Electronic Supplementary Information (ESI) to accompany:

Influence of Adsorption Thermodynamics on Guest Diffusivities in Nanoporous Crystalline Materials

Rajamani Krishna* and Jasper M. van Baten

Van 't Hoff Institute for Molecular Sciences, University of Amsterdam, Science Park 904,

1098 XH Amsterdam, The Netherlands

*CORRESPONDING AUTHOR Tel +31 20 6270990; Fax: + 31 20 5255604;

email: r.krishna@uva.nl

Listing of Sequence of Figures with data relating diffusivities to adsorption thermodynamics.

The structural details, pore landscapes, surface area vs pore size distributions, CBMC and MD simulation results, along with available experimental data. The data for each material are arranged and presented in the accompanying Figures in the following order.

Cage-type structures with narrow windows

For cage-type zeolites, the accompanying Figures demonstrate the validity of the QC model to describe the loading dependence of CH_4.

CHA

DDR

ERI

ITQ-29

LTA-Si (all-silica)

LTA-4A

LTA-5A

SOD-Si (all silica)

TSC

ZIF-8: In this case, experimental data on diffusivities obtained from Leipzig using Infra-Red Microscopy are presented to demonstrate the influence of molecular clustering.

1D meso-porous channels

BTP-COF

1D micro-porous channels

For 1D microporous channels, the data comparing the loading dependence of diffusivities with the inverse thermodynamic factor for variety of guest molecules are presented for the following structures.

AFI

MTW

TON

MgMOF-74

ZnMOF-74

NiMOF-74

FeMOF-74

CoMOF-74

MIL-47

MIL-53(Cr)-lp

1D micro-porous channels with side pockets

For MOR, the accompanying Figures present data comparing the loading dependence of diffusivities with the inverse thermodynamic factor for variety of guest molecules.

MOR

"Open" structures with large cavities

For each structure listed below, the accompanying Figures present data comparing the loading dependence of diffusivities with the inverse thermodynamic factor for variety of guest molecules.

FAU-Si

NaY

NaX

CuBTC

IRMOF-1

MOF-177

Intersecting channels

For each structure listed below, the accompanying Figures present data comparing the loading dependence of diffusivities with the inverse thermodynamic factor for variety of guest molecules.

BEA

BOG

FER

ISV

MFI

Zn(bdc)dabco

Electronic Supplementary Material (ESI) for Physical Chemistry Chemical Physics

Cage-type structures with narrow windows

CHA landscape

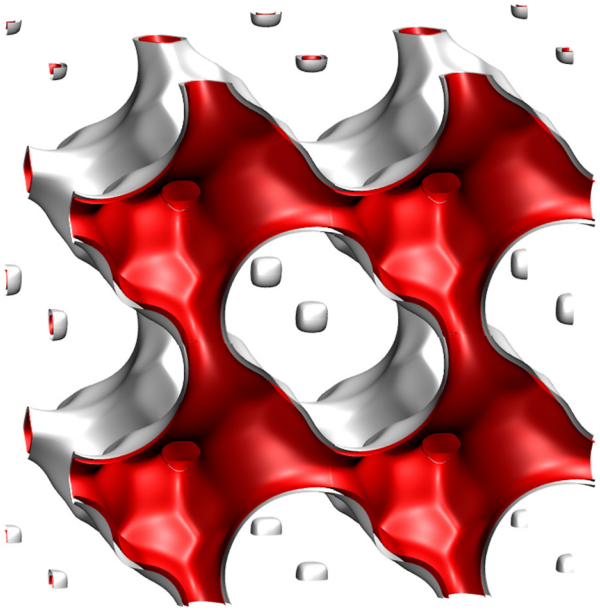

There are 6 cages per unit cell. The volume of one CHA cage is 316.4 Å^3, slightly larger than that of a single cage of DDR (278 Å^3), but significantly lower than FAU (786 Å^3).

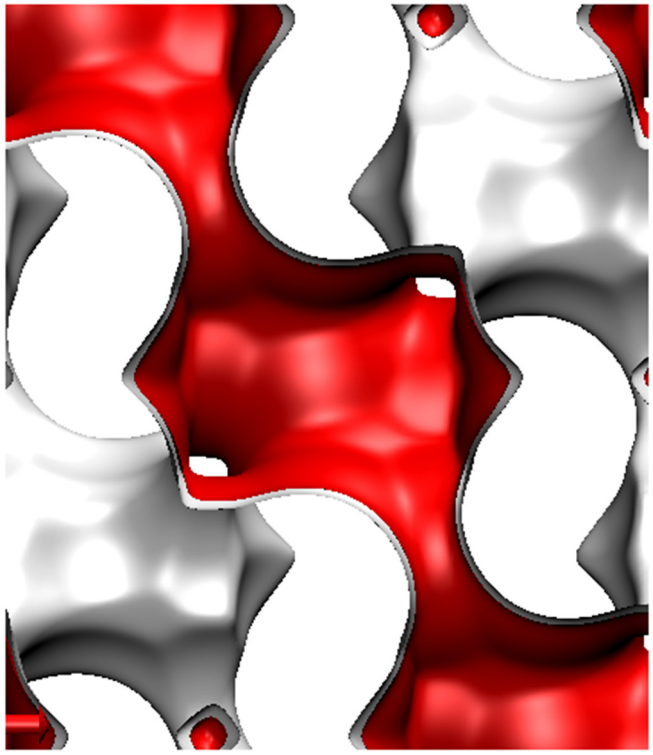

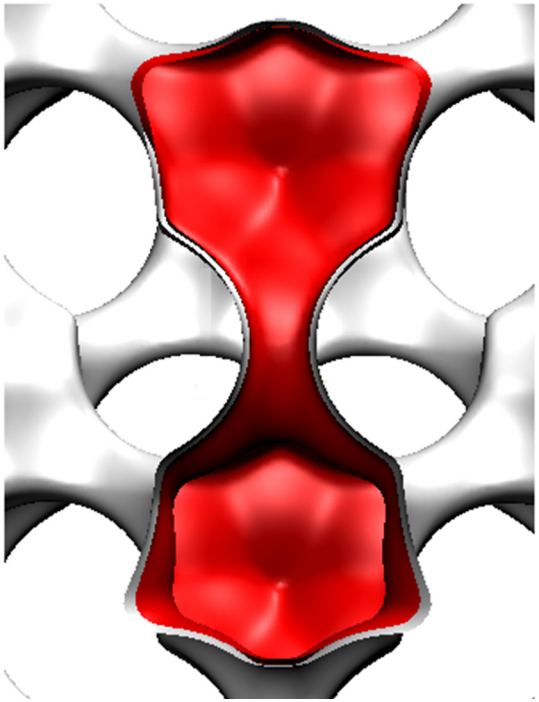

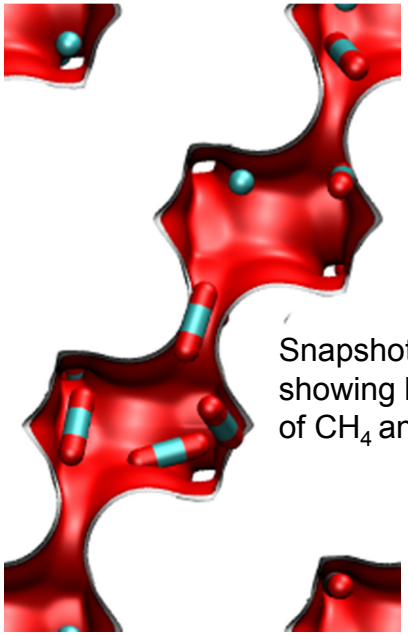

Snapshots showing location of CH_4 and CO_2

Snapshots showing location of CH_4

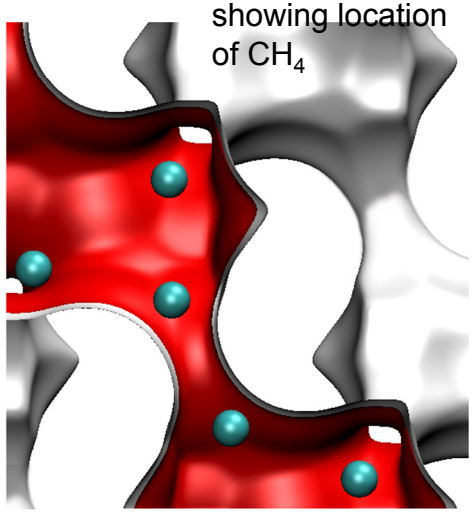

Structural information from: C. Baerlocher, L.B. McCusker, Database of Zeolite Structures, International Zeolite Association, http://www.iza-structure.org/databases/

CHA window and pore dimensions

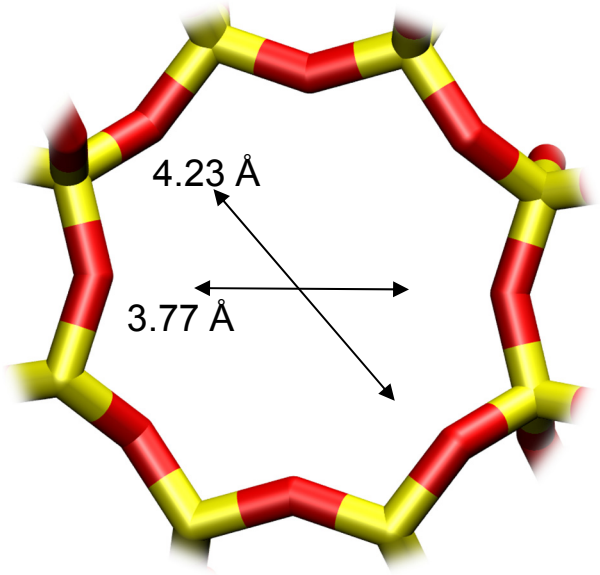

CHA

The window dimensions calculated using the van der Waals diameter of framework atoms = 2.7 Å are indicated above by the arrows.

This plot of surface area versus pore dimension is determined using a combination of the DeLaunay triangulation method for pore dimension determination, and the procedure of Düren for determination of the surface area.

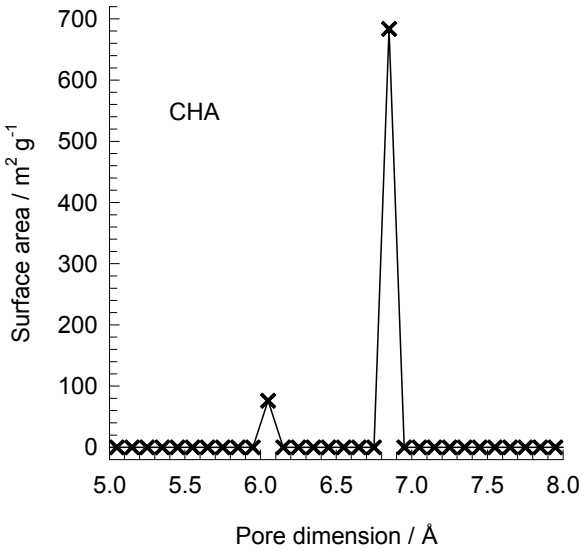

	CHA
a /Å	15.075
b /Å	23.907
c /Å	13.803
Cell volume / Å^3	4974.574
conversion factor for [molec/uc] to [mol per kg Framework]	0.2312
conversion factor for [molec/uc] to [kmol/m^3]	0.8747
ρ [kg/m3]	1444.1
MW unit cell [g/mol(framework)]	4326.106
ϕ, fractional pore volume	0.382
open space / Å^3/uc	1898.4
Pore volume / cm^3/g	0.264
Surface area /m^2/g	758.0
DeLaunay diameter /Å	3.77

CHA CBMC simulations of isotherms, and isosteric heats of adsorption

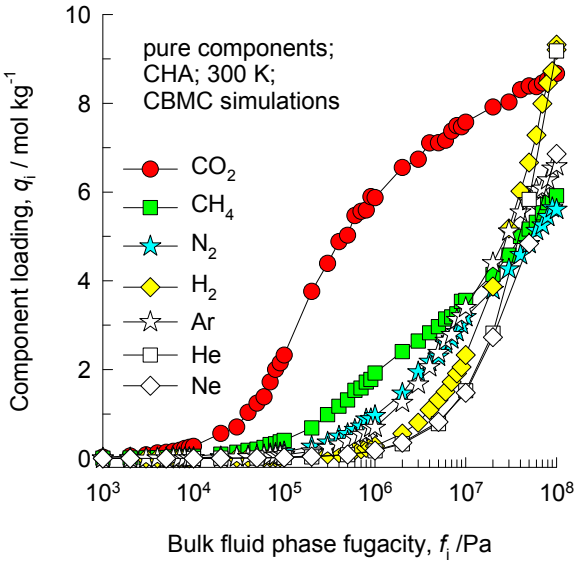

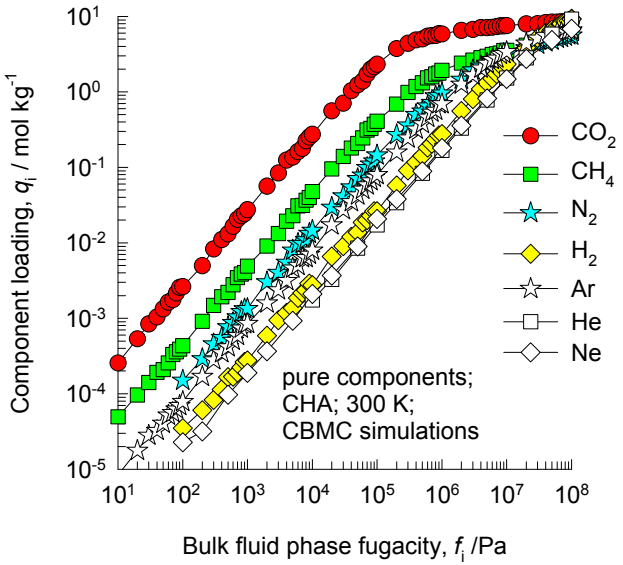

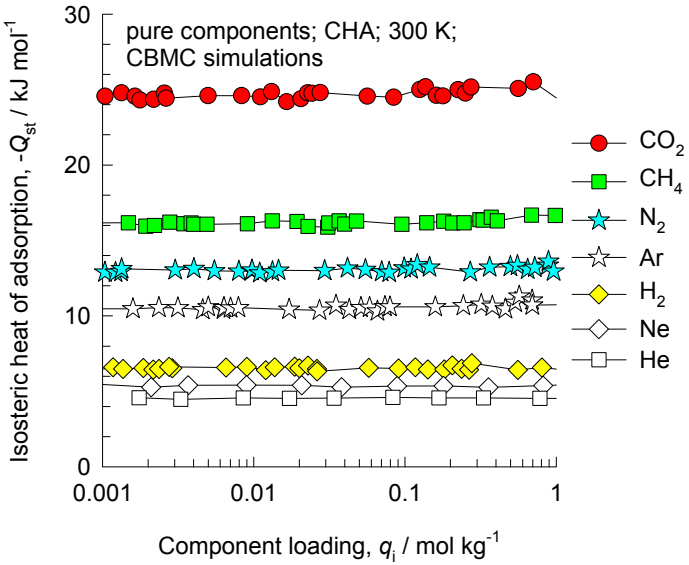

CHA MD simulations of unary self- , and M-S diffusivities

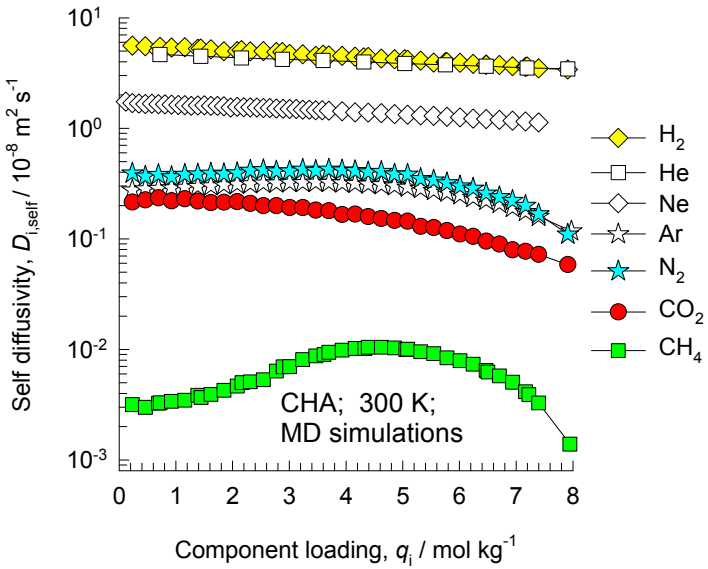

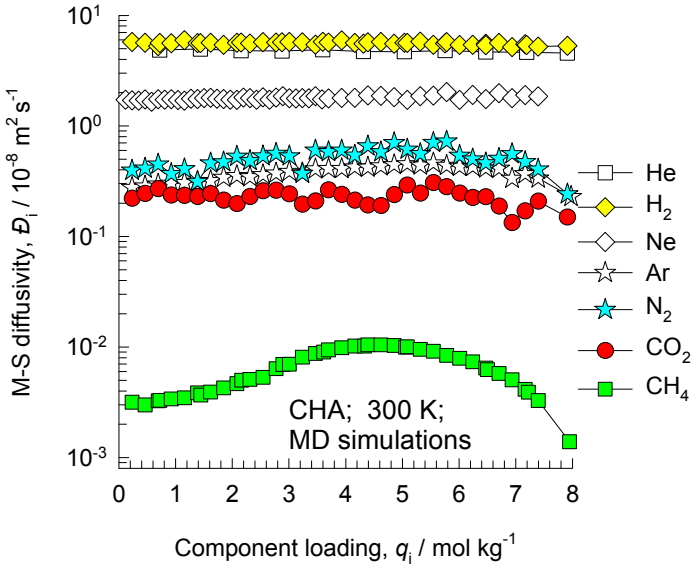

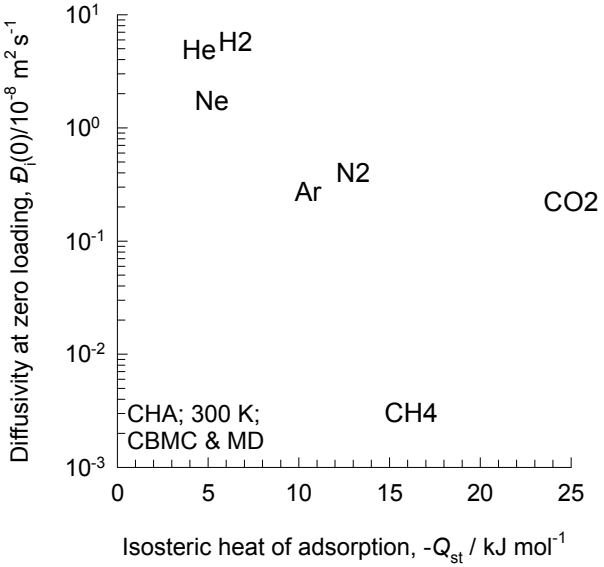

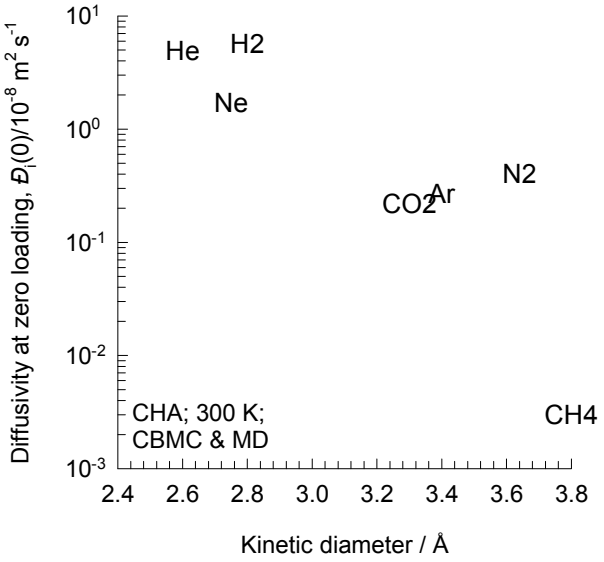

CHA Modeling the loading dependence of CH_4 diffusivity

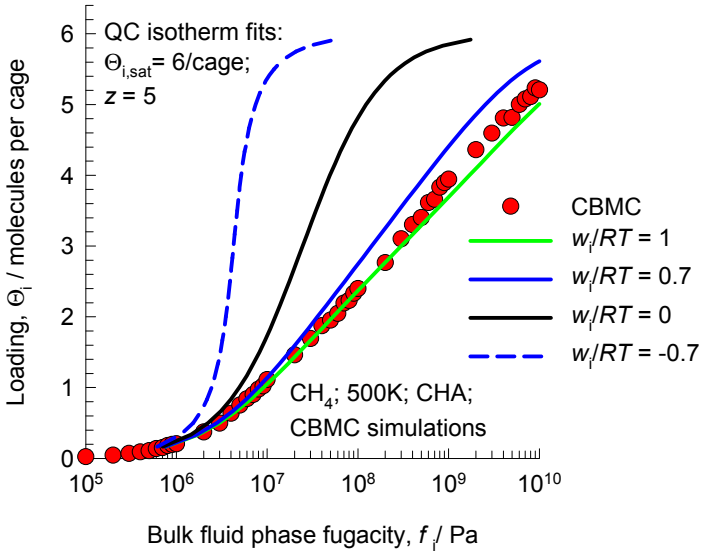

Quasi - Chemical isotherm

$$b_i f_i = \frac{\theta_i}{(1-\theta_i)}\left(\frac{2\,(1-\theta_i)}{\varsigma_i + 1 - 2\theta_i}\right)^z$$

$$\theta_i = c_i / c_{i,sat} = q_i / q_{i,sat} = \Theta_i / \Theta_{i,sat}$$

$$\varsigma_i = \sqrt{1 - 4\,\theta_i(1-\theta_i)(1-\exp(-w_i/RT))}$$

$$\Gamma_i = \frac{1}{(1-\theta_i)}\left(1 + \frac{z}{2}\frac{(1-\varsigma_i)}{\varsigma_i}\right)$$

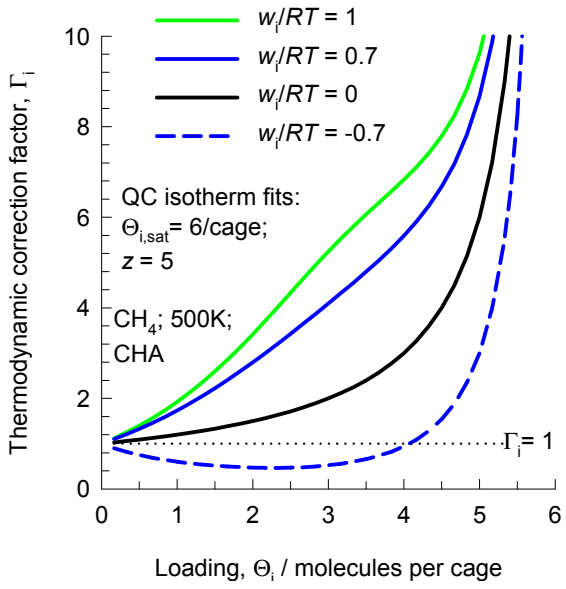

Krishna, Paschek and Baur (2004) model

$$Đ_i = Đ_i(0)\left(\frac{1+\varsigma_i}{2\,(1-\theta_i)}\right)^{-z}\left(1 + \frac{(\varsigma_i - 1 + 2\theta_i)\exp(w_i/RT)}{2\,(1-\theta_i)}\right)^{z-1}$$

$$\varsigma_i = \sqrt{1 - 4\,\theta_i(1-\theta_i)(1-\exp(-w_i/RT))}$$

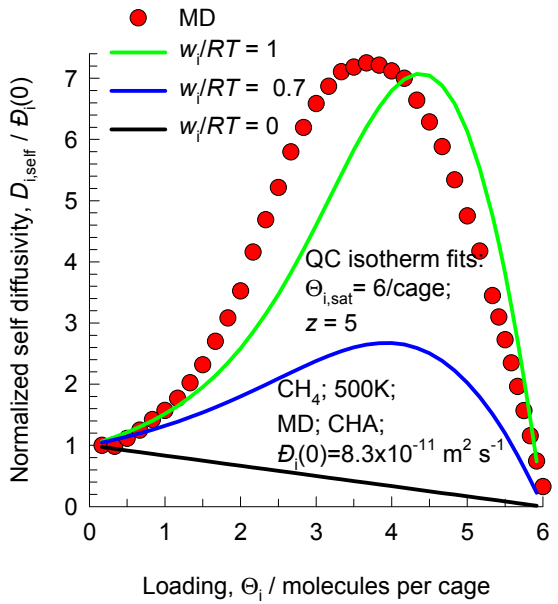

The model used to describe the concentration dependence of $Đ_i$ is described in detail in Krishna, R.; Paschek, D.; Baur, R. Modelling the occupancy dependence of diffusivities in zeolites, Microporous Mesoporous Mater. 2004, 76, 233-246.

CHA: Transient uptake of methanol – ethanol mixture

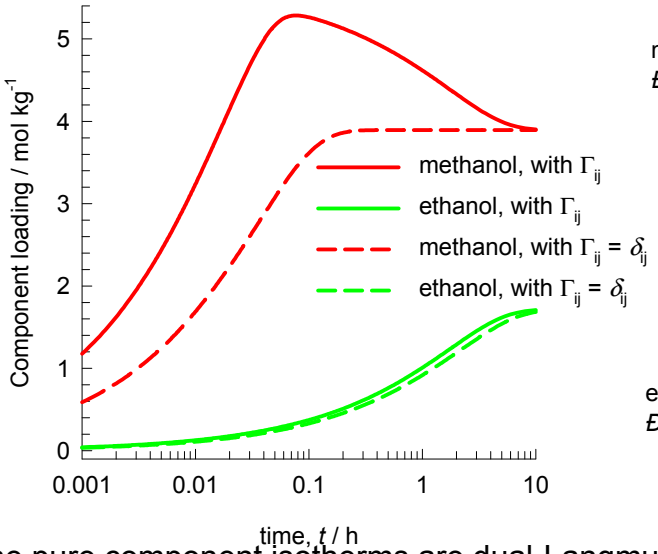

methanol diffusivity:
$Đ_1 / r_c^2 = 6 \times 10^{-4}$ s^{-1}

CHA; 300 K;
methanol(1)/ethanol(2)
f_1 = 10000 Pa; f_2= 10000 Pa;

ethanol diffusivity:
$Đ_2 / r_c^2 = 1 \times 10^{-5}$ s^{-1}

In these simulations, both the M-S diffusivities are assumed to be independent of loading. The overshoot in methanol is not, therefore, a result of the loading dependence of its M-S diffusivity.

The pure component isotherms are dual-Langmuir-Freundlich fits of CBMC simulated pure component isotherms of alcohols in CHA available in
Krishna, R.; van Baten, J. M. Entropy-based separation of linear chain molecules by exploiting differences in the saturation capacities in cage-type zeolites, Sep. Purif. Technol. 2011, 76, 325-330.

The overshoot in the methanol uptake is a direct consequence of thermodynamic coupling caused by the off-diagonal elements of $\begin{bmatrix} \Gamma_{11} & \Gamma_{12} \\ \Gamma_{21} & \Gamma_{21} \end{bmatrix}$ where $\Gamma_{ij} = \frac{q_i}{f_i}\frac{\partial f_i}{\partial q_j}$

If the thermodynamic coupling is ignored, i.e. we assume $\Gamma_i = \delta_{ij}$; Kronecker delta $\begin{bmatrix} \Gamma_{11} & \Gamma_{12} \\ \Gamma_{21} & \Gamma_{21} \end{bmatrix} = \begin{bmatrix} 1 & 0 \\ 0 & 1 \end{bmatrix}$

the methanol overshoot disappears.

CHA: Transient uptake of methanol – 1-propanol mixture

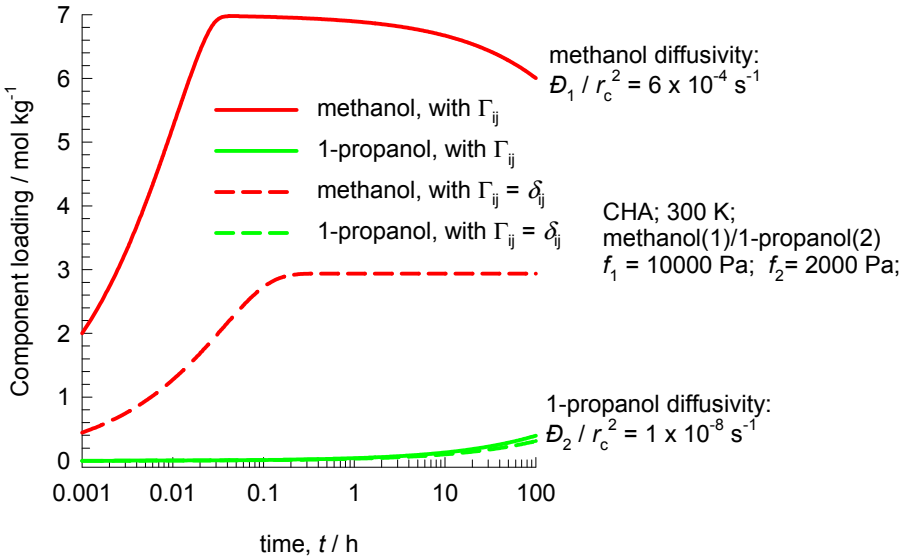

In these simulations, both the M-S diffusivities are assumed to be independent of loading. The overshoot in methanol is not, therefore, a result of the loading dependence of its M-S diffusivity.

The pure component isotherms are dual-Langmuir-Freundlich fits of CBMC simulated pure component isotherms of alcohols in CHA available in
Krishna, R.; van Baten, J. M. Entropy-based separation of linear chain molecules by exploiting differences in the saturation capacities in cage-type zeolites, Sep. Purif. Technol. 2011, 76, 325-330.

The overshoot in the methanol uptake is a direct consequence of thermodynamic coupling caused by the off-diagonal elements of $\begin{bmatrix}\Gamma_{11} & \Gamma_{12}\\ \Gamma_{21} & \Gamma_{21}\end{bmatrix}$ where $\Gamma_{ij} = \frac{q_i}{f_i}\frac{\partial f_i}{\partial q_j}$

If the thermodynamic coupling is ignored, i.e. we assume $\Gamma_i = \delta_{ij}$; Kronecker delta $\begin{bmatrix}\Gamma_{11} & \Gamma_{12}\\ \Gamma_{21} & \Gamma_{21}\end{bmatrix} = \begin{bmatrix}1 & 0\\ 0 & 1\end{bmatrix}$

the methanol overshoot disappears.

CHA: Transient uptake of ethanol – 1-propanol mixture

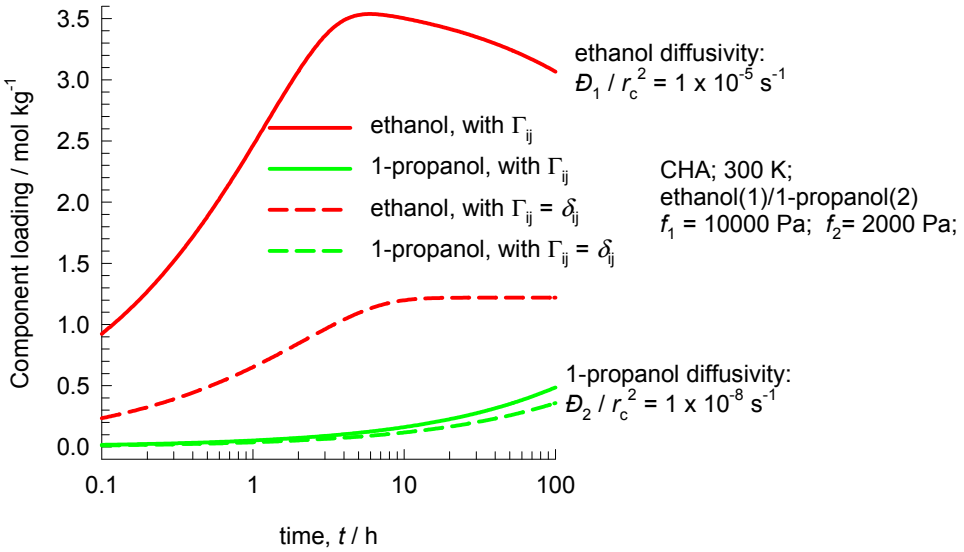

In these simulations, both the M-S diffusivities are assumed to be independent of loading. The overshoot in ethanol is not, therefore, a result of the loading dependence of its M-S diffusivity.

The pure component isotherms are dual-Langmuir-Freundlich fits of CBMC simulated pure component isotherms of alcohols in CHA available in
Krishna, R.; van Baten, J. M. Entropy-based separation of linear chain molecules by exploiting differences in the saturation capacities in cage-type zeolites, Sep. Purif. Technol. 2011, 76, 325-330.

The overshoot in the ethanol uptake is a direct consequence of thermodynamic coupling caused by the off-diagonal elements of $\begin{bmatrix}\Gamma_{11} & \Gamma_{12}\\ \Gamma_{21} & \Gamma_{21}\end{bmatrix}$ where $\Gamma_{ij} = \frac{q_i}{f_i}\frac{\partial f_i}{\partial q_j}$

If the thermodynamic coupling is ignored, i.e. we assume $\Gamma_i = \delta_{ij}$; Kronecker delta $\begin{bmatrix}\Gamma_{11} & \Gamma_{12}\\ \Gamma_{21} & \Gamma_{21}\end{bmatrix} = \begin{bmatrix}1 & 0\\ 0 & 1\end{bmatrix}$

the ethanol overshoot disappears.

Electronic Supplementary Material (ESI) for Physical Chemistry Chemical Physics

DDR landscape

There are 12 cages per unit cell. The volume of one DDR cage is 278 Å^3, significantly smaller than that of a single cage of FAU (786 Å^3), or ZIF-8 (1168 Å^3).

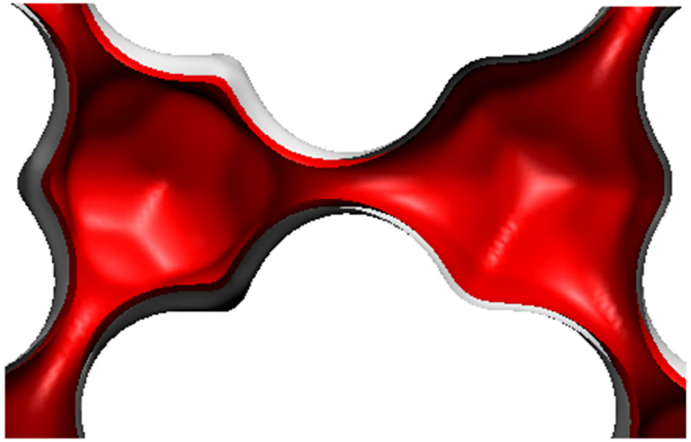

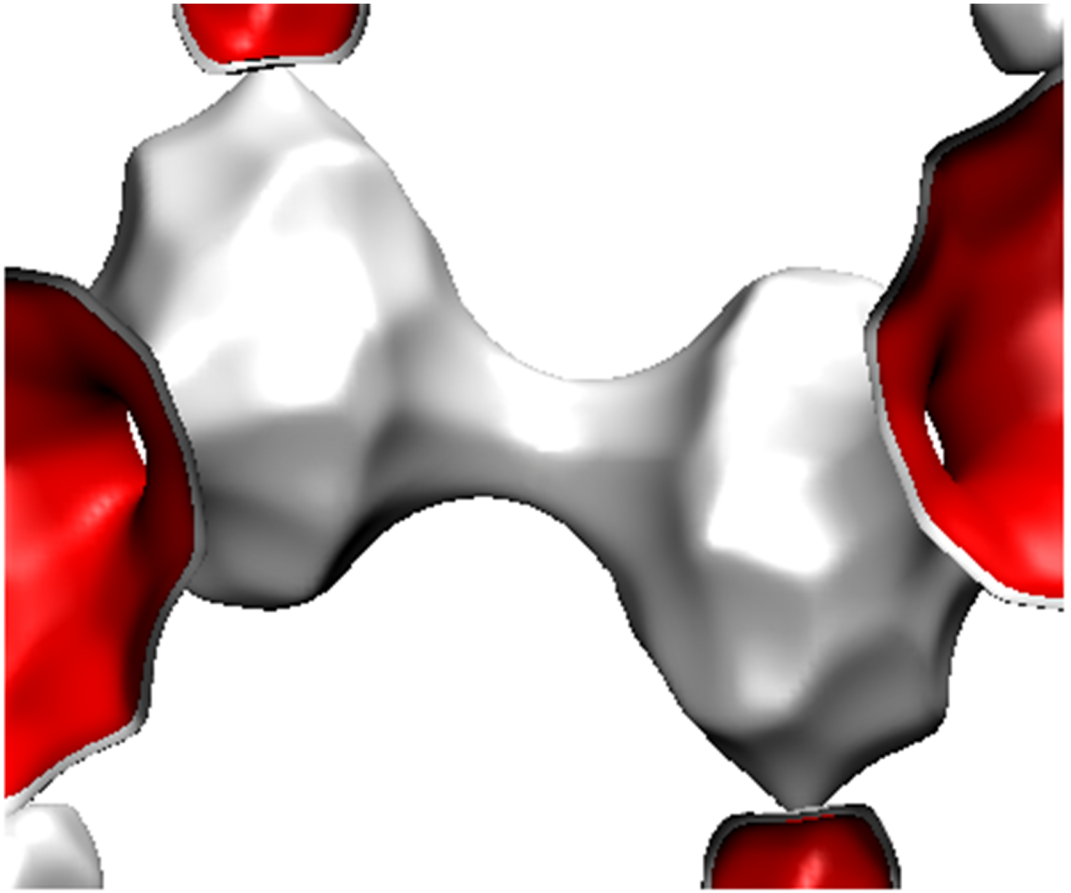

Structural information from: C. Baerlocher, L.B. McCusker, Database of Zeolite Structures, International Zeolite Association, http://www.iza-structure.org/databases/

To convert from molecules per unit cell to mol kg^{-1}, multiply by 0.06936.
The pore volume is 0.182 cm^3/g.

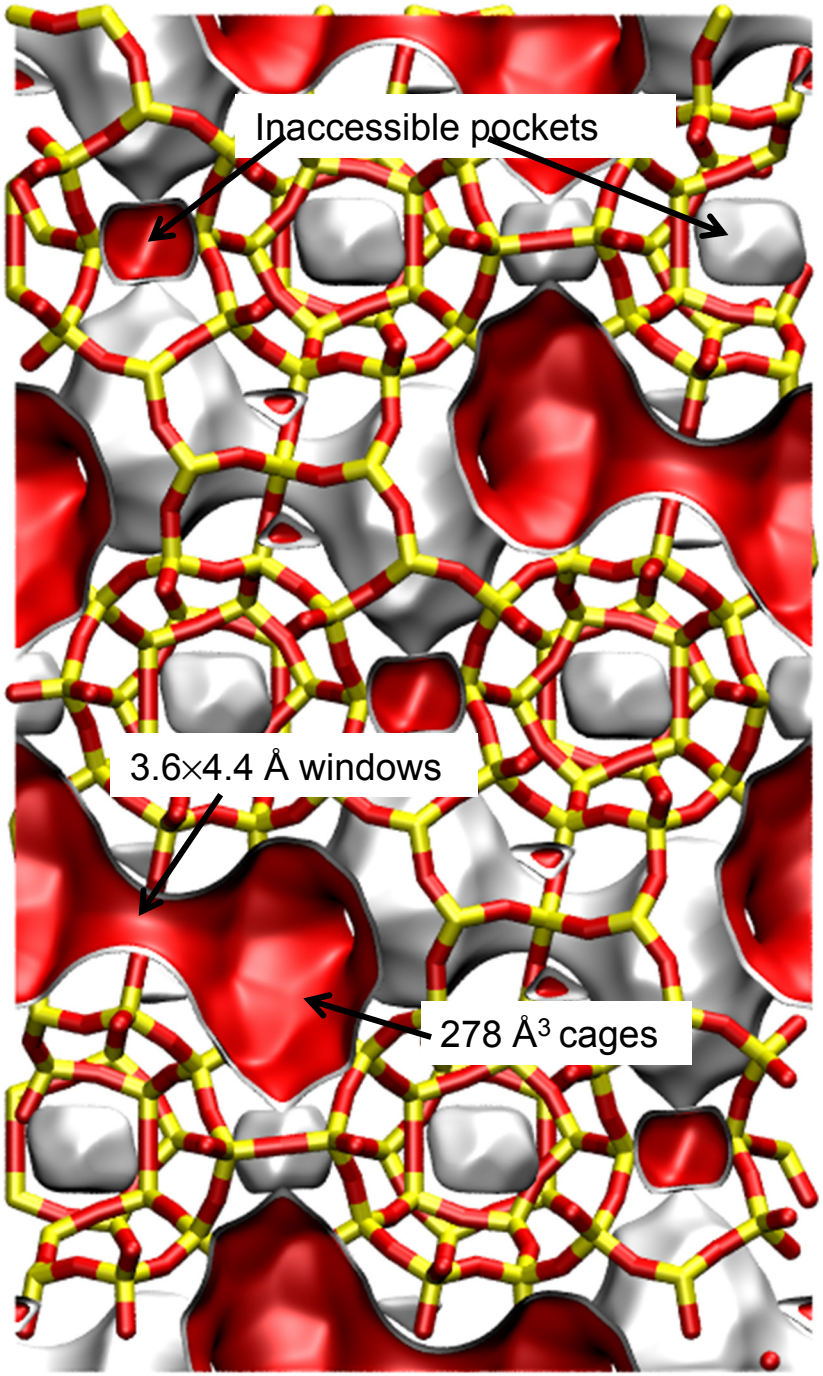

DDR landscapes without blocking

In all our simulations the inaccessible pockets of DDR were blocked. This aspect is explained in our paper
R. Krishna and J.M. van Baten, Comment on Comparative Molecular Simulation Study of CO2/N2 and CH4/N2 Separation in Zeolites and Metal-Organic Frameworks, Langmuir, 26 (2010) 2975-2978

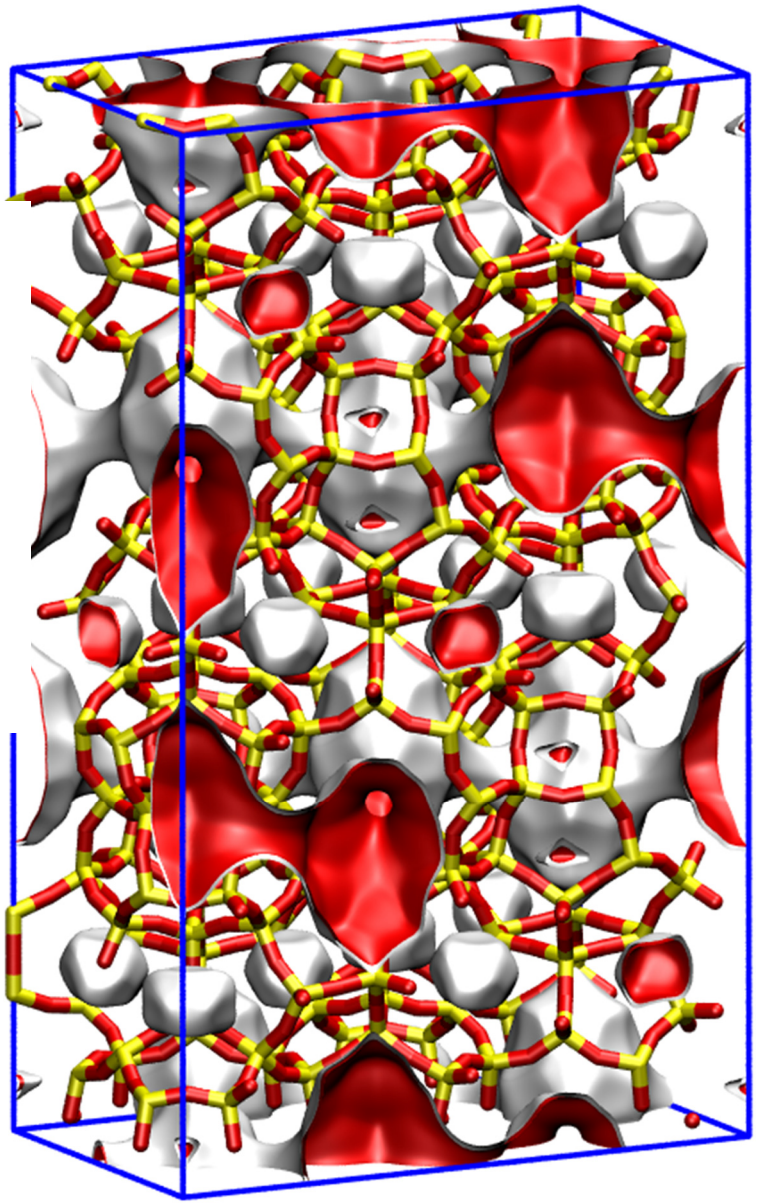

DDR window and pore dimensions

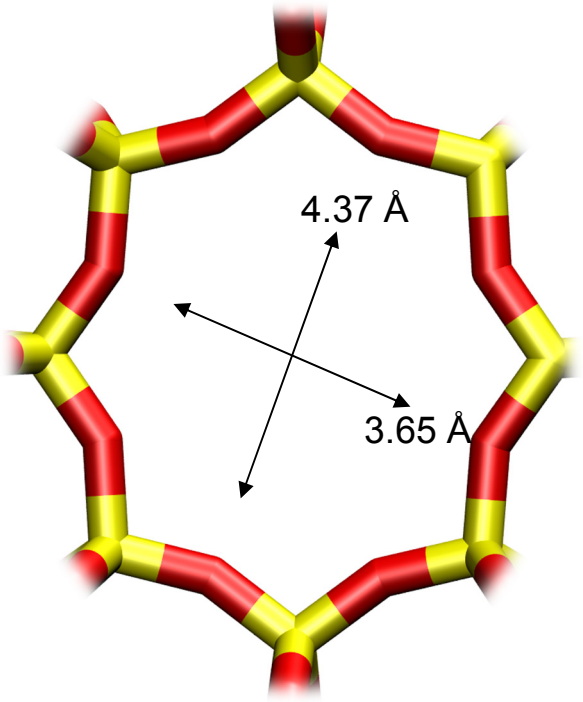

DDR

The window dimensions calculated using the van der Waals diameter of framework atoms = 2.7 Å are indicated above by the arrows.

This plot of surface area versus pore dimension is determined using a combination of the DeLaunay triangulation method for pore dimension determination, and the procedure of Düren for determination of the surface area.

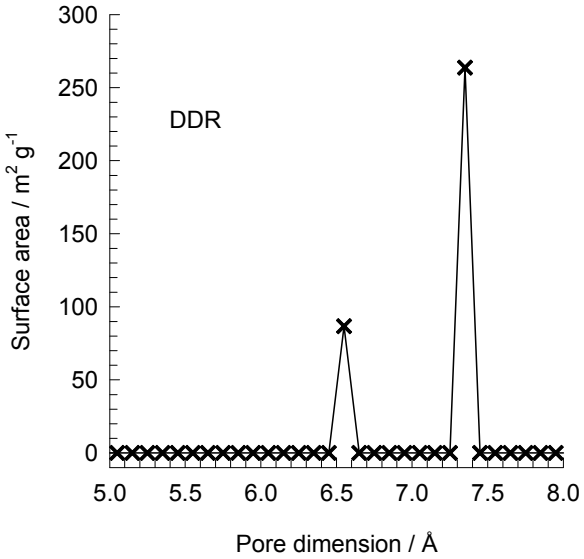

	DDR
a /Å	24.006
b /Å	13.86
c /Å	40.892
Cell volume / Å^3	13605.72
conversion factor for [molec/uc] to [mol per kg Framework]	0.0693
conversion factor for [molec/uc] to [kmol/m^3]	0.4981
ρ [kg/m3]	1759.991
MW unit cell [g/mol(framework)]	14420.35
ϕ, fractional pore volume	0.245
open space / Å^3/uc	3333.5
Pore volume / cm^3/g	0.139
Surface area /m^2/g	350.0
DeLaunay diameter /Å	3.65

DDR CBMC simulations of isotherms, and isosteric heats of adsorption

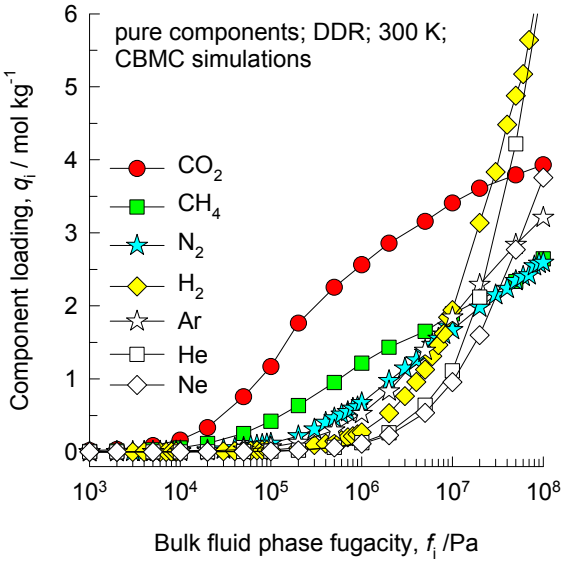

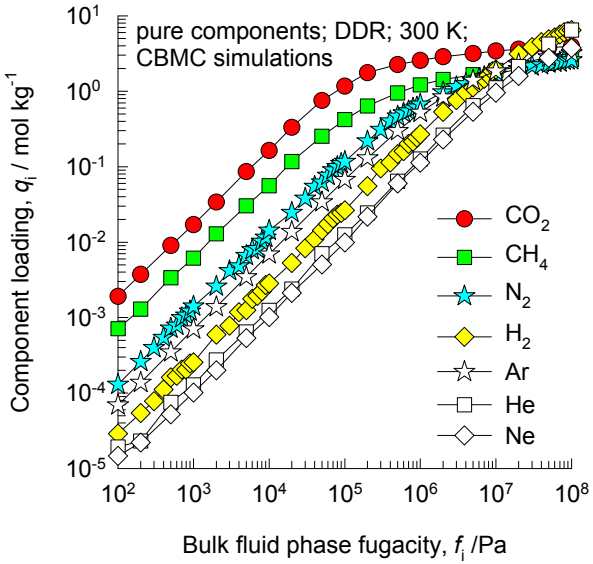

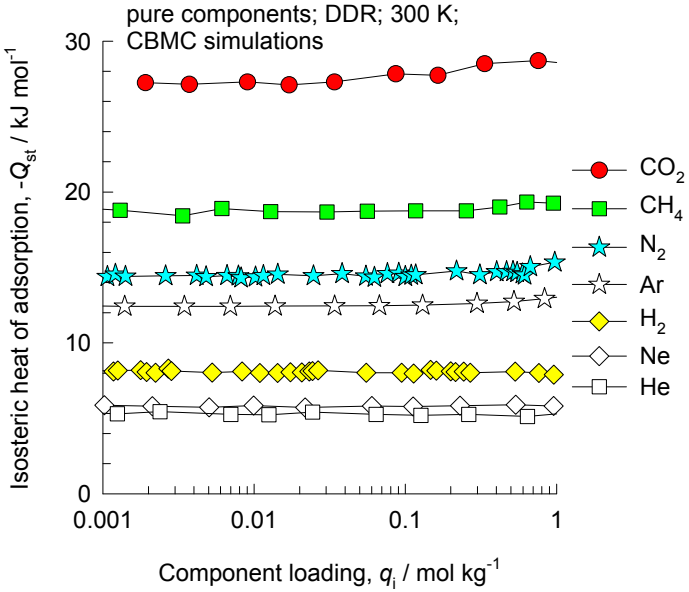

DDR Modeling the loading dependence of CH_4 diffusivity

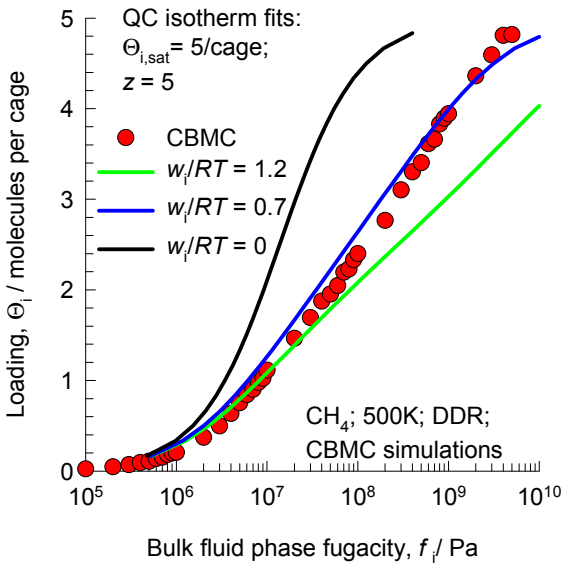

Quasi - Chemical isotherm

$$b_i f_i = \frac{\theta_i}{(1-\theta_i)}\left(\frac{2\,(1-\theta_i)}{\varsigma_i + 1 - 2\theta_i}\right)^z$$

$$\theta_i = c_i / c_{i,sat} = q_i / q_{i,sat} = \Theta_i / \Theta_{i,sat}$$

$$\varsigma_i = \sqrt{1 - 4\,\theta_i (1-\theta_i)\left(1 - \exp(-w_i/RT)\right)}$$

$$\Gamma_i = \frac{1}{(1-\theta_i)}\left(1 + \frac{z}{2}\frac{(1-\varsigma_i)}{\varsigma_i}\right)$$

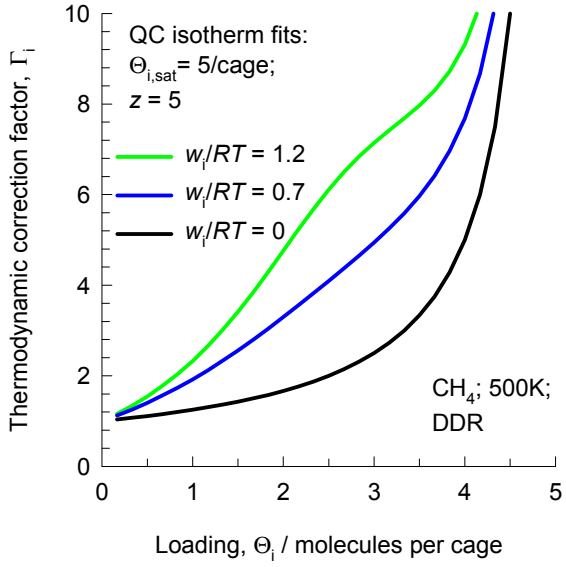

Krishna, Paschek and Baur (2004) model

$$Đ_i = Đ_i(0)\left(\frac{1+\varsigma_i}{2\,(1-\theta_i)}\right)^{-z}\left(1 + \frac{(\varsigma_i - 1 + 2\theta_i)\exp(w_i/RT)}{2\,(1-\theta_i)}\right)^{z-1}$$

$$\varsigma_i = \sqrt{1 - 4\,\theta_i (1-\theta_i)\left(1 - \exp(-w_i/RT)\right)}$$

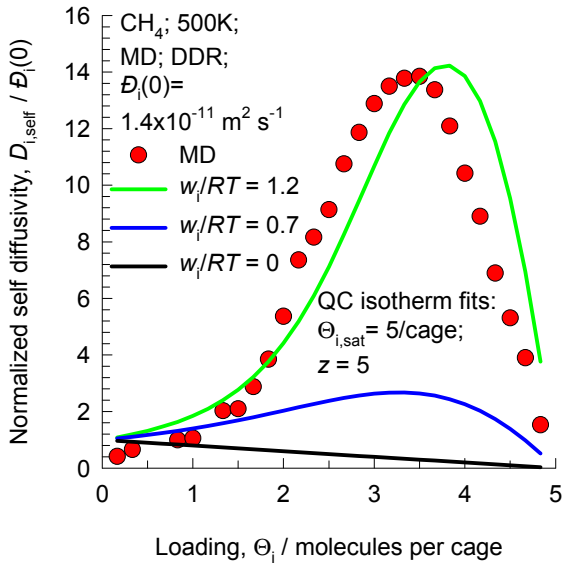

The model used to describe the concentration dependence of $Đ_i$ is described in detail in Krishna, R.; Paschek, D.; Baur, R. Modelling the occupancy dependence of diffusivities in zeolites, Microporous Mesoporous Mater. 2004, 76, 233-246.

ERI pore landscape

There are 4 cages per unit cell.
The volume of one ERI cage is 408.7 Å^3, significantly smaller than that of a single cage of FAU-Si (786 Å^3), or ZIF-8 (1168 Å^3).

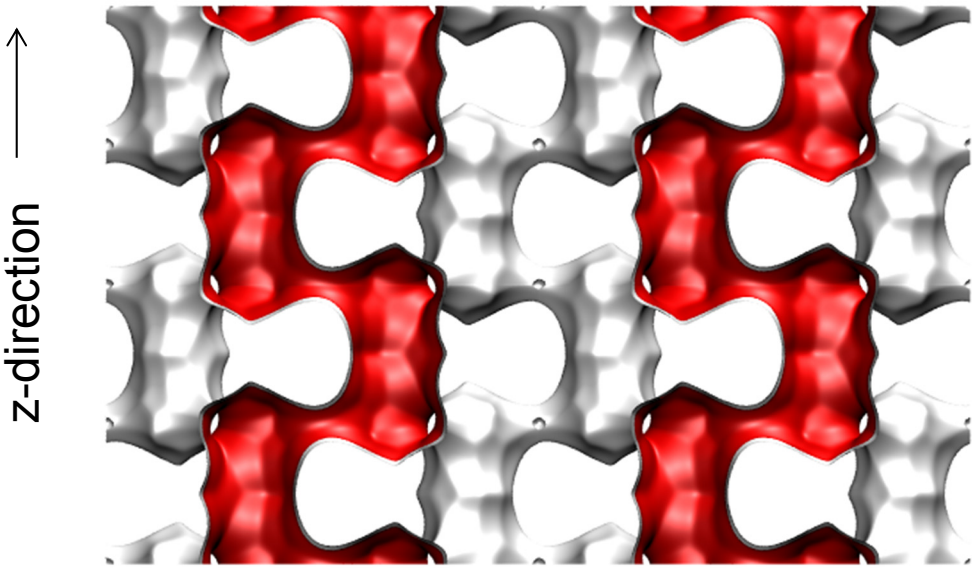

x-y projection

Snapshots showing location of CH_4 and CO_2

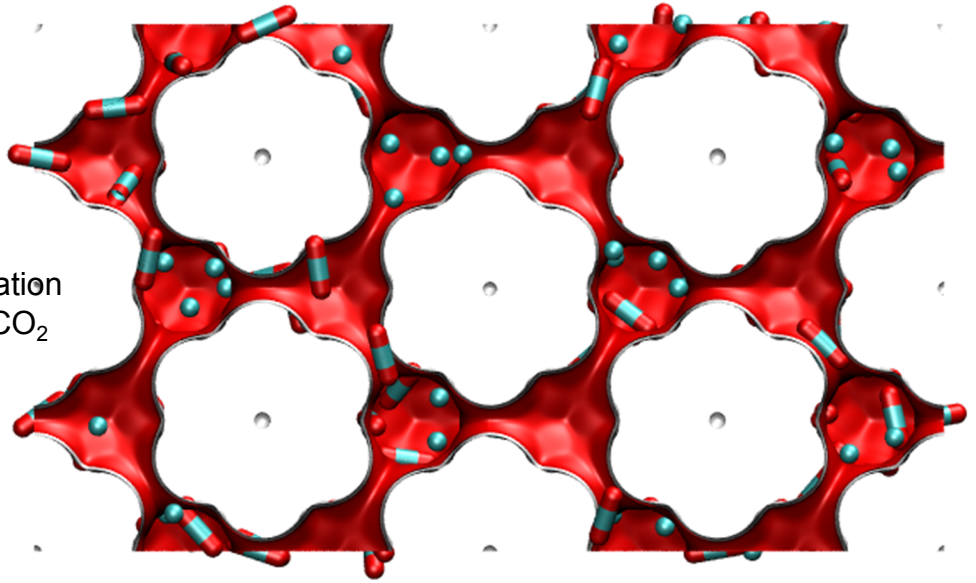

Structural information from: C. Baerlocher, L.B. McCusker, Database of Zeolite Structures, International Zeolite Association, http://www.iza-structure.org/databases/

ERI window and pore dimensions

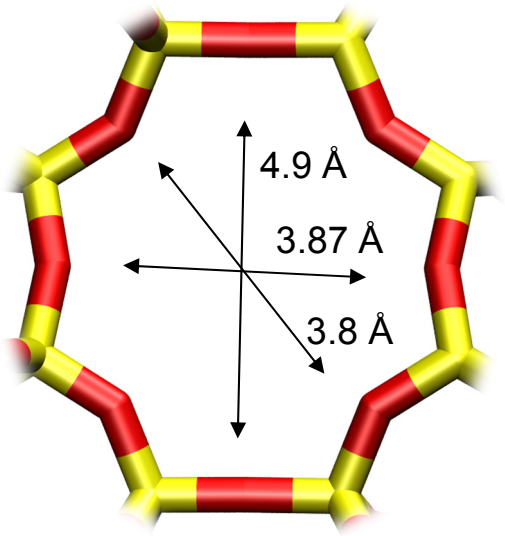

ERI

The window dimensions calculated using the van der Waals diameter of framework atoms = 2.7 Å are indicated above by the arrows.

This plot of surface area versus pore dimension is determined using a combination of the DeLaunay triangulation method for pore dimension determination, and the procedure of Düren for determination of the surface area.

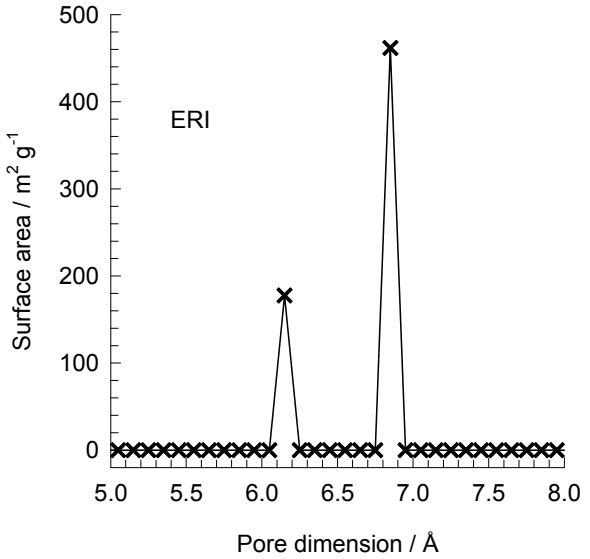

	ERI
a /Å	22.953
b /Å	13.252
c /Å	14.81
Cell volume / Å^3	4504.804
conversion factor for [molec/uc] to [mol per kg Framework]	0.2312
conversion factor for [molec/uc] to [kmol/m^3]	1.0156
ρ [kg/m3]	1594.693
MW unit cell [g/mol(framework)]	4326.106
ϕ, fractional pore volume	0.363
open space / Å^3/uc	1635.0
Pore volume / cm^3/g	0.228
Surface area /m^2/g	635.0
DeLaunay diameter /Å	3.81

Electronic Supplementary Material (ESI) for Physical Chemistry Chemical Physics

ERI MD simulations of unary self- diffusivities

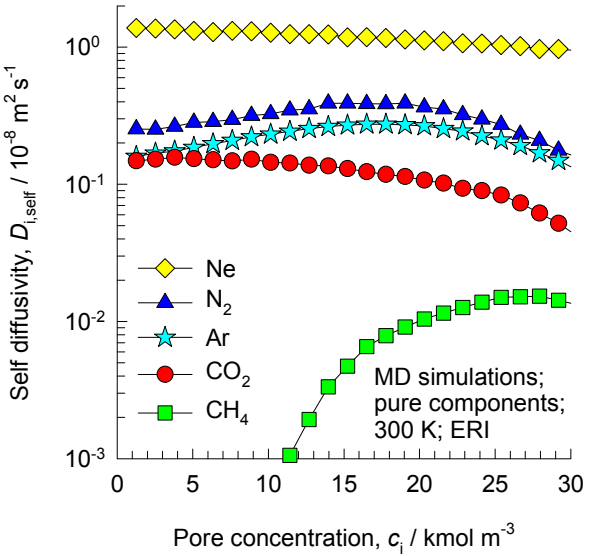

ITQ-29 pore landscape

There is 1 cage per unit cell.
The volume of one ITQ-29 cage is 677.6 Å^3, intermediate in size between a single cage of ZIF-8 (1168 Å^3) and of DDR (278 Å^3).

The structural information for ITQ-29 is not available in the IZA atlas and is taken from Corma, Nature, 437 (2004) 287. The window size is slightly smaller than that of LTA Si.

Inaccessible sodalite cages have been blocked in these simulations

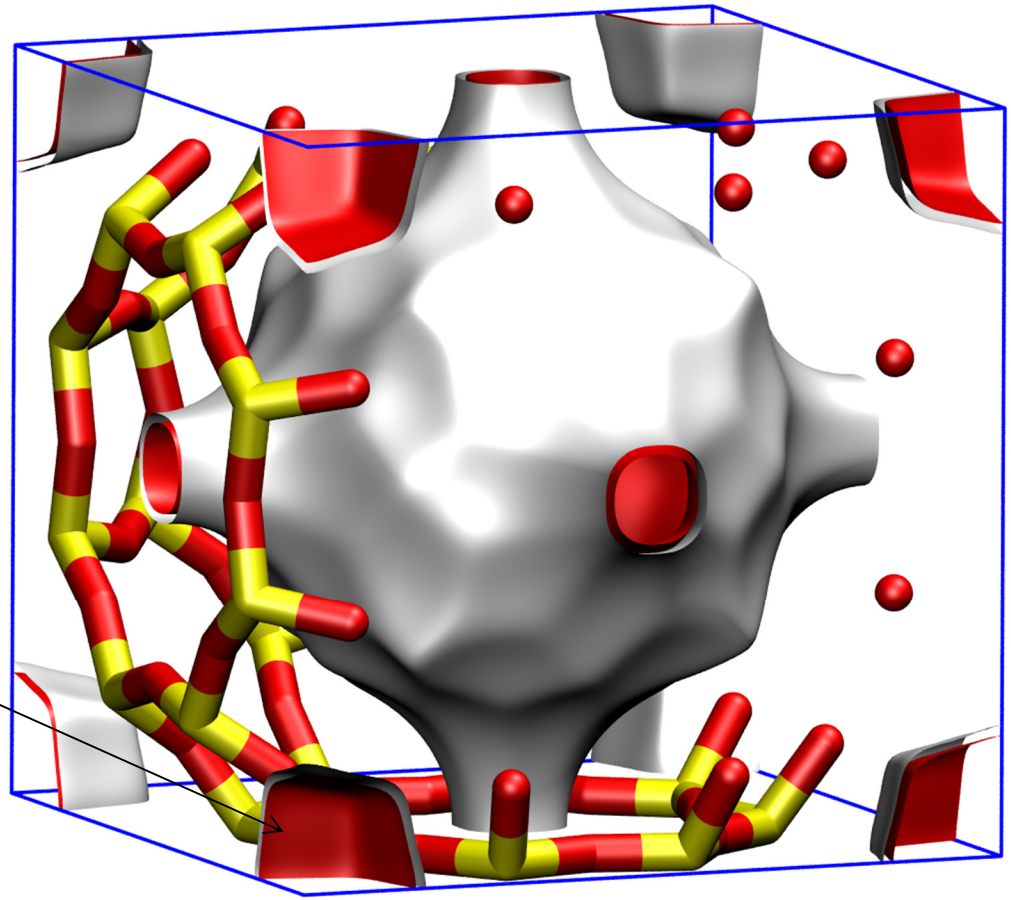

Electronic Supplementary Material (ESI) for Physical Chemistry Chemical Physics

ITQ-29 window and pore dimensions

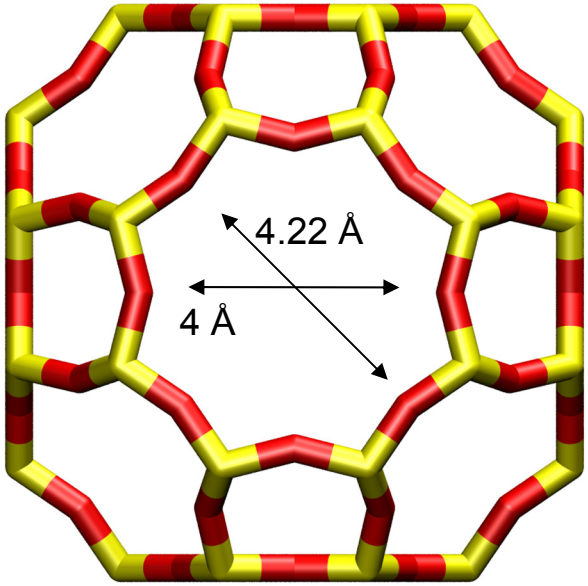

The window dimension calculated using the van der Waals diameter of framework atoms = 2.7 Å is indicated above by the arrows.

This plot of surface area versus pore dimension is determined using a combination of the DeLaunay triangulation method for pore dimension determination, and the procedure of Düren for determination of the surface area.

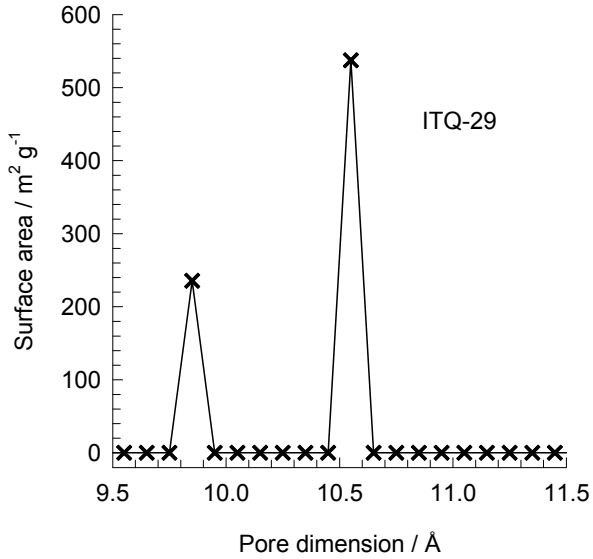

	ITQ-29
a /Å	11.867
b /Å	11.867
c /Å	11.867
Cell volume / Å^3	1671.178
conversion factor for [molec/uc] to [mol per kg Framework]	0.6935
conversion factor for [molec/uc] to [kmol/m^3]	2.4508
ρ [kg/m3]	1432.877
MW unit cell [g/mol(framework)]	1442.035
ϕ, fractional pore volume	0.405
open space / Å^3/uc	677.6
Pore volume / cm^3/g	0.283
Surface area /m^2/g	773.0
DeLaunay diameter /Å	3.98

Electronic Supplementary Material (ESI) for Physical Chemistry Chemical Physics

ITQ-29 MD simulations of unary self- diffusivities

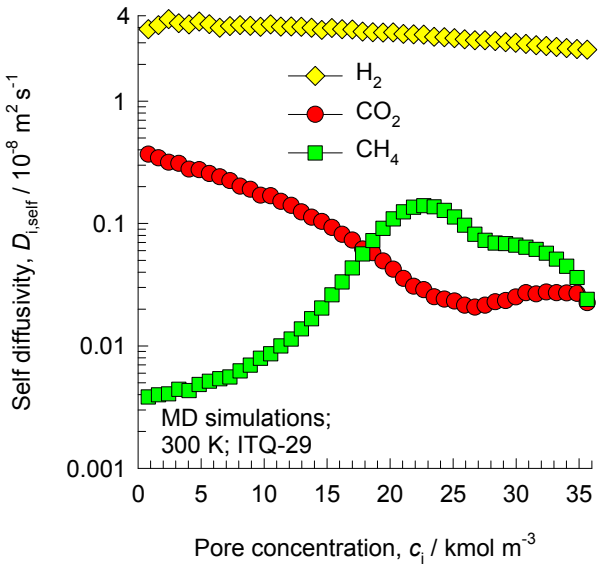

ITQ-29 Modeling the loading dependence of CH_4 diffusivity

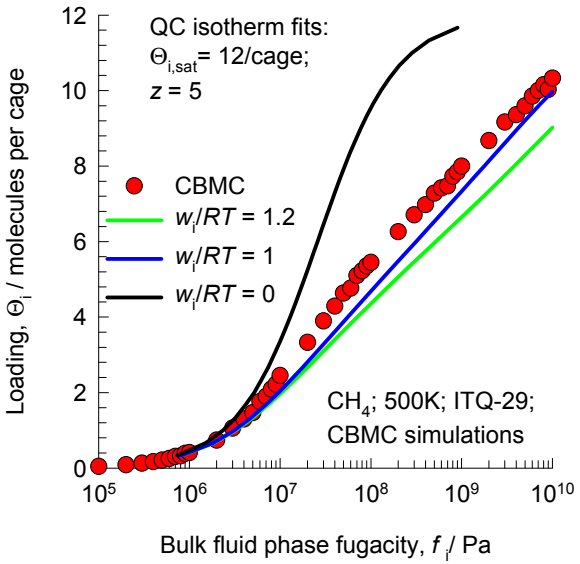

Quasi - Chemical isotherm

$$b_i f_i = \frac{\theta_i}{(1-\theta_i)}\left(\frac{2\,(1-\theta_i)}{\varsigma_i + 1 - 2\theta_i}\right)^z$$

$$\theta_i = c_i / c_{i,sat} = q_i / q_{i,sat} = \Theta_i / \Theta_{i,sat}$$

$$\varsigma_i = \sqrt{1 - 4\,\theta_i (1-\theta_i)\left(1 - \exp(-w_i / RT)\right)}$$

$$\Gamma_i = \frac{1}{(1-\theta_i)}\left(1 + \frac{z}{2}\frac{(1-\varsigma_i)}{\varsigma_i}\right)$$

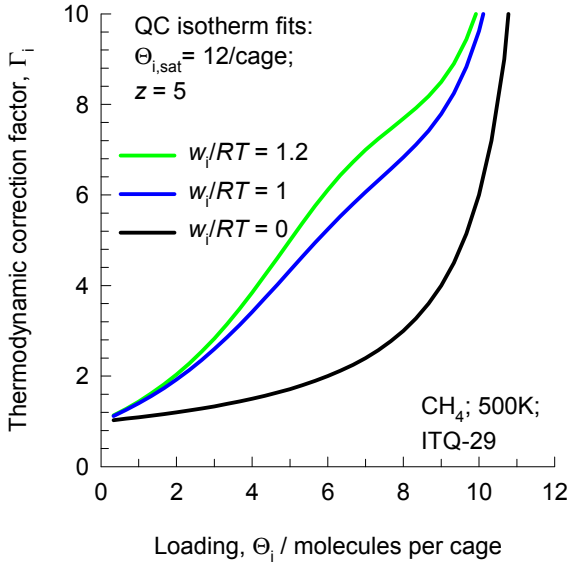

Krishna, Paschek and Baur (2004) model

$$Đ_i = Đ_i(0)\left(\frac{1+\varsigma_i}{2\,(1-\theta_i)}\right)^{-z}\left(1 + \frac{(\varsigma_i - 1 + 2\theta_i)\exp(w_i/RT)}{2\,(1-\theta_i)}\right)^{z-1}$$

$$\varsigma_i = \sqrt{1 - 4\,\theta_i (1-\theta_i)\left(1 - \exp(-w_i / RT)\right)}$$

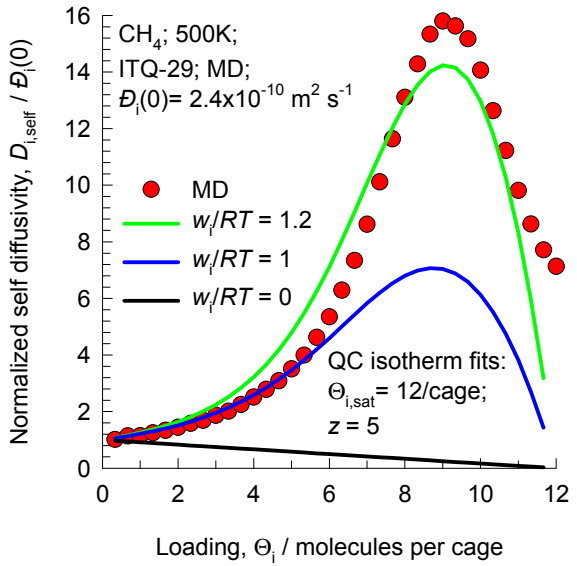

The model used to describe the concentration dependence of $Đ_i$ is described in detail in Krishna, R.; Paschek, D.; Baur, R. Modelling the occupancy dependence of diffusivities in zeolites, Microporous Mesoporous Mater. 2004, 76, 233-246.

ITQ-29, diffusivity of CH_4

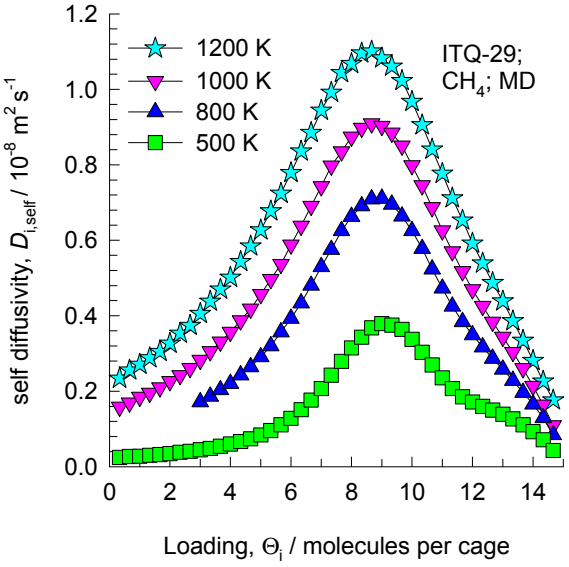

These data are for rigid frameworks

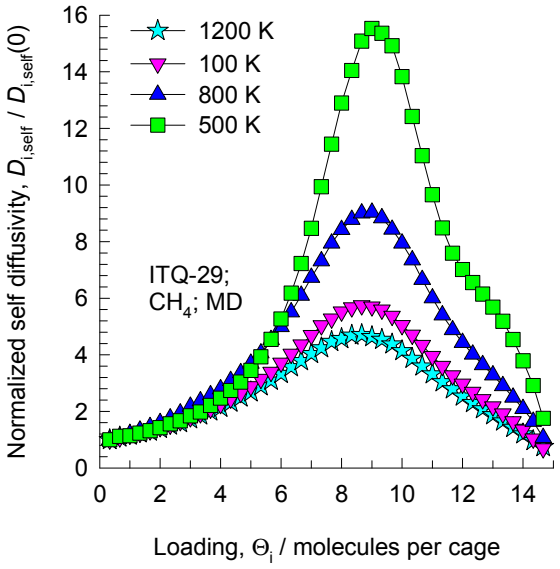

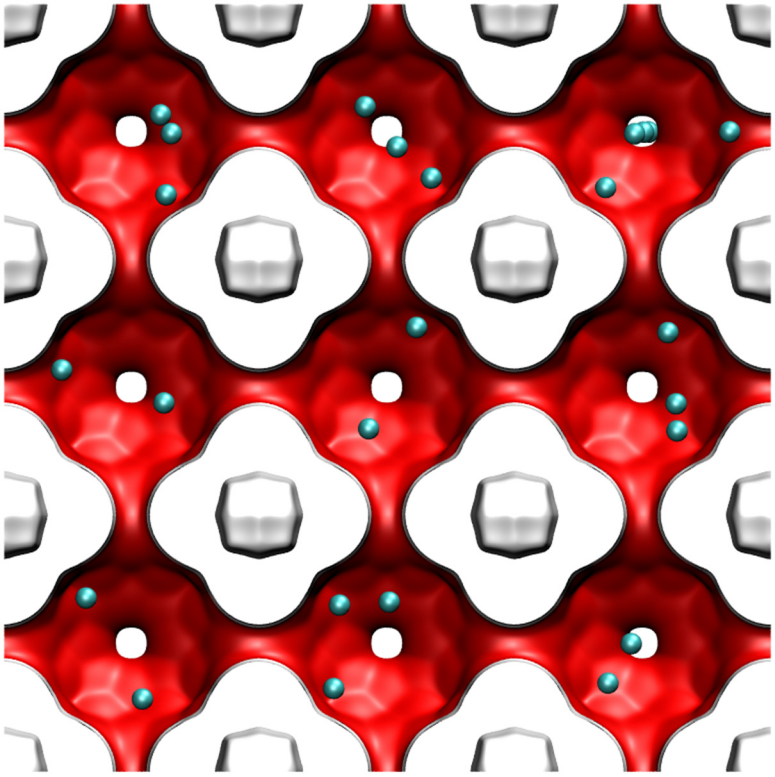

LTA-Si landscapes

This is a *hypothetical* structure constructed from dealuminized LTA-5A structure

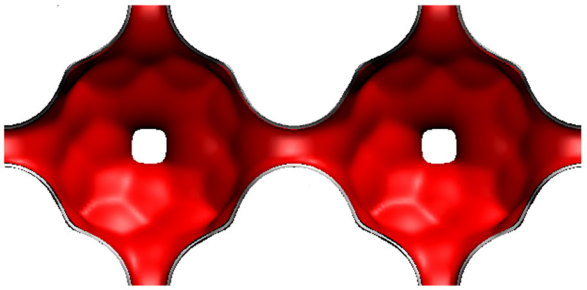

There are 8 cages per unit cell. The volume of one LTA cage is 743 Å^3, intermediate in size between a single cage of ZIF-8 (1168 Å^3) and of DDR (278 Å^3).

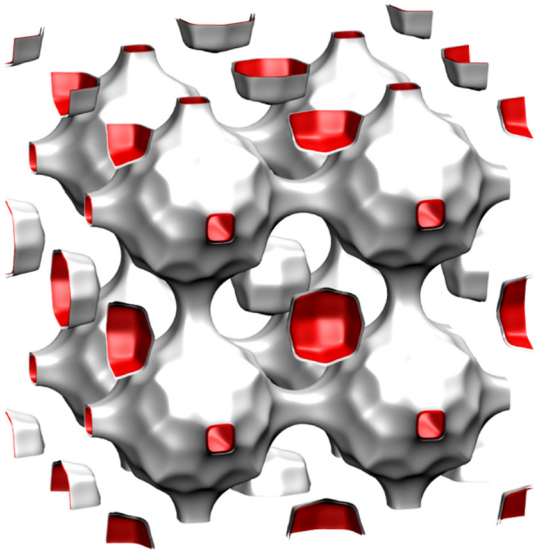

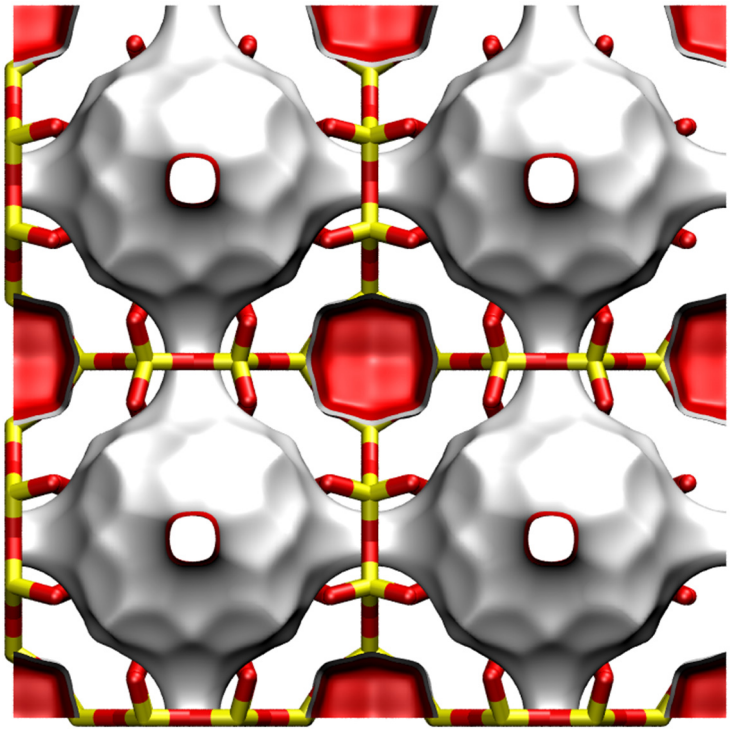

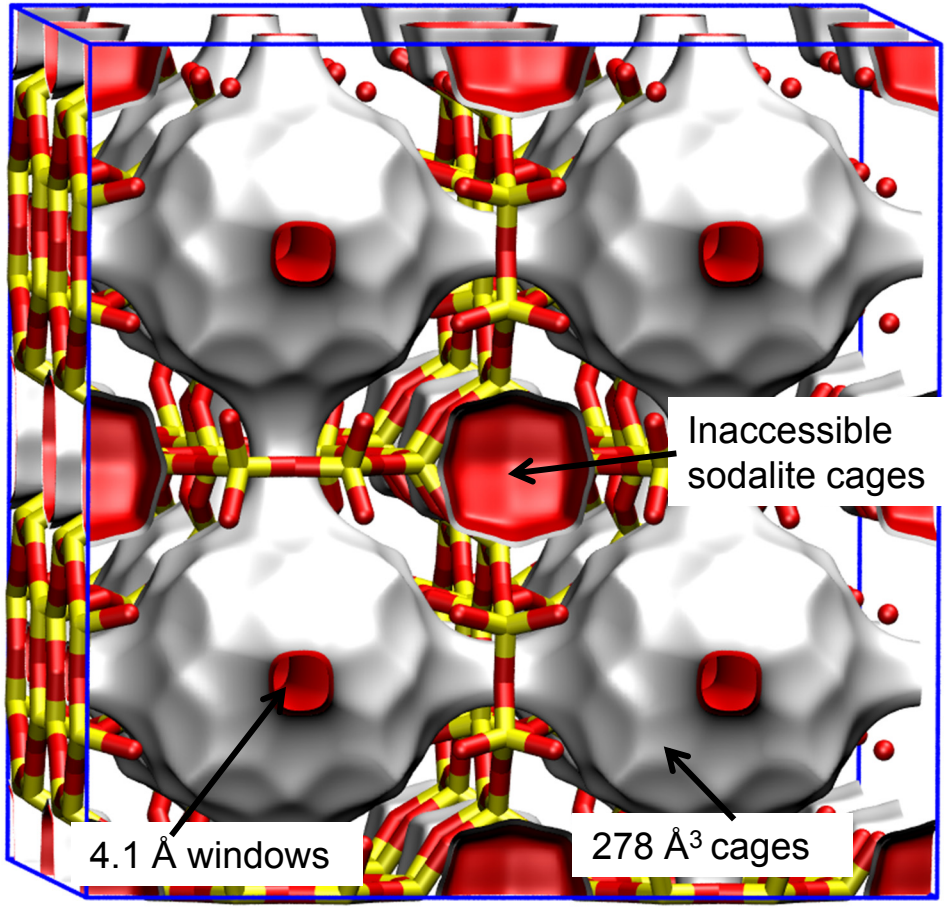

LTA-Si window and pore dimensions

8-ring window of LTA

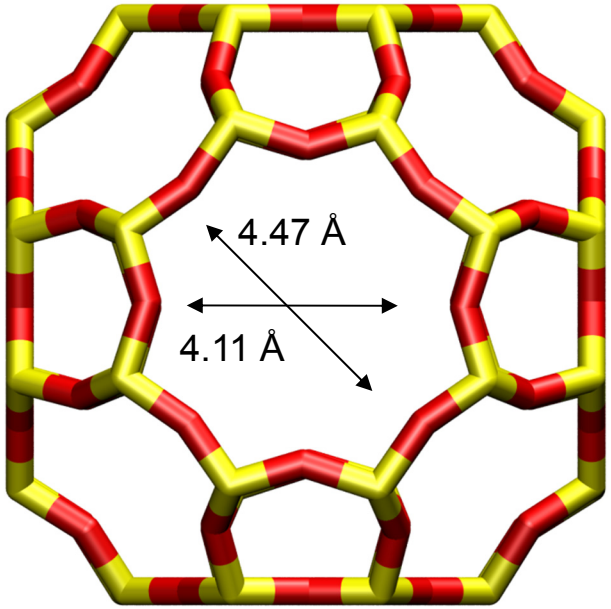

The window dimension calculated using the van der Waals diameter of framework atoms = 2.7 Å is indicated above by the arrows.

This plot of surface area versus pore dimension is determined using a combination of the DeLaunay triangulation method for pore dimension determination, and the procedure of Düren for determination of the surface area.

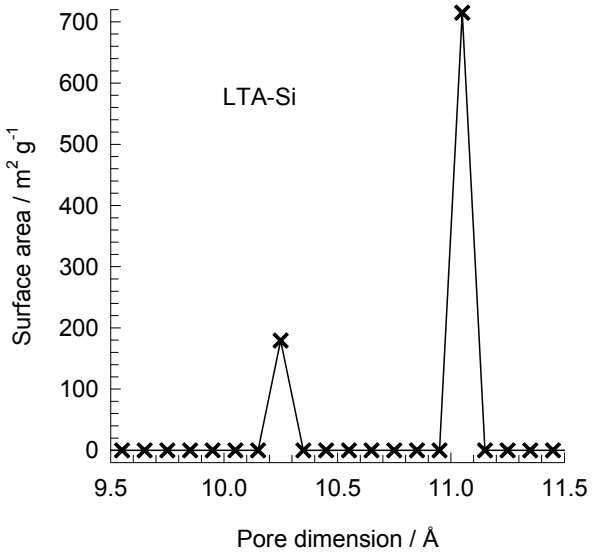

	LTA-Si
a /Å	24.61
b /Å	24.61
c /Å	24.61
Cell volume / Å^3	14905.1
conversion factor for [molec/uc] to [mol per kg Framework]	0.0867
conversion factor for [molec/uc] to [kmol/m^3]	0.2794
ρ [kg/m3]	1285.248
MW unit cell [g/mol(framework)]	11536.28
ϕ, fractional pore volume	0.399
open space / Å^3/uc	5944.4
Pore volume / cm^3/g	0.310
Surface area /m^2/g	896.0
DeLaunay diameter /Å	4.10

Electronic Supplementary Material (ESI) for Physical Chemistry Chemical Physics

LTA-Si CBMC simulations of isotherms, and isosteric heats of adsorption

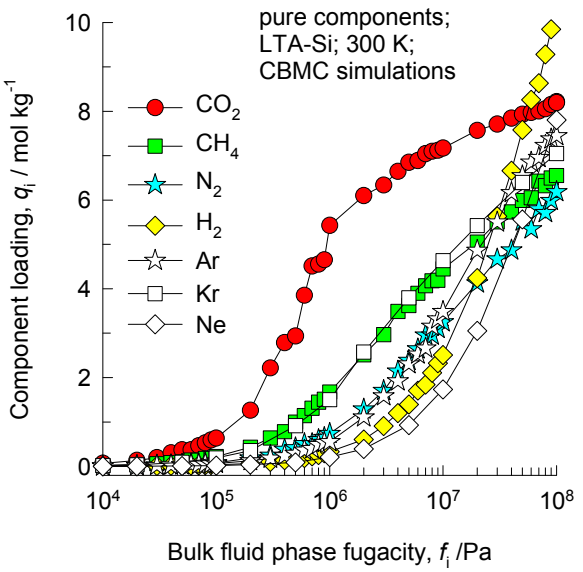

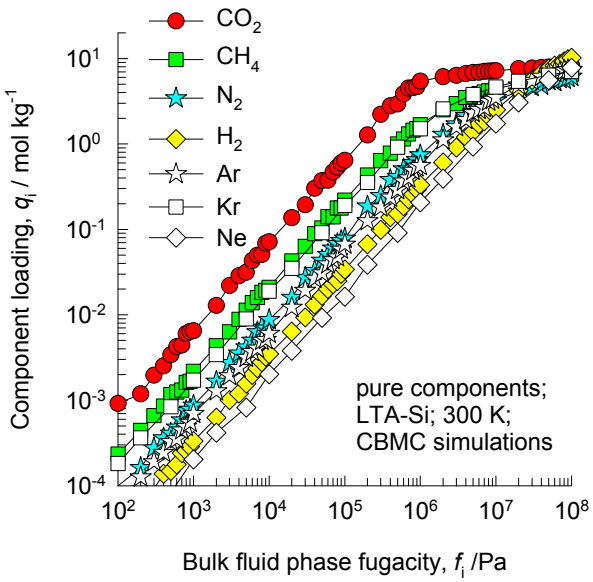

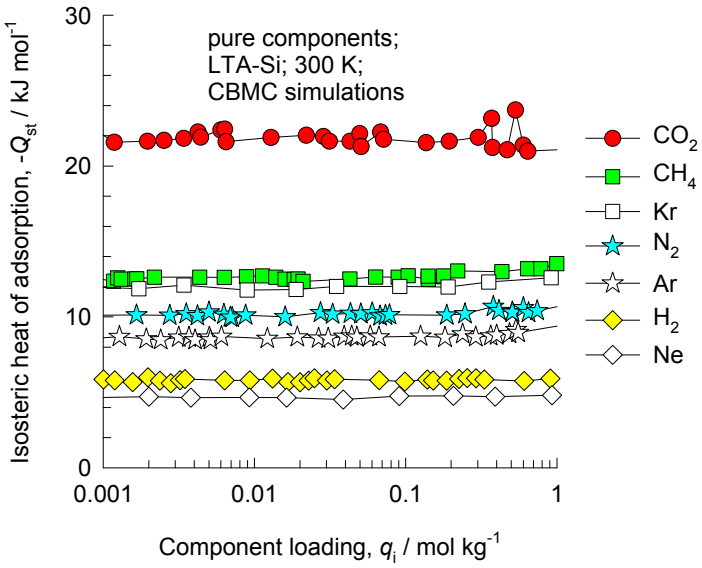

LTA-Si Modeling the loading dependence of CH_4 diffusivity

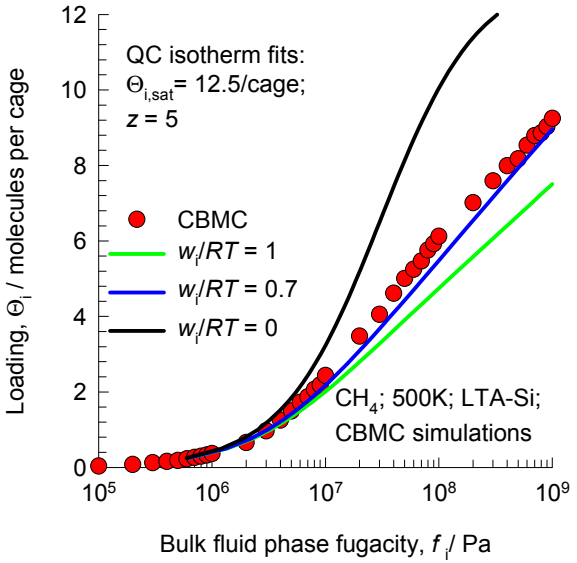

Quasi - Chemical isotherm

$$b_i f_i = \frac{\theta_i}{(1-\theta_i)}\left(\frac{2(1-\theta_i)}{\varsigma_i + 1 - 2\theta_i}\right)^z$$

$$\theta_i = c_i / c_{i,sat} = q_i / q_{i,sat} = \Theta_i / \Theta_{i,sat}$$

$$\varsigma_i = \sqrt{1 - 4\,\theta_i(1-\theta_i)(1-\exp(-w_i/RT))}$$

$$\Gamma_i = \frac{1}{(1-\theta_i)}\left(1 + \frac{z}{2}\frac{(1-\varsigma_i)}{\varsigma_i}\right)$$

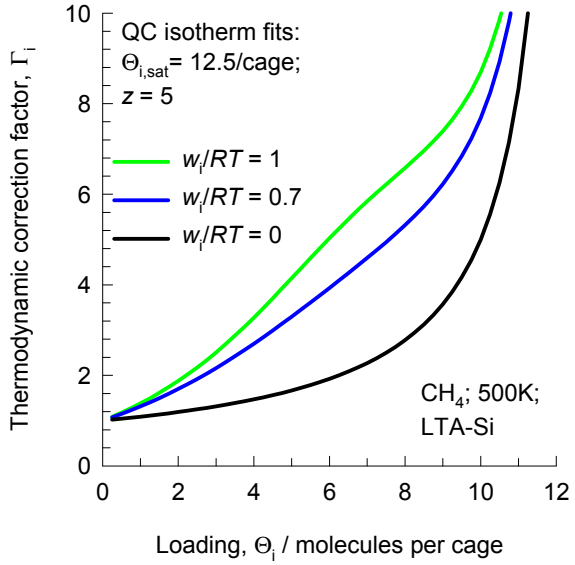

Krishna, Paschek and Baur (2004) model

$$Đ_i = Đ_i(0)\left(\frac{1+\varsigma_i}{2(1-\theta_i)}\right)^{-z}\left(1 + \frac{(\varsigma_i - 1 + 2\theta_i)\exp(w_i/RT)}{2(1-\theta_i)}\right)^{z-1}$$

$$\varsigma_i = \sqrt{1 - 4\,\theta_i(1-\theta_i)(1-\exp(-w_i/RT))}$$

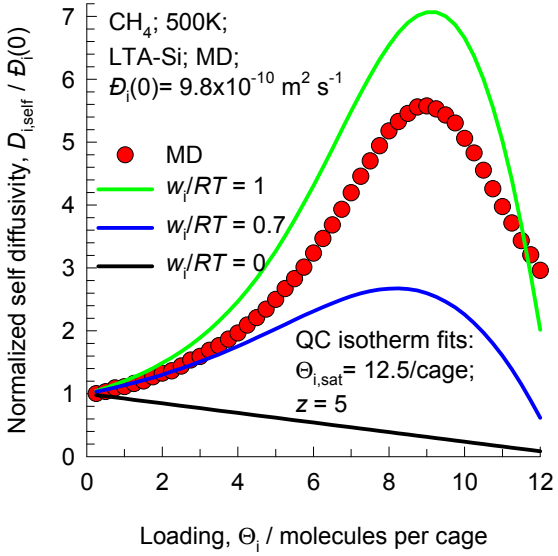

The model used to describe the concentration dependence of $Đ_i$ is described in detail in Krishna, R.; Paschek, D.; Baur, R. Modelling the occupancy dependence of diffusivities in zeolites, Microporous Mesoporous Mater. 2004, 76, 233-246.

LTA-Si, self-diffusivities of various guest molecules

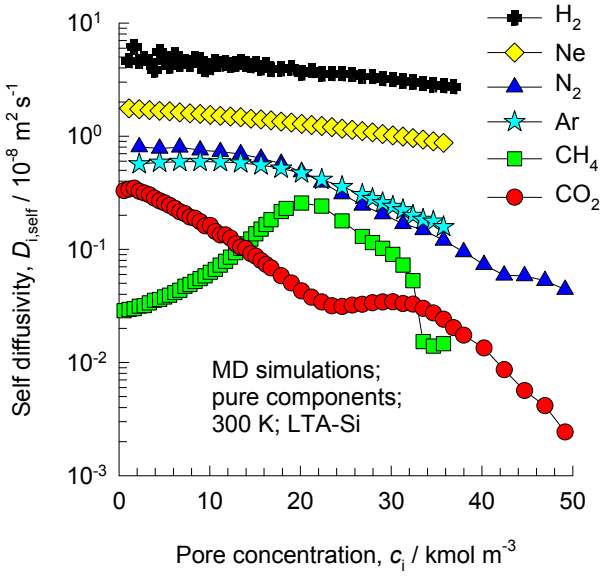

These data are for rigid frameworks

LTA-Si, self-diffusivity of CH_4

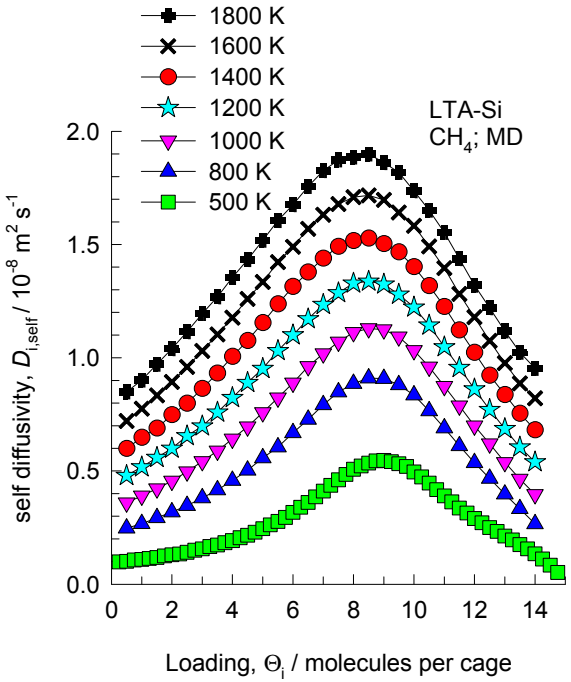

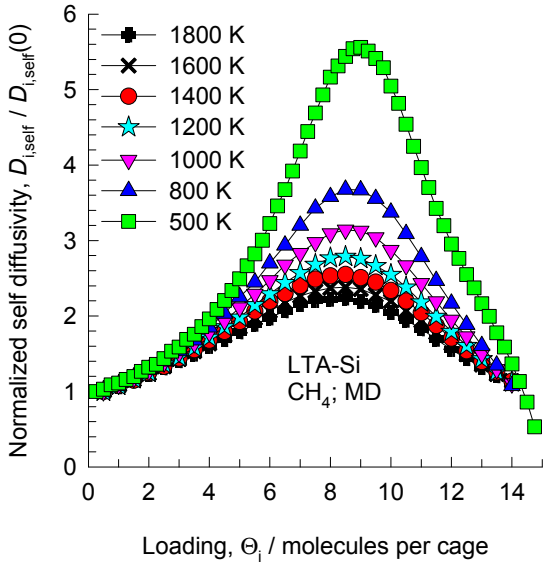

These data are for rigid frameworks

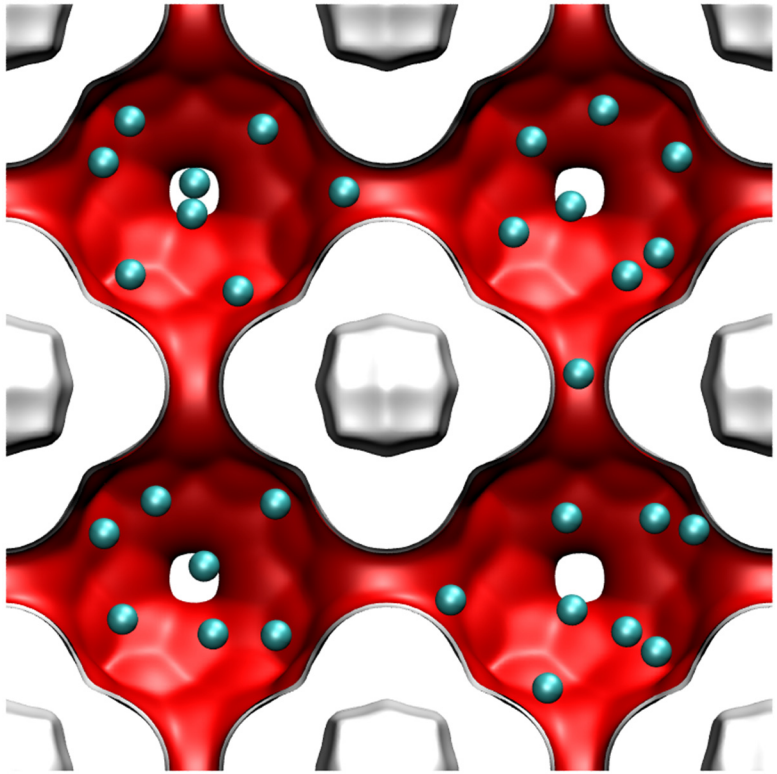

Electronic Supplementary Material (ESI) for Physical Chemistry Chemical Physics

LTA-4A

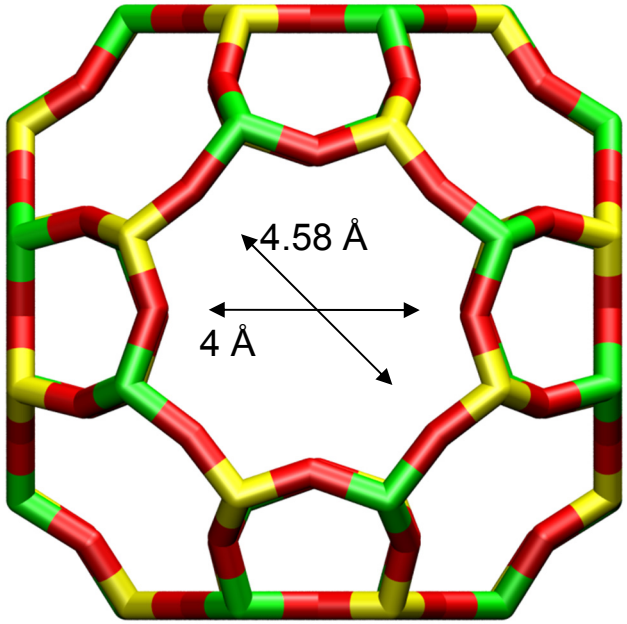

LTA-4A

	LTA-4A
a /Å	24.555
b /Å	24.555
c /Å	24.555
Cell volume / Å^3	14805.39
conversion factor for [molec/uc] to [mol per kg Framework]	0.0733
conversion factor for [molec/uc] to [kmol/m^3]	0.2991
ρ [kg/m3] (with cations)	1529.55
MW unit cell [g/mol(framework+cations)]	13637.27
ϕ, fractional pore volume	0.375
open space / Å^3/uc	5552.0
Pore volume / cm^3/g	0.245
Surface area /m^2/g	
DeLaunay diameter /Å	4.00

The window dimension calculated using the van der Waals diameter of framework atoms = 2.7 Å is indicated above by the arrow.

Note that the Na^+ ions partially block the windows and therefore the diffusivities in LTA-4A are significantly lower than that for LTA Si. These cannot be determined from MD.

Electronic Supplementary Material (ESI) for Physical Chemistry Chemical Physics

LTA-4A

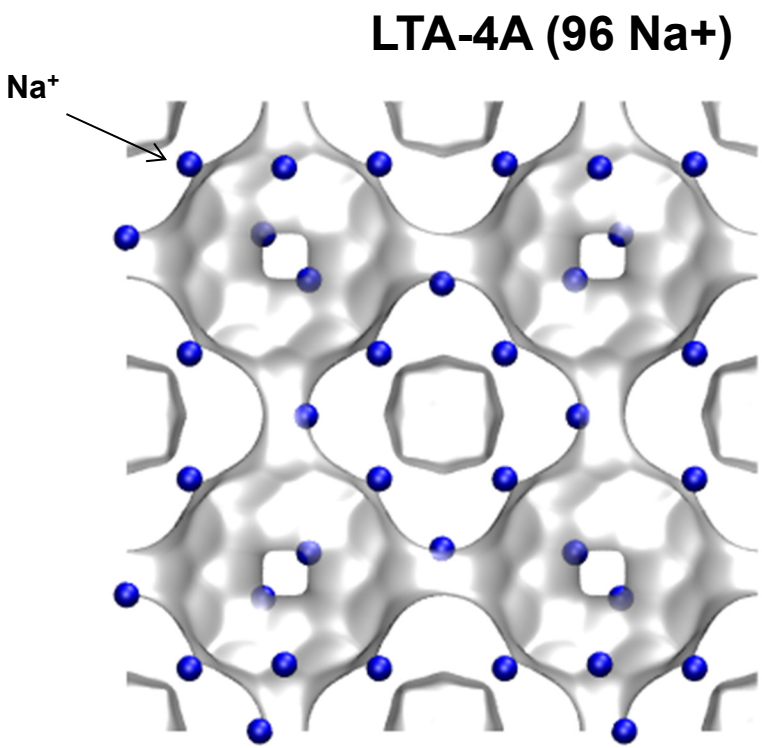

LTA-4A: Transient uptake of C_2H_6

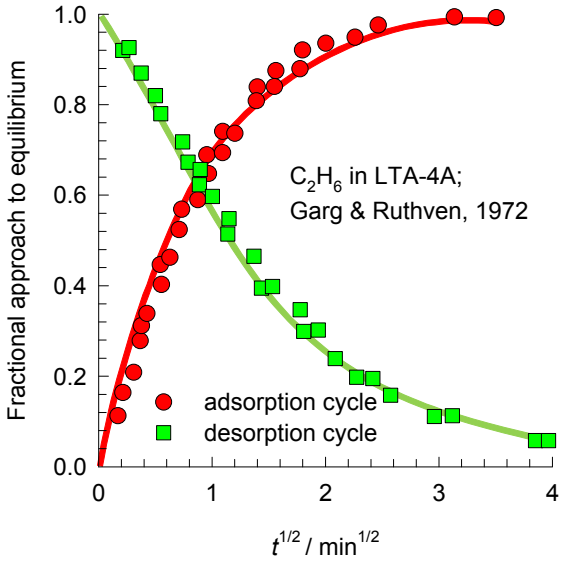

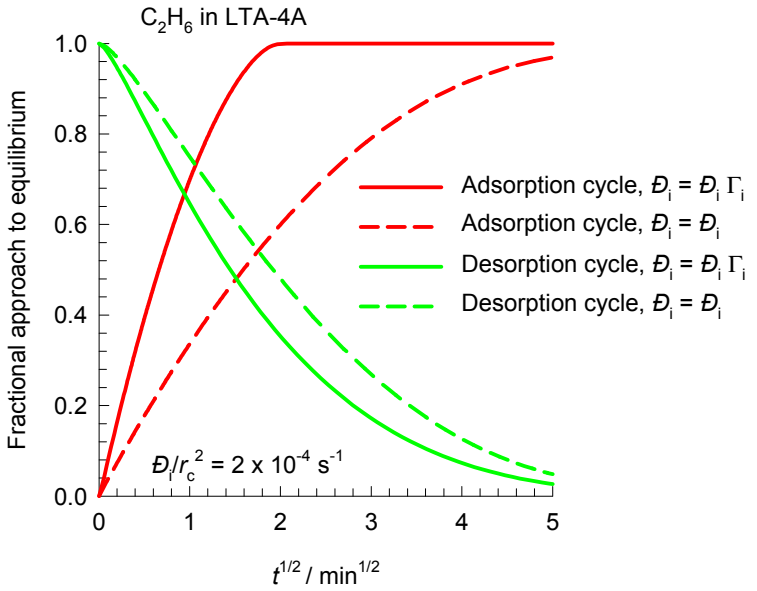

The data are re-plotted using the information contained in
Garg, D. R.; Ruthven, D. M. Effect of the concentration dependence of diffusivity on zeolitic sorption curves, Chem. Eng. Sci. 1972, 27, 417-423. .

The continuous solid lines are simulations including the thermodynamic correction factor, Γ_i.
These simulations capture the asymmetry in the adsorption and desorption cycles.

The dashed lines are simulations in which $\Gamma_i = 1$.
These simulations anticipate that the adsorption and desorption cycles are symmetric.

The simulations assume a constant, loading independent M-S diffusivity, $Đ_i$. We take $Đ_i/r_c^2 = 0.0002$ s^{-1} where r_c is the crystal radius.

LTA-4A: Transient uptake of N_2 and CH_4

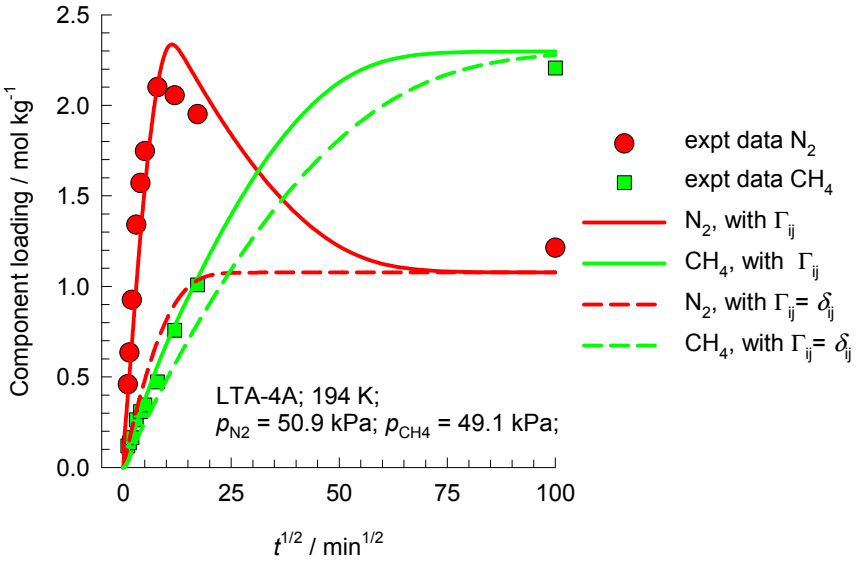

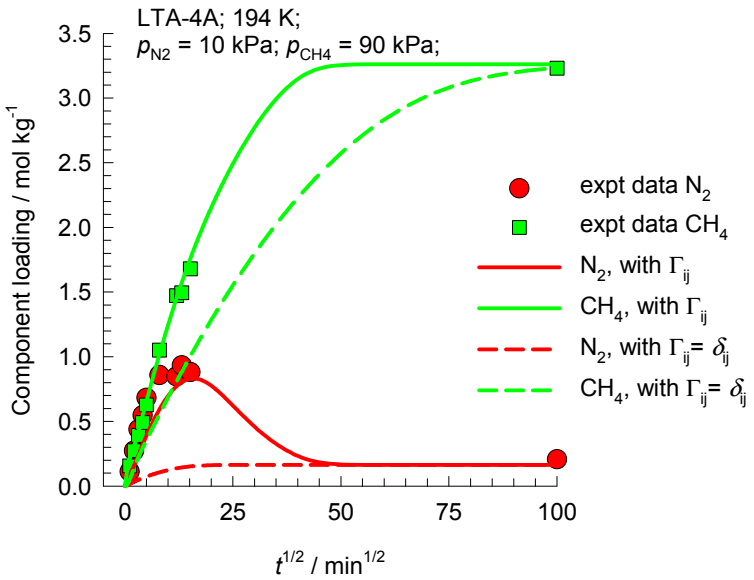

The experimental data are re-plotted using the information contained in
Habgood, H. W. The kinetics of molecular sieve action. Sorption of nitrogen-methane mixtures by Linde molecular sieve 4A, Canad. J. Chem. 1958, 36, 1384-1397.

In these simulations, both the M-S diffusivities are assumed to be independent of loading. The overshoot in N_2 is not, therefore, a result of the loading dependence of its M-S diffusivity.

The overshoot in the N_2 uptake is a direct consequence of thermodynamic coupling caused by the off-diagonal elements of

$$\begin{bmatrix} \Gamma_{11} & \Gamma_{12} \\ \Gamma_{21} & \Gamma_{21} \end{bmatrix} \quad \text{where} \quad \Gamma_{ij} = \frac{q_i}{f_i}\frac{\partial f_i}{\partial q_j}$$

This has been demonstrated by
Krishna, R.; Baur, R. Modelling issues in zeolite based separation processes, Sep. Purif. Technol. 2003, 33, 213-254.

If the thermodynamic coupling is ignored, i.e. we assume $\Gamma_i = \delta_{ij}$; Kronecker delta $\begin{bmatrix} \Gamma_{11} & \Gamma_{12} \\ \Gamma_{21} & \Gamma_{21} \end{bmatrix} = \begin{bmatrix} 1 & 0 \\ 0 & 1 \end{bmatrix}$

the N_2 overshoot disappears.

LTA-4A: Transient uptake of CH_4 and C_2H_6

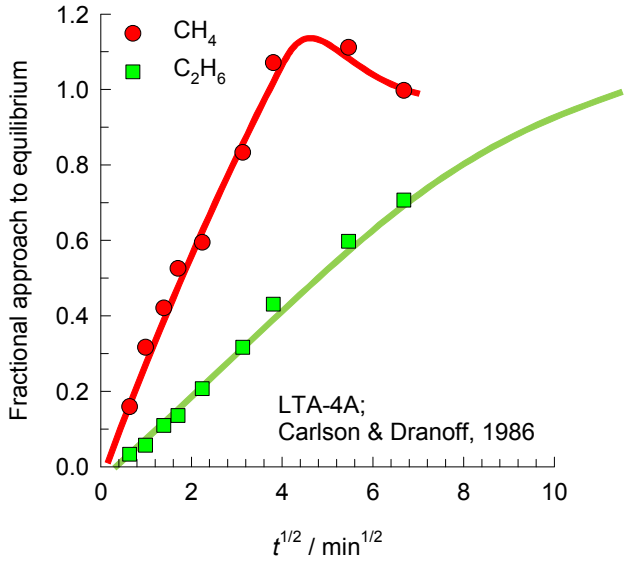

The data are re-plotted using the information contained in
Carlson, N. W.; Dranoff, J. S. Competitive adsorption of methane and ethane on 4A zeolite. Fundamentals of Adsorption; Edited by A.I. Liapis, AIChE: New York, 1986.

In these simulations, both the M-S diffusivities are assumed to be independent of loading. The overshoot in CH_4 is not, therefore, a result of the loading dependence of its M-S diffusivity.

The overshoot in the CH_4 uptake is a direct consequence of thermodynamic coupling caused by the off-diagonal elements of $\begin{bmatrix} \Gamma_{11} & \Gamma_{12} \\ \Gamma_{21} & \Gamma_{21} \end{bmatrix}$ where $\Gamma_{ij} = \frac{q_i}{f_i}\frac{\partial f_i}{\partial q_j}$

This has been demonstrated by
Krishna, R. Diffusion of binary mixtures in microporous materials: Overshoot and roll-up phenomena, Int. Commun. Heat Mass Transf. 2000, 27, 893-902.

If the thermodynamic coupling is ignored, i.e. we assume $\begin{bmatrix} \Gamma_{11} & \Gamma_{12} \\ \Gamma_{21} & \Gamma_{21} \end{bmatrix} = \begin{bmatrix} 1 & 0 \\ 0 & 1 \end{bmatrix}$

the CH_4 overshoot disappears.

LTA-4A vs LTA-5A diffusivities of CO_2

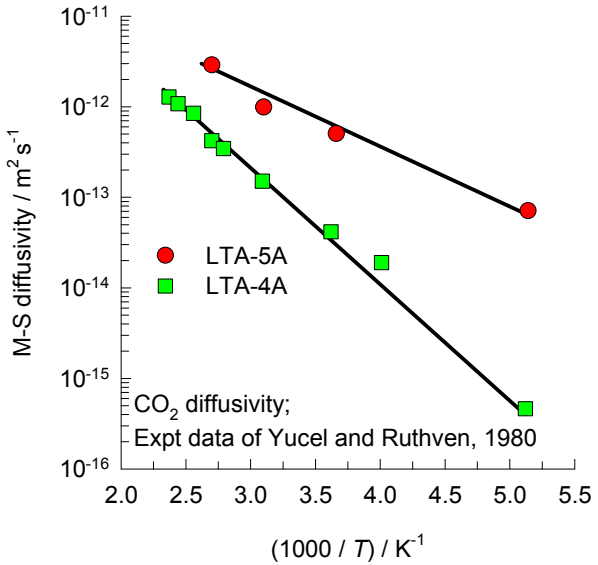

The experimental data are from
Yucel, H.; Ruthven, D.M. Diffusion of CO_2 in 4A and 5A zeolite crystals. Journal of Colloid and Interface Science 1980, 74, 186-195.

Note that no MD simulation results are presented for LTA-4A because the diffusivities are too low to be determined accurately.

LTA-5A

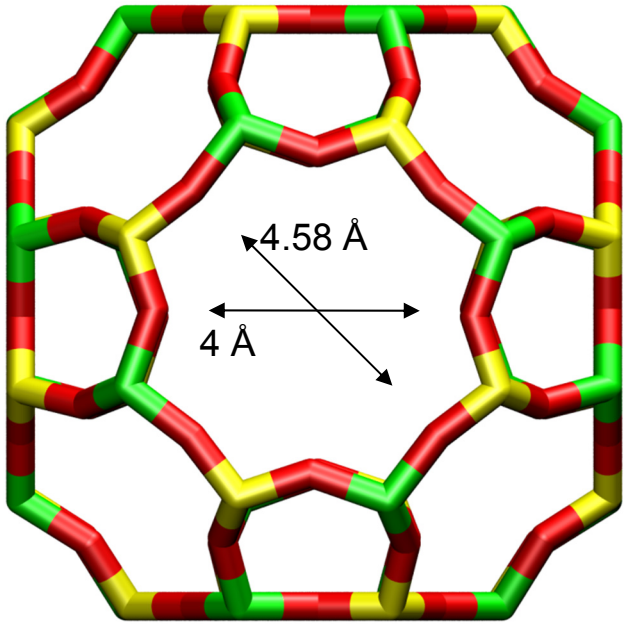

LTA-5A

The window dimension calculated using the van der Waals diameter of framework atoms = 2.7 Å is indicated above by the arrow.

	LTA-5A
a /Å	24.555
b /Å	24.555
c /Å	24.555
Cell volume / Å^3	14805.39
conversion factor for [molec/uc] to [mol per kg Framework]	0.0744
conversion factor for [molec/uc] to [kmol/m^3]	0.2955
ρ [kg/m3] (with cations)	1508.376
MW unit cell [g/mol(framework+cations)]	13448.48
ϕ, fractional pore volume	0.380
open space / Å^3/uc	5620.4
Pore volume / cm^3/g	0.252
Surface area /m^2/g	
DeLaunay diameter /Å	4.00

Electronic Supplementary Material (ESI) for Physical Chemistry Chemical Physics

LTA-5A

LTA-5A (32 Na+, 32 Ca++)

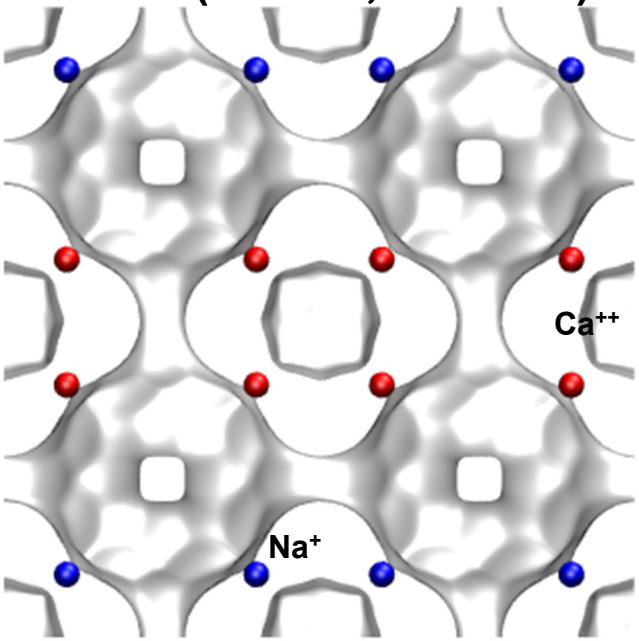

LTA-5A Modeling the loading dependence of CH_4 diffusivity at 300 K

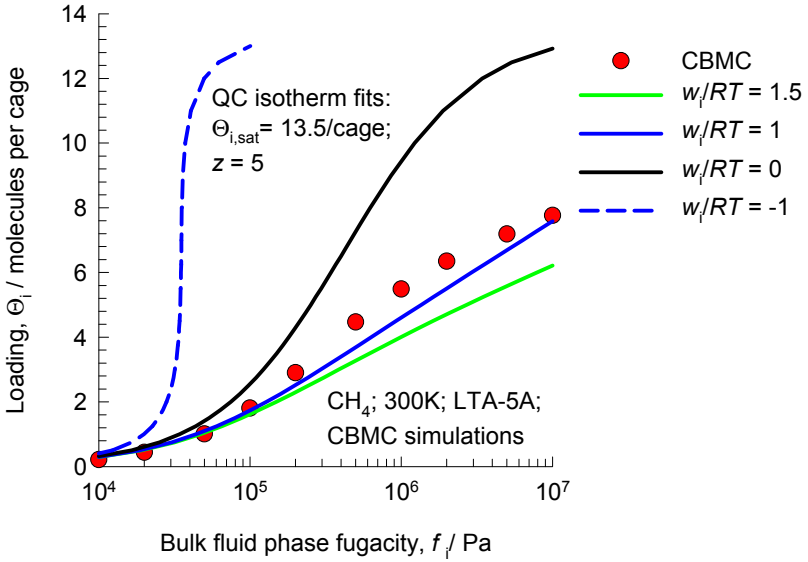

Quasi - Chemical isotherm

$$b_i f_i = \frac{\theta_i}{(1-\theta_i)}\left(\frac{2\,(1-\theta_i)}{\varsigma_i + 1 - 2\theta_i}\right)^z$$

$$\theta_i = c_i / c_{i,sat} = q_i / q_{i,sat} = \Theta_i / \Theta_{i,sat}$$

$$\varsigma_i = \sqrt{1 - 4\,\theta_i (1-\theta_i)\left(1 - \exp(-w_i/RT)\right)}$$

$$\Gamma_i = \frac{1}{(1-\theta_i)}\left(1 + \frac{z}{2}\frac{(1-\varsigma_i)}{\varsigma_i}\right)$$

Krishna, Paschek and Baur (2004) model

$$Đ_i = Đ_i(0)\left(\frac{1+\varsigma_i}{2\,(1-\theta_i)}\right)^{-z}\left(1 + \frac{(\varsigma_i - 1 + 2\theta_i)\exp(w_i/RT)}{2\,(1-\theta_i)}\right)^z$$

$$\varsigma_i = \sqrt{1 - 4\,\theta_i (1-\theta_i)\left(1 - \exp(-w_i/RT)\right)}$$

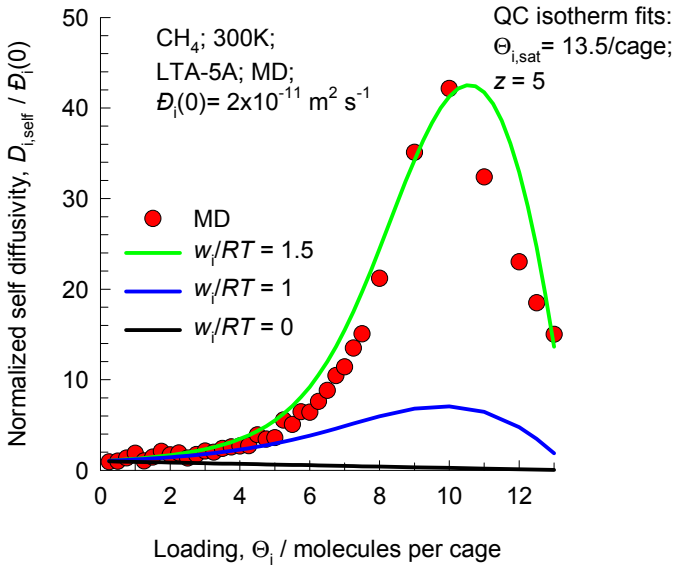

The model used to describe the concentration dependence of $Đ_i$ is described in detail in Krishna, R.; Paschek, D.; Baur, R. Modelling the occupancy dependence of diffusivities in zeolites, Microporous Mesoporous Mater. 2004, 76, 233-246.

LTA-5A Modeling the loading dependence of CH_4 diffusivity at 500 K

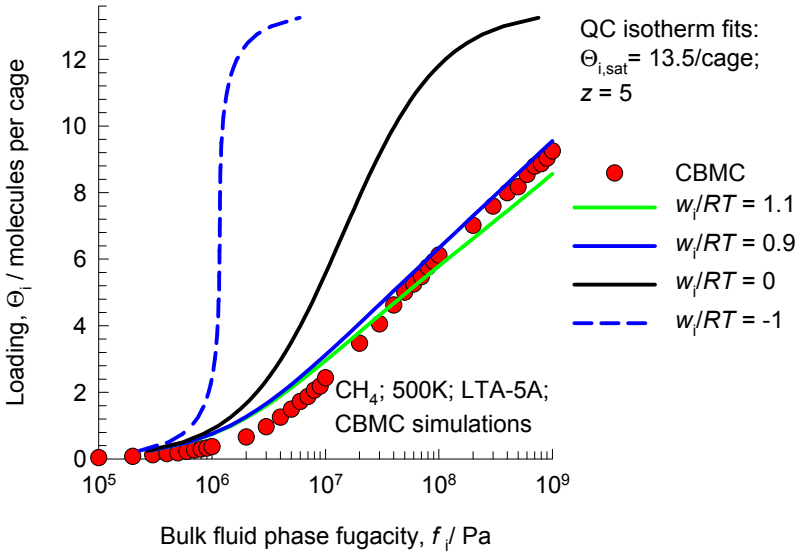

Quasi - Chemical isotherm

$$b_i f_i = \frac{\theta_i}{(1-\theta_i)}\left(\frac{2\,(1-\theta_i)}{\varsigma_i + 1 - 2\theta_i}\right)^z$$

$$\vartheta_i = c_i / c_{i,sat} = q_i / q_{i,sat} = \Theta_i / \Theta_{i,sat}$$

$$\varsigma_i = \sqrt{1 - 4\,\theta_i(1-\theta_i)\left(1-\exp(-w_i/RT)\right)}$$

$$\Gamma_i = \frac{1}{(1-\theta_i)}\left(1 + \frac{z}{2}\frac{(1-\varsigma_i)}{\varsigma_i}\right)$$

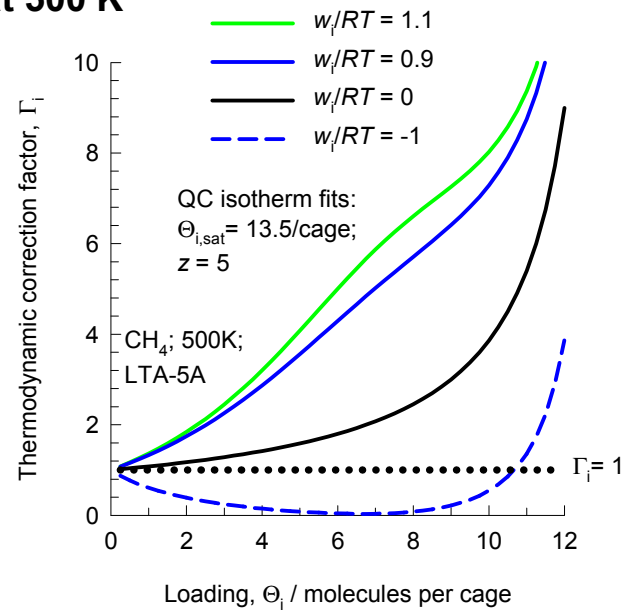

Krishna, Paschek and Baur (2004) model

$$Đ_i = Đ_i(0)\left(\frac{1+\varsigma_i}{2\,(1-\theta_i)}\right)^{-z}\left(1 + \frac{(\varsigma_i - 1 + 2\theta_i)\exp(w_i/RT)}{2\,(1-\theta_i)}\right)^{z-1}$$

$$\varsigma_i = \sqrt{1 - 4\,\theta_i(1-\theta_i)\left(1-\exp(-w_i/RT)\right)}$$

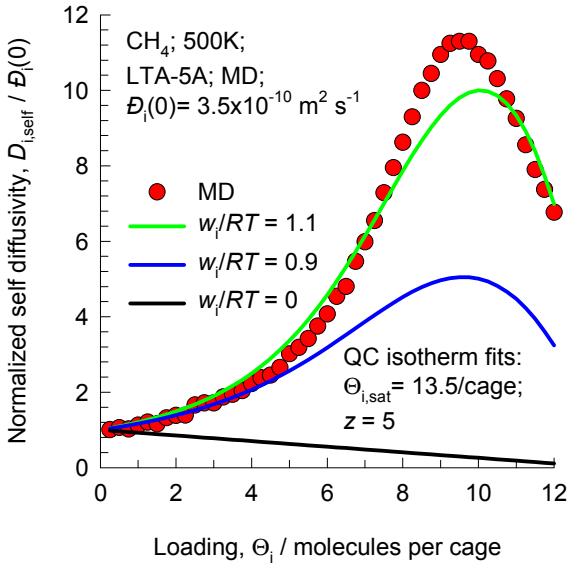

The model used to describe the concentration dependence of $Đ_i$ is described in detail in Krishna, R.; Paschek, D.; Baur, R. Modelling the occupancy dependence of diffusivities in zeolites, Microporous Mesoporous Mater. 2004, 76, 233-246.

LTA-5A, diffusivity of CH_4

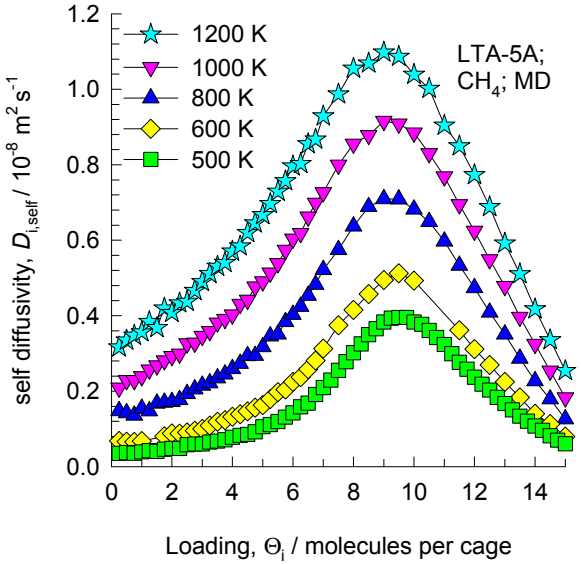

These data are for rigid frameworks

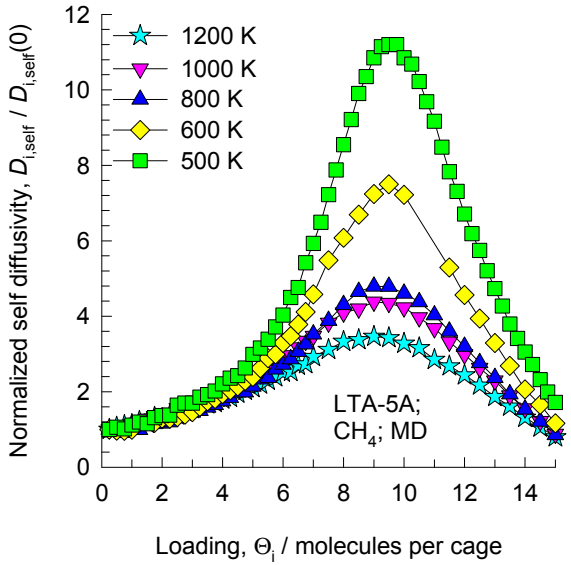

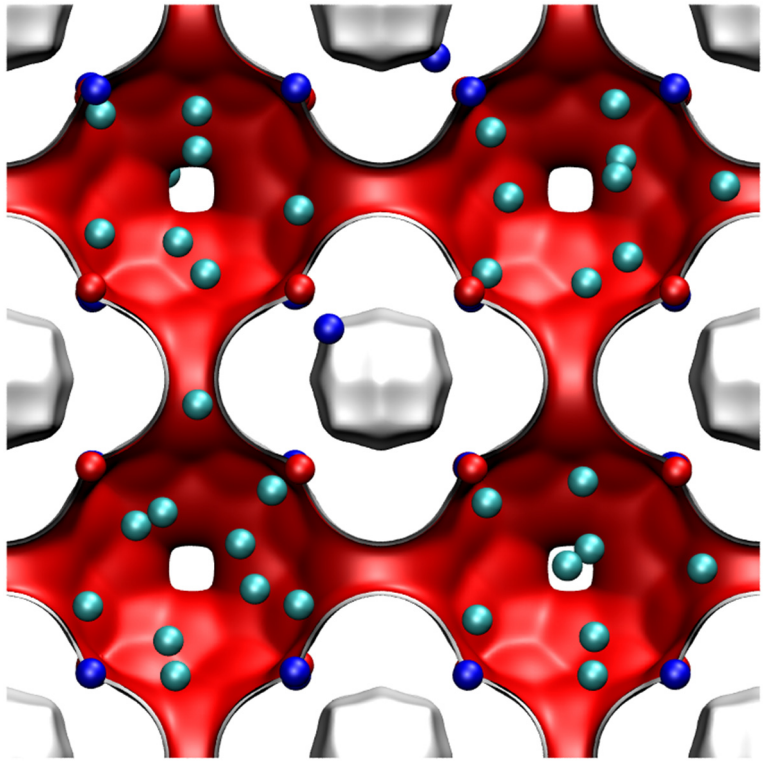

LTA-5A Modeling the MR experiments of Caro

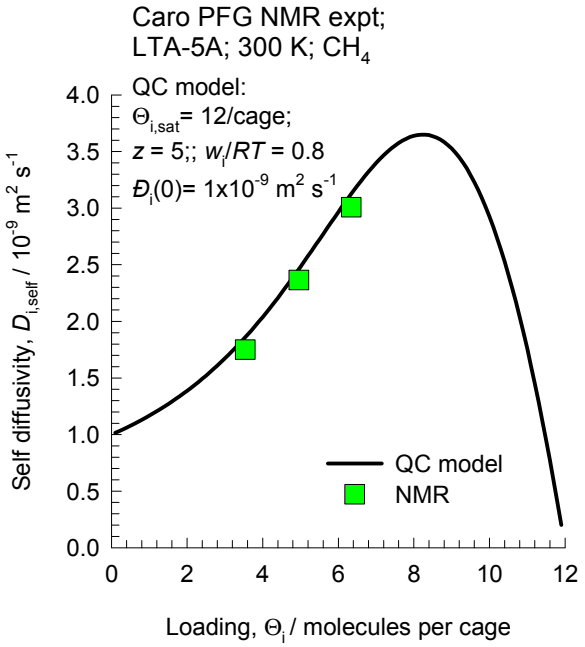

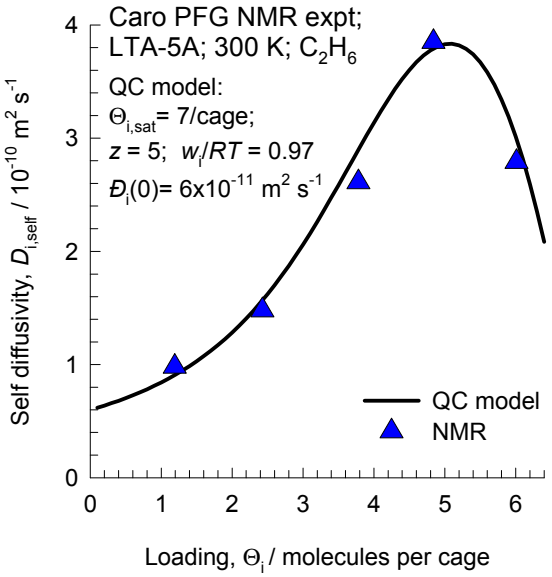

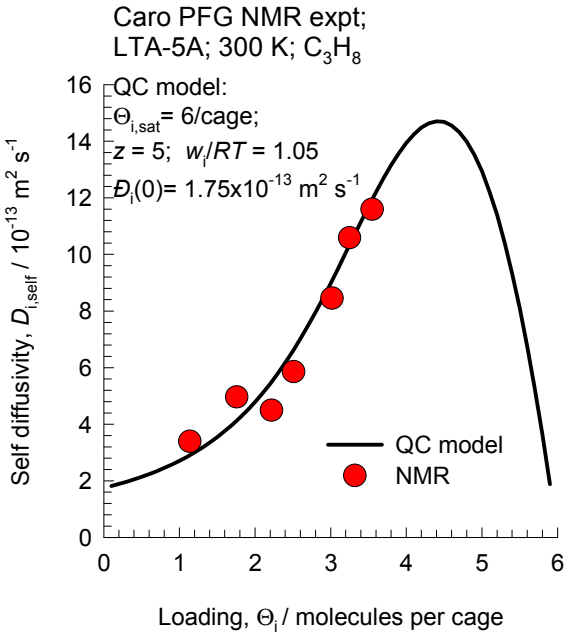

The experimental data are from
Caro, J.; Bülow, M.; Schirmer, W.; Kärger, J.; Heink, W.; Pfeifer, H. Microdynamics of methane, ethane and propane in ZSM-5 type zeolites. Journal of the Chemical Society, Faraday Transactions 1985, 81, 2541-2550.

Electronic Supplementary Material (ESI) for Physical Chemistry Chemical Physics

SOD-Si pore landscape

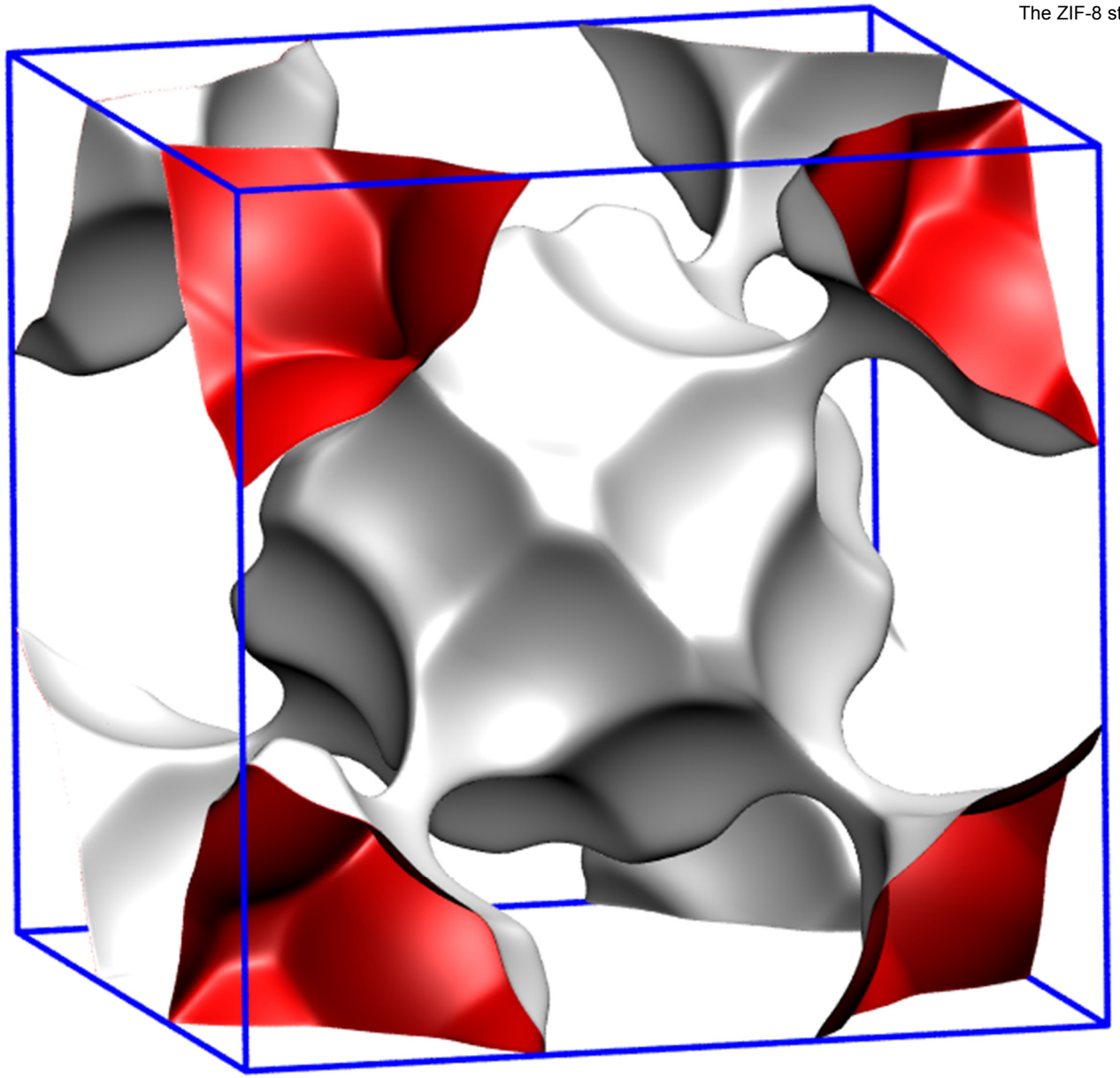

The ZIF-8 structure is analogous to that of SOD.

There are 2 cages per unit cell. The volume of one SOD cage is 84.8 Å^3, significantly smaller than that of ZIF-8 (1168 Å^3), its structural analog.

Structural information from: C. Baerlocher, L.B. McCusker, Database of Zeolite Structures, International Zeolite Association, http://www.iza-structure.org/databases/

Electronic Supplementary Material (ESI) for Physical Chemistry Chemical Physics

SOD-Si dimensions

	SOD-Si
a /Å	8.89
b /Å	8.89
c /Å	8.89
Cell volume / Å^3	702.5954
conversion factor for [molec/uc] to [mol per kg Framework]	1.3869
conversion factor for [molec/uc] to [kmol/m^3]	9.7908
ρ [kg/m3]	1704.106
MW unit cell [g/mol(framework)]	721.0176
ϕ, fractional pore volume	0.241
open space / Å^3/uc	169.6
Pore volume / cm^3/g	0.142
Surface area /m^2/g	
DeLaunay diameter /Å	2.47

Electronic Supplementary Material (ESI) for Physical Chemistry Chemical Physics

TSC landscape

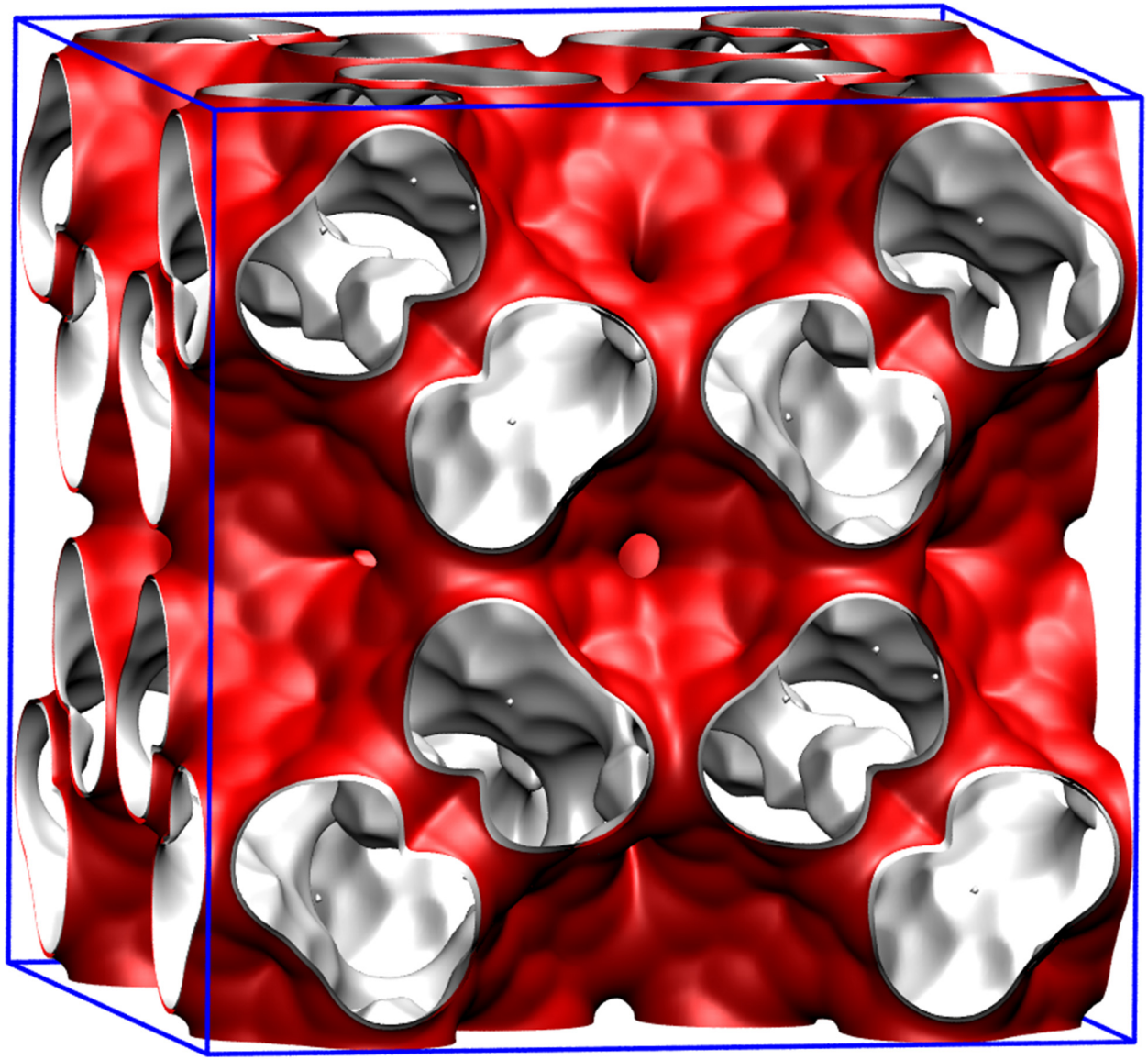

Unit cell of TSC

Structural information from: C. Baerlocher, L.B. McCusker, Database of Zeolite Structures, International Zeolite Association, http://www.iza-structure.org/databases/

Electronic Supplementary Material (ESI) for Physical Chemistry Chemical Physics

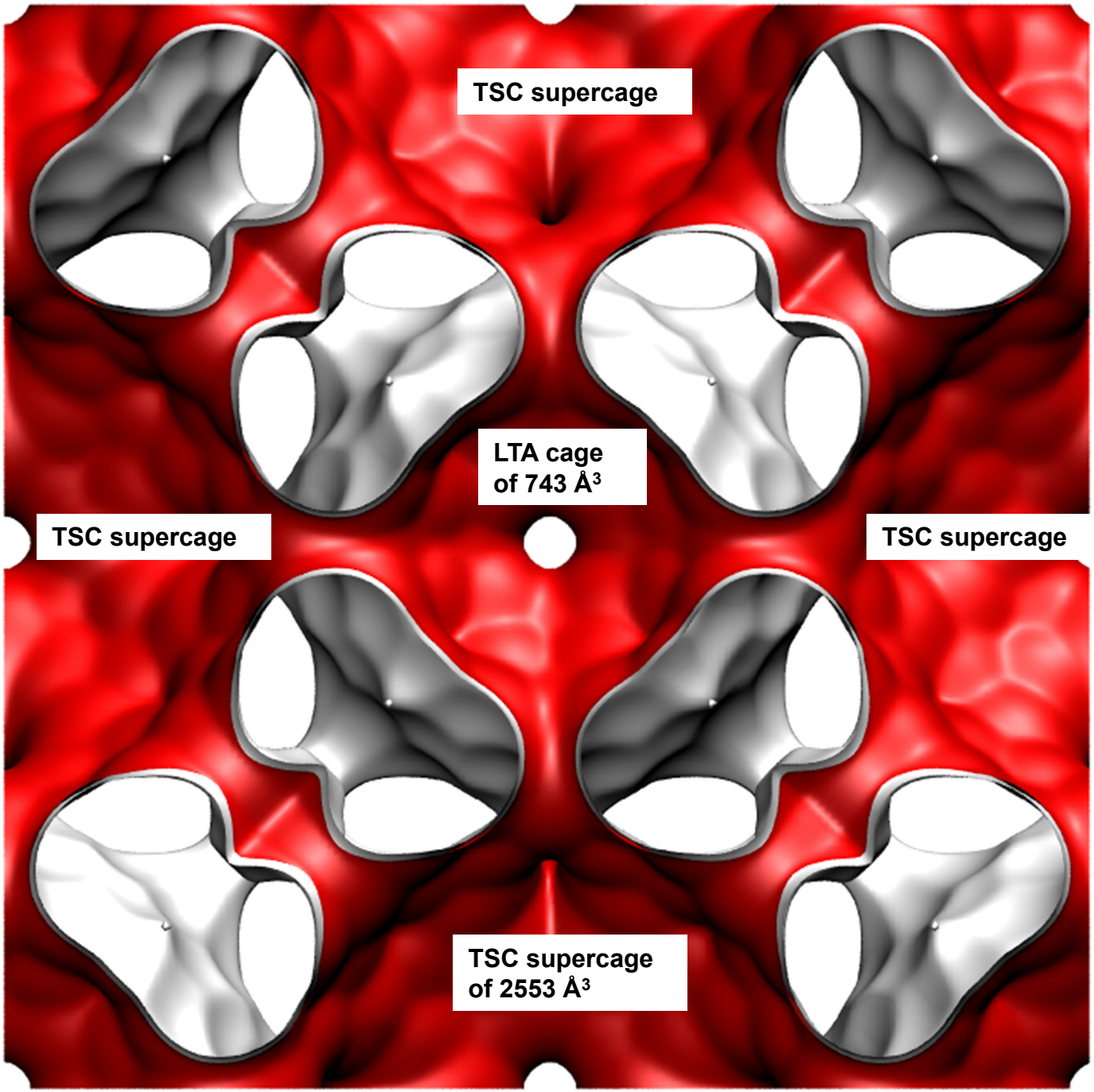

8-ring windows of two sizes:
4.2x4.2 Å along [100]
3.1x5.6 Å along [110]

Front plane of unit cell of TSC

Electronic Supplementary Material (ESI) for Physical Chemistry Chemical Physics

TSC window and pore dimensions

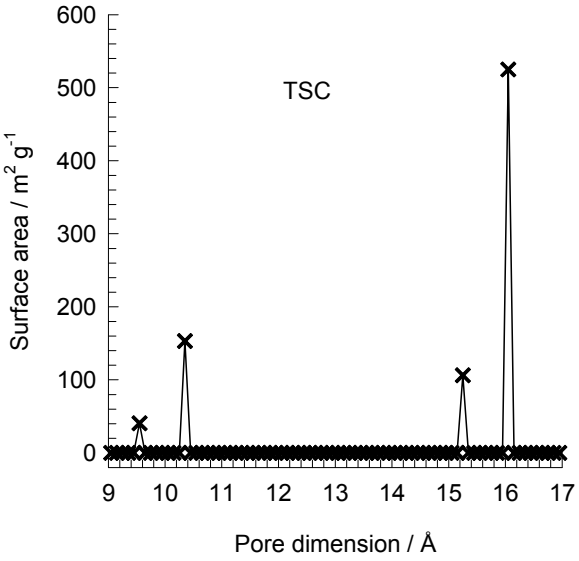

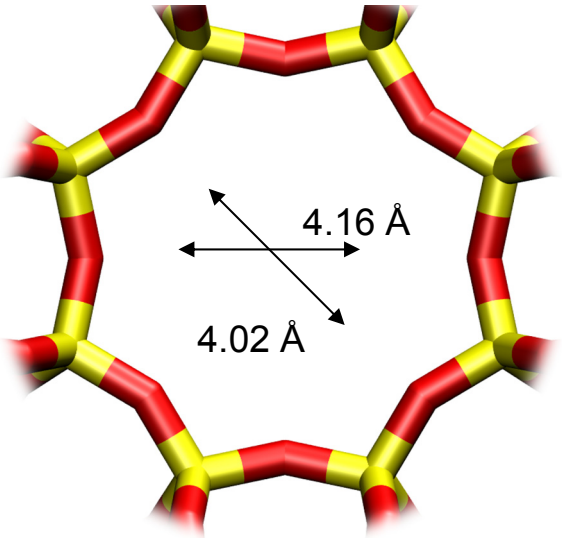

TSC
(supercage - cage)

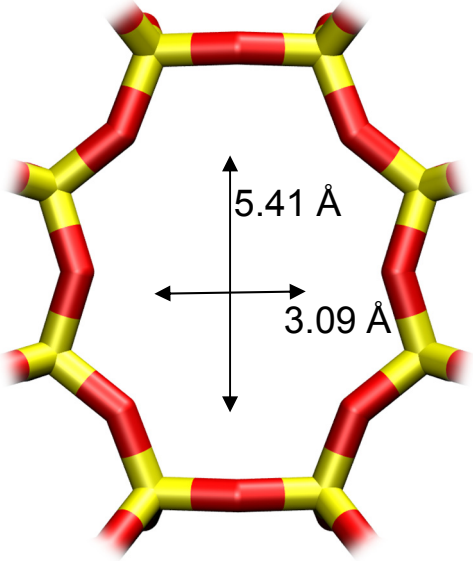

TSC
(supercage - pocket)

	TSC
a /Å	30.742
b /Å	30.742
c /Å	30.742
Cell volume / Å^3	29053.36
conversion factor for [molec/uc] to [mol per kg Framework]	0.0433
conversion factor for [molec/uc] to [kmol/m^3]	0.1260
ρ [kg/m3]	1318.729
MW unit cell [g/mol(framework)]	23072.56
ϕ, fractional pore volume	0.454
open space / Å^3/uc	13182.6
Pore volume / cm^3/g	0.344
Surface area /m^2/g	829.0
DeLaunay diameter /Å	4.02

The window dimension calculated using the van der Waals diameter of framework atoms = 2.7 Å are indicated above by the arrows. It is likely that the pockets are inaccessible due to the narrow constriction of 3.092 Å. Another point to note is that the dimensions provided in the IZA website do not appear to be correct for the window on the left.

Electronic Supplementary Material (ESI) for Physical Chemistry Chemical Physics

TSC MD simulations of unary self- diffusivities

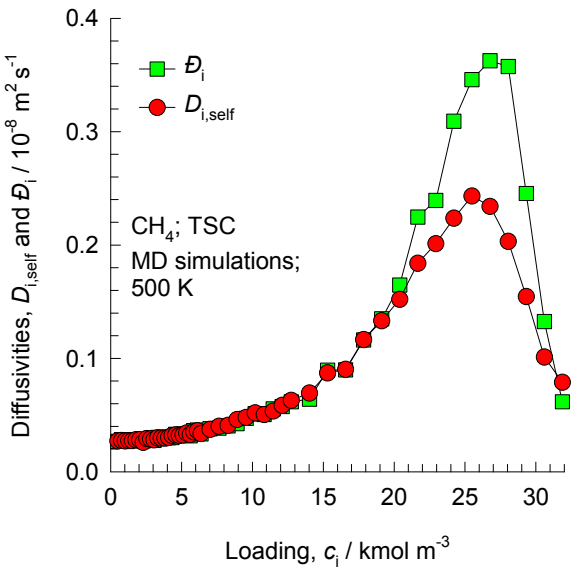

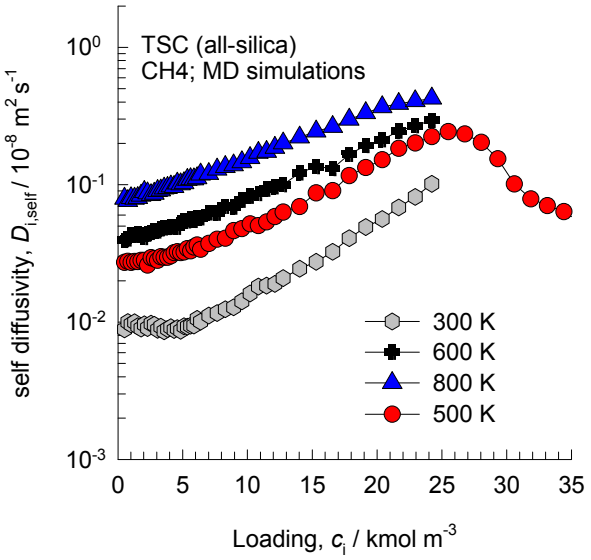

Comparing CH_4 diffusivities in 8-ring zeolites

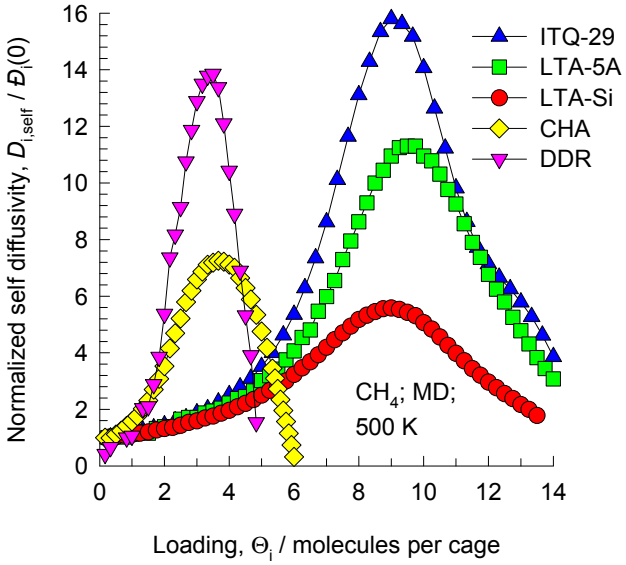

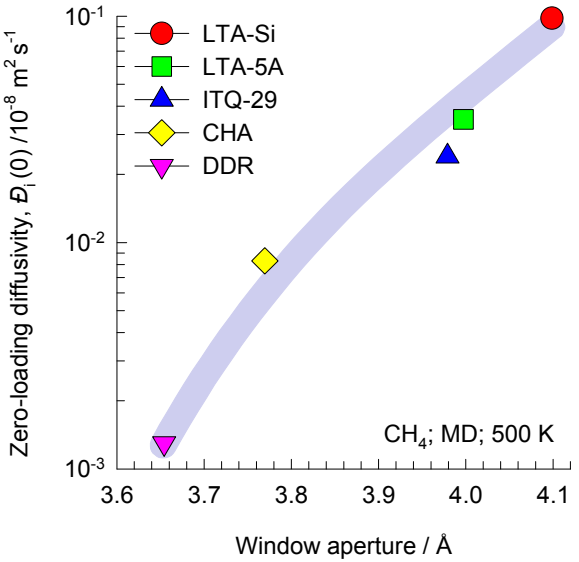

ZIF-8 pore landscapes

The ZIF-8 = Zn(methylimidazole)$_2$ structure was taken from
R. Banerjee, A. Phan, B. Wang, C. Knobler, H. Furukawa, M. O'Keeffe, O.M. Yaghi, High-Throughput Synthesis of Zeolitic Imidazolate Frameworks and Application to CO_2 Capture, Science 319 (2008) 939-943.
The original structural data (cif file) contains solvent molecules; these were removed and the solvent-free structures were simulated.

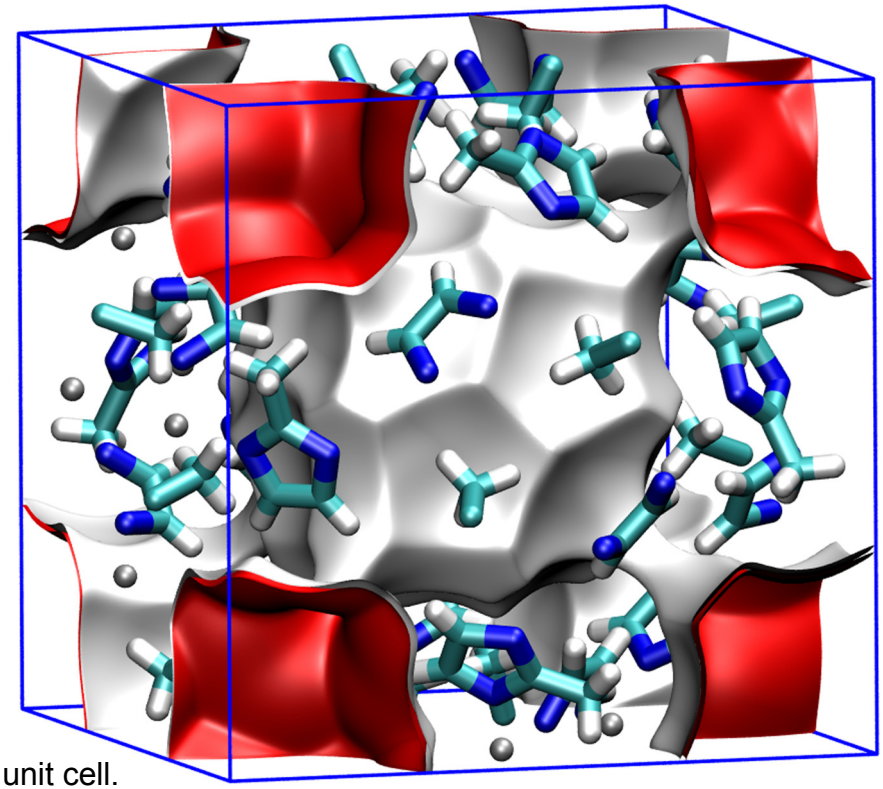

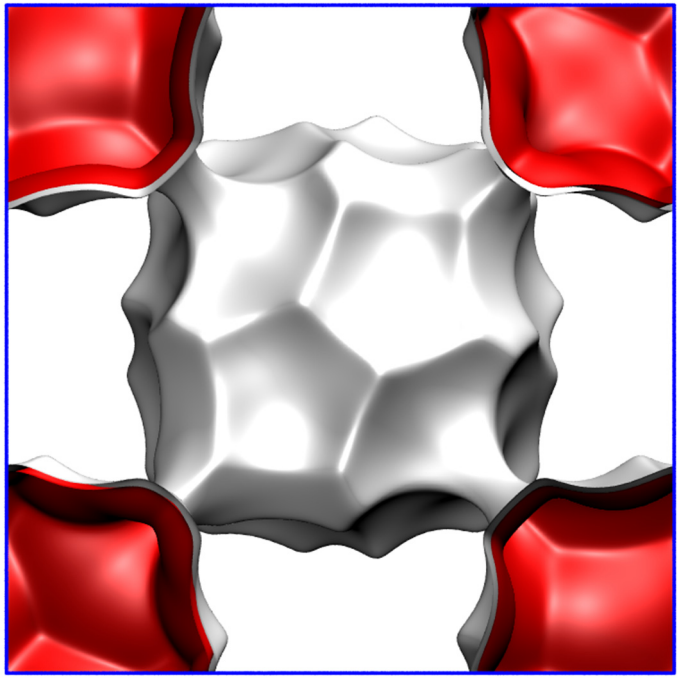

There are 2 cages per unit cell. The volume of one ZIF-8 cage is 1168 Å^3, significantly larger than that of a single cage of DDR (278 Å^3), or FAU (786 Å^3).

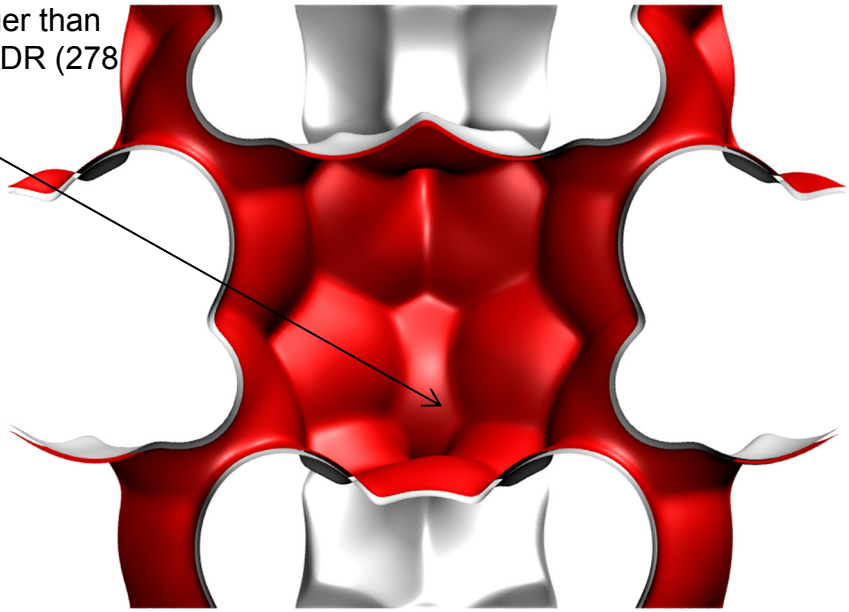

Electronic Supplementary Material (ESI) for Physical Chemistry Chemical Physics

ZIF-8 dimensions

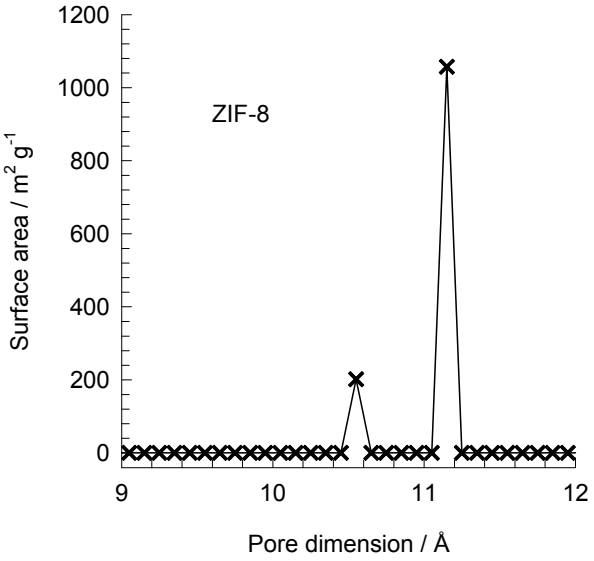

This plot of surface area versus pore dimension is determined using a combination of the DeLaunay triangulation method for pore dimension determination, and the procedure of Düren for determination of the surface area.

	ZIF-8
a /Å	16.991
b /Å	16.991
c /Å	16.991
Cell volume / Å^3	4905.201
conversion factor for [molec/uc] to [mol per kg Framework]	0.3663
conversion factor for [molec/uc] to [kmol/m^3]	0.7106
ρ [kg/m3]	924.253
MW unit cell [g/mol(framework)]	2730.182
ϕ, fractional pore volume	0.476
open space / Å^3/uc	2337.0
Pore volume / cm^3/g	0.515
Surface area /m^2/g	1164.7
DeLaunay diameter /Å	3.26

ZIF-8 methanol, ethanol, and ethane isotherms at 298 K

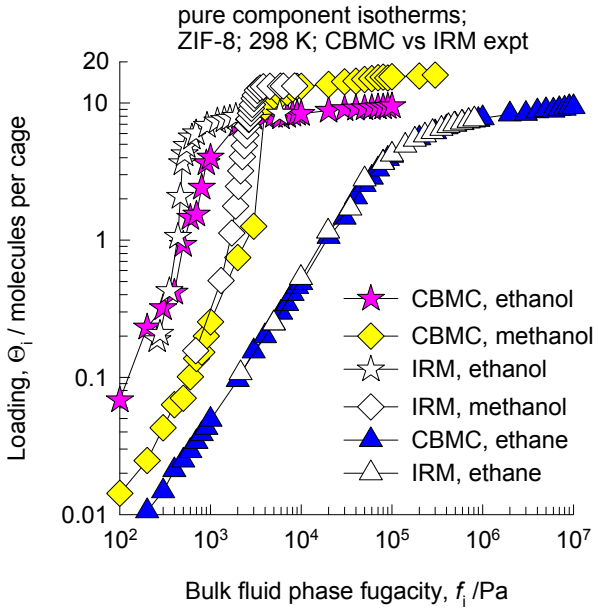

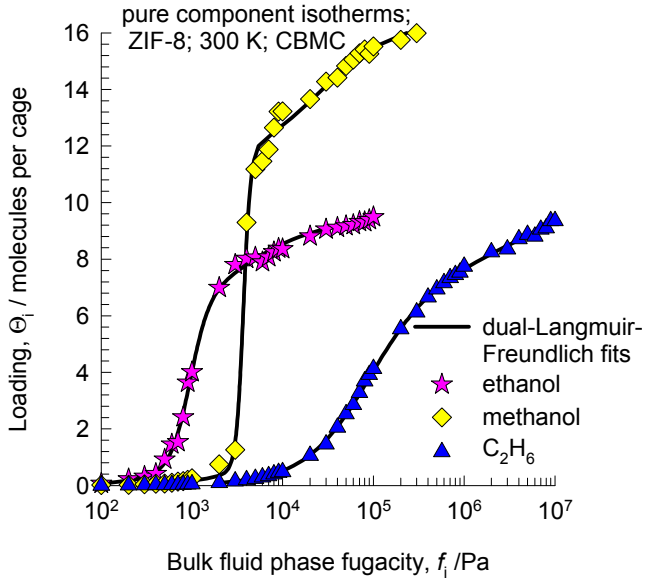

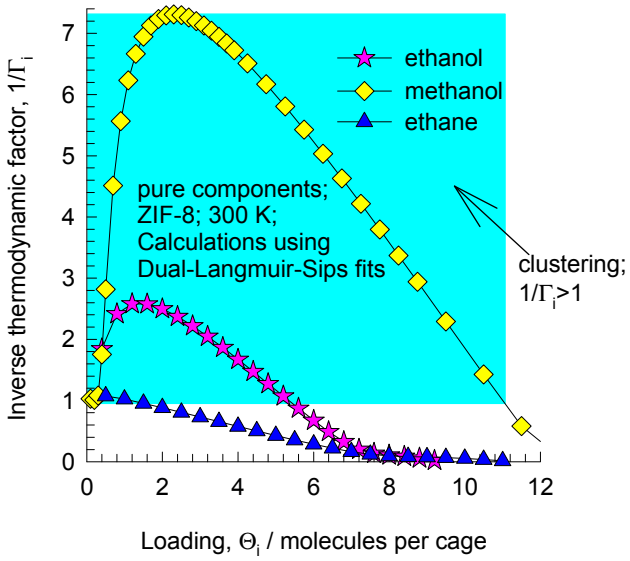

The experimental data are re-plotted using the information in:
C. Chmelik, H. Bux, J. Caro, L. Heinke, F. Hibbe, T. Titze, J. Kärger, Mass transfer in a nanoscale material enhanced by an opposing flux, Phys. Rev. Lett. 104 (2010) 085902.

The steep isotherms for methanol and ethanol are indicative of molecular clustering. This is confirmed by the inverse thermodynamic factors that significantly exceed unity for a range of molecular loadings. We should therefore expect the hierarchy of diffusivities to be “abnormal” for methanol, and ethanol.

ZIF-8 methanol, ethanol, and ethane diffusivities at 298 K

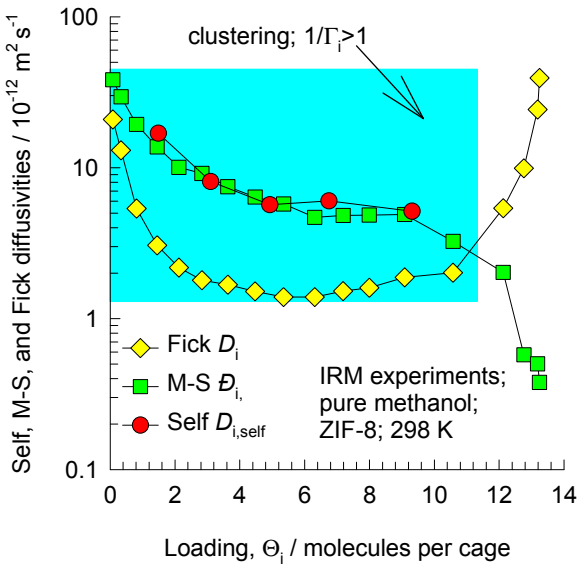

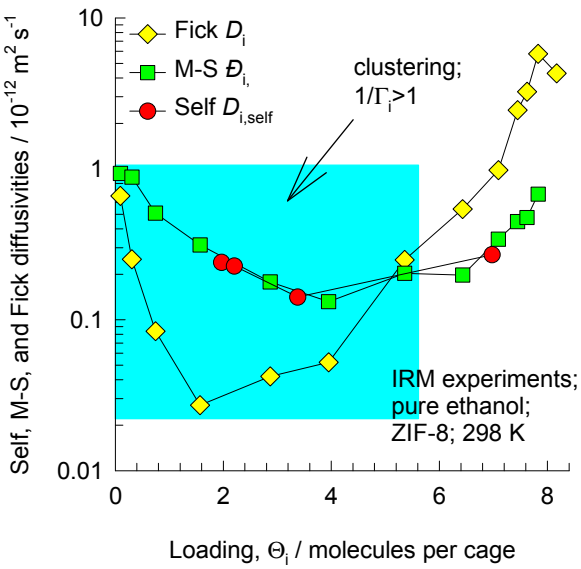

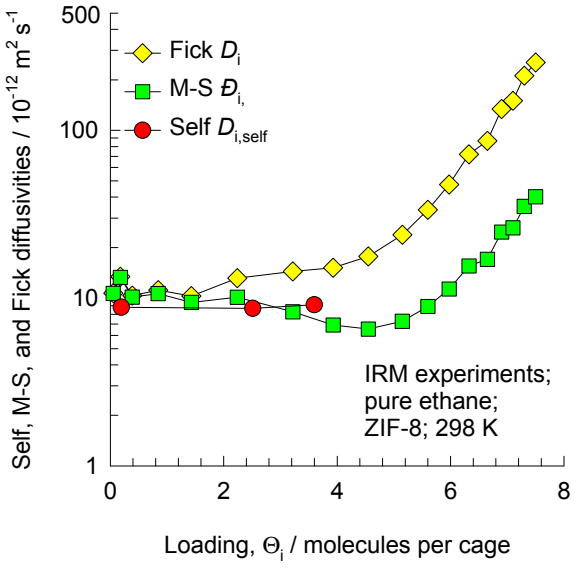

The experimental data are re-plotted using the information in:
C. Chmelik, H. Bux, J. Caro, L. Heinke, F. Hibbe, T. Titze, J. Kärger, Mass transfer in a nanoscale material enhanced by an opposing flux, Phys. Rev. Lett. 104 (2010) 085902.

The hierarchy of diffusivities is M-S = Self > Fick in regions where molecular clustering occurs.

Electronic Supplementary Material (ESI) for Physical Chemistry Chemical Physics

ZIF-8 snapshot of methanol clusters

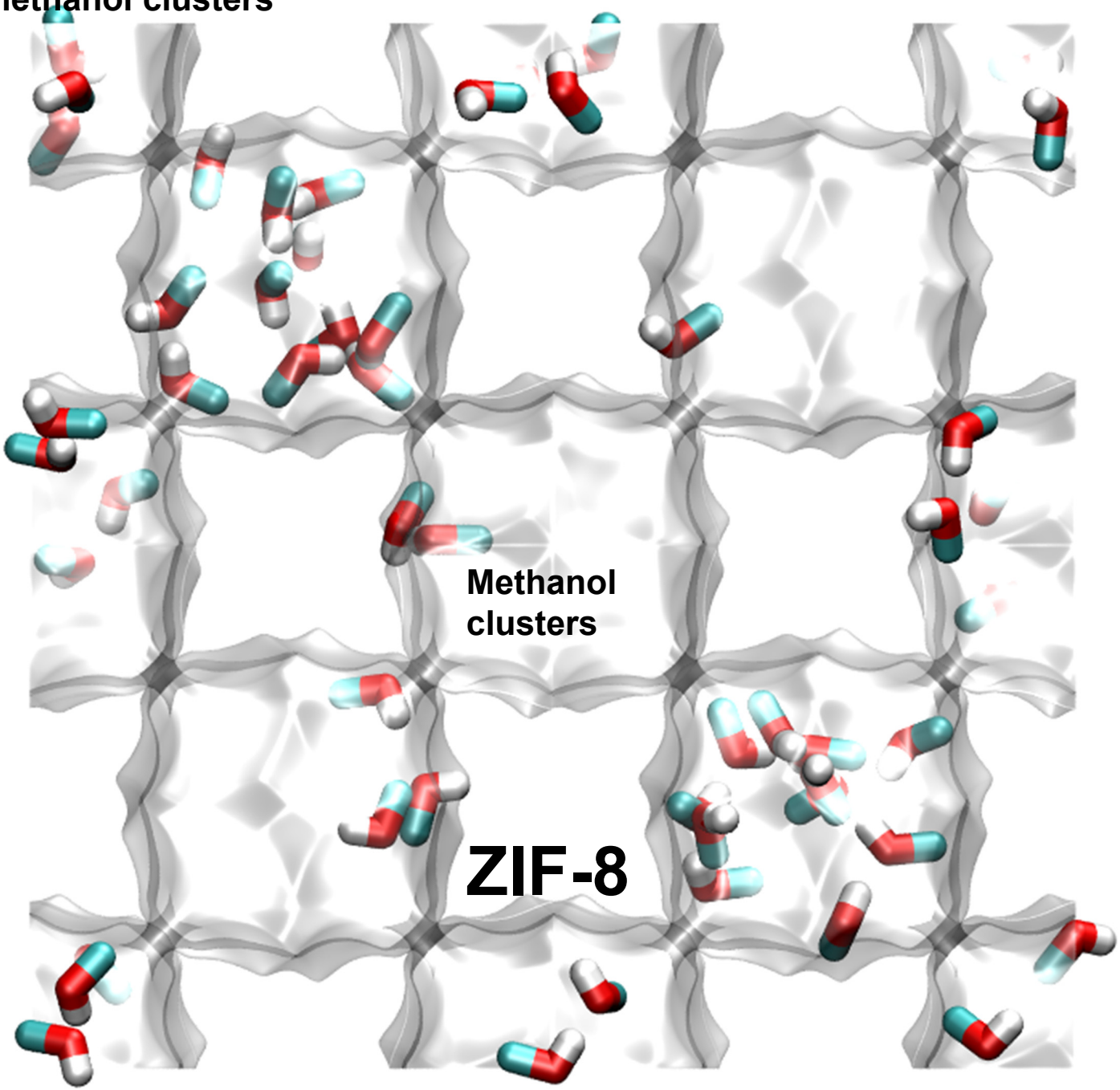

Electronic Supplementary Material (ESI) for Physical Chemistry Chemical Physics

ZIF-8 snapshot of ethanol clusters

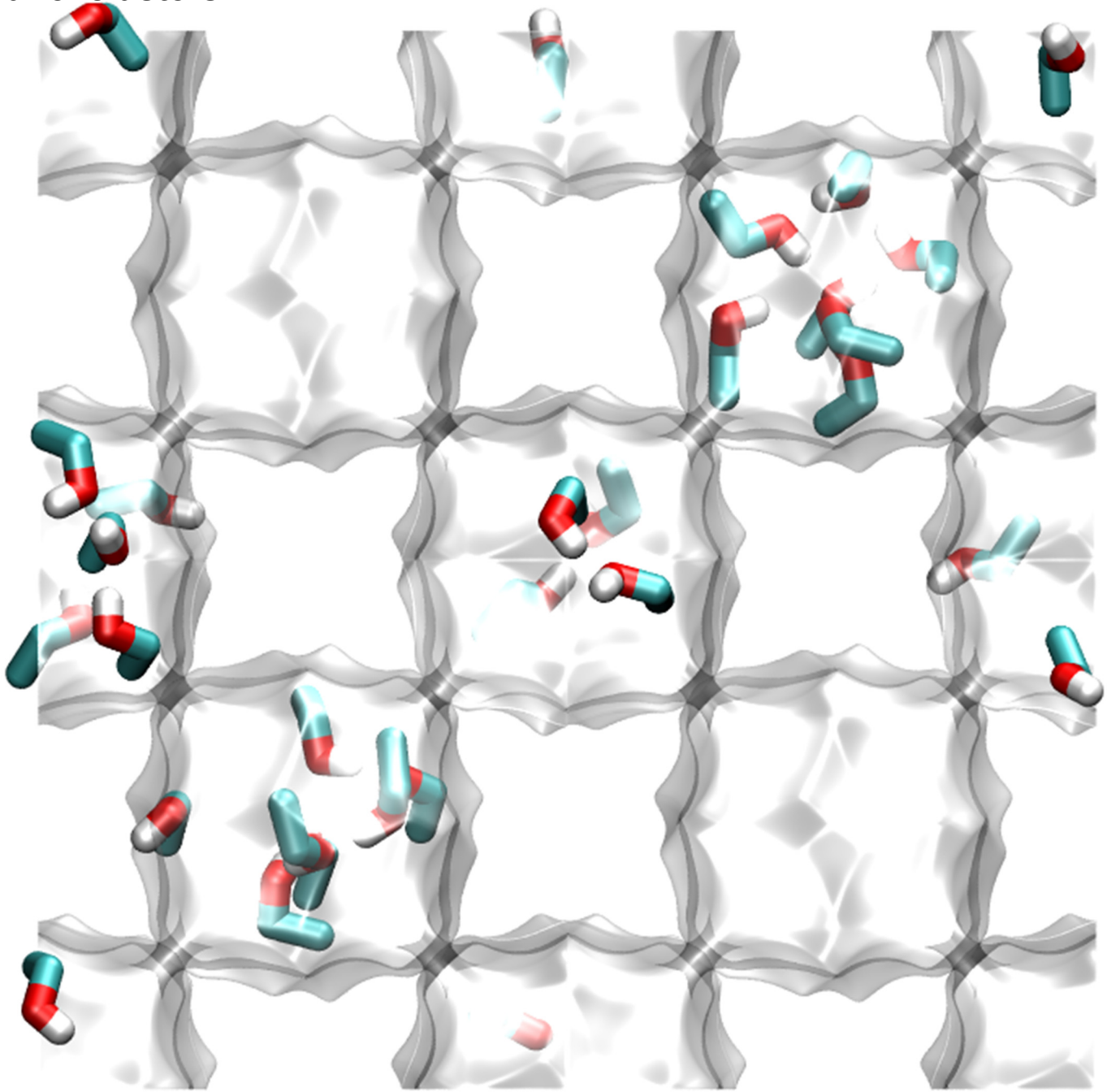

Electronic Supplementary Material (ESI) for Physical Chemistry Chemical Physics

1D mesoporous channels

BTP-COF landscape

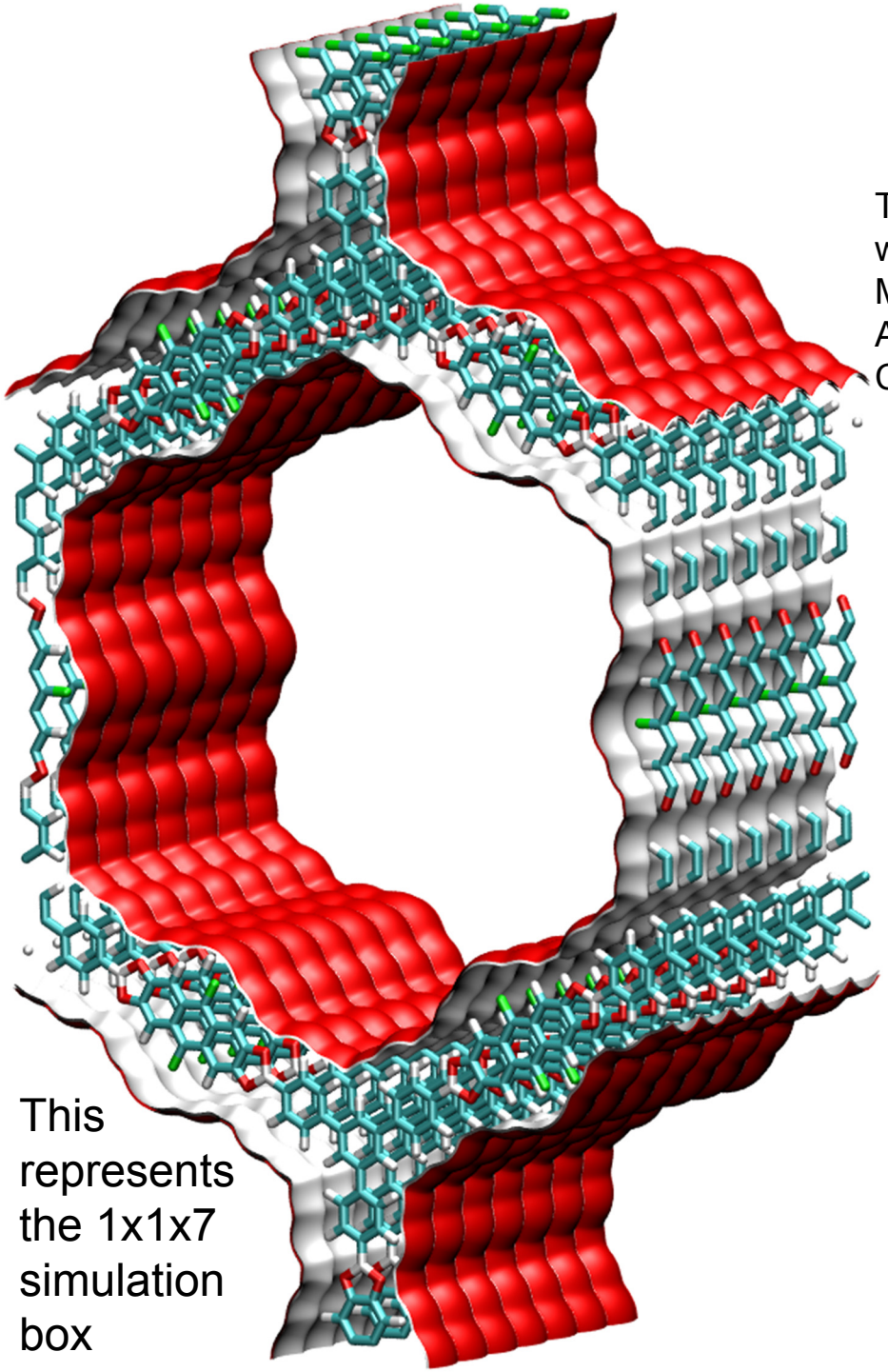

This represents the 1x1x7 simulation box

The crystallographic structural information for BTP-COF was obtained from
M. Dogru, A. Sonnauer, A. Gavryushin, P. Knochel, T. Bein, A Covalent Organic Framework with 4 nm open pores, Chem. Commun. 47 (2011) 1707-1709.

	BTP-COF
a /Å	43.65
b /Å	75.604
c /Å	3.52
Cell volume / Å^3	11616.4
conversion factor for [molec/uc] to [mol per kg Framework]	0.3403
conversion factor for [molec/uc] to [kmol/m^3]	0.1900
ρ [kg/m3]	420.0831
MW unit cell [g/mol(framework)]	2938.67
ϕ, fractional pore volume	0.752
open space / Å^3/uc	8738.7
Pore volume / cm^3/g	1.791
Surface area /m^2/g	
DeLaunay diameter /Å	34.26

BTP-COF CBMC simulations of isotherms, and isosteric heats of adsorption

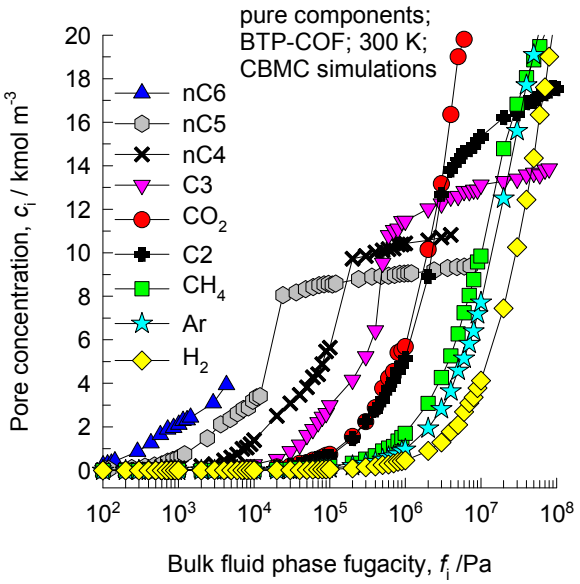

Note that C2 and C3 refer to saturated alkanes

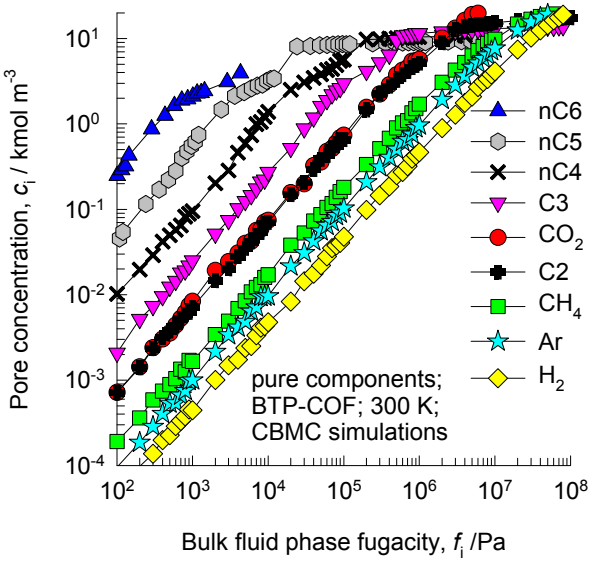

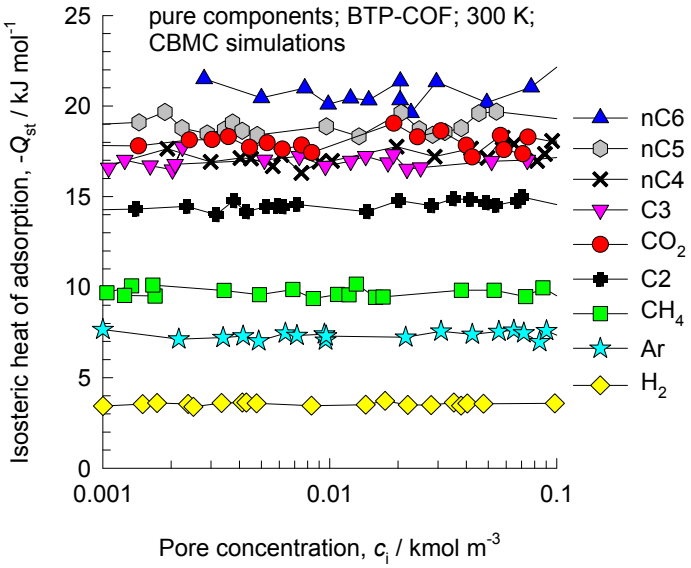

The isosteric heats of adsorption correlate with the Henry coefficients determined from CBMC

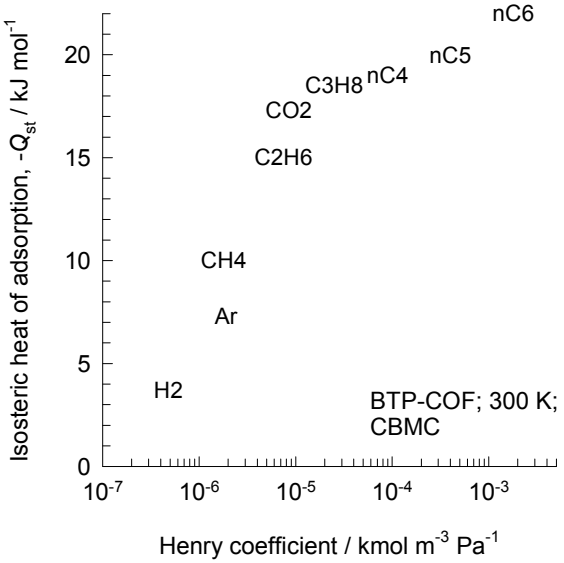

BTP-COF MD simulations of unary self- , and M-S diffusivities

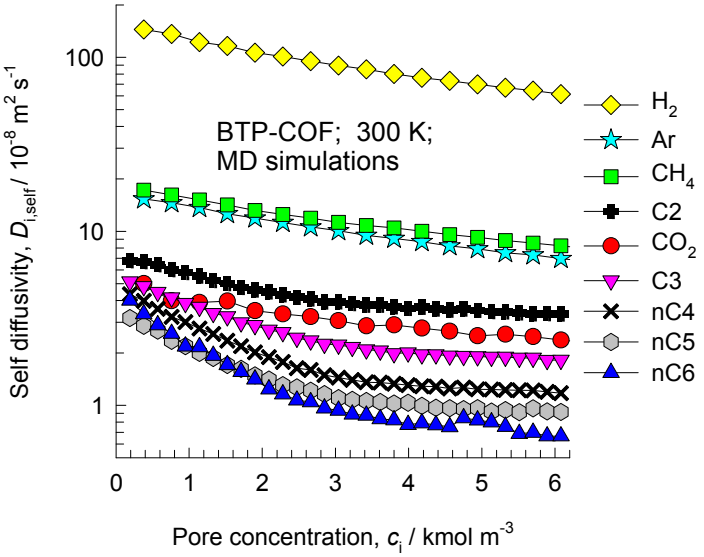

Note that C2 and C3 refer to saturated alkanes

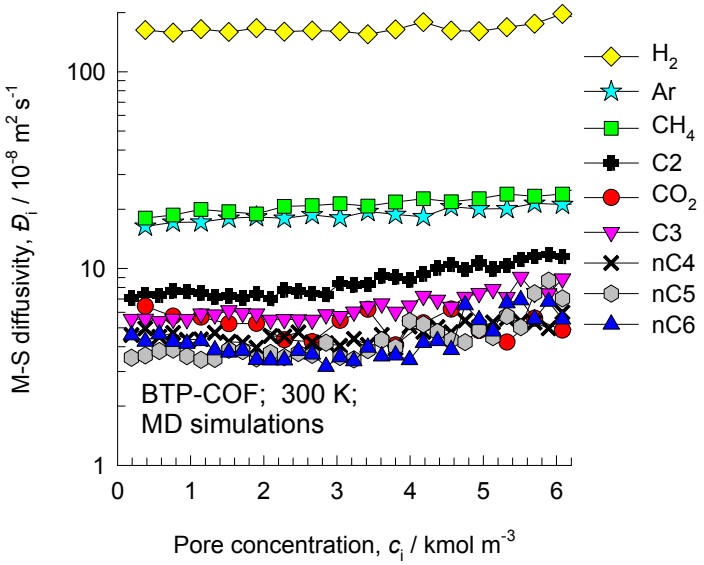

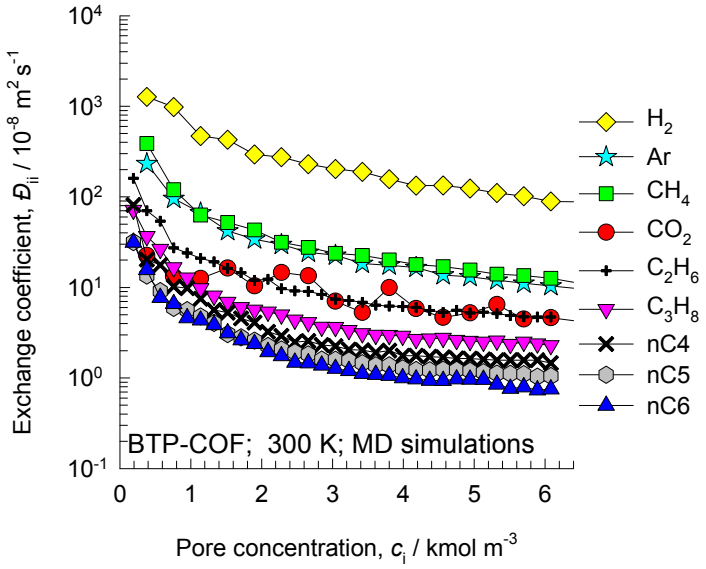

Electronic Supplementary Material (ESI) for Physical Chemistry Chemical Physics

1D micro-porous channels

AFI landscapes

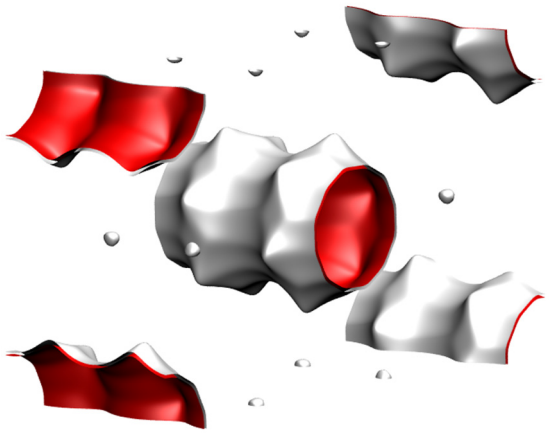

12-ring
1D channel of AFI

Snapshots showing location of CH_4 and CO_2

Structural information from: C. Baerlocher, L.B. McCusker, Database of Zeolite Structures, International Zeolite Association, http://www.iza-structure.org/databases/

Electronic Supplementary Material (ESI) for Physical Chemistry Chemical Physics

AFI pore dimensions

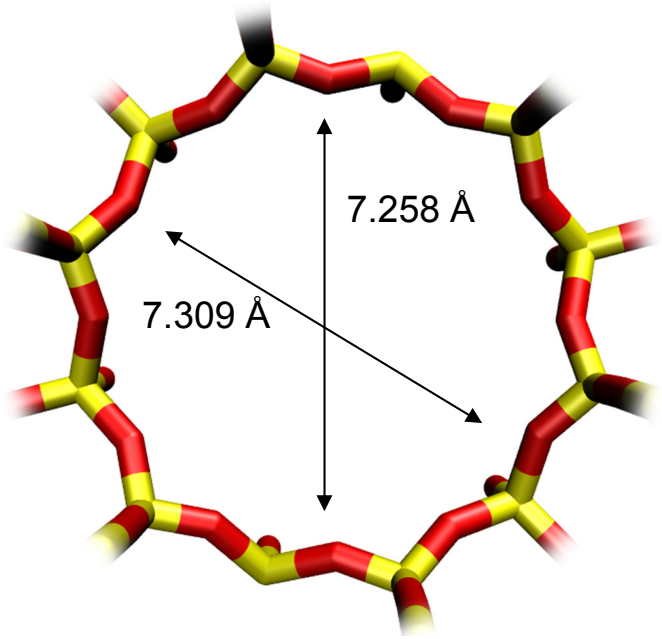

	AFI
a /Å	23.774
b /Å	13.726
c /Å	8.484
Cell volume / Å^3	2768.515
conversion factor for [molec/uc] to [mol per kg Framework]	0.3467
conversion factor for [molec/uc] to [kmol/m^3]	2.1866
ρ [kg/m3]	1729.876
MW unit cell [g/mol(framework)]	2884.07
ϕ, fractional pore volume	0.274
open space / Å^3/uc	759.4
Pore volume / cm^3/g	0.159
Surface area /m^2/g	466.0
DeLaunay diameter /Å	7.26

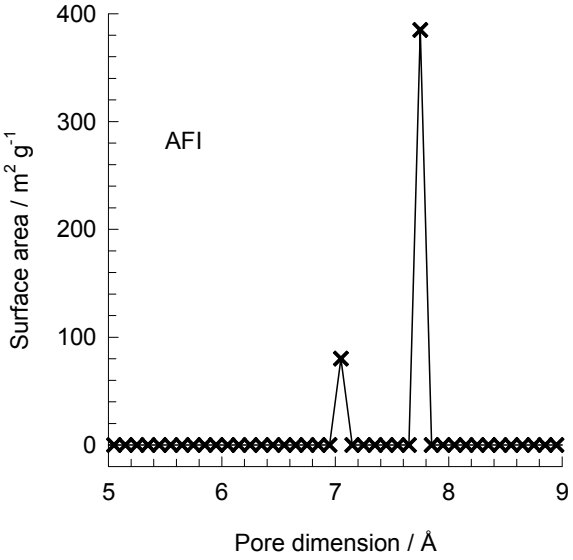

This plot of surface area versus pore dimension is determined using a combination of the DeLaunay triangulation method for pore dimension determination, and the procedure of Düren for determination of the surface area.

AFI CBMC simulations of isotherms, and isosteric heats of adsorption

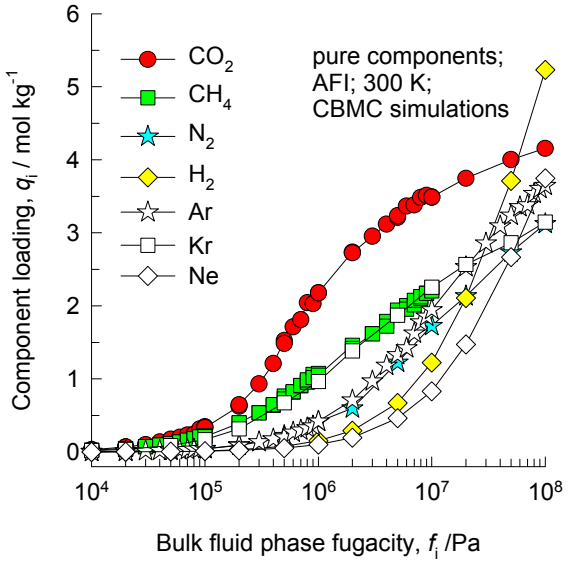

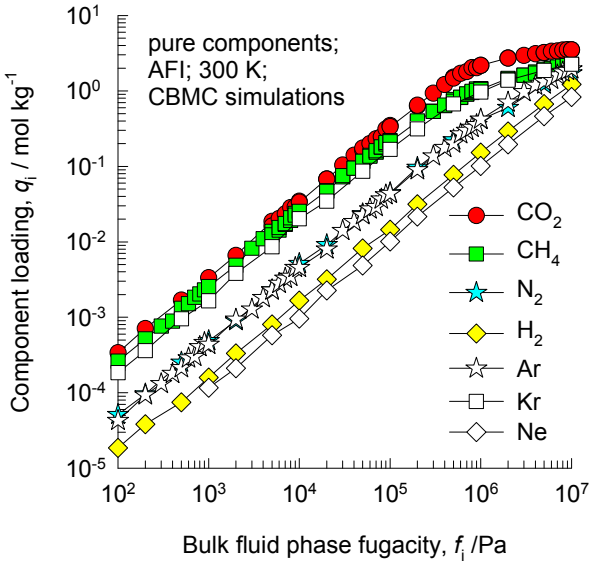

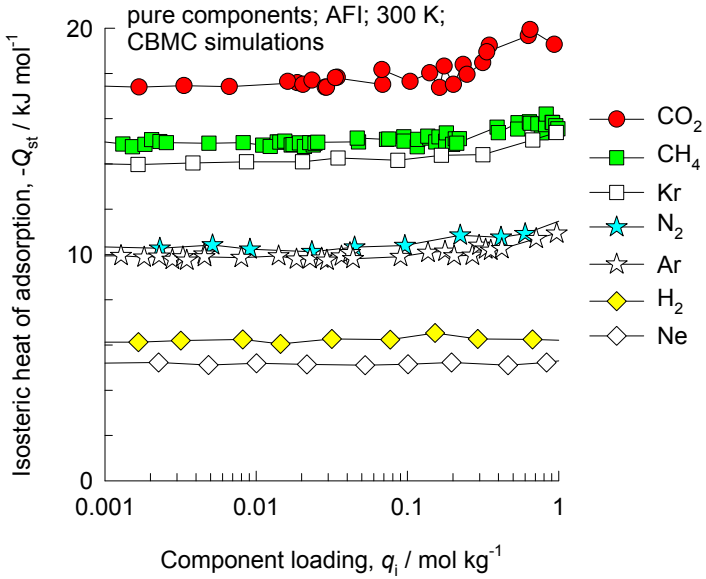

Influence of Inverse Thermodynamic Factor on diffusivities

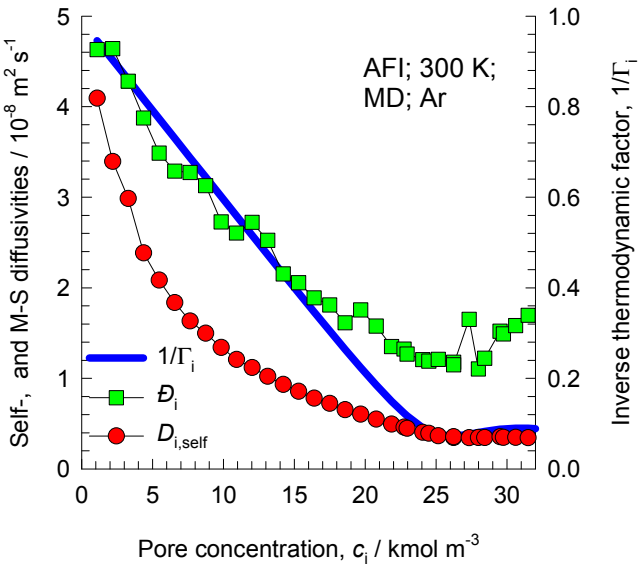

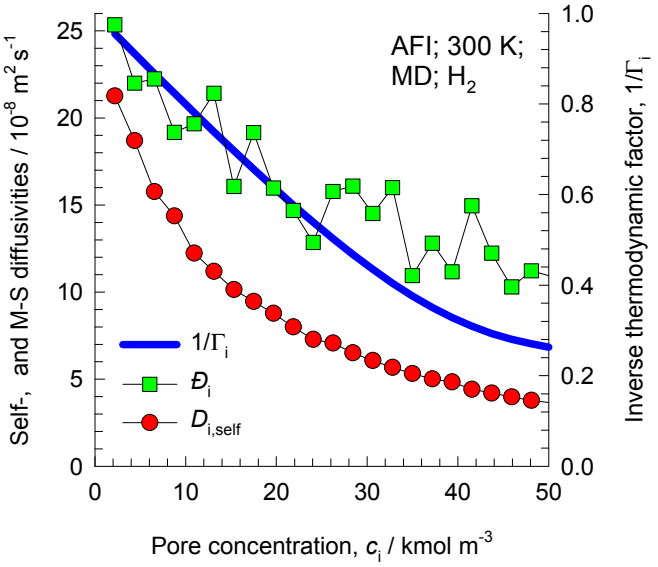

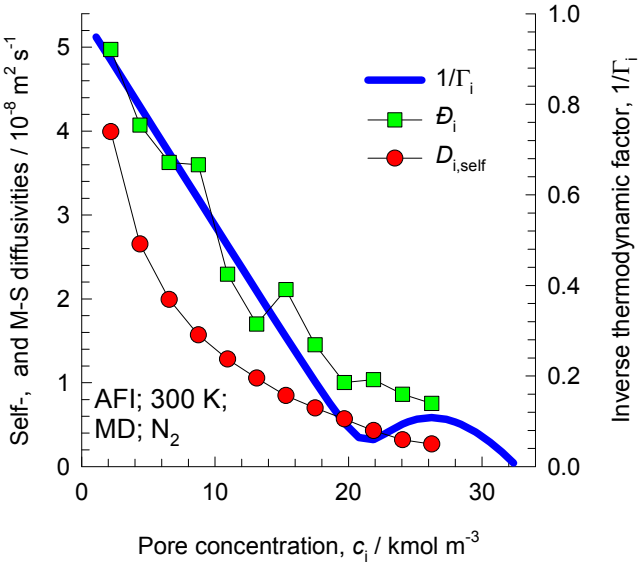

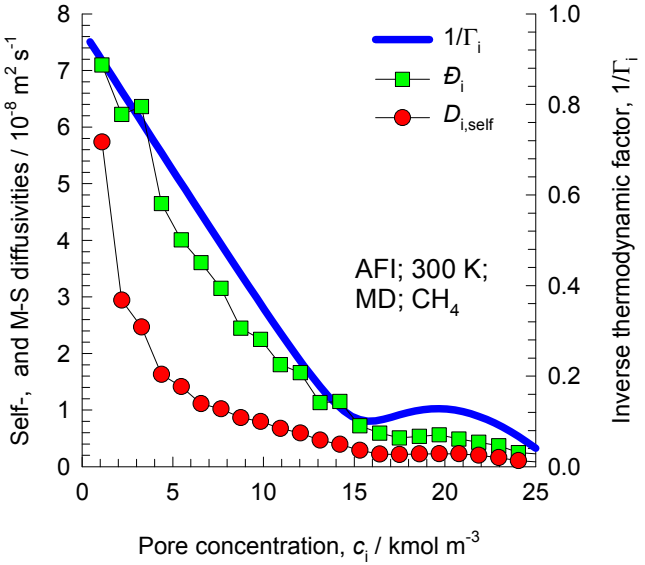

MTW pore landscape

MTW has 1D 12-ring channels

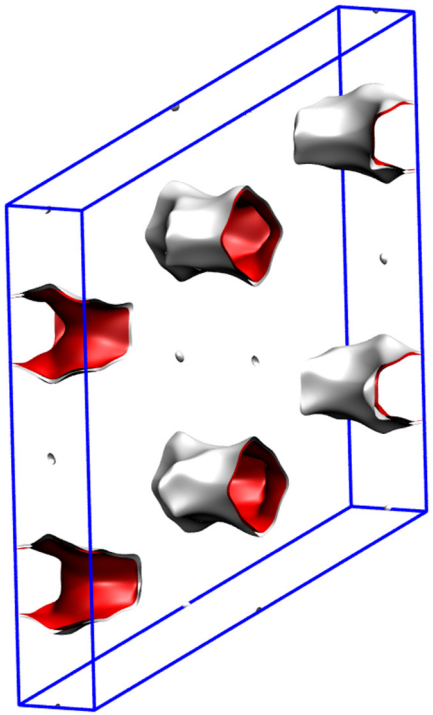

Structural information from: C. Baerlocher, L.B. McCusker, Database of Zeolite Structures, International Zeolite Association, http://www.iza-structure.org/databases/

MTW pore dimensions

This plot of surface area versus pore dimension is determined using a combination of the DeLaunay triangulation method for pore dimension determination, and the procedure of Düren for determination of the surface area.

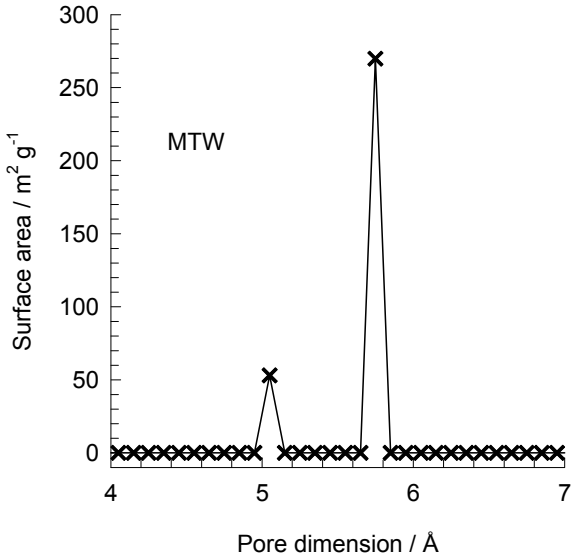

MTW has 1D, 12-ring channels

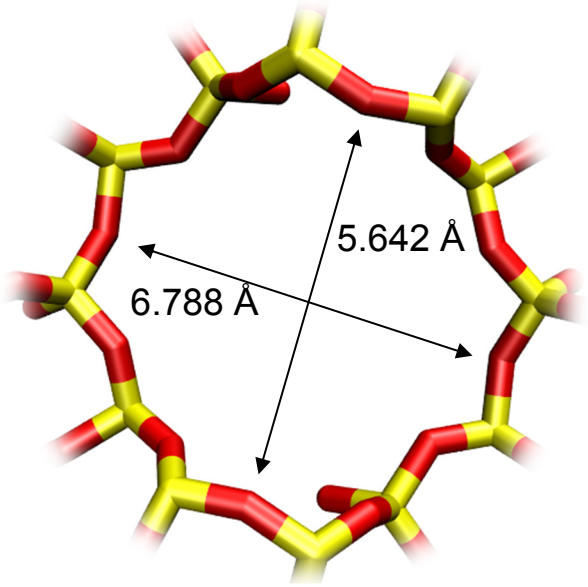

	MTW
a /Å	24.863
b /Å	5.012
c /Å	24.326
Cell volume / Å^3	2887.491
conversion factor for [molec/uc] to [mol per kg Framework]	0.2972
conversion factor for [molec/uc] to [kmol/m^3]	2.6759
ρ [kg/m3]	1935.031
MW unit cell [g/mol(framework)]	3364.749
ϕ, fractional pore volume	0.215
open space / Å^3/uc	620.6
Pore volume / cm^3/g	0.111
Surface area /m^2/g	323.0
DeLaunay diameter /Å	5.69

MTW MD simulations of unary self- , and M-S diffusivities

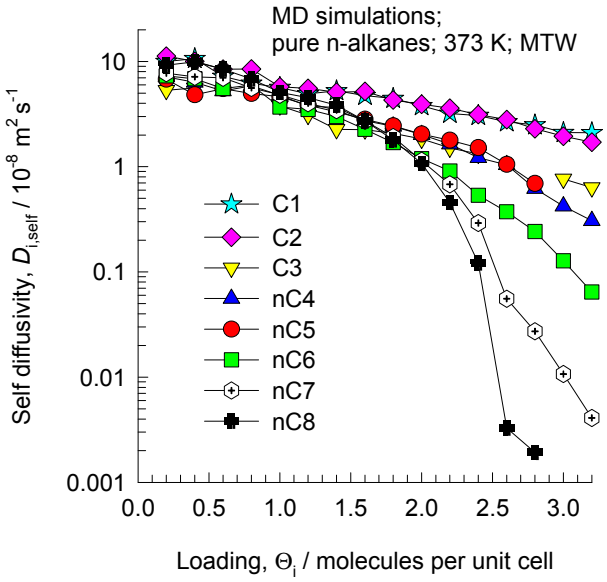

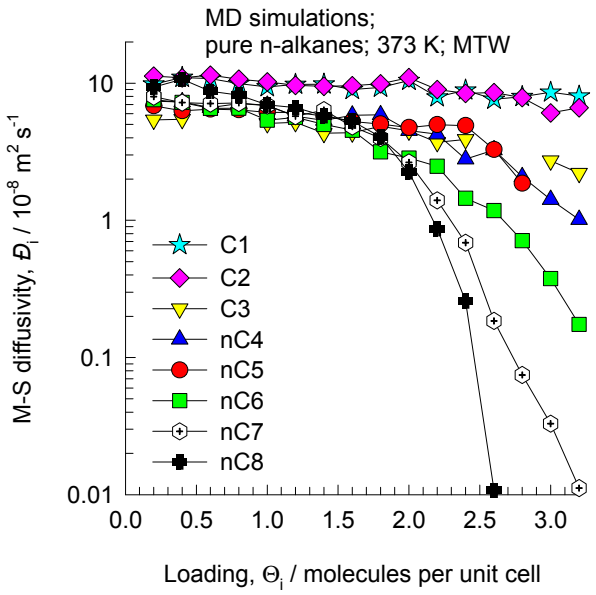

MTW adsorption of CO_2

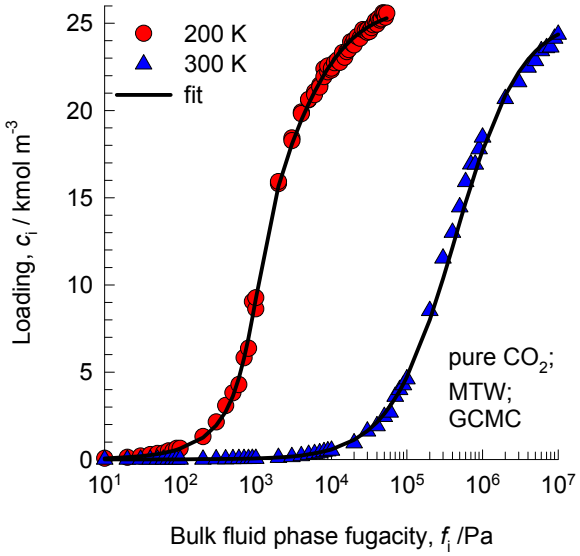

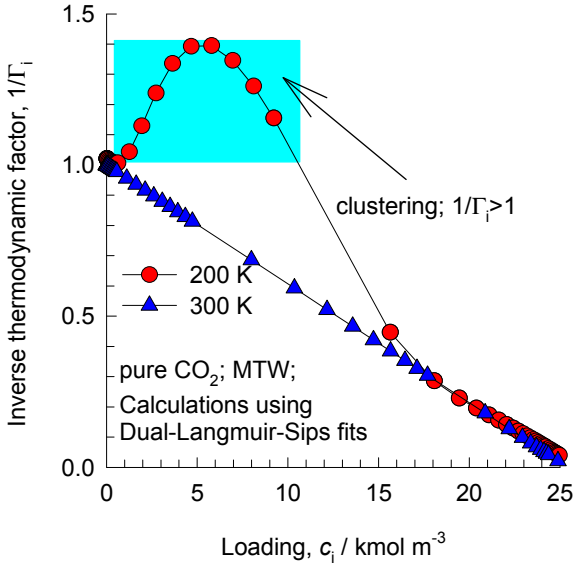

TON pore landscape

10-ring 1D channel of TON

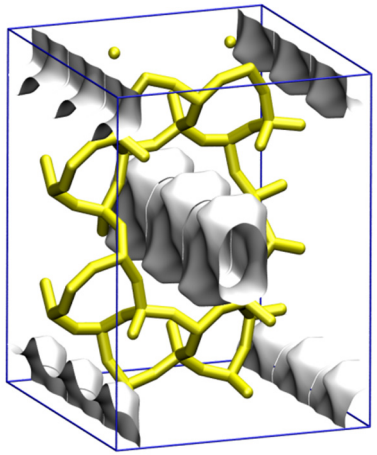

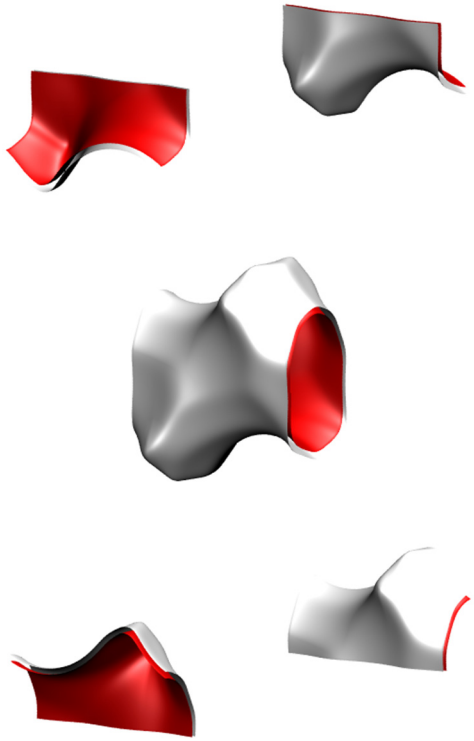

Structural information from: C. Baerlocher, L.B. McCusker, Database of Zeolite Structures, International Zeolite Association, http://www.iza-structure.org/databases/

TON pore dimensions

This plot of surface area versus pore dimension is determined using a combination of the DeLaunay triangulation method for pore dimension determination, and the procedure of Düren for determination of the surface area.

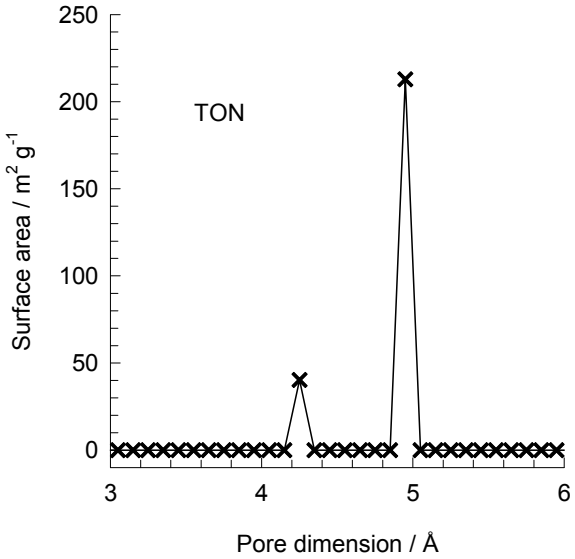

10-ring channel of TON

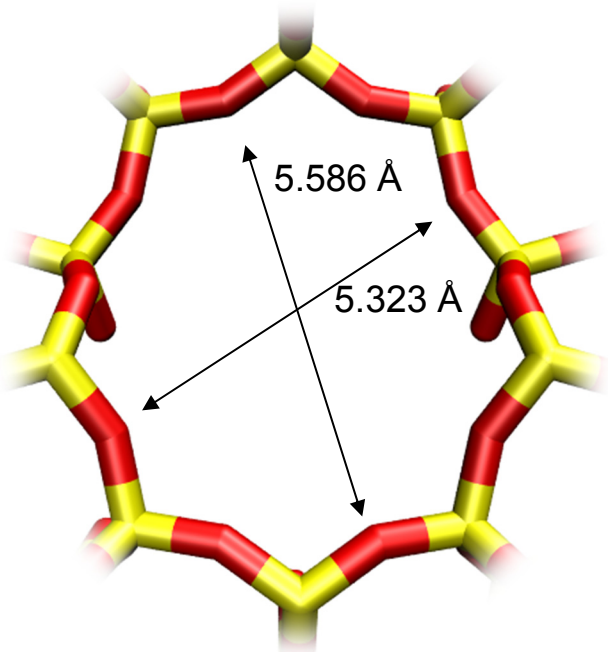

	TON
a /Å	13.859
b /Å	17.42
c /Å	5.038
Cell volume / Å^3	1216.293
conversion factor for [molec/uc] to [mol per kg Framework]	0.6935
conversion factor for [molec/uc] to [kmol/m^3]	7.1763
ρ [kg/m3]	1968.764
MW unit cell [g/mol(framework)]	1442.035
ϕ, fractional pore volume	0.190
open space / Å^3/uc	231.4
Pore volume / cm^3/g	0.097
Surface area /m^2/g	253.0
DeLaunay diameter /Å	4.88

MgMOF-74 pore landscapes

The structural information on MgMOF-74 (= Mg_2(dobdc) = Mg\(dobdc = CPO-27-Mg) with dobdc = ($dobdc^{4-}$ = 2,5-dioxido-1,4-benzenedicarboxylate)) were obtained from

A.Ö. Yazaydın, R.Q. Snurr, T.H. Park, K. Koh, J. Liu, M.D. LeVan, A.I. Benin, P. Jakubczak, M. Lanuza, D.B. Galloway, J.J. Low, R.R. Willis, Screening of Metal-Organic Frameworks for Carbon Dioxide Capture from Flue Gas using a Combined Experimental and Modeling Approach, J. Am. Chem. Soc. 131 (2009) 18198-18199.
D. Britt, H. Furukawa, B. Wang, T.G. Glover, O.M. Yaghi, Highly efficient separation of carbon dioxide by a metal-organic framework replete with open metal sites, Proc. Natl. Acad. Sci. U.S.A. 106 (2009) 20637-20640.
N.L. Rosi, J. Kim, M. Eddaoudi, B. Chen, M. O'Keeffe, O.M. Yaghi, Rod Packings and Metal-Organic Frameworks Constructed from Rod-Shaped Secondary Building Units, J. Am. Chem. Soc. 127 (2005) 1504-1518.
P.D.C. Dietzel, B. Panella, M. Hirscher, R. Blom, H. Fjellvåg, Hydrogen adsorption in a nickel based coordination polymer with open metal sites in the cylindrical cavities of the desolvated framework, Chem. Commun. (2006) 959-961.
P.D.C. Dietzel, V. Besikiotis, R. Blom, Application of metal–organic frameworks with coordinatively unsaturated metal sites in storage and separation of methane and carbon dioxide, J. Mater. Chem. 19 (2009) 7362-7370.
S.R. Caskey, A.G. Wong-Foy, A.J. Matzger, Dramatic Tuning of Carbon Dioxide Uptake via Metal Substitution in a Coordination Polymer with Cylindrical Pores, J. Am. Chem. Soc. 130 (2008) 10870-10871.

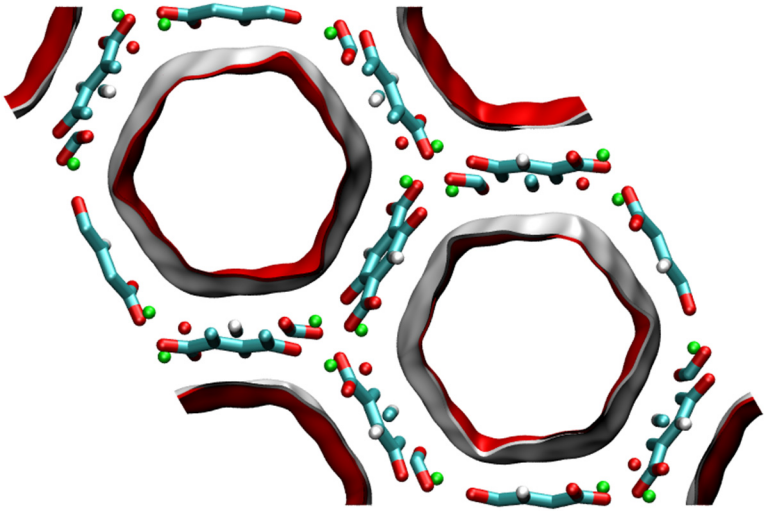

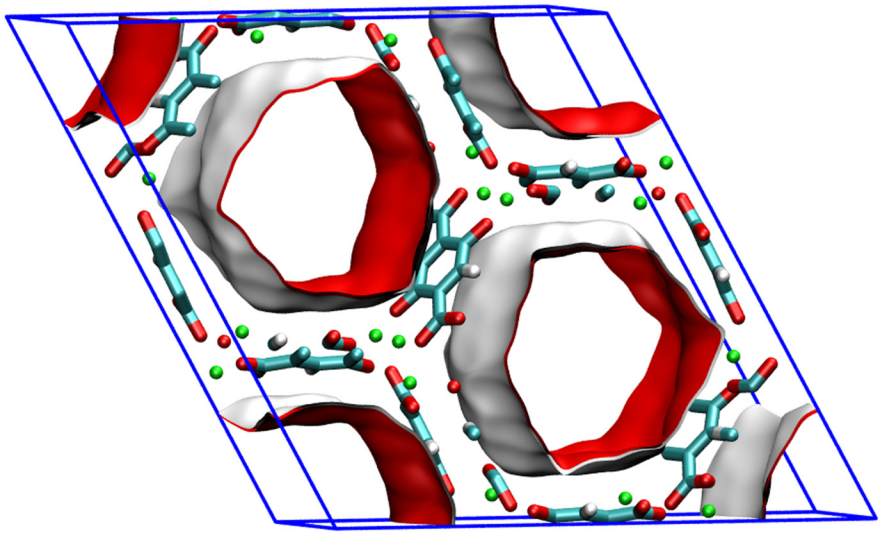

MgMOF-74 pore dimensions

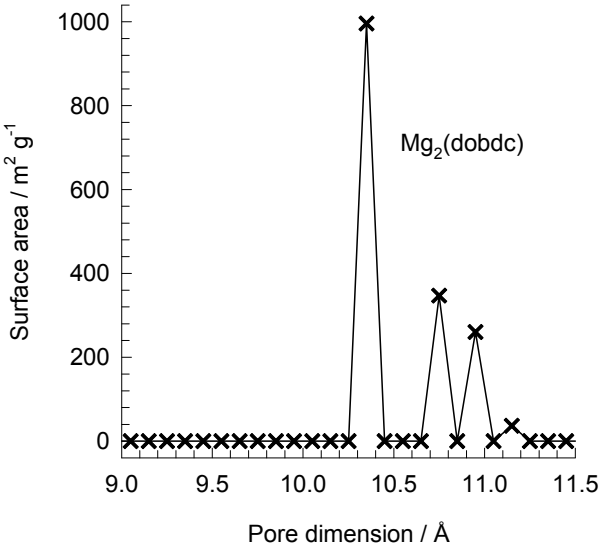

This plot of surface area versus pore dimension is determined using a combination of the DeLaunay triangulation method for pore dimension determination, and the procedure of Düren for determination of the surface area.

	MgMOF-74
a /Å	25.8621
b /Å	25.8621
c /Å	6.91427
Cell volume / Å^3	4005.019
conversion factor for [molec/uc] to [mol per kg Framework]	0.4580
conversion factor for [molec/uc] to [kmol/m^3]	0.5856
ρ [kg/m3]	905.367
MW unit cell [g/mol(framework)]	2183.601
ϕ, fractional pore volume	0.708
open space / Å^3/uc	2835.6
Pore volume / cm^3/g	0.782
Surface area /m^2/g	1640.0
DeLaunay diameter /Å	10.66

MgMOF-74 isotherms and isosteric heats of adsorption from experiments

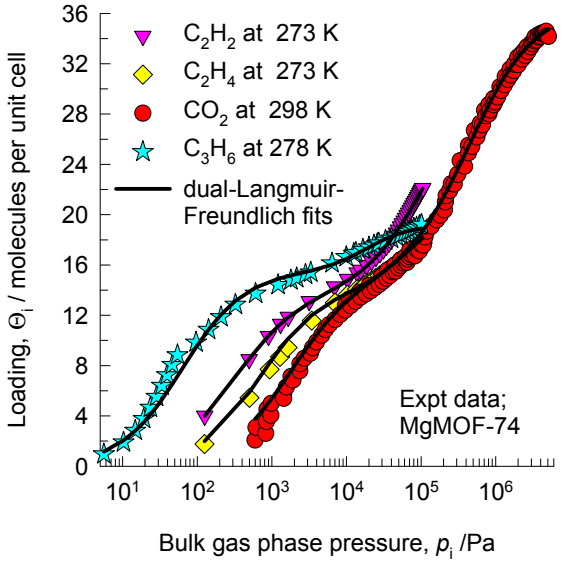

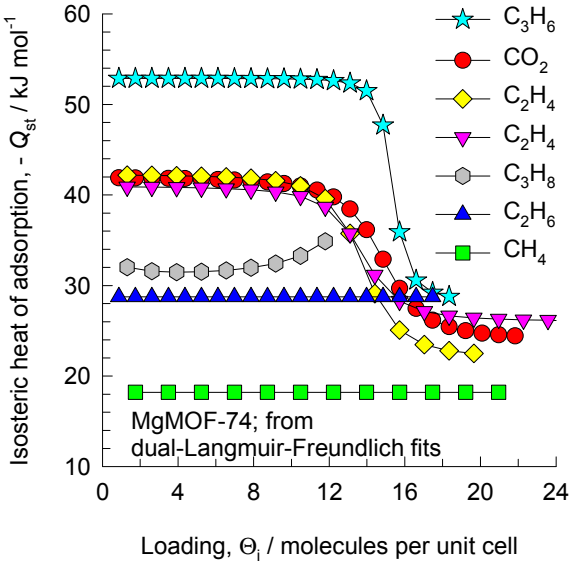

The pure component isotherms, with fits, and isosteric heats of adsorption are those reported by:
He, Y.; Krishna, R.; Chen, B. Metal-Organic Frameworks with Potential for Energy-Efficient Adsorptive Separation of Light Hydrocarbons. Energy Environ. Sci. 2012, 5, 9107-9120.

The unary diffusivities are taken to be identical to those in MgMOF-74; the Maxwell-Stefan diffusivities are the ones presented by:
Krishna, R.; van Baten, J.M. Investigating the Relative Influences of Molecular Dimensions and Binding Energies on Diffusivities of Guest Species Inside Nanoporous Crystalline Materials J. Phys. Chem. C 2012, 116, 23556-23568.

MgMOF-74 dependence of diffusivity on the isosteric heats of adsorption

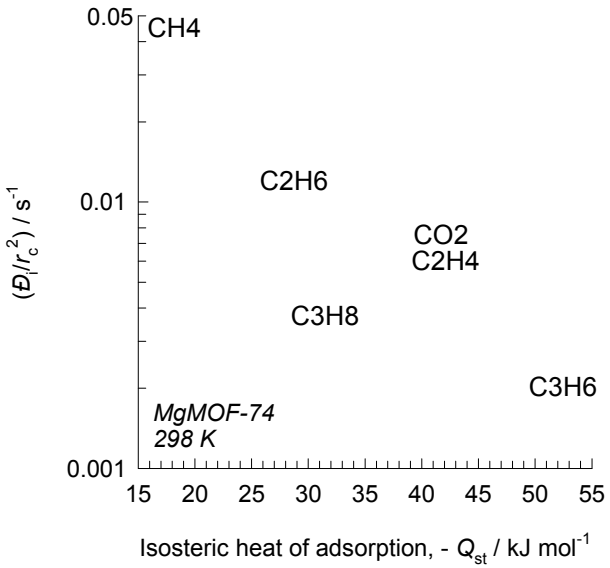

The pure component isotherms, with fits, and isosteric heats of adsorption are those reported by:
He, Y.; Krishna, R.; Chen, B. Metal-Organic Frameworks with Potential for Energy-Efficient Adsorptive Separation of Light Hydrocarbons. Energy Environ. Sci. 2012, 5, 9107-9120.

The unary diffusivities Maxwell-Stefan diffusivities are the ones presented by:
Krishna, R.; van Baten, J.M. Investigating the Relative Influences of Molecular Dimensions and Binding Energies on Diffusivities of Guest Species Inside Nanoporous Crystalline Materials J. Phys. Chem. C 2012, 116, 23556-23568.

Electronic Supplementary Material (ESI) for Physical Chemistry Chemical Physics

ZnMOF-74 pore landscapes

The structural information on ZnMOF-74 (= Zn_2(dobdc) = Zn\(dobdc= CPO-27-Zn) with dobdc = ($dobdc^{4-}$ = 2,5-dioxido-1,4-benzenedicarboxylate)) were obtained from

A.Ö. Yazaydın, R.Q. Snurr, T.H. Park, K. Koh, J. Liu, M.D. LeVan, A.I. Benin, P. Jakubczak, M. Lanuza, D.B. Galloway, J.J. Low, R.R. Willis, Screening of Metal-Organic Frameworks for Carbon Dioxide Capture from Flue Gas using a Combined Experimental and Modeling Approach, J. Am. Chem. Soc. 131 (2009) 18198-18199.
D. Britt, H. Furukawa, B. Wang, T.G. Glover, O.M. Yaghi, Highly efficient separation of carbon dioxide by a metal-organic framework replete with open metal sites, Proc. Natl. Acad. Sci. U.S.A. 106 (2009) 20637-20640.
N.L. Rosi, J. Kim, M. Eddaoudi, B. Chen, M. O'Keeffe, O.M. Yaghi, Rod Packings and Metal-Organic Frameworks Constructed from Rod-Shaped Secondary Building Units, J. Am. Chem. Soc. 127 (2005) 1504-1518.
P.D.C. Dietzel, B. Panella, M. Hirscher, R. Blom, H. Fjellvåg, Hydrogen adsorption in a nickel based coordination polymer with open metal sites in the cylindrical cavities of the desolvated framework, Chem. Commun. (2006) 959-961.
P.D.C. Dietzel, V. Besikiotis, R. Blom, Application of metal–organic frameworks with coordinatively unsaturated metal sites in storage and separation of methane and carbon dioxide, J. Mater. Chem. 19 (2009) 7362-7370.
S.R. Caskey, A.G. Wong-Foy, A.J. Matzger, Dramatic Tuning of Carbon Dioxide Uptake via Metal Substitution in a Coordination Polymer with Cylindrical Pores, J. Am. Chem. Soc. 130 (2008) 10870-10871.

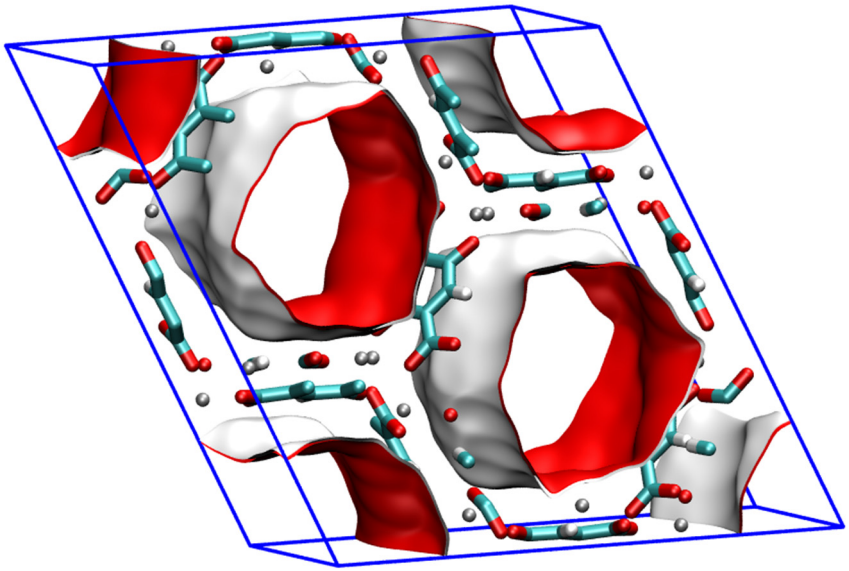

ZnMOF-74 pore dimensions

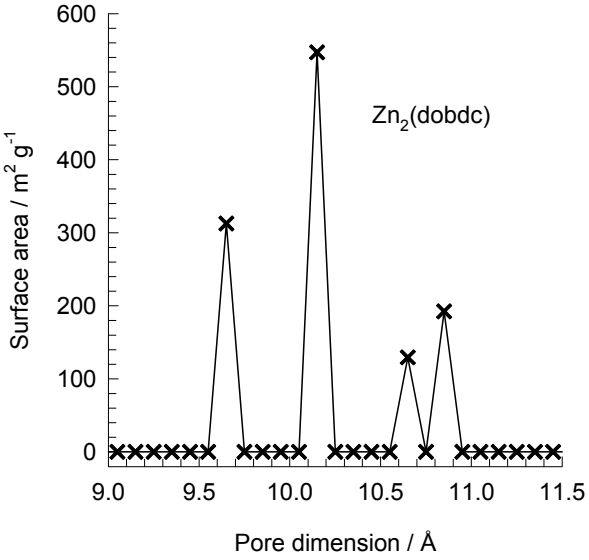

This plot of surface area versus pore dimension is determined using a combination of the DeLaunay triangulation method for pore dimension determination, and the procedure of Düren for determination of the surface area.

	ZnMOF-74
a /Å	25.9322
b /Å	25.9322
c /Å	6.8365
Cell volume / Å^3	3981.467
conversion factor for [molec/uc] to [mol per kg Framework]	0.3421
conversion factor for [molec/uc] to [kmol/m^3]	0.5881
ρ [kg/m3]	1219.304
MW unit cell [g/mol(framework)]	2923.473
ϕ, fractional pore volume	0.709
open space / Å^3/uc	2823.8
Pore volume / cm^3/g	0.582
Surface area /m^2/g	1176.0
DeLaunay diameter /Å	9.49

ZnMOF-74 CBMC simulations of isotherms, and isosteric heats of adsorption

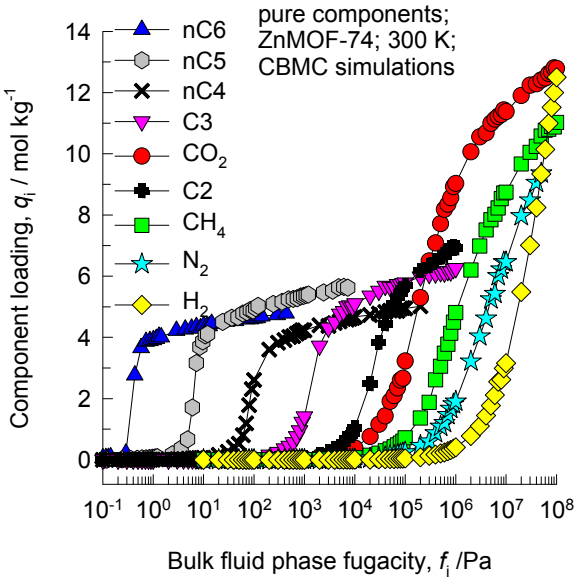

Note that C2 and C3 above refer to saturated alkanes.

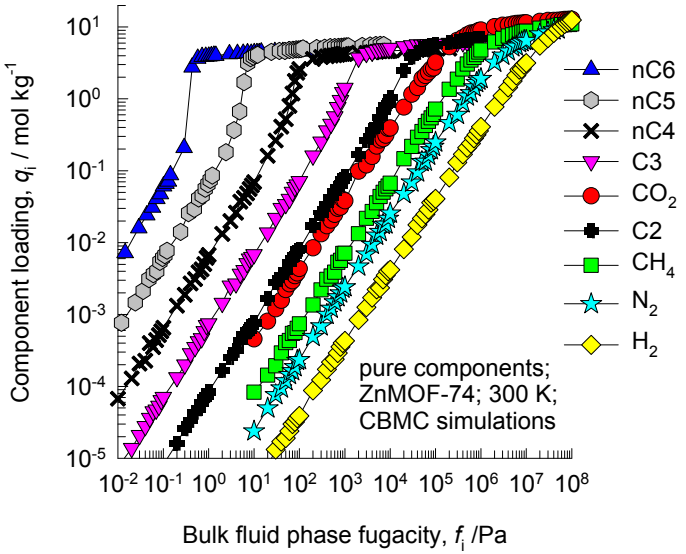

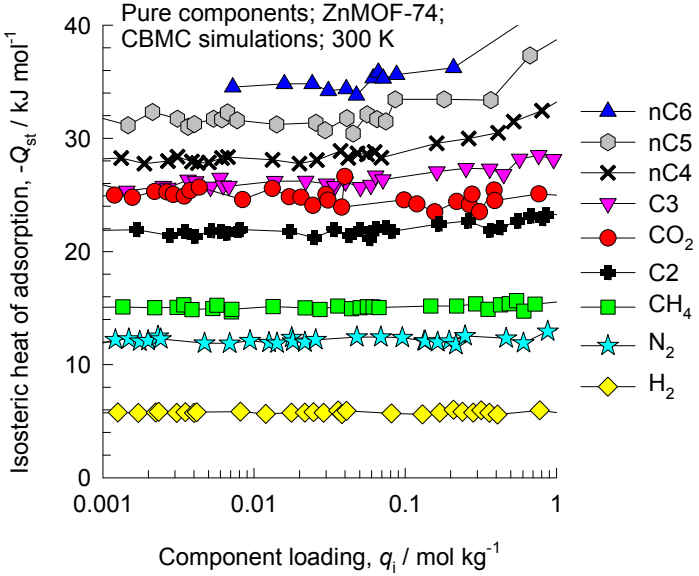

Influence of Inverse Thermodynamic Factor on diffusivities

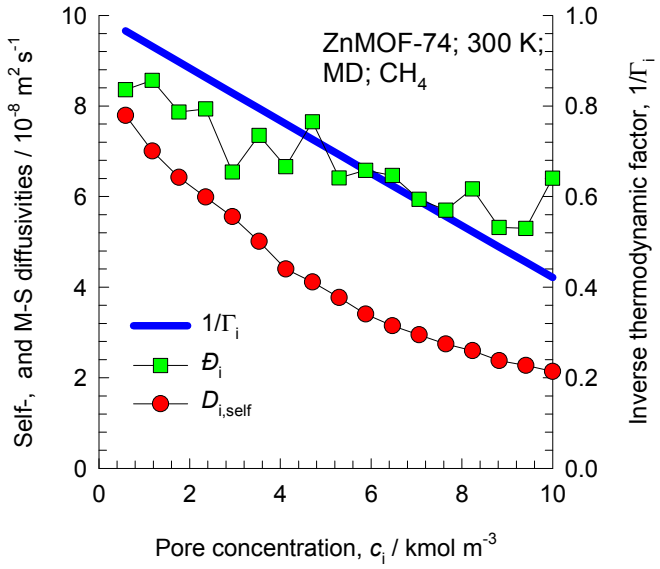

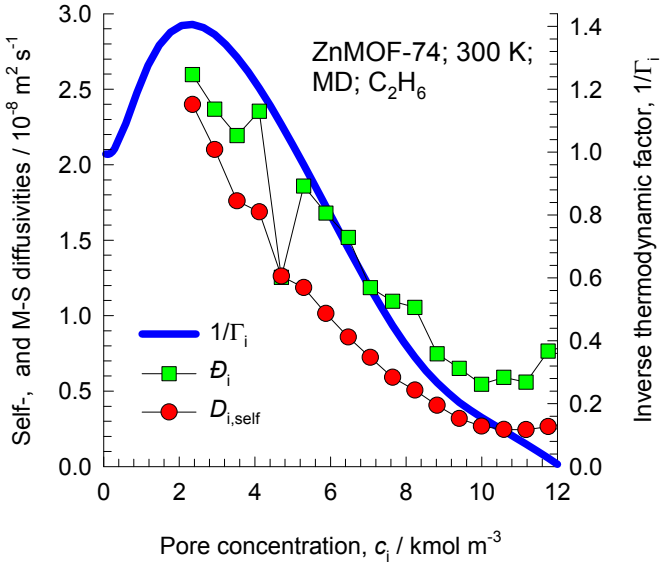

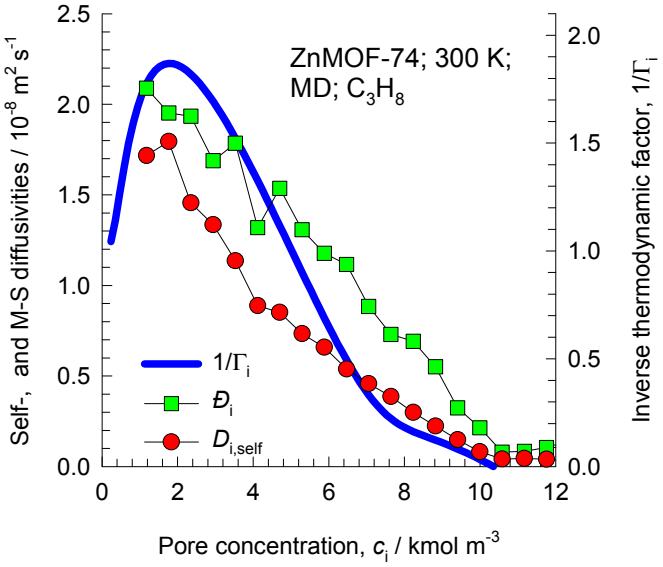

NiMOF-74 pore landscapes

The structural information on NiMOF-74 (= Ni_2(dobdc) = Ni\(dobdc = CPO-27-Ni) with dobdc = ($dobdc^{4-}$ = 2,5-dioxido-1,4-benzenedicarboxylatee)) were obtained from

A.Ö. Yazaydın, R.Q. Snurr, T.H. Park, K. Koh, J. Liu, M.D. LeVan, A.I. Benin, P. Jakubczak, M. Lanuza, D.B. Galloway, J.J. Low, R.R. Willis, Screening of Metal-Organic Frameworks for Carbon Dioxide Capture from Flue Gas using a Combined Experimental and Modeling Approach, J. Am. Chem. Soc. 131 (2009) 18198-18199.
D. Britt, H. Furukawa, B. Wang, T.G. Glover, O.M. Yaghi, Highly efficient separation of carbon dioxide by a metal-organic framework replete with open metal sites, Proc. Natl. Acad. Sci. U.S.A. 106 (2009) 20637-20640.
N.L. Rosi, J. Kim, M. Eddaoudi, B. Chen, M. O'Keeffe, O.M. Yaghi, Rod Packings and Metal-Organic Frameworks Constructed from Rod-Shaped Secondary Building Units, J. Am. Chem. Soc. 127 (2005) 1504-1518.
P.D.C. Dietzel, B. Panella, M. Hirscher, R. Blom, H. Fjellvåg, Hydrogen adsorption in a nickel based coordination polymer with open metal sites in the cylindrical cavities of the desolvated framework, Chem. Commun. (2006) 959-961.
P.D.C. Dietzel, V. Besikiotis, R. Blom, Application of metal–organic frameworks with coordinatively unsaturated metal sites in storage and separation of methane and carbon dioxide, J. Mater. Chem. 19 (2009) 7362-7370.
S.R. Caskey, A.G. Wong-Foy, A.J. Matzger, Dramatic Tuning of Carbon Dioxide Uptake via Metal Substitution in a Coordination Polymer with Cylindrical Pores, J. Am. Chem. Soc. 130 (2008) 10870-10871.

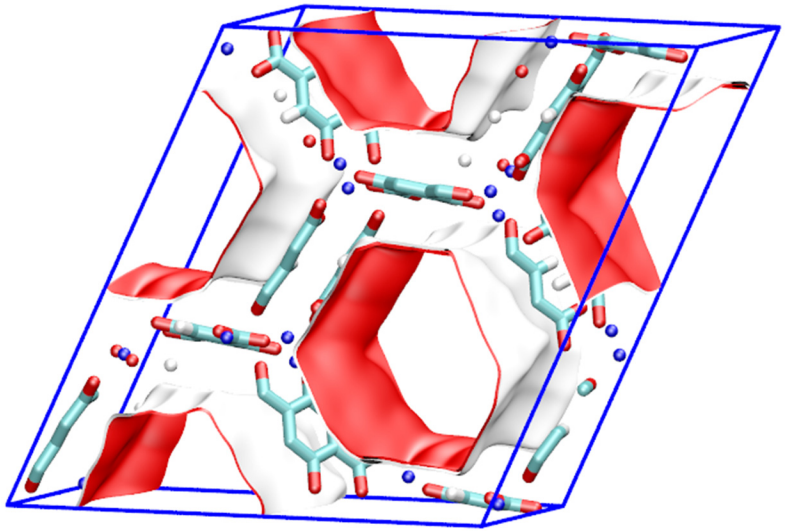

Electronic Supplementary Material (ESI) for Physical Chemistry Chemical Physics

NiMOF-74 pore dimensions

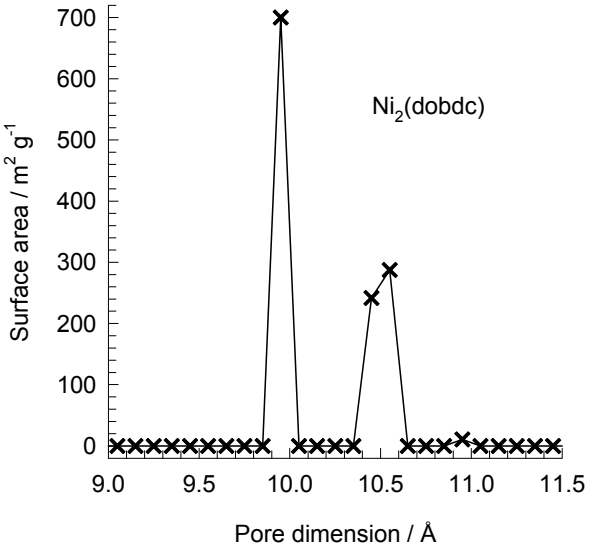

This plot of surface area versus pore dimension is determined using a combination of the DeLaunay triangulation method for pore dimension determination, and the procedure of Düren for determination of the surface area.

	NiMOF-74
a /Å	25.7856
b /Å	25.7856
c /Å	6.7701
Cell volume / Å^3	3898.344
conversion factor for [molec/uc] to [mol per kg Framework]	0.3568
conversion factor for [molec/uc] to [kmol/m^3]	0.6133
ρ [kg/m3]	1193.811
MW unit cell [g/mol(framework)]	2802.592
ϕ, fractional pore volume	0.695
open space / Å^3/uc	2707.6
Pore volume / cm^3/g	0.582
Surface area /m^2/g	1239.0
DeLaunay diameter /Å	9.80

NiMOF-74 isotherms and isosteric heats of adsorption from experiments

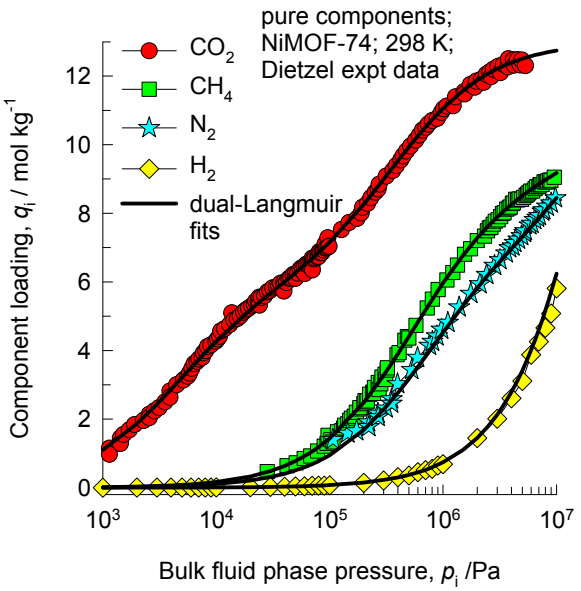

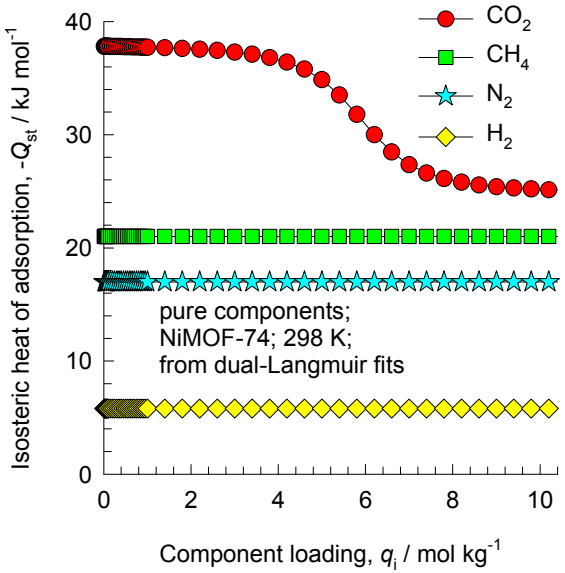

The pure component isotherms, with fits, and isosteric heats of adsorption are those reported by:

Krishna, R.; van Baten, J.M. Investigating the Relative Influences of Molecular Dimensions and Binding Energies on Diffusivities of Guest Species Inside Nanoporous Crystalline Materials J. Phys. Chem. C 2012, 116, 23556-23568.

NiMOF-74: Analysis of membrane permeation experiments

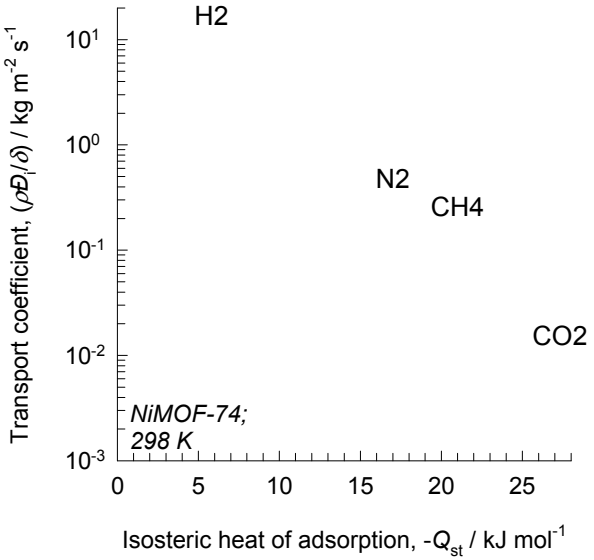

The membrane transport coefficients are the ones presented by:
Krishna, R.; van Baten, J.M. Investigating the Relative Influences of Molecular Dimensions and Binding Energies on Diffusivities of Guest Species Inside Nanoporous Crystalline Materials J. Phys. Chem. C 2012, 116, 23556-23568.

FeMOF-74 pore landscapes

The structural information on FeMOF-74 (= Fe_2(dobdc) = Fe\(dobdc = CPO-27-Fe) with dobdc = (dobdc^{4-} = 2,5-dioxido-1,4-benzenedicarboxylate)) was obtained from

Bloch et al. E.D. Bloch, L. Murray, W.L. Queen, S.M. Chavan, S.N. Maximoff, J.P. Bigi, R. Krishna, V.K. Peterson, F. Grandjean, G.J. Long, B. Smit, S. Bordiga, C.M. Brown, J.R. Long, Selective Binding of O_2 over N_2 in a Redox-Active Metal-Organic Framework with Open Iron(II) Coordination Sites, J. Am. Chem. Soc. 133 (2011) 14814-14822.

E.D. Bloch, W.L. Queen, R. Krishna, J.M. Zadrozny, C.M. Brown, J.R. Long, Hydrocarbon Separations in a Metal-Organic Framework with Open Iron(II) Coordination Sites, Science 335 (2012) 1606-1610.

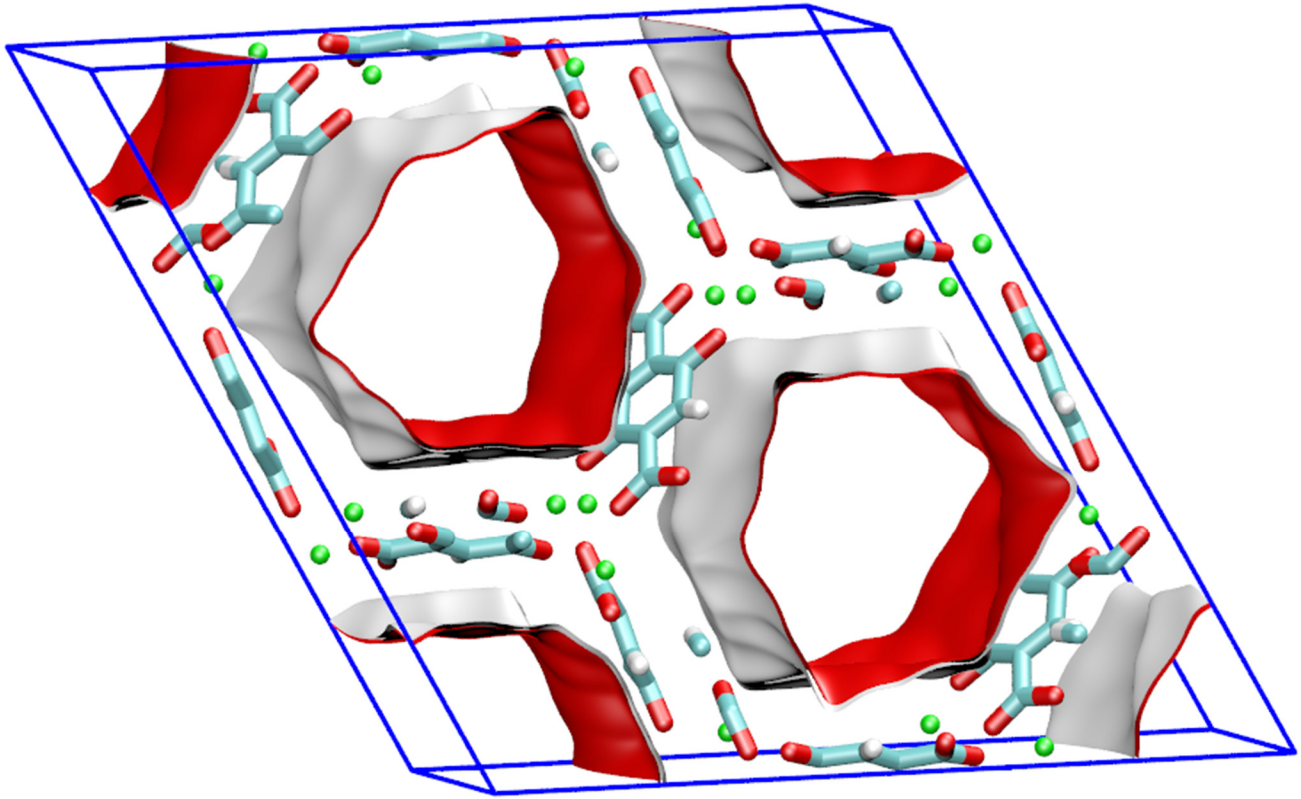

FeMOF-74 pore dimensions

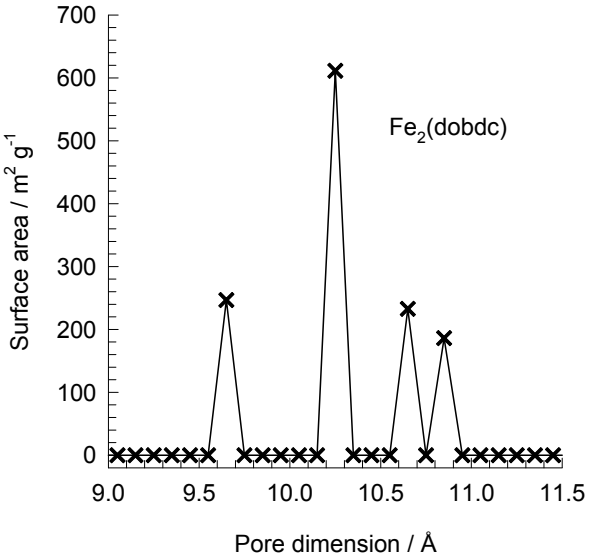

This plot of surface area versus pore dimension is determined using a combination of the DeLaunay triangulation method for pore dimension determination, and the procedure of Düren for determination of the surface area.

	FeMOF-74
a /Å	26.1627
b /Å	26.1627
c /Å	6.8422
Cell volume / Å^3	4055.94
conversion factor for [molec/uc] to [mol per kg Framework]	0.3635
conversion factor for [molec/uc] to [kmol/m^3]	0.5807
ρ [kg/m3]	1126.434
MW unit cell [g/mol (framework)]	2751.321
ϕ, fractional pore volume	0.705
open space / Å^3/uc	2859.7
Pore volume / cm^3/g	0.626
Surface area /m^2/g	1277.4
DeLaunay diameter /Å	11.12

FeMOF-74 isotherms and isosteric heats of adsorption from experiments

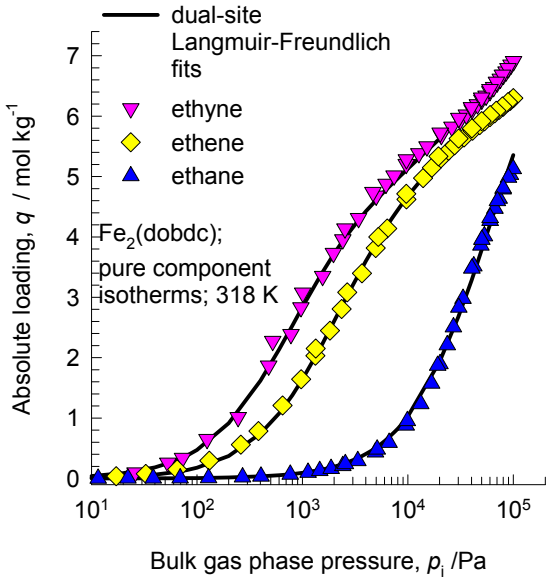

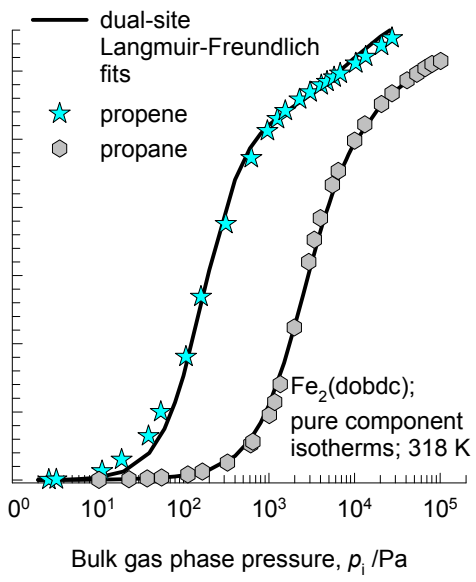

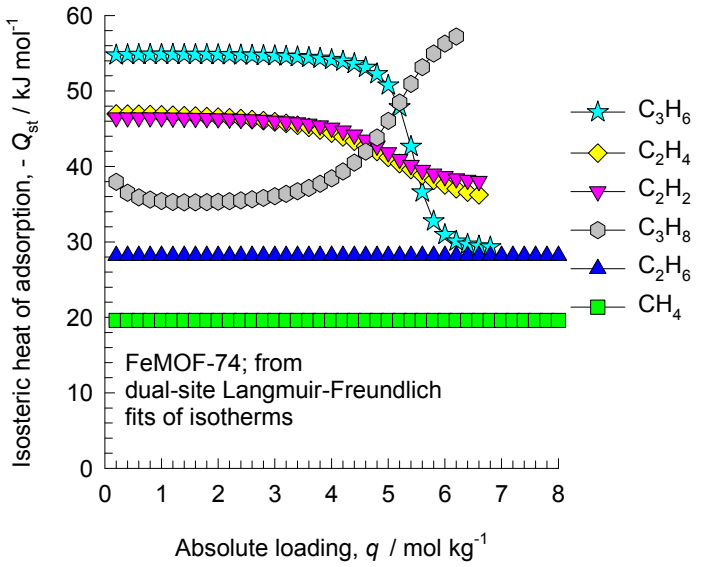

The pure component isotherms, with fits, and isosteric heats of adsorption are those reported by:
He, Y.; Krishna, R.; Chen, B. Metal-Organic Frameworks with Potential for Energy-Efficient Adsorptive Separation of Light Hydrocarbons. Energy Environ. Sci. 2012, 5, 9107-9120.

Electronic Supplementary Material (ESI) for Physical Chemistry Chemical Physics

CoMOF-74 pore landscapes

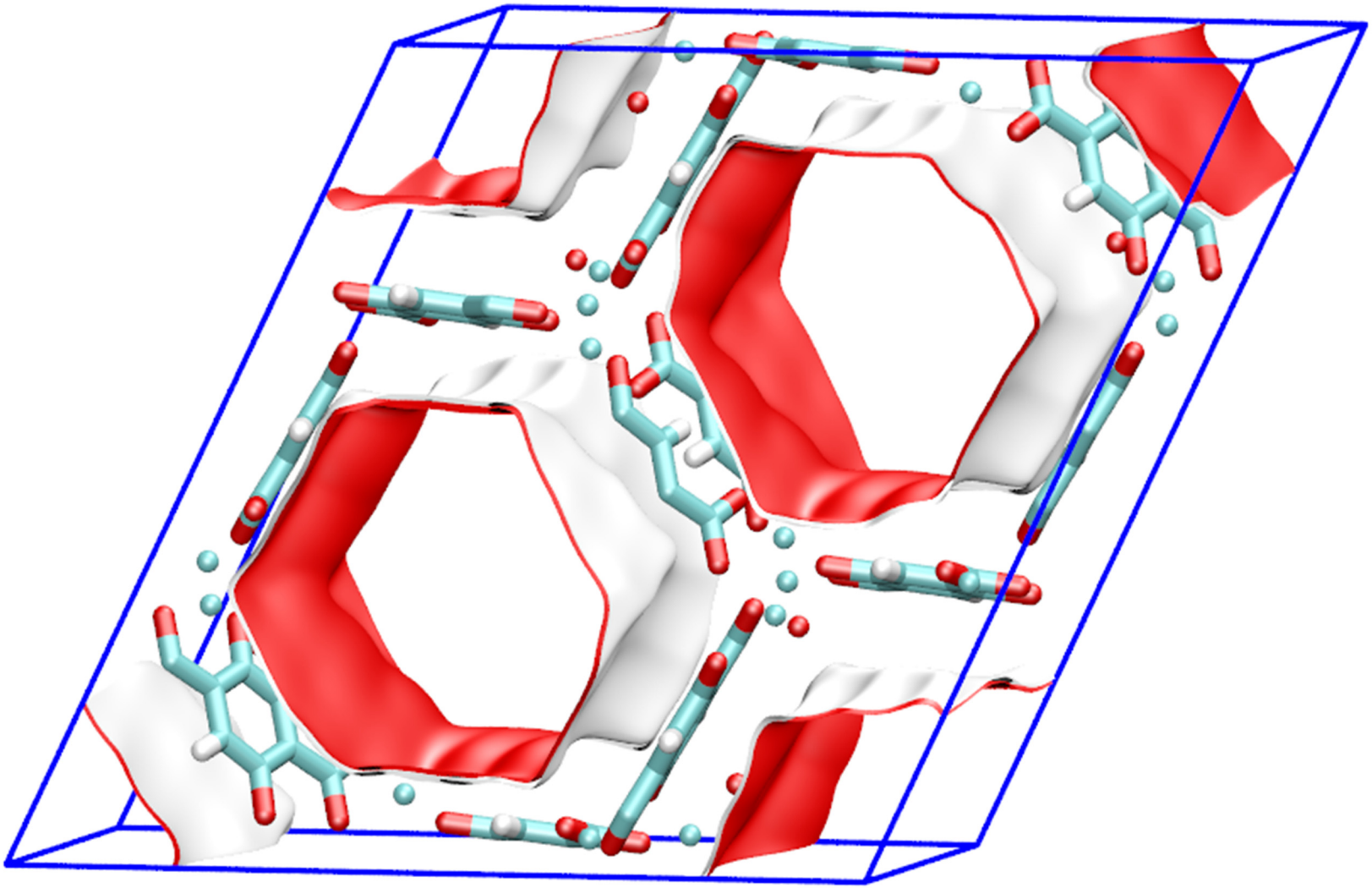

Electronic Supplementary Material (ESI) for Physical Chemistry Chemical Physics

CoMOF-74 pore dimensions

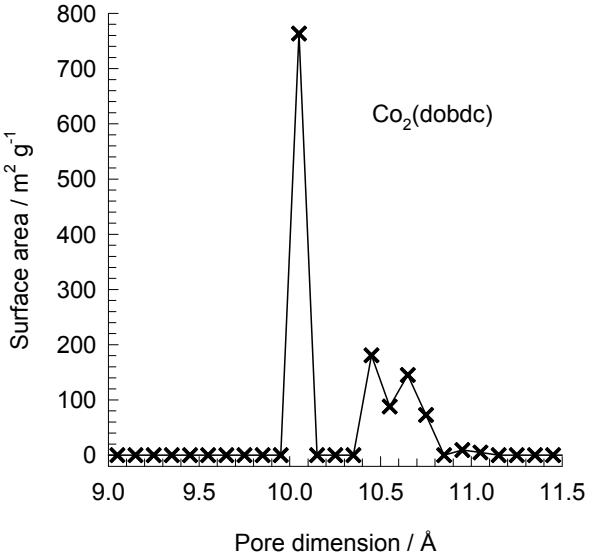

This plot of surface area versus pore dimension is determined using a combination of the DeLaunay triangulation method for pore dimension determination, and the procedure of Düren for determination of the surface area. The computational details will be described in detail in a forthcoming publication.

	CoMOF-74
a /Å	25.885
b /Å	25.885
c /Å	6.8058
Cell volume / Å^3	3949.173
conversion factor for [molec/uc] to [mol per kg Framework]	0.3563
conversion factor for [molec/uc] to [kmol/m^3]	0.5945
ρ [kg/m3]	1180.261
MW unit cell [g/mol(framework)]	2806.908
ϕ, fractional pore volume	0.707
open space / Å^3/uc	2793.1
Pore volume / cm^3/g	0.599
Surface area /m^2/g	1274.0
DeLaunay diameter /Å	9.52

CoMOF-74 isotherms and isosteric heats of adsorption from experiments

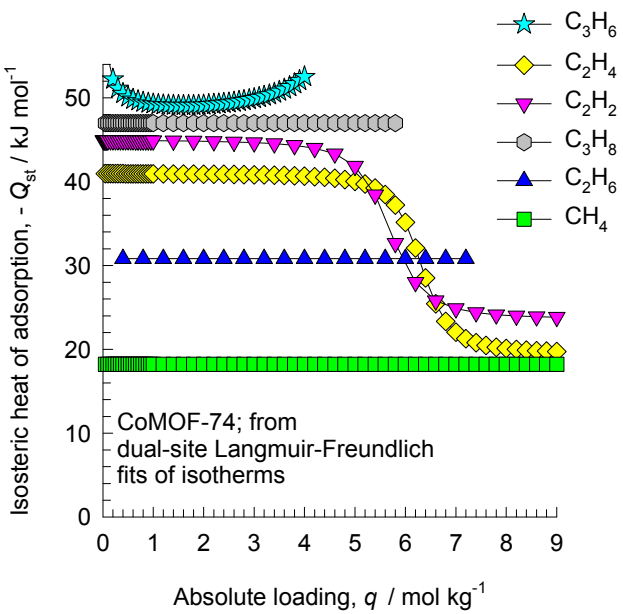

The pure component isotherms, with fits, and isosteric heats of adsorption are those reported by:
He, Y.; Krishna, R.; Chen, B. Metal-Organic Frameworks with Potential for Energy-Efficient Adsorptive Separation of Light Hydrocarbons. Energy Environ. Sci. 2012, 5, 9107-9120.

Electronic Supplementary Material (ESI) for Physical Chemistry Chemical Physics

MIL–47 pore landscape

The structural information for MIL-47 was taken from

L. Alaerts, C.E.A. Kirschhock, M. Maes, M. van der Veen, V. Finsy, A. Depla, J.A. Martens, G.V. Baron, P.A. Jacobs, J.F.M. Denayer, D. De Vos, Selective Adsorption and Separation of Xylene Isomers and Ethylbenzene with the Microporous Vanadium(IV) Terephthalate MIL-47, Angew. Chem. Int. Ed. 46 (2007) 4293-4297.

V. Finsy, H. Verelst, L. Alaerts, D. De Vos, P.A. Jacobs, G.V. Baron, J.F.M. Denayer, Pore-Filling-Dependent Selectivity Effects in the Vapor-Phase Separation of Xylene Isomers on the Metal-Organic Framework MIL-47, J. Am. Chem. Soc. 130 (2008) 7110-7118.

K. Barthelet, J. Marrot, D. Riou, G. Férey, A Breathing Hybrid Organic - Inorganic Solid with Very Large Pores and High Magnetic Characteristics, Angew. Chem. Int. Ed. 41 (2007) 281-284.

Snapshot of CO_2/CH_4 mixture

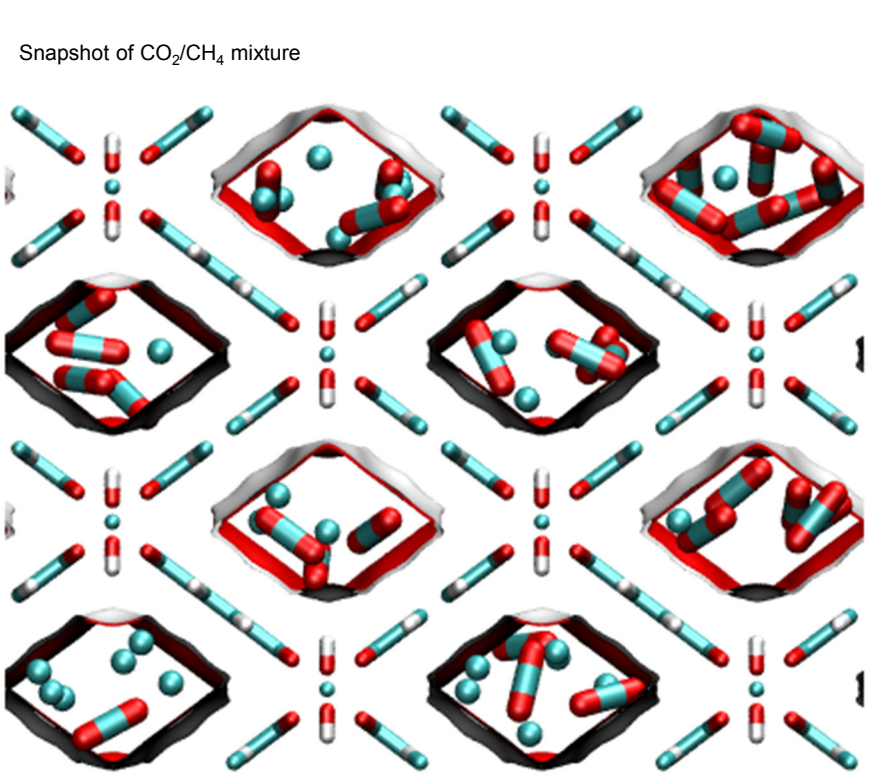

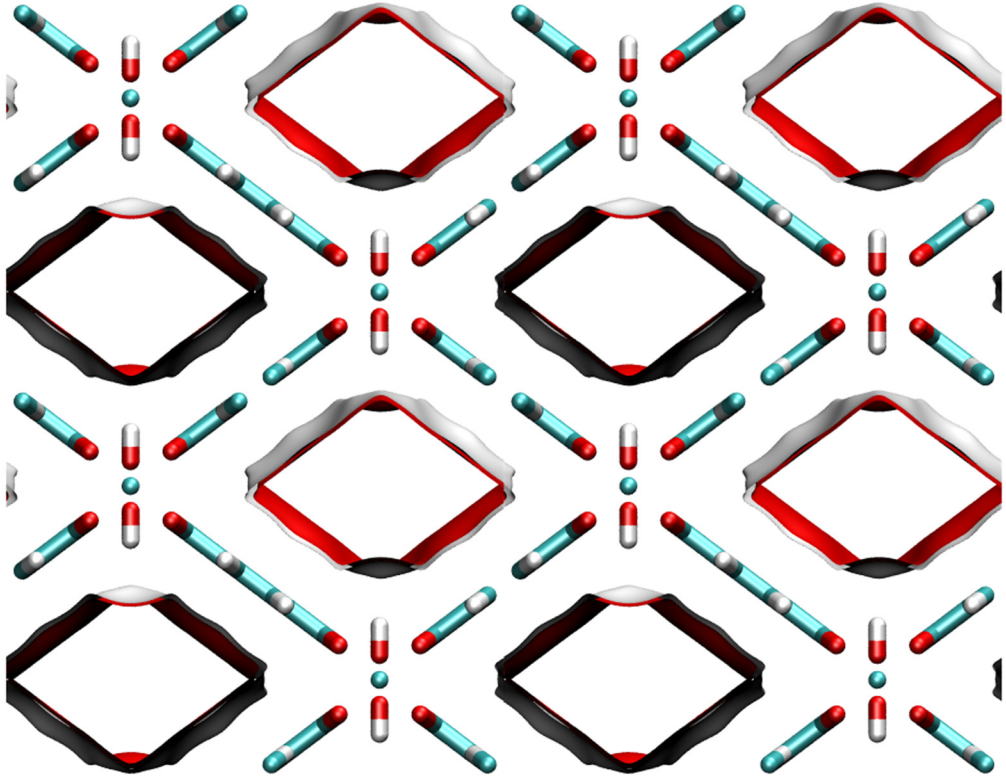

Electronic Supplementary Material (ESI) for Physical Chemistry Chemical Physics

MIL–47 dimensions

	MIL-47
a /Å	6.808
b /Å	16.12
c /Å	13.917
Cell volume / Å^3	1527.321
conversion factor for [molec/uc] to [mol per kg Framework]	1.0824
conversion factor for [molec/uc] to [kmol/m^3]	1.7868
ρ [kg/m3]	1004.481
MW unit cell [g/mol(framework)]	923.881
ϕ, fractional pore volume	0.608
open space / Å^3/uc	929.3
Pore volume / cm^3/g	0.606
Surface area /m^2/g	1472.8
DeLaunay diameter /Å	8.03

One-dimensional diamond-shaped channels with free internal diameter of 8Å

MIL-47 CBMC simulations of isotherms, and isosteric heats of adsorption

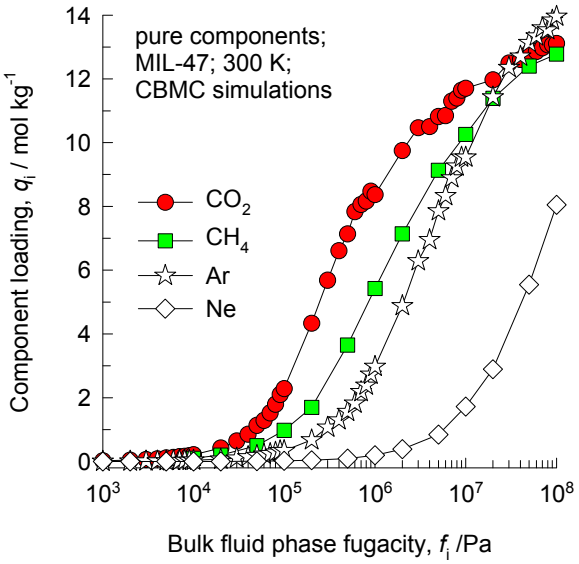

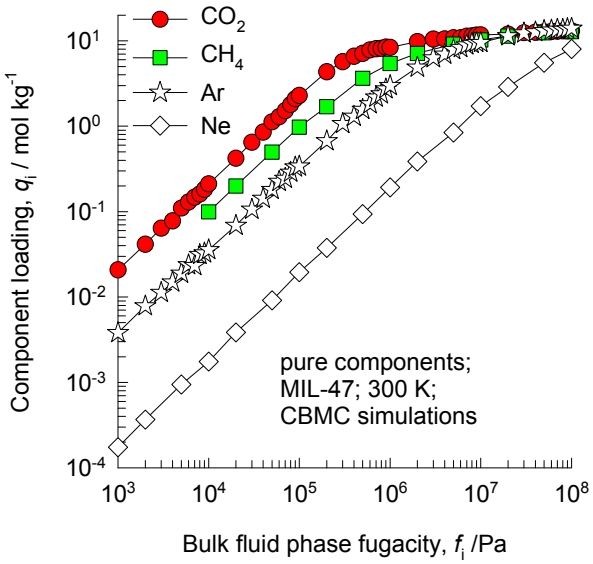

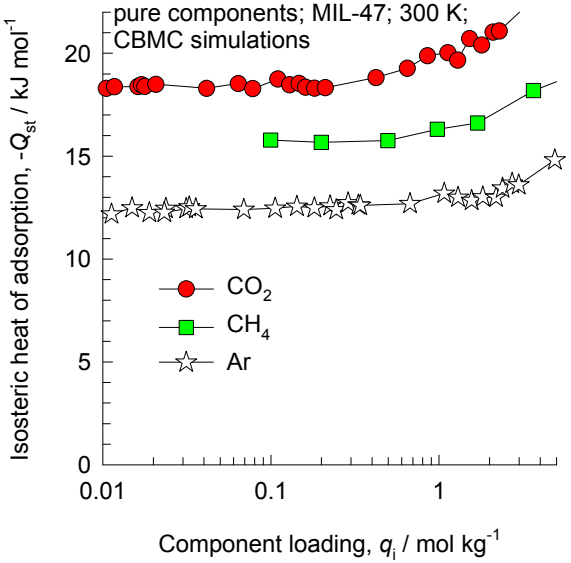

Influence of Inverse Thermodynamic Factor on diffusivities

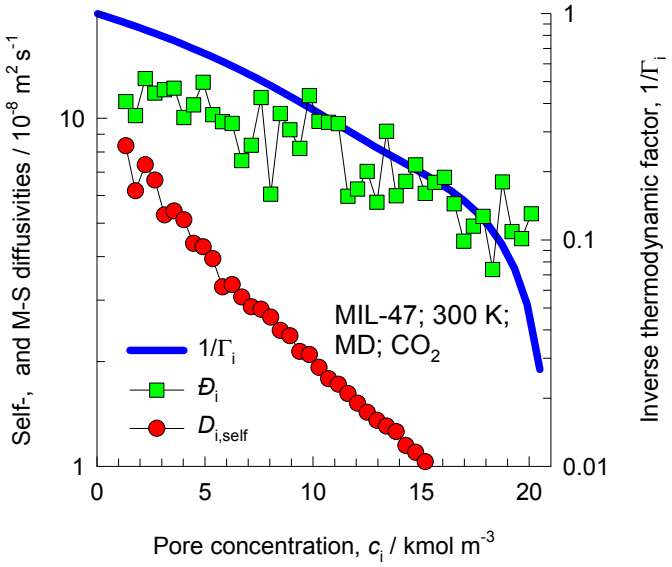

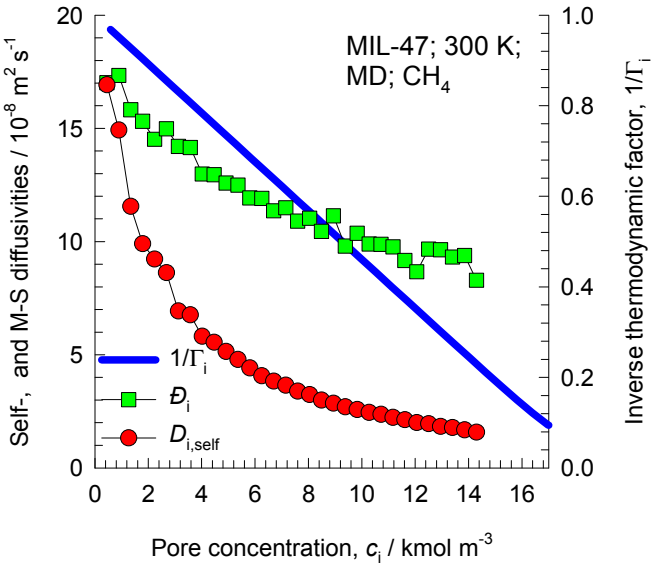

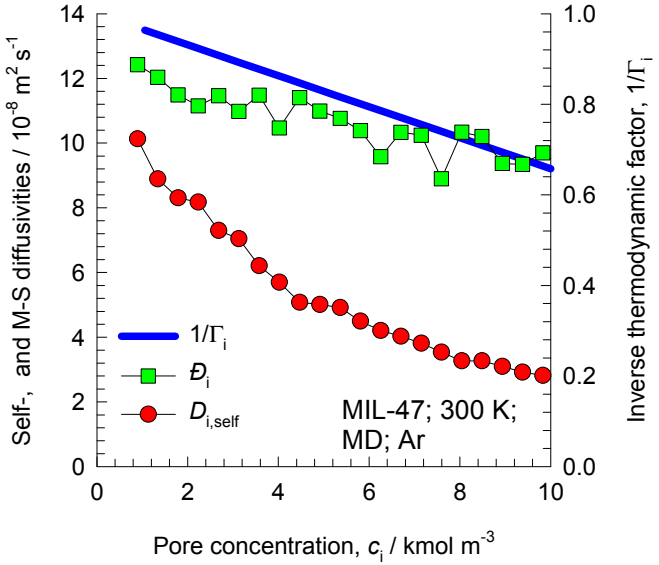

Influence of Inverse Thermodynamic Factor on diffusivities

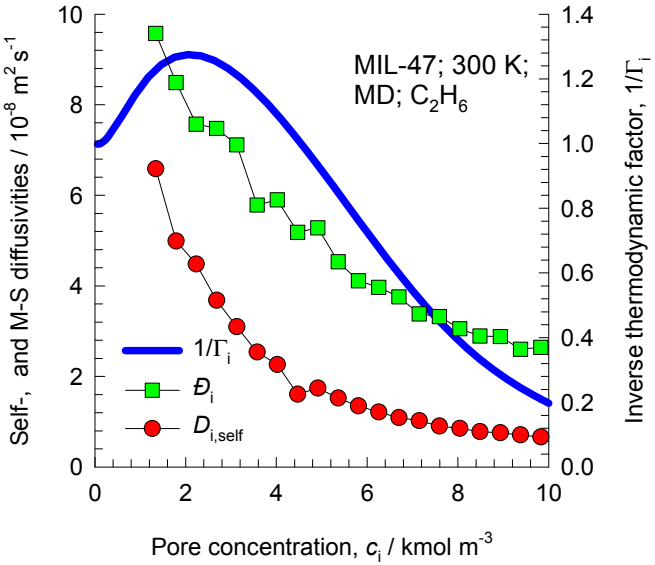

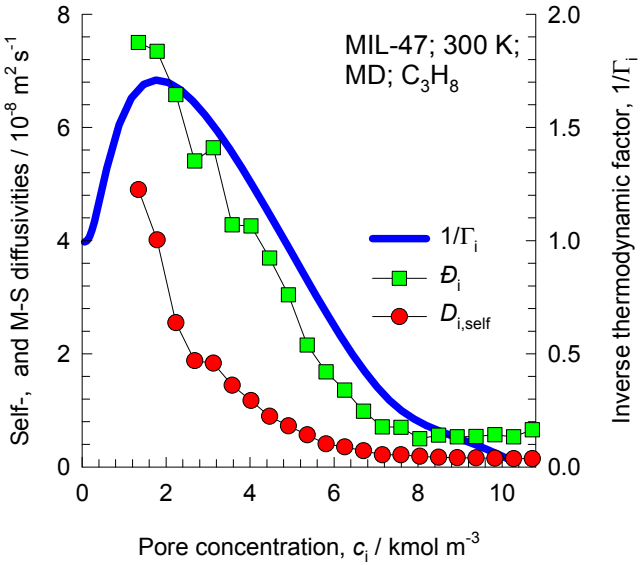

MIL-47 CO_2 adsorption and diffusion

The RDFs show that the degree of clustering increases as the temperature is decreased.

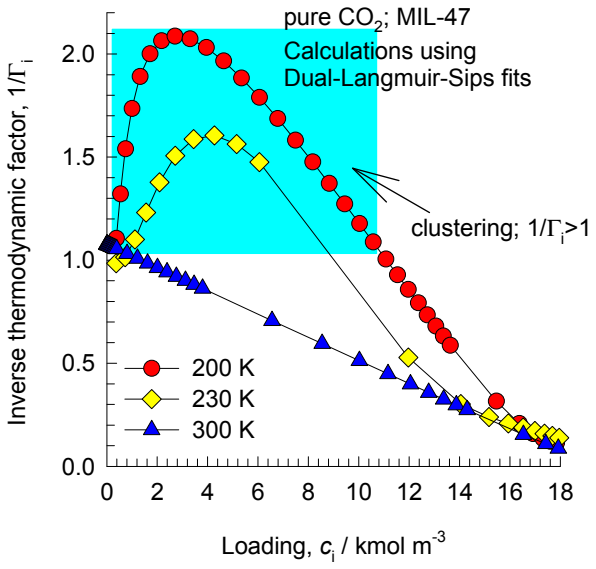

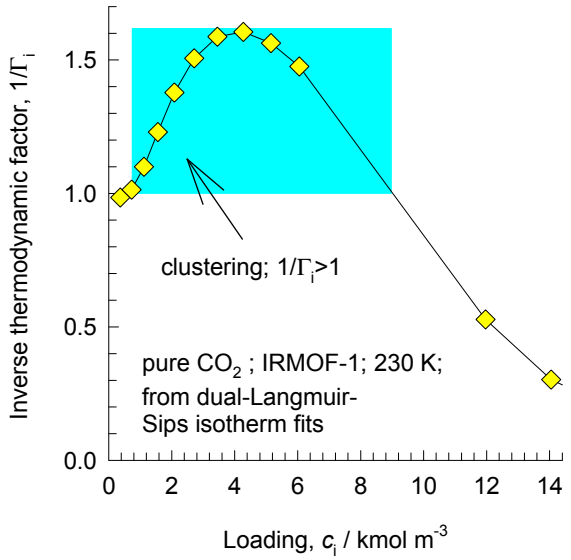

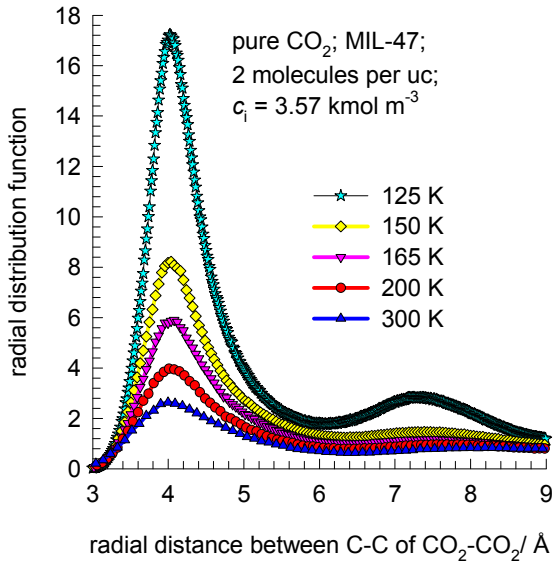

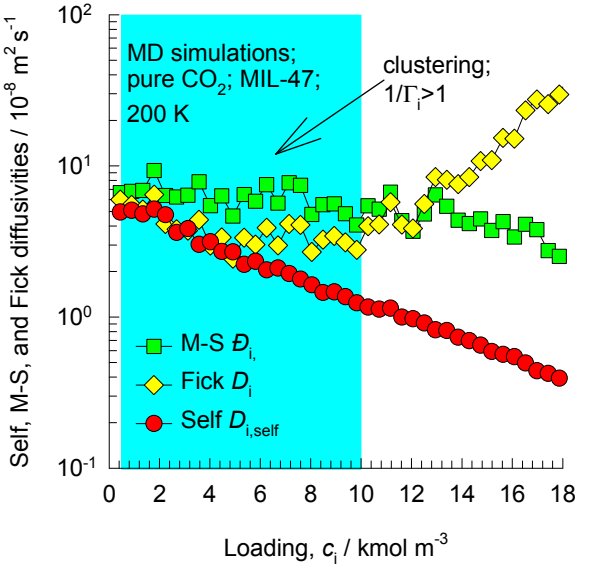

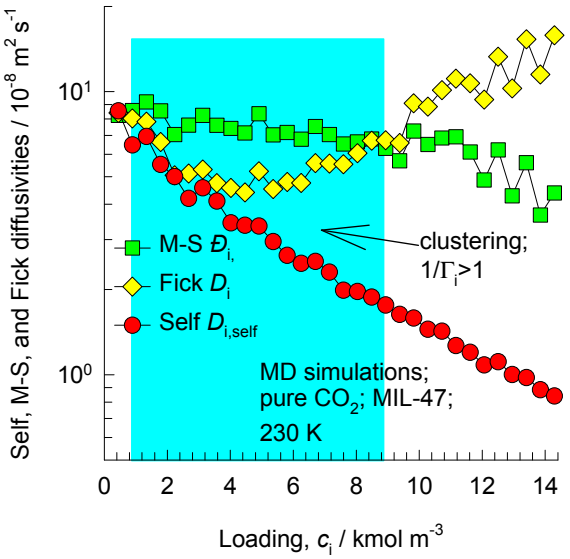

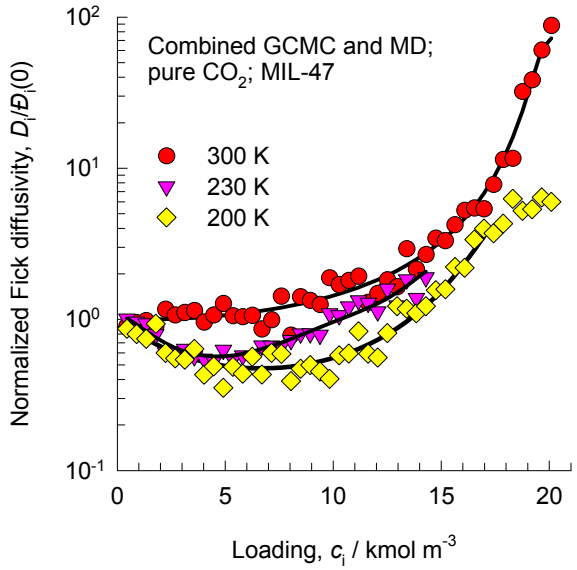

MIL-47 CO_2 adsorption and diffusion; analysis of Salles et al. expt data

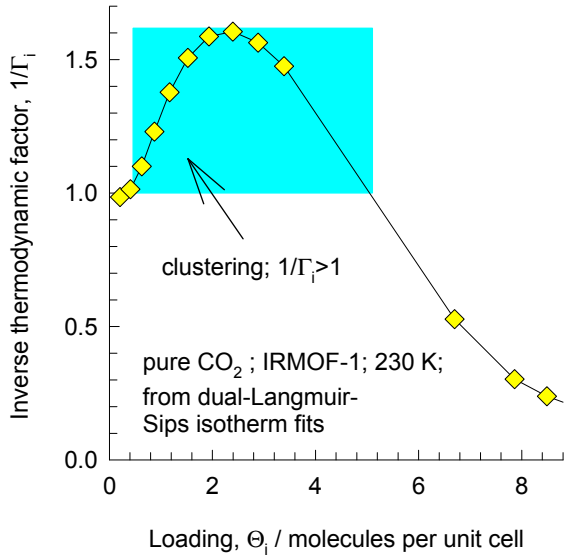

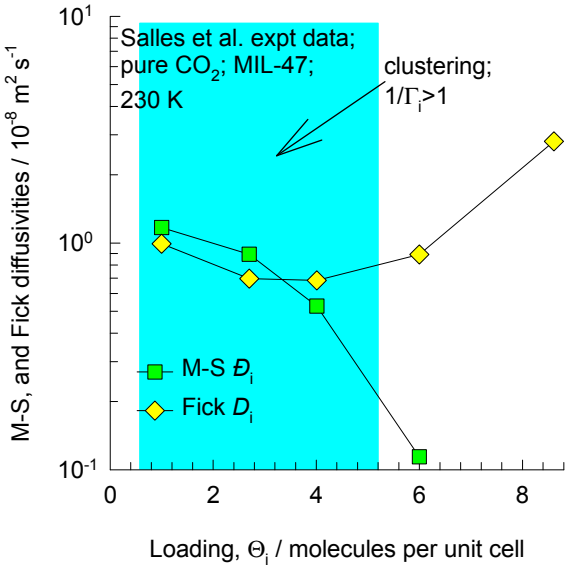

These are our CBMC simulation results, not those of Salles et al.

The experimental results of F. Salles, H. Jobic, T. Devic, P.L. Llewellyn, C. Serre, G. Férey, G. Maurin, Self and Transport Diffusivity of CO2 in the Metal-Organic Framework MIL-47(V) Explored by Quasi-elastic Neutron Scattering Experiments and Molecular Dynamics Simulations, ACS Nano 2010, 4, 143-152, show that the Fick diffusivity can be lower than the Maxwell-Stefan diffusivity in regions where clustering of molecules occurs. The Fick diffusivity decreases with loading in the regions in which $1/\Gamma_i > 1$. Please also note that the Salles data on diffusivities is spatially averaged over x, y, and z directions. Our MD data in the previous slide is for diffusion in the x-direction. So our diffusivities are expected to be about 3 times higher.

Electronic Supplementary Material (ESI) for Physical Chemistry Chemical Physics

MIL-47 CH_4 adsorption and diffusion

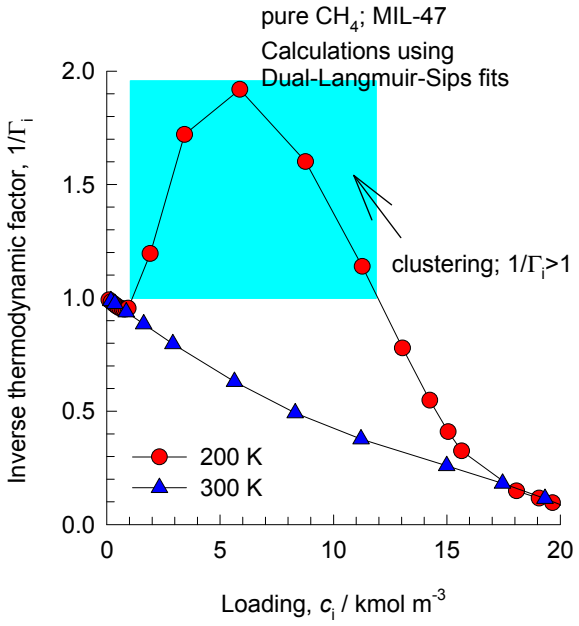

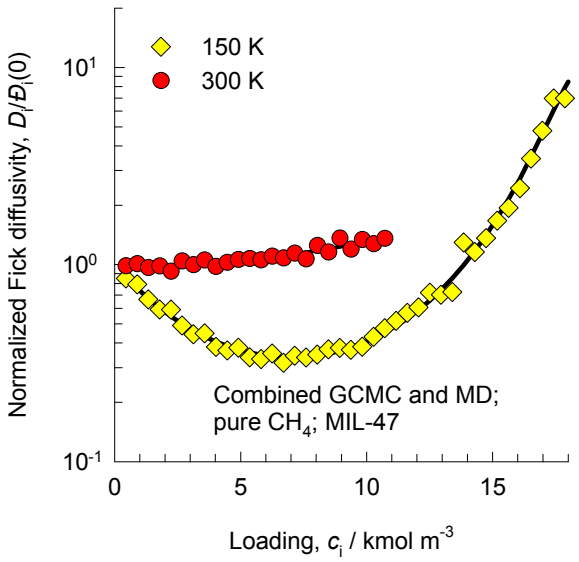

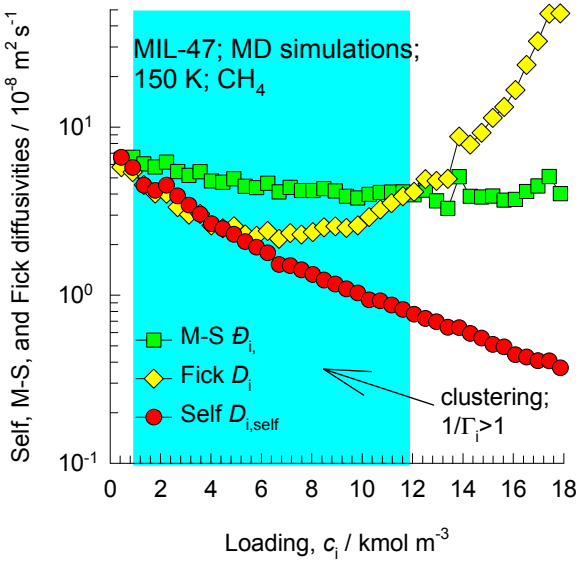

Electronic Supplementary Material (ESI) for Physical Chemistry Chemical Physics

MIL-47 Ar adsorption and diffusion

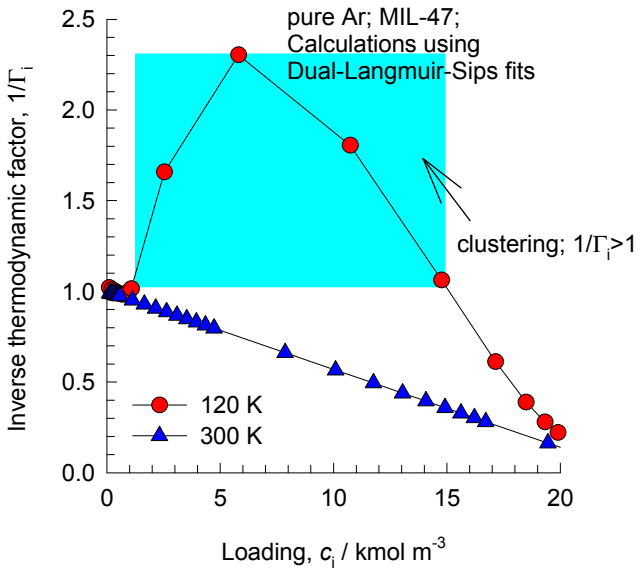

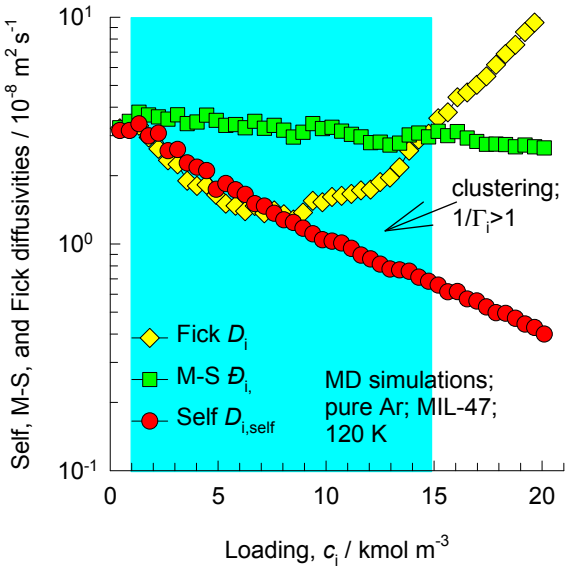

MIL-47 CBMC simulation results for CO_2-CH_4 mixtures

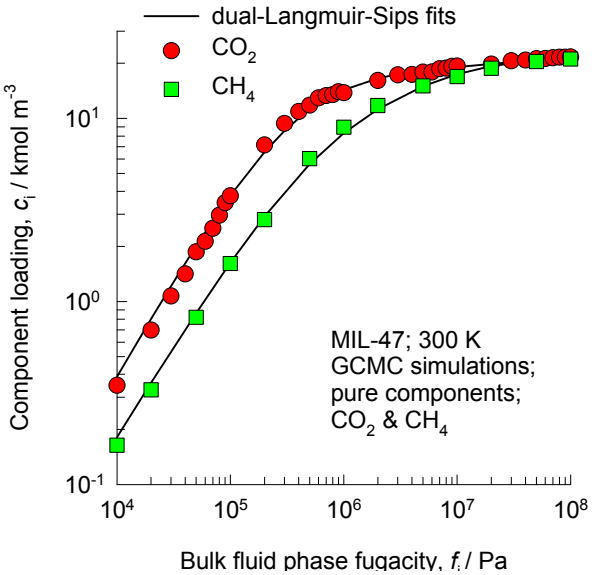

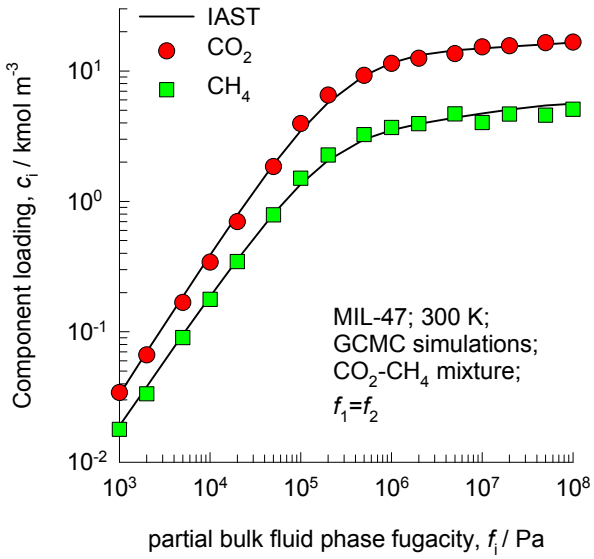

The IAST provides a good estimation of component loadings in the mixture.

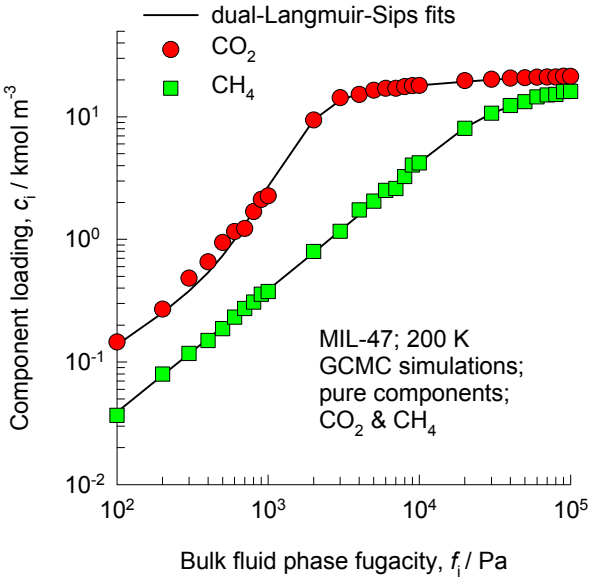

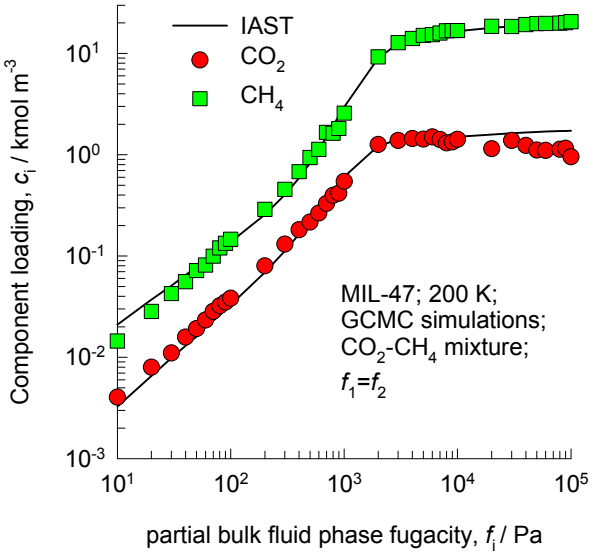

MIL-47 RDFs for CO_2-CH_4 mixtures

The RDFs are based on distances between the centres of mass of the molecules.

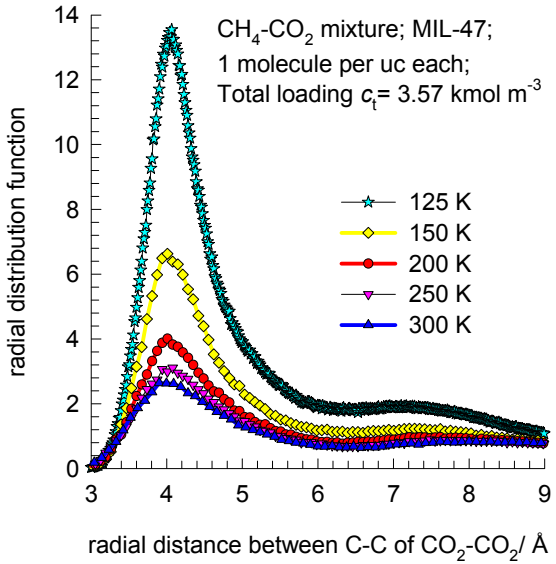

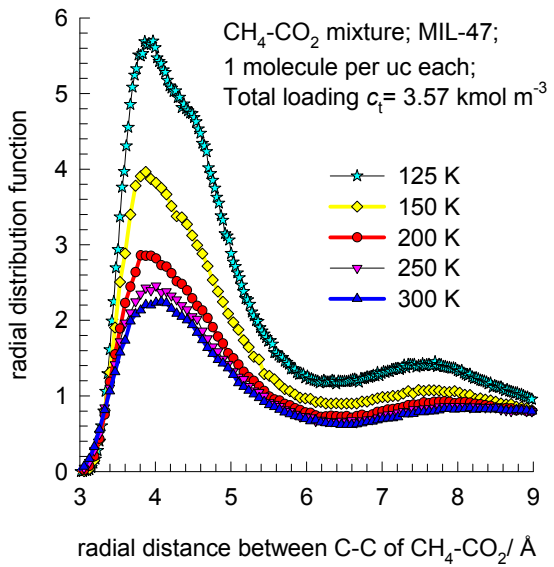

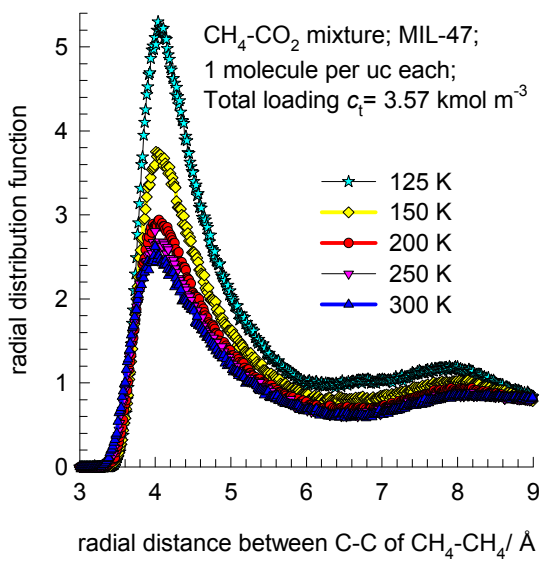

The RDFs demonstrate that clustering persists in mixtures, and increases with decreasing temperature

Electronic Supplementary Material (ESI) for Physical Chemistry Chemical Physics

MIL-47 adsorption of xylene isomers

These simulation results are from Castillo, J. M.; Vlugt, T. J. H.; Calero, S. J. Phys. Chem. C 2009, 113, 20869-20874.

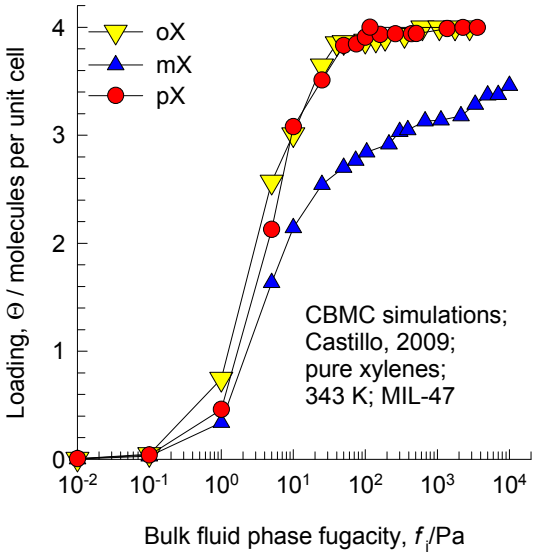

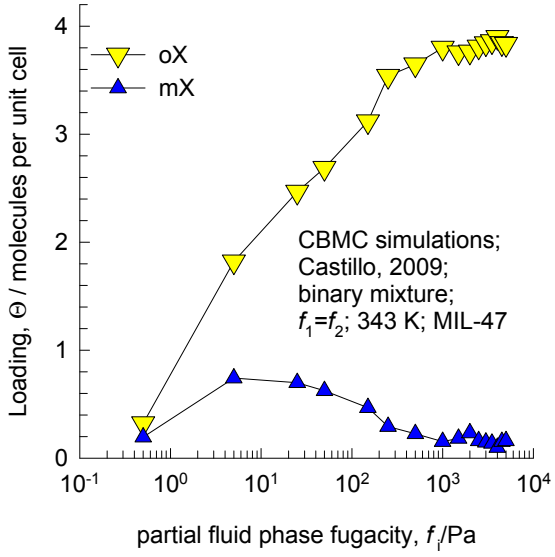

The adsorption selectivity hierarchy oX>mX is dictated by the hierarchy of critical temperatures, i.e. degree of clustering. The degree of clustering has to be interpreted somewhat differently. As can be seen in the snapshots of the location of o-, p-, and m- xylenes in the following three slides, the xylene isomers stack nicely within the channels of MIL-47. The stacking efficiency for o- and p- isomers are significantly superior to that of the m- isomer, as evidenced from the snapshots.

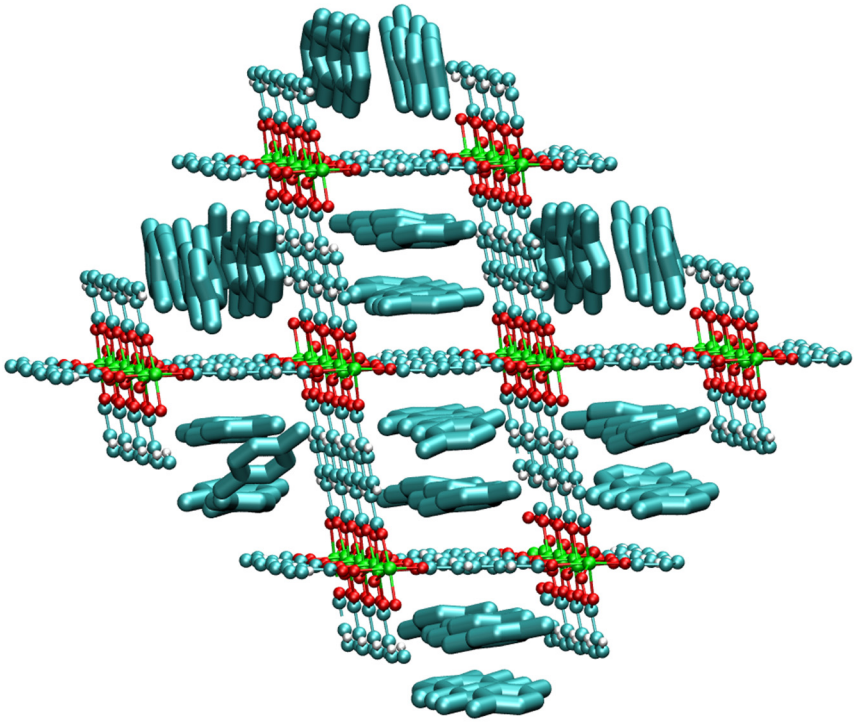

p-xylene

o-xylene and p-xylene appear to pack the channels very well

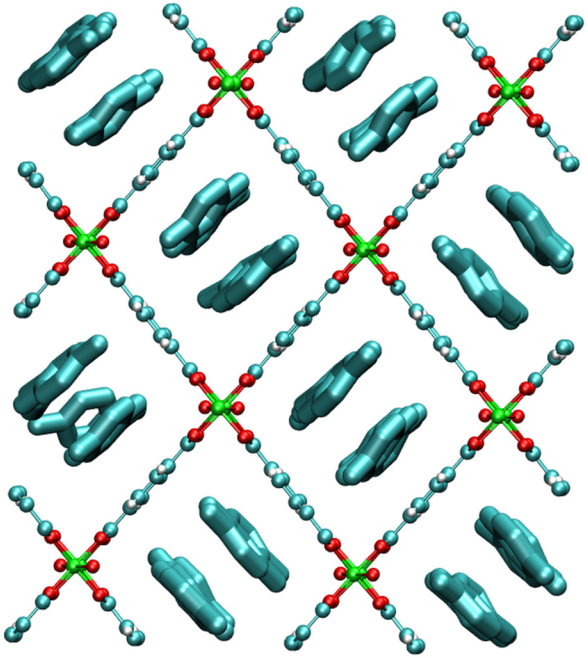

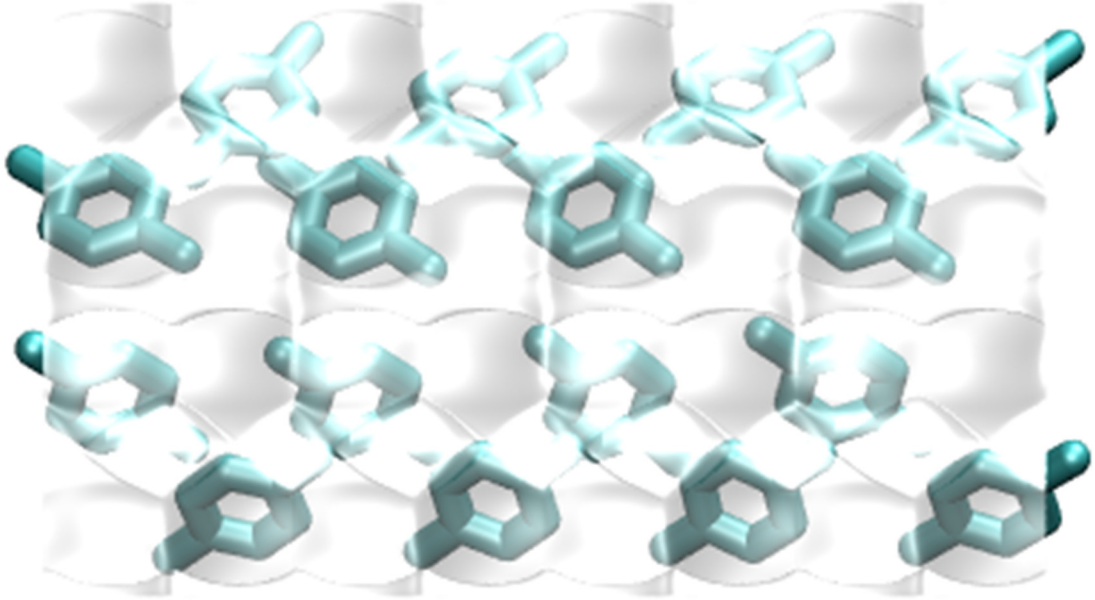

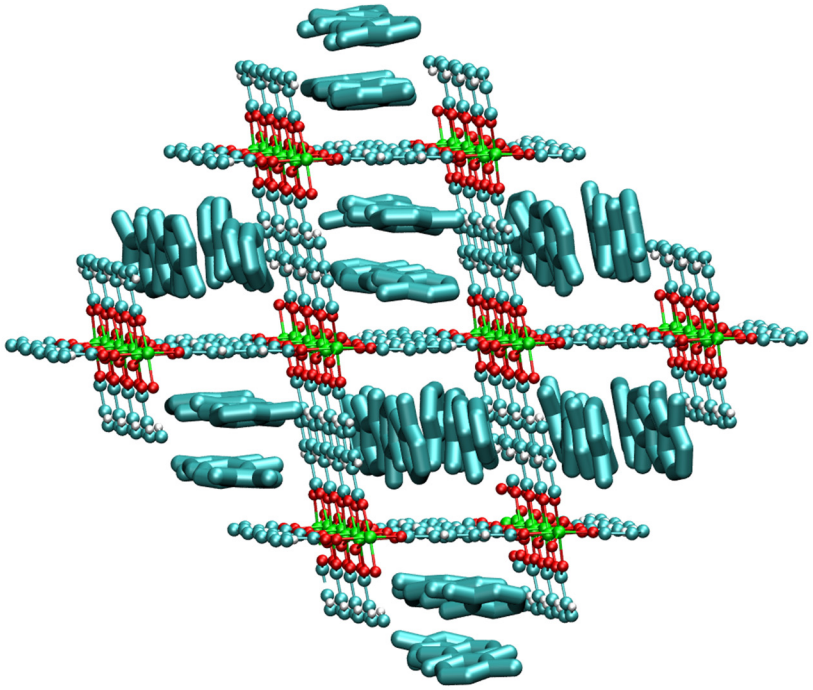

o-xylene

o-xylene and p-xylene appear to pack the channels very well

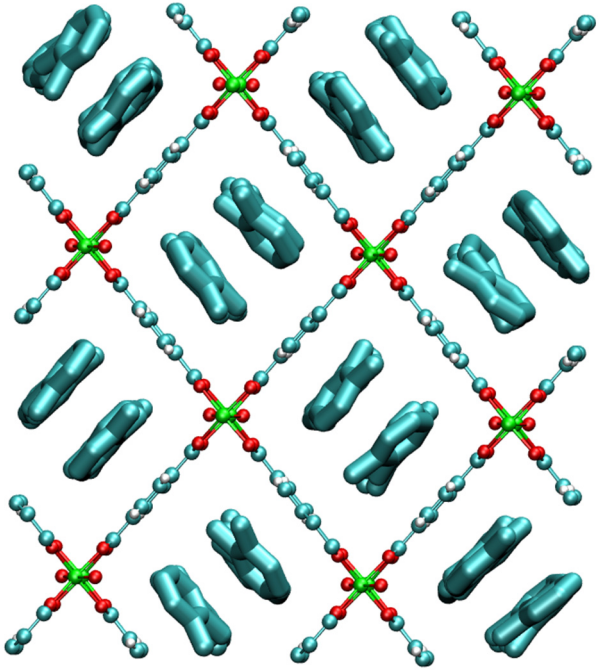

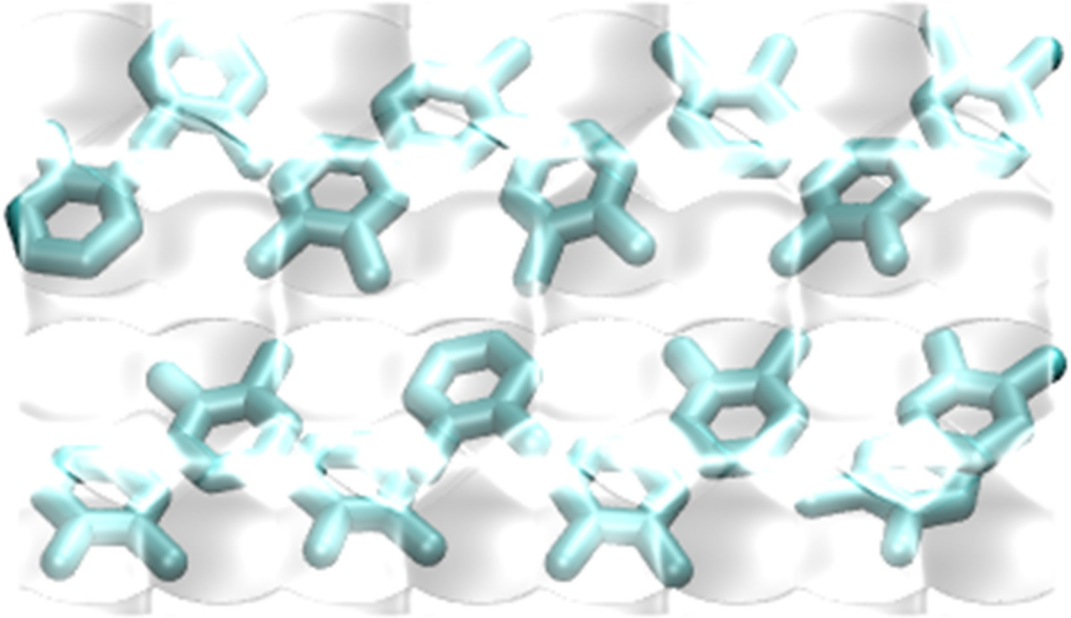

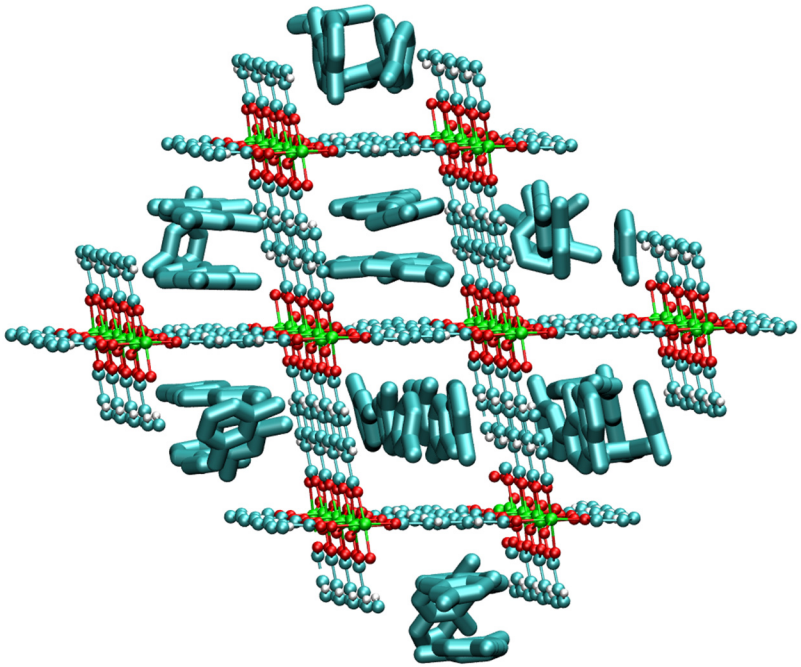

m-xylene

m-xylene does not pack the channels as well as o- and p-xylene. This is also evidenced in the snapshots.

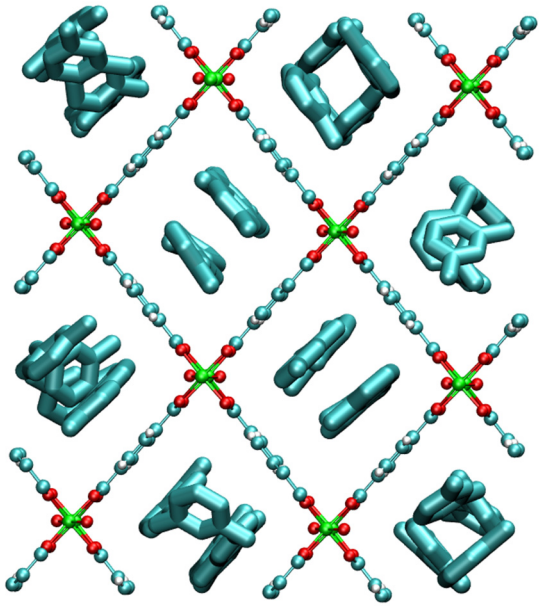

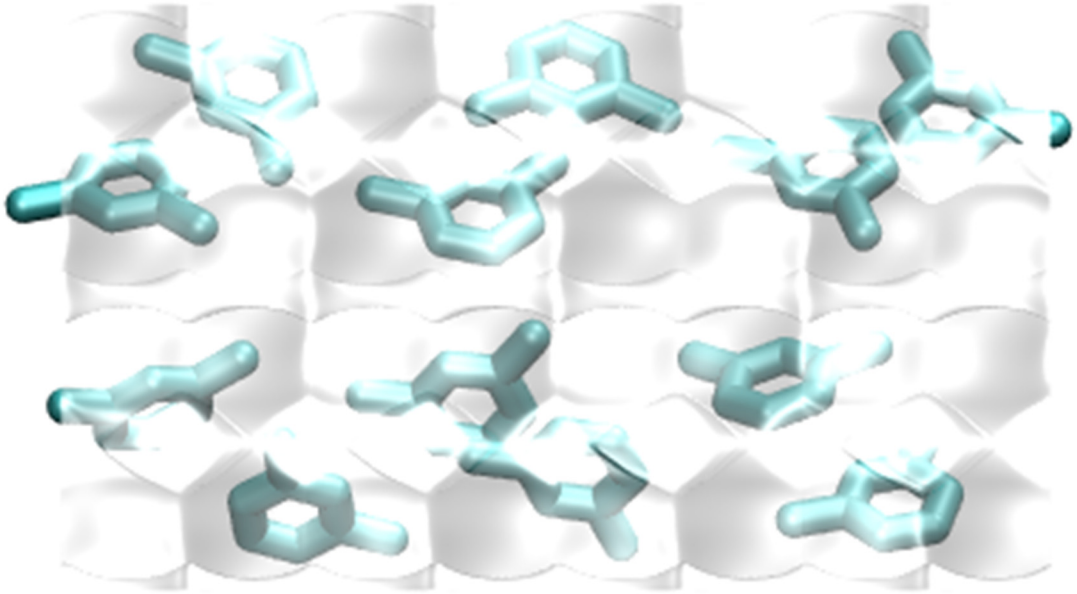

MIL – 53 (Cr) pore landscape

The structural data for MIL-53 (Cr) = $Cr(OH)(O_2C\text{-}C_6H_4\text{-}CO_2)$ was taken from

D.S. Coombes, F. Corà, C. Mellot-Draznieks, R.G. Bell, Sorption-Induced Breathing in the Flexible Metal Organic Framework CrMIL-53: Force-Field Simulations and Electronic Structure Analysis, J. Phys. Chem. C 113 (2009) 544-552.

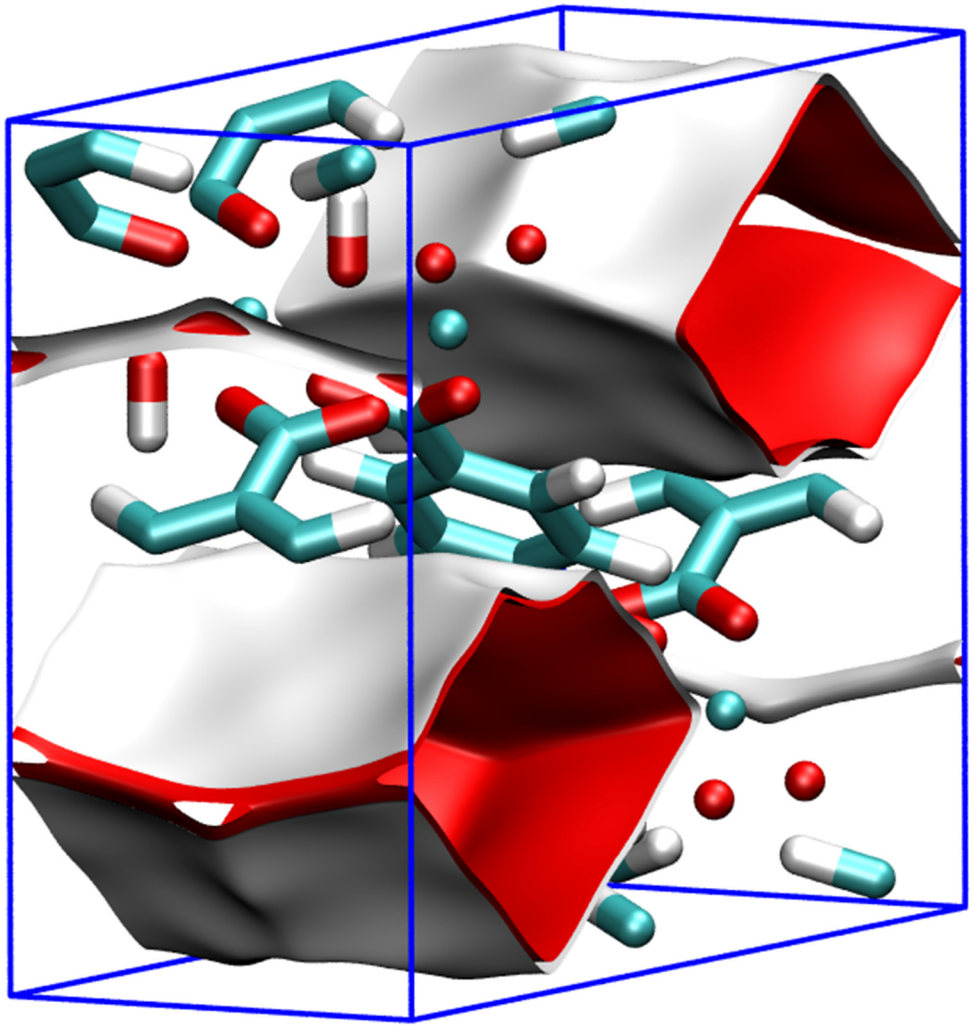

Simulation results presented are for –lp structure, i.e. large pore

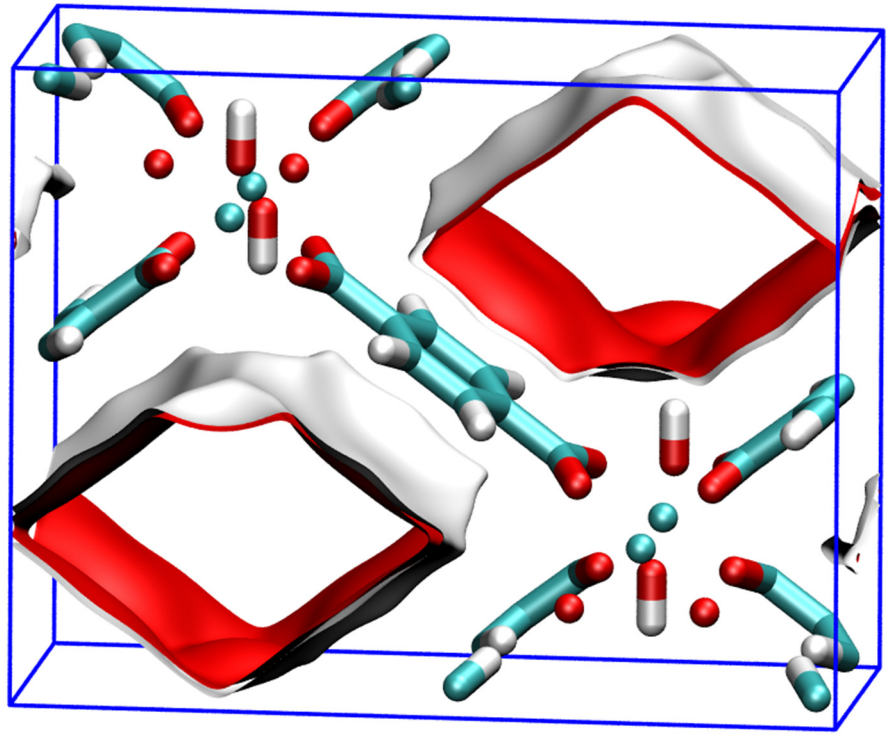

MIL–53 (Cr) pore dimensions

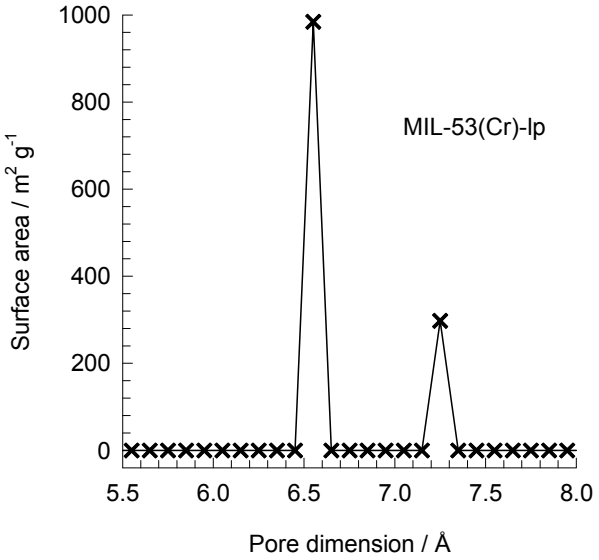

This plot of surface area versus pore dimension is determined using a combination of the DeLaunay triangulation method for pore dimension determination, and the procedure of Düren for determination of the surface area.

	MIL53(Cr)-lp
a /Å	16.733
b /Å	13.038
c /Å	6.812
Cell volume / Å^3	1486.139
conversion factor for [molec/uc] to [mol per kg Framework]	1.0728
conversion factor for [molec/uc] to [kmol/m^3]	2.0716
ρ [kg/m3]	1041.534
MW unit cell [g/mol(framework)]	932.1312
ϕ, fractional pore volume	0.539
open space / Å^3/uc	801.6
Pore volume / cm^3/g	0.518
Surface area /m^2/g	1280.5
DeLaunay diameter /Å	7.40

One-dimensional lozenge-shaped channels

Influence of Inverse Thermodynamic Factor on diffusivities

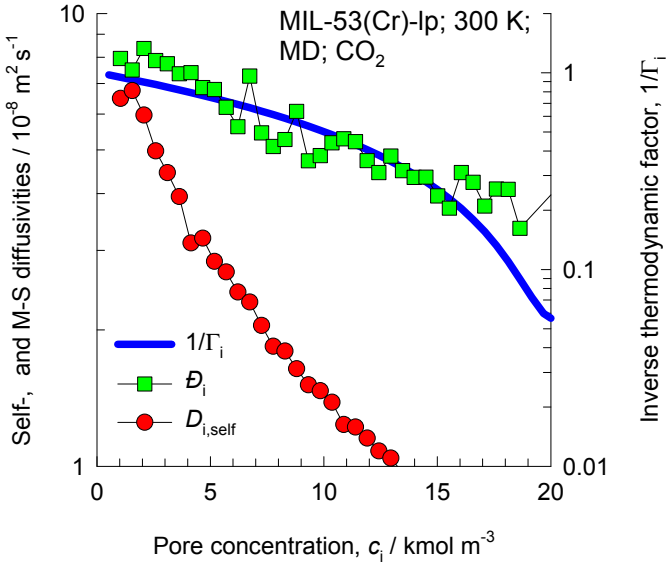

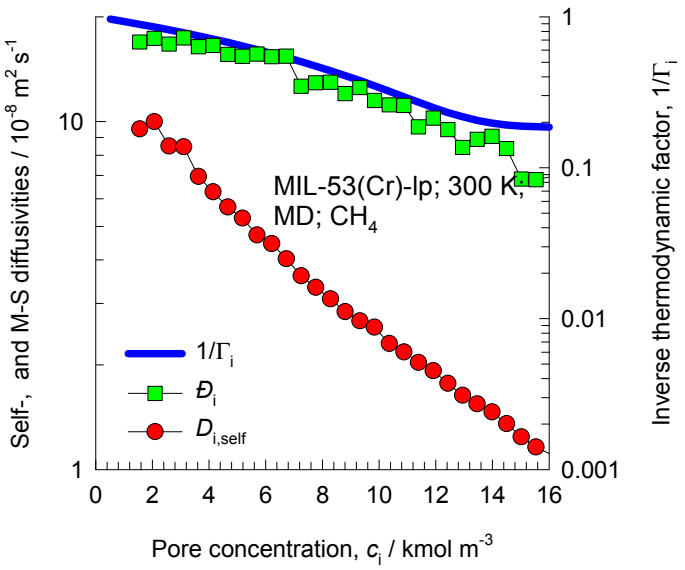

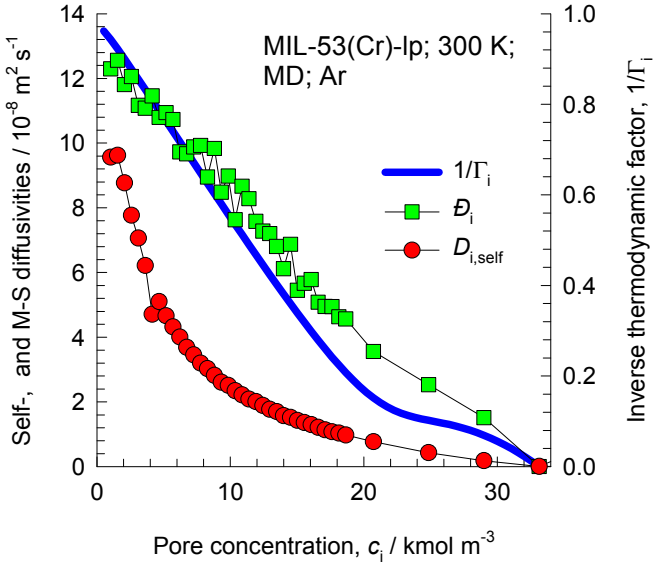

MIL-53 (Cr) -lp

CBMC simulation results for adsorption of pure CO_2

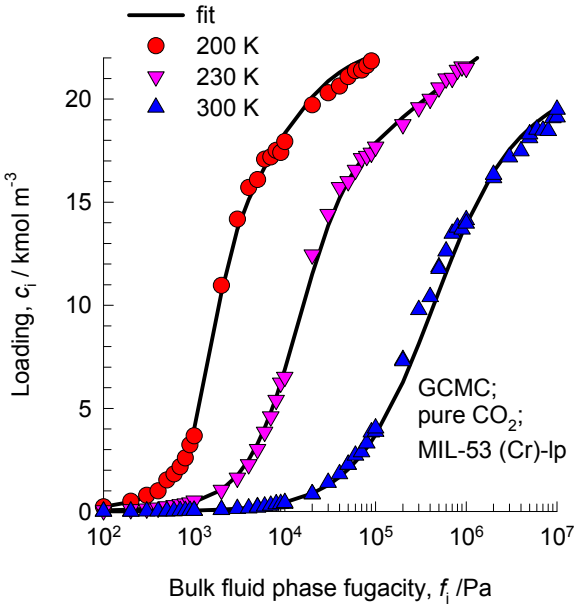

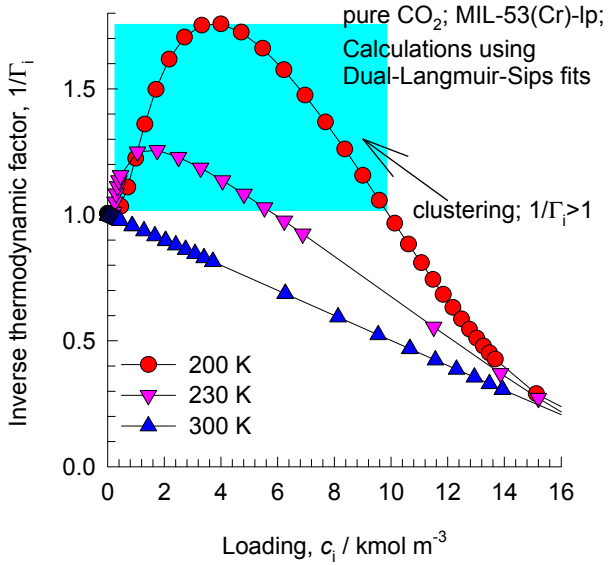

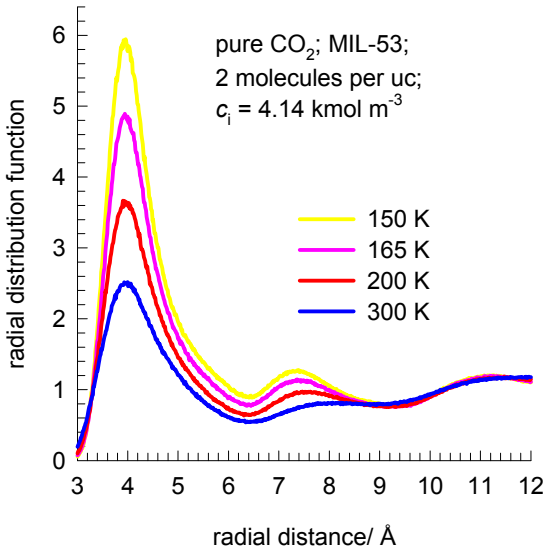

MIL-53 (Cr)-lp

MD simulations for CO_2 and CH_4 diffusion at 300 K

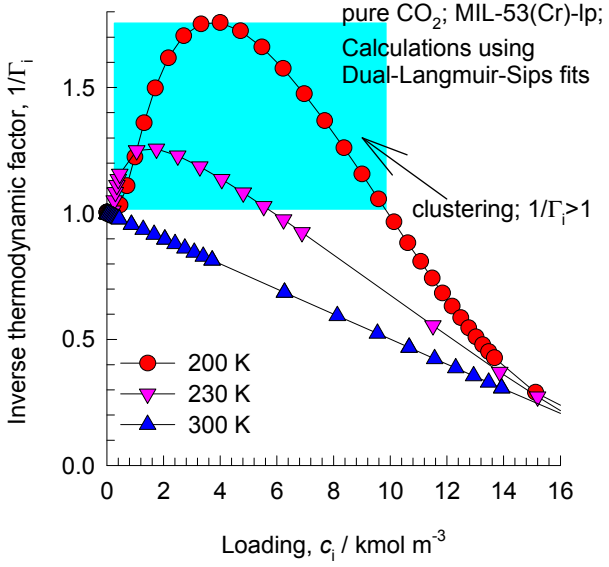

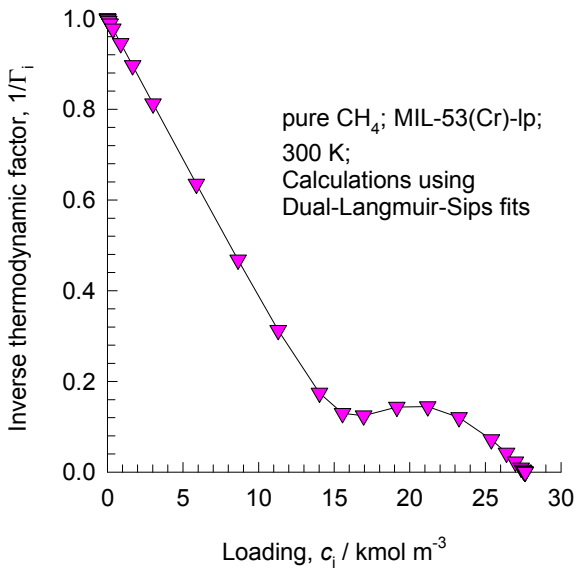

No clustering of either component at 300 K

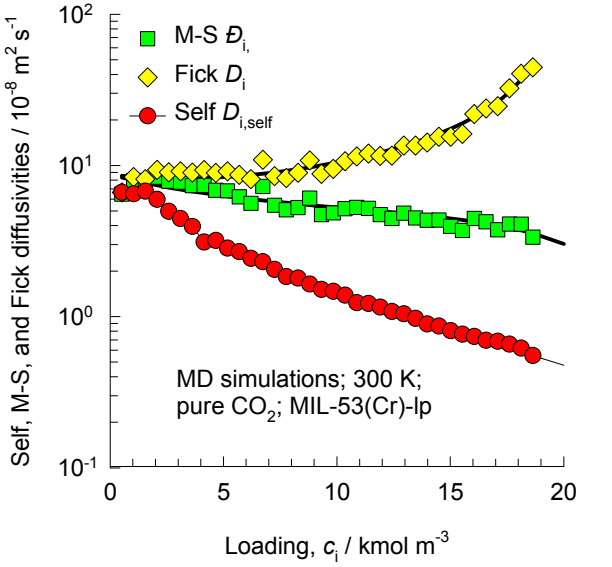

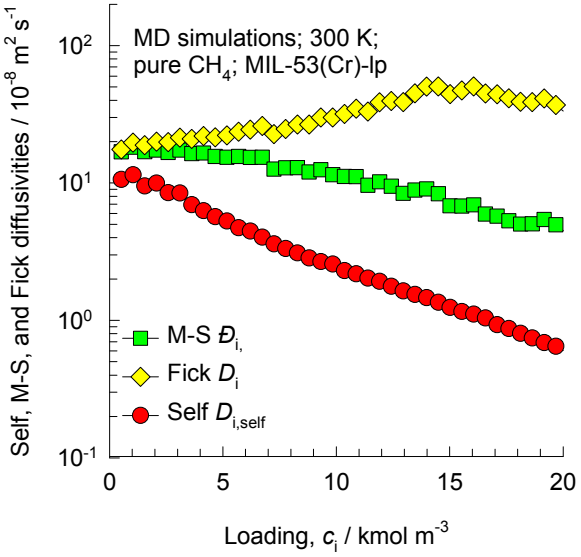

MIL-53 (Cr)-lp

MD simulations for CO_2 diffusion at 200 K and 230 K

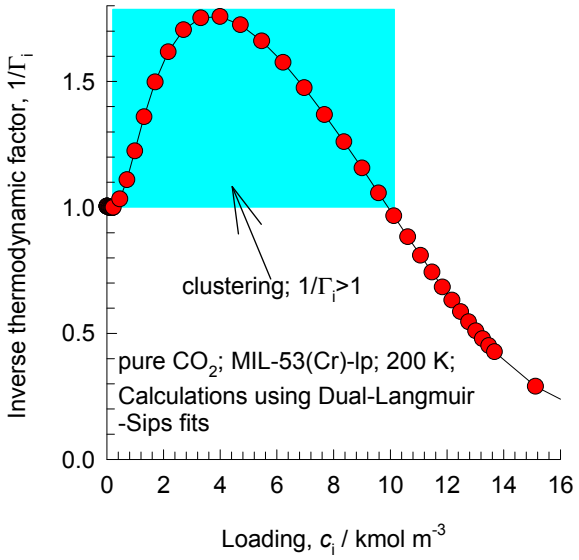

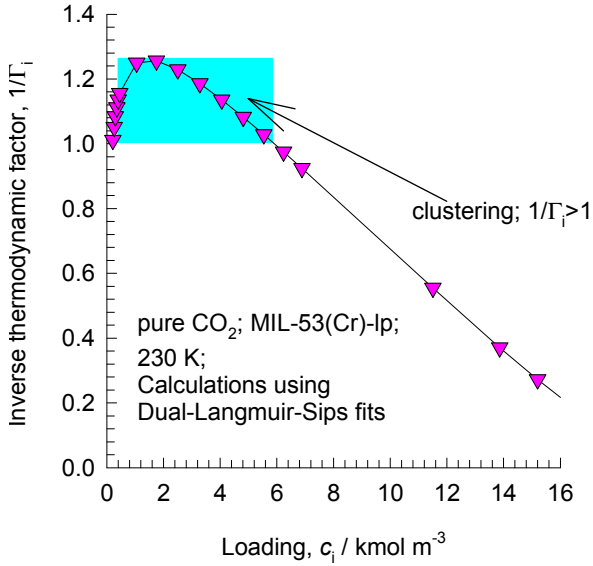

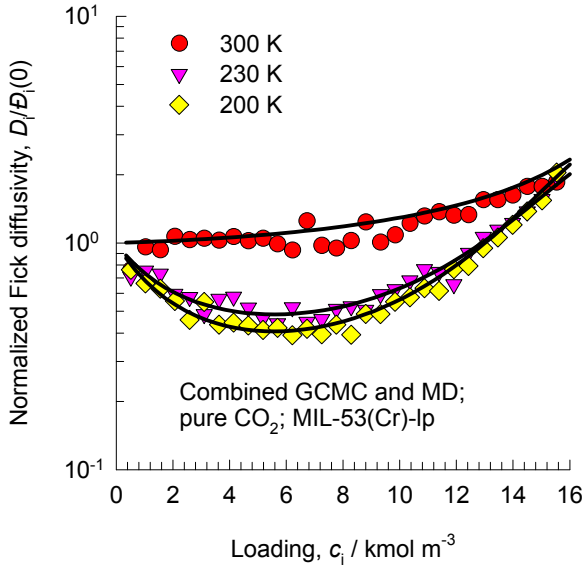

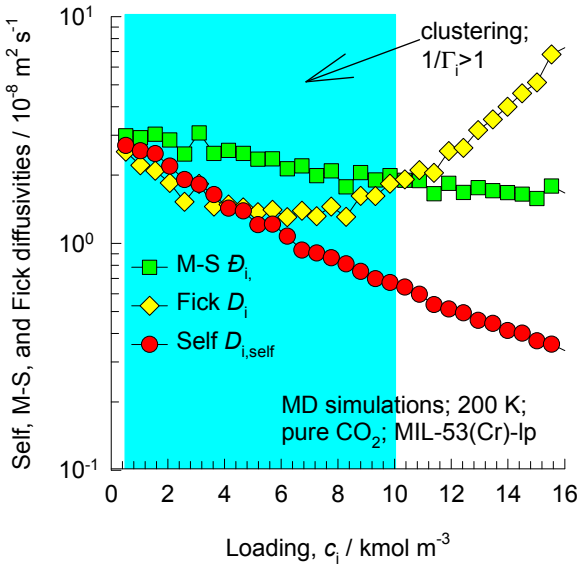

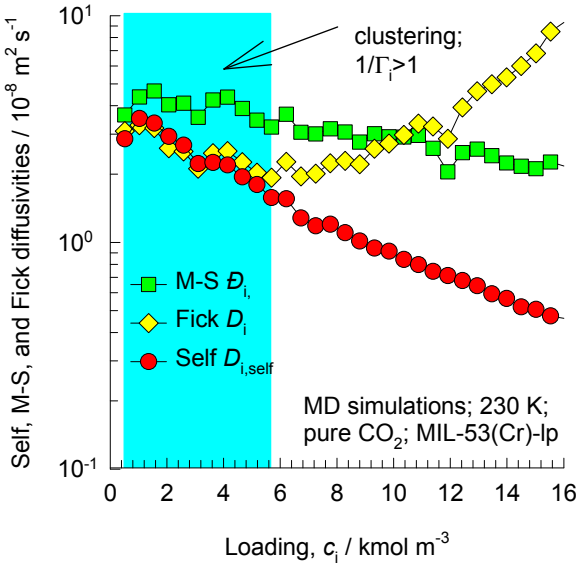

The experimental data of the Fick diffusivity at 230 K, published by Salles et al. (Angew. Chem. Int. Ed. 2009, 48, 8335-8339), shows that for the regions in which $1/\Gamma_i > 1$ the Fick diffusivity decreases with the loading.

Electronic Supplementary Material (ESI) for Physical Chemistry Chemical Physics

1D micro-porous channels With side pockets

MOR pore landscape

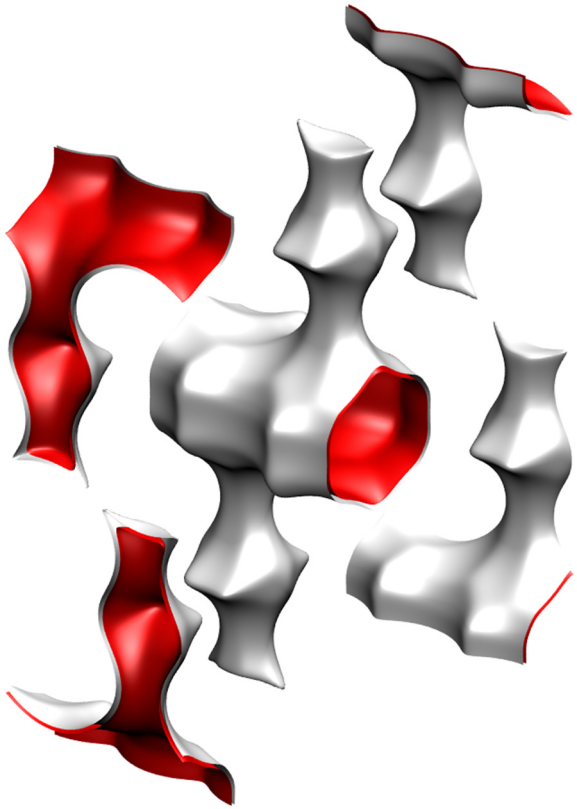

	MOR
a /Å	18.094
b /Å	20.516
c /Å	7.524
Cell volume / Å^3	2793.033
conversion factor for [molec/uc] to [mol per kg Framework]	0.3467
conversion factor for [molec/uc] to [kmol/m^3]	2.0877
ρ [kg/m3]	1714.691
MW unit cell [g/mol(framework)]	2884.07
ϕ, fractional pore volume	0.285
open space / Å^3/uc	795.4
Pore volume / cm^3/g	0.166
Surface area /m^2/g	417.0
DeLaunay diameter /Å	6.44

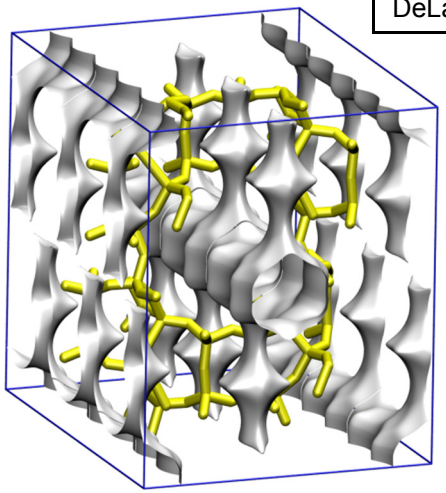

Structural information from: C. Baerlocher, L.B. McCusker, Database of Zeolite Structures, International Zeolite Association, http://www.iza-structure.org/databases/

MOR pore dimensions

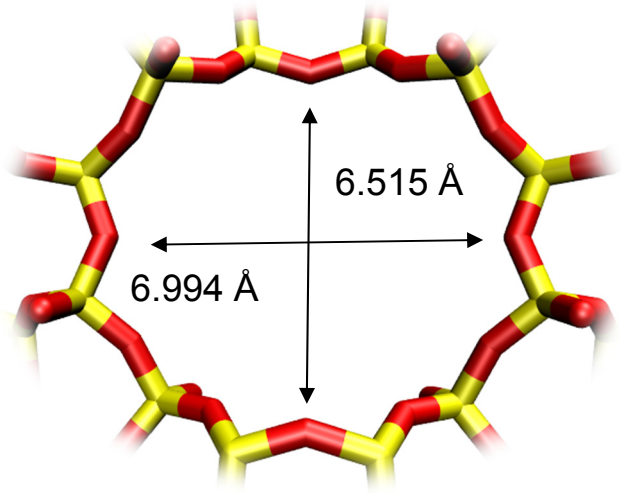

MOR Channel [1 0 0]

12-ring
main channels

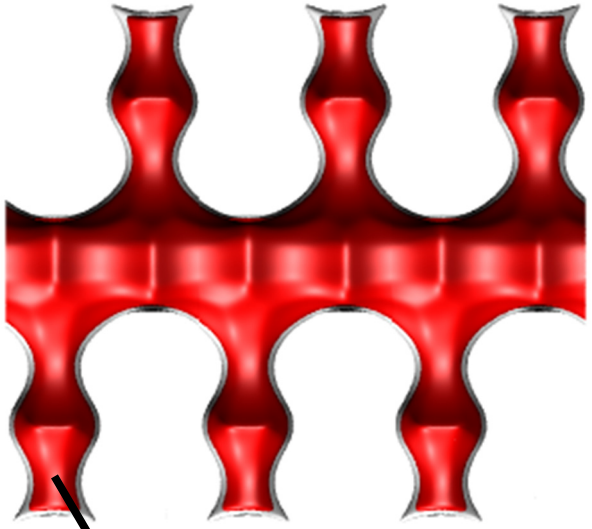

8-ring

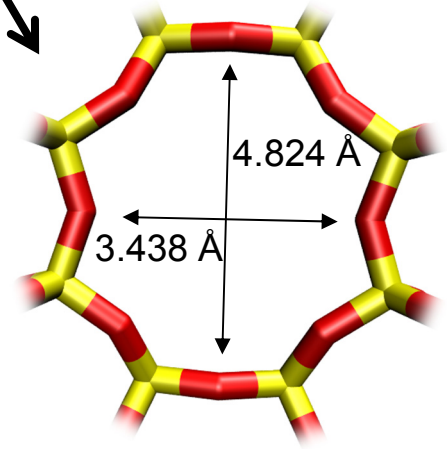

MOR [0 1 0]

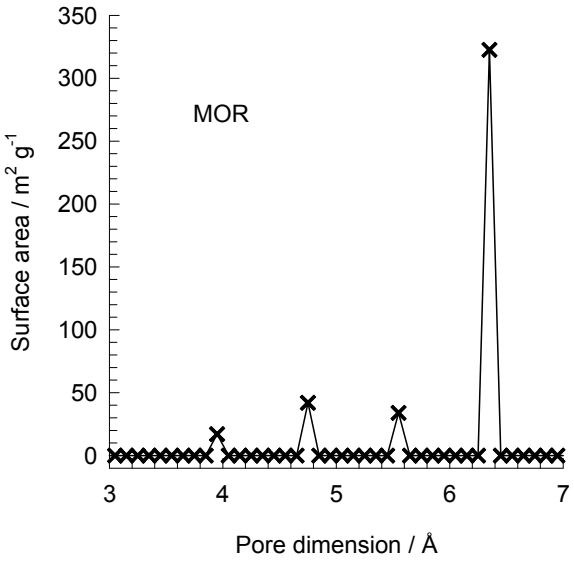

This plot of surface area versus pore dimension is determined using a combination of the DeLaunay triangulation method for pore dimension determination, and the procedure of Düren for determination of the surface area.

MOR CBMC simulations of isotherms, and -Q_{st}; MD simulations of diffusivities

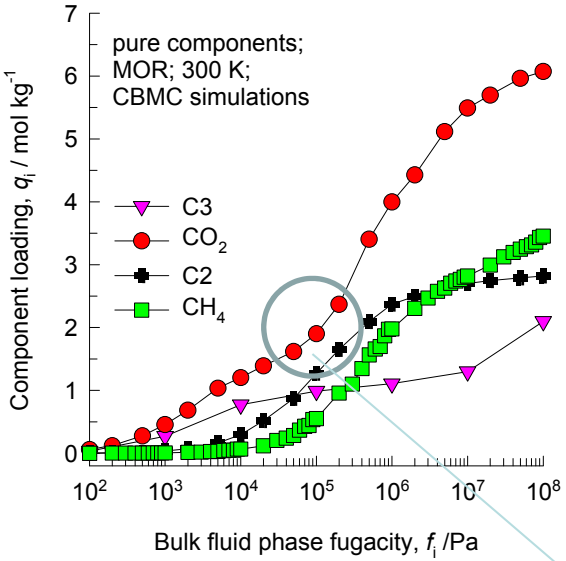

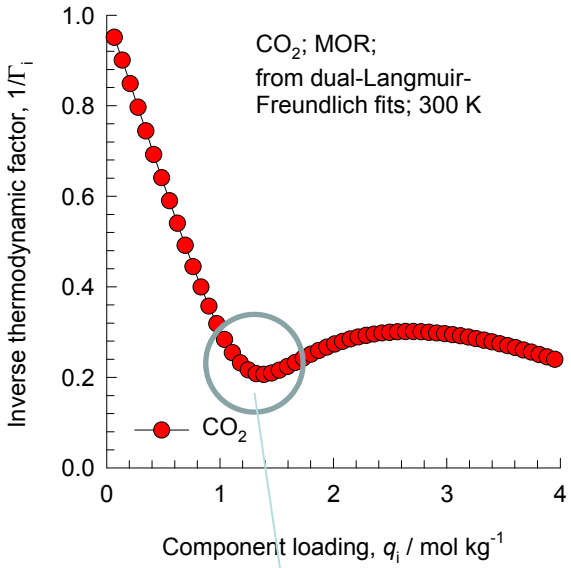

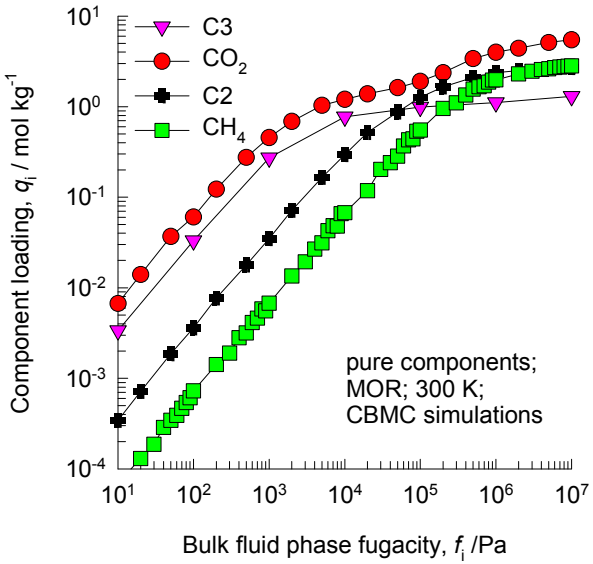

Note that C2 and C3 above refer to saturated alkanes.

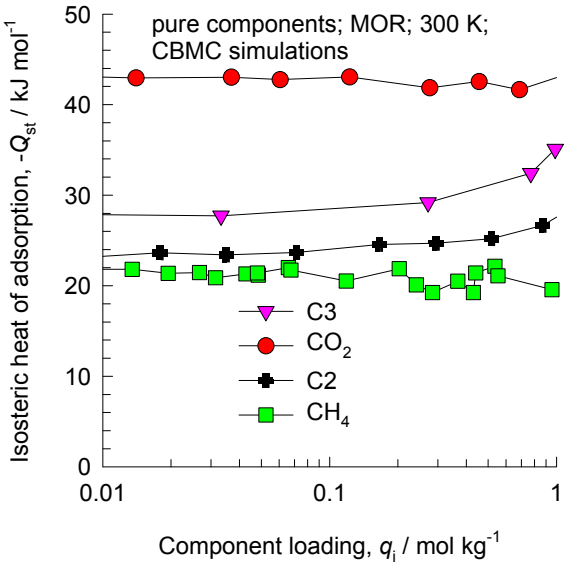

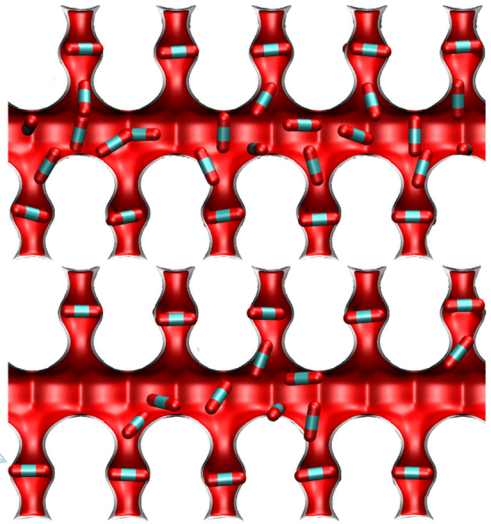

CO_2 preferentially locates in the side pockets as shown in snapshot. At a loading of 4/uc = 1.39 mol/kg, the pockets are full. This causes an infection. This also explains the high heat of adsorption due to snug fits in the side pockets

MOR MD simulations of unary diffusivities

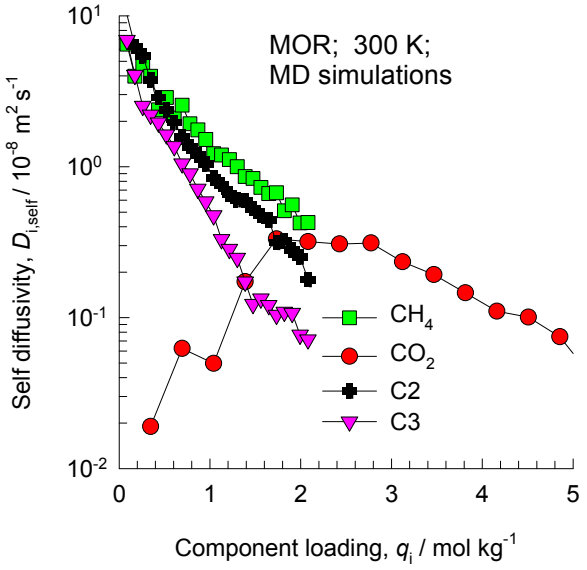

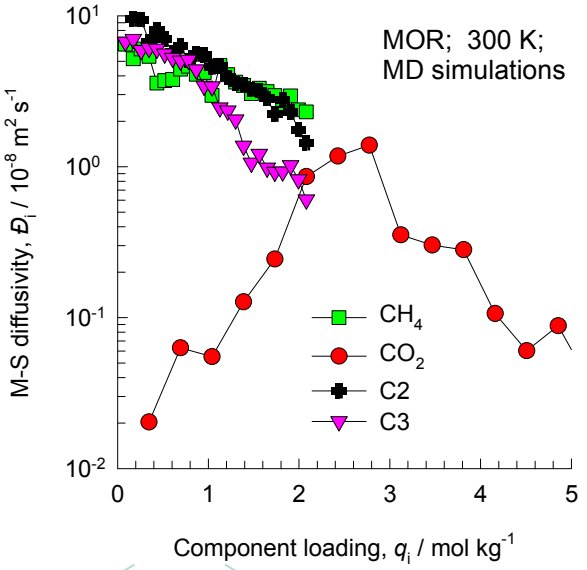

CO_2 preferentially locates in the side pockets in this loading range. This explains the low diffusivities.

Side pockets

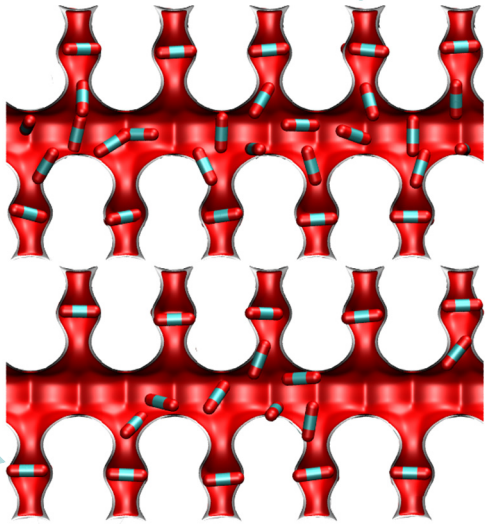

Influence of $1/\Gamma_i$ and $-Q_{st}$ on diffusivities

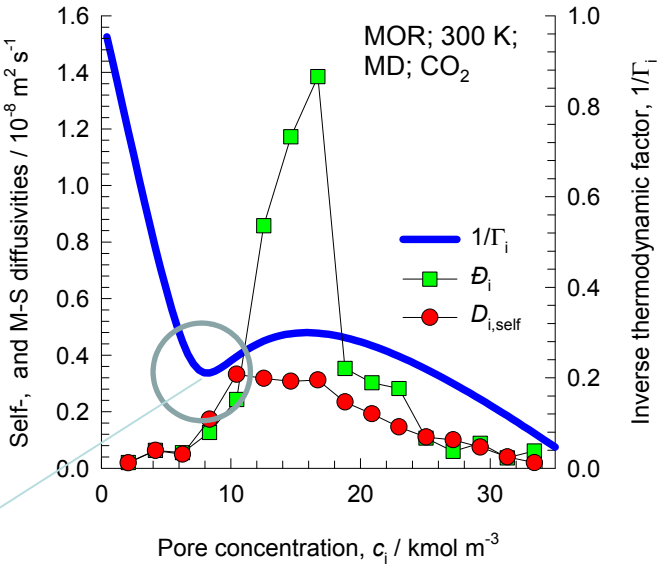

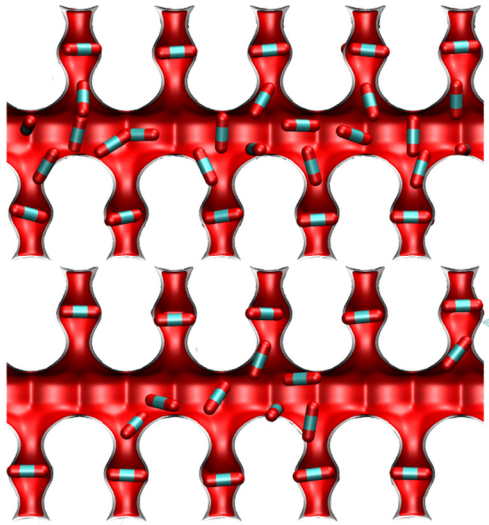

Side pockets

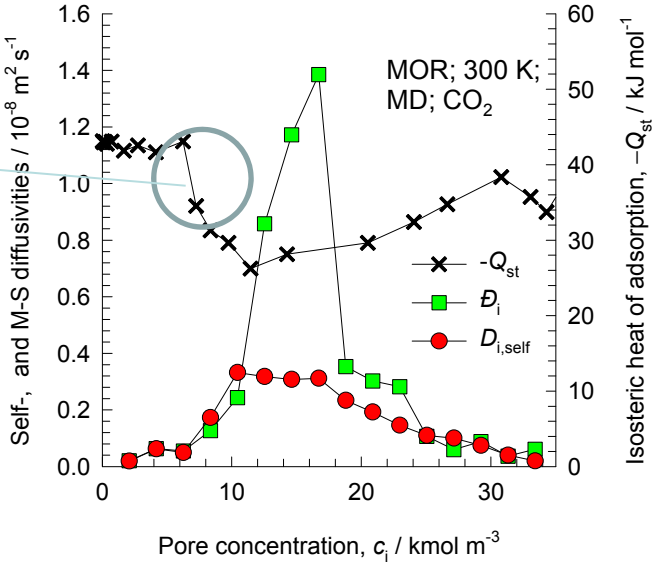

CO_2 preferentially locates in the side pockets as shown in snapshot. At a loading of 4/uc = 8.35 kmol m^{-3}, the pockets are full. This causes an infection. This also explains the high heat of adsorption due to snug fits in the side pockets

Electronic Supplementary Material (ESI) for Physical Chemistry Chemical Physics

“Open” structures with large cavities

FAU-Si pore landscape

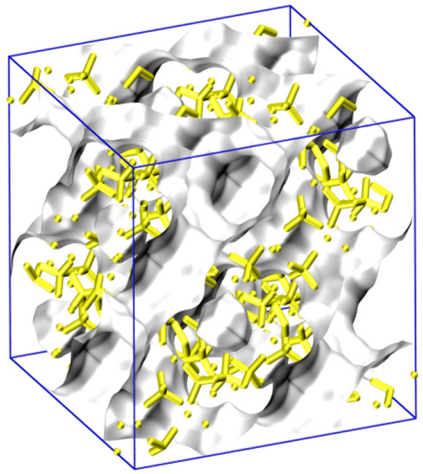

The sodalite cages are blocked in simulations and are not accessible to guest molecules; these are excluded for pore volume determination.

12-ring window of FAU

There are 8 cages per unit cell. The volume of one FAU cage is 786 Å^3, larger in size than that of LTA (743 Å^3) and DDR (278 Å^3).

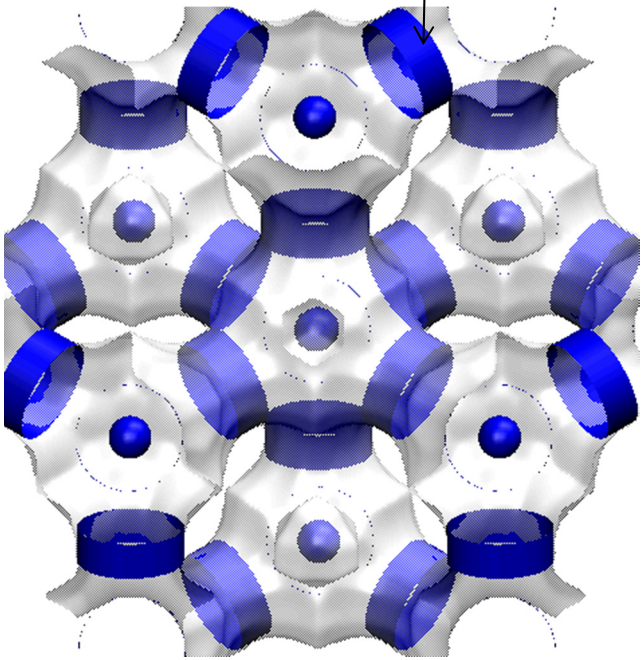

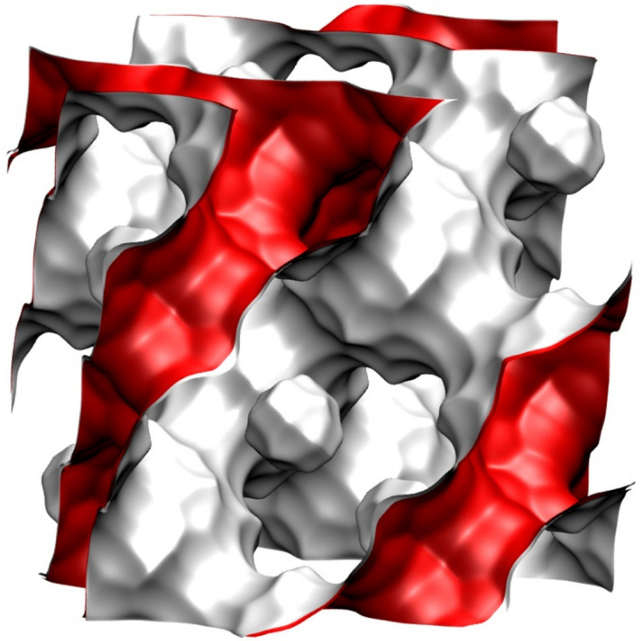

Structural information from: C. Baerlocher, L.B. McCusker, Database of Zeolite Structures, International Zeolite Association, http://www.iza-structure.org/databases/

FAU-Si window and pore dimensions

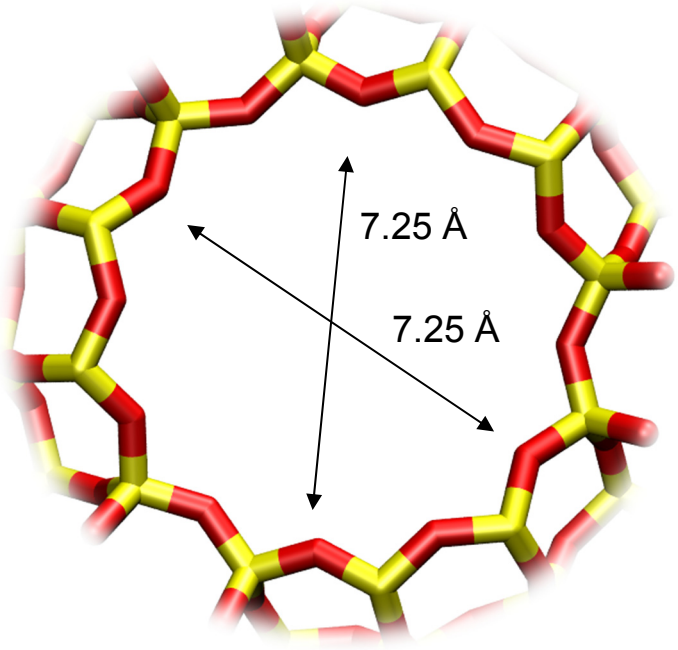

This plot of surface area versus pore dimension is determined using a combination of the DeLaunay triangulation method for pore dimension determination, and the procedure of Düren for determination of the surface area.

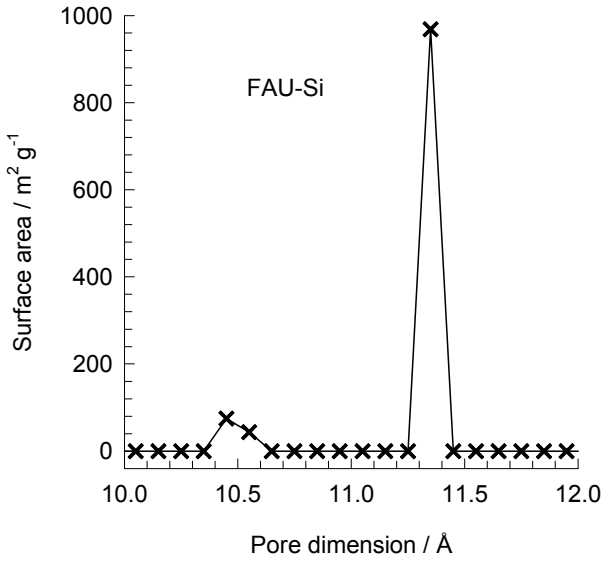

	FAU-Si
a /Å	24.28
b /Å	24.28
c /Å	24.28
Cell volume / Å^3	14313.51
conversion factor for [molec/uc] to [mol per kg Framework]	0.0867
conversion factor for [molec/uc] to [kmol/m^3]	0.2642
ρ [kg/m3]	1338.369
MW unit cell [g/mol (framework)]	11536.28
ϕ, fractional pore volume	0.439
open space / Å^3/uc	6285.6
Pore volume / cm^3/g	0.328
Surface area /m^2/g	1086.0
DeLaunay diameter /Å	7.37

FAU-Si CBMC simulations of isotherms, and isosteric heats of adsorption

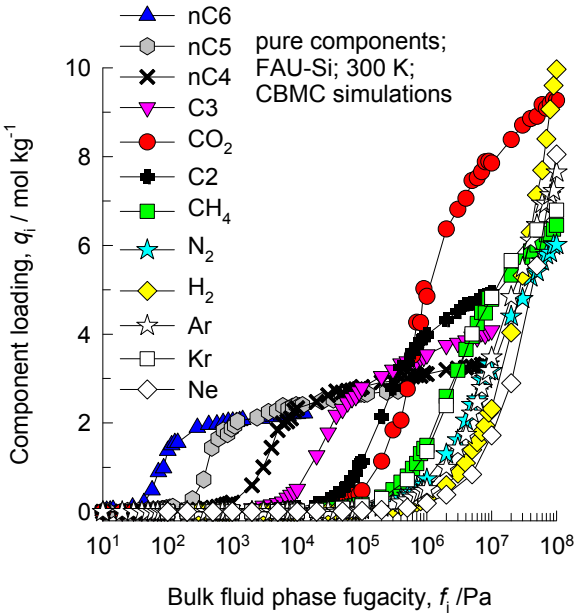

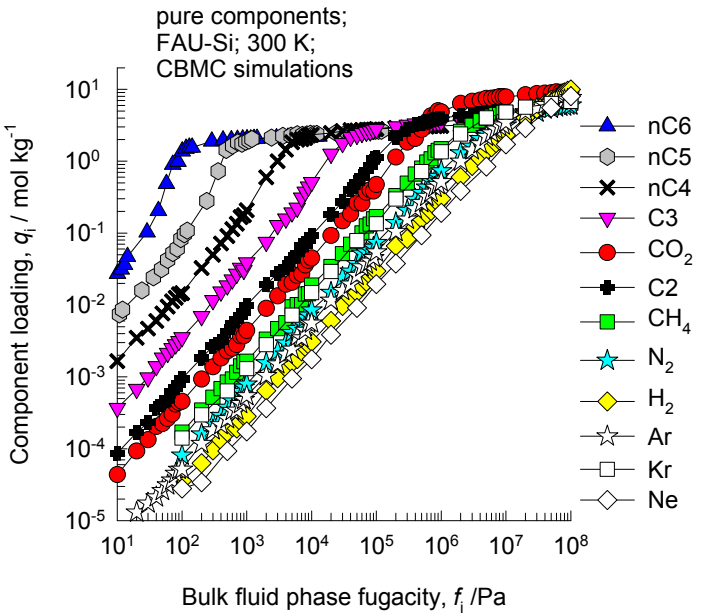

Note that C2 and C3 above refer to saturated alkanes

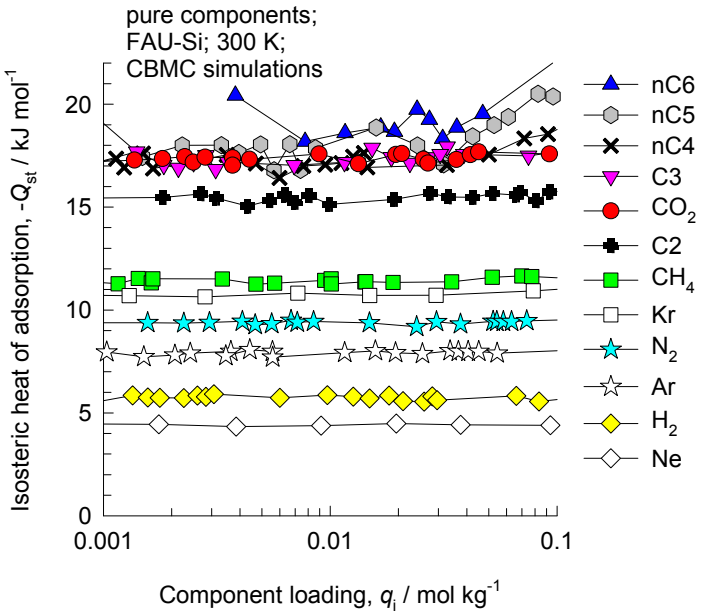

Influence of Inverse Thermodynamic Factor on diffusivities

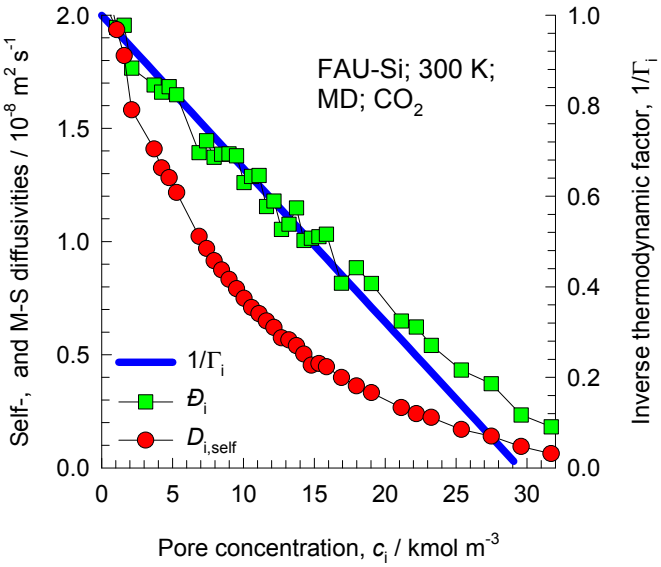

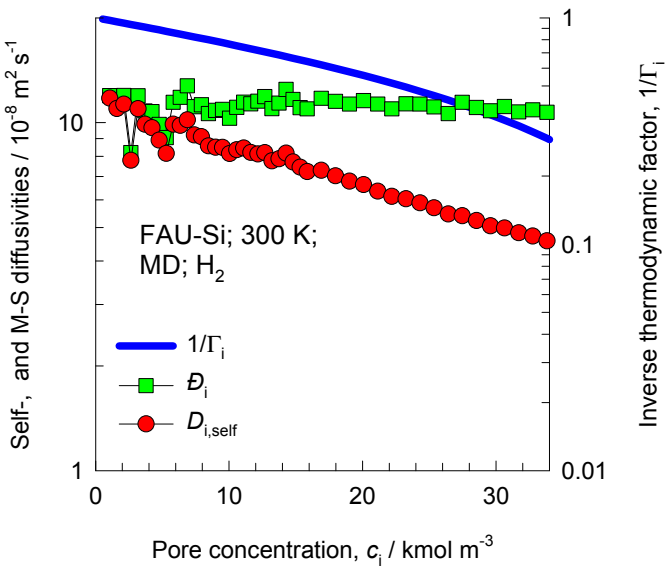

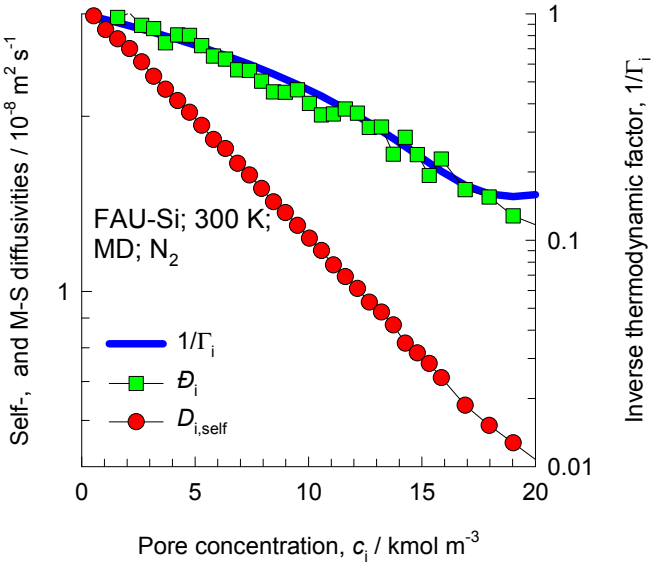

Influence of Inverse Thermodynamic Factor on diffusivities

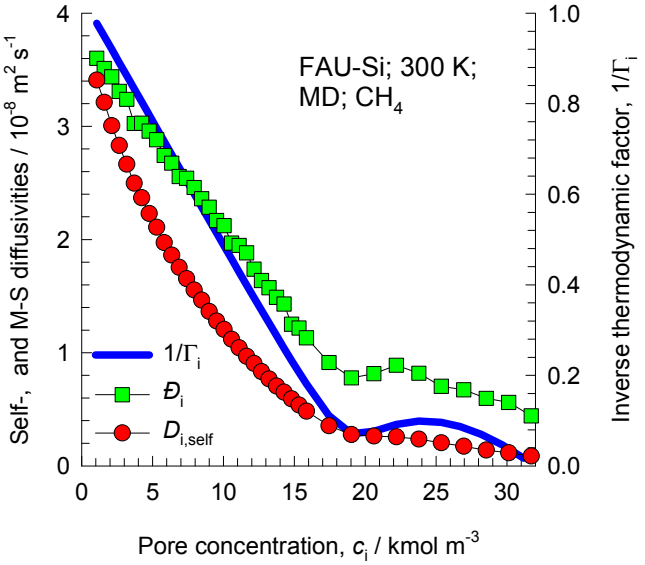

The isotherm inflection for methane gets reflected in the concentration dependence of the M-S diffusivity.

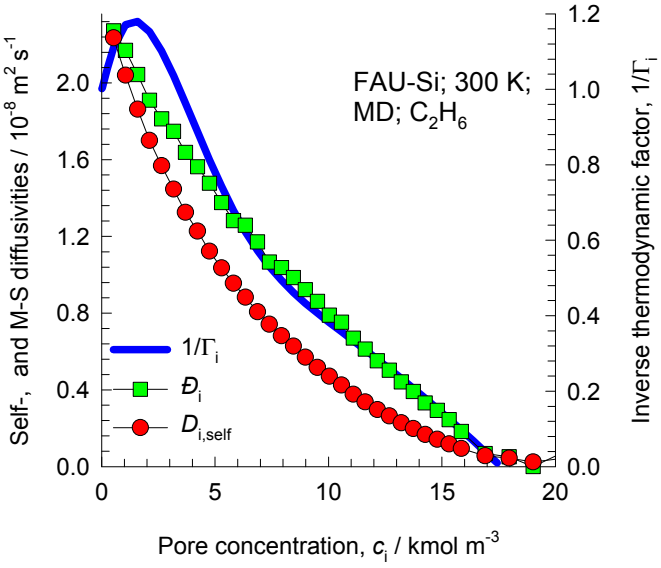

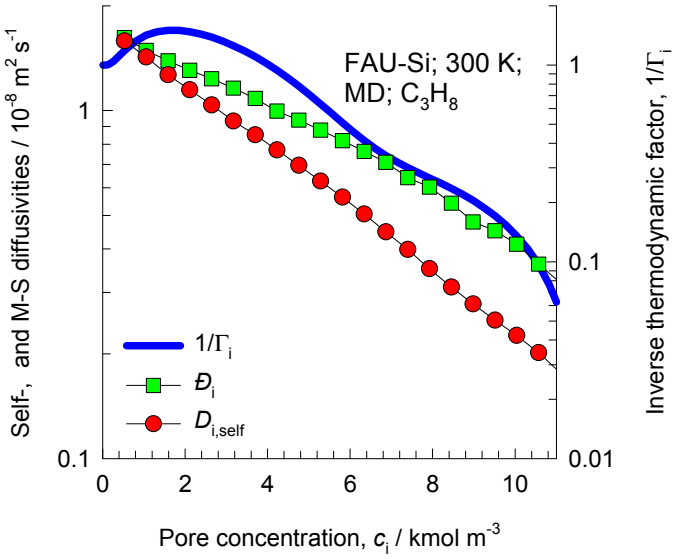

Influence of Inverse Thermodynamic Factor on diffusivities

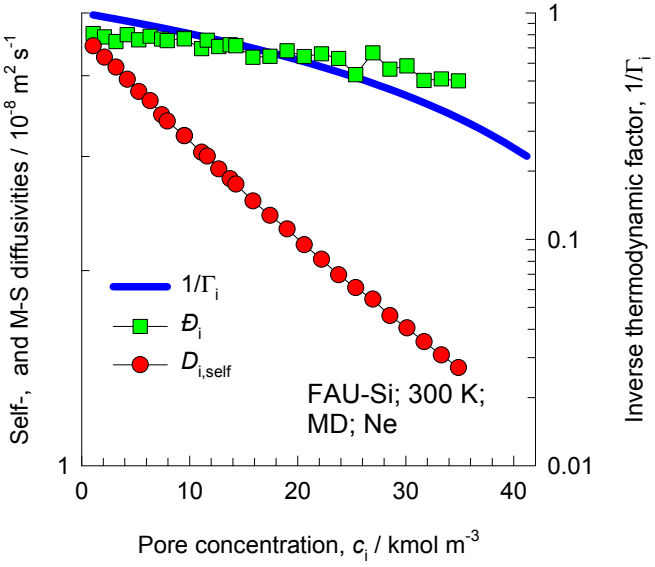

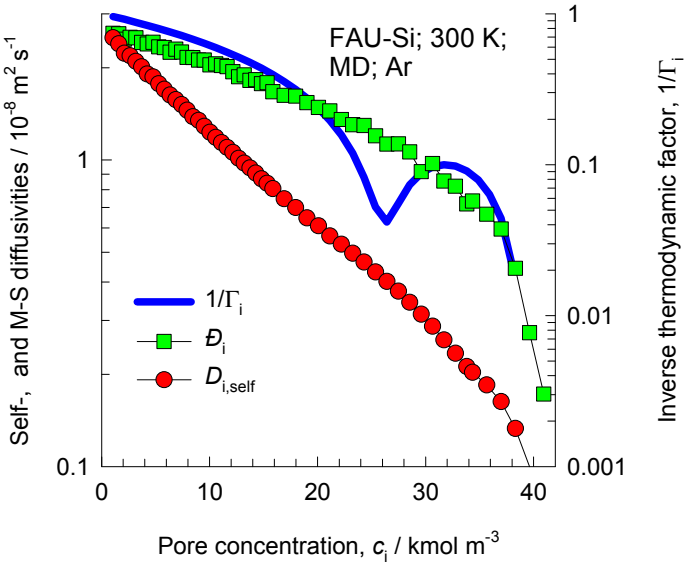

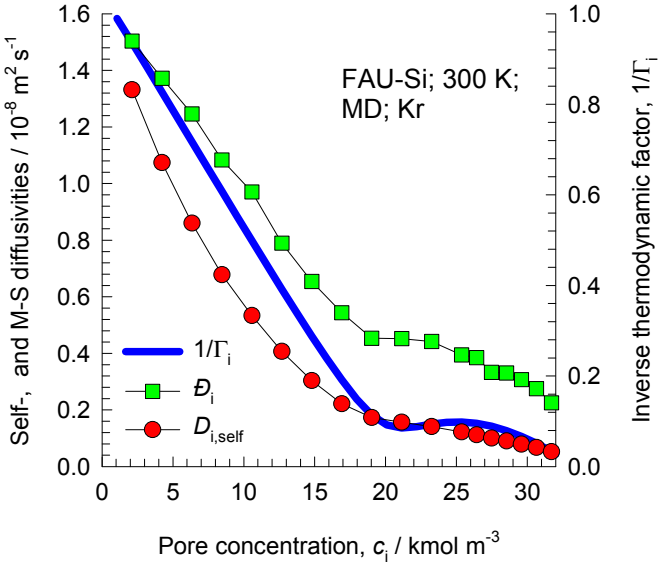

FAU-Si CO_2 adsorption and diffusion

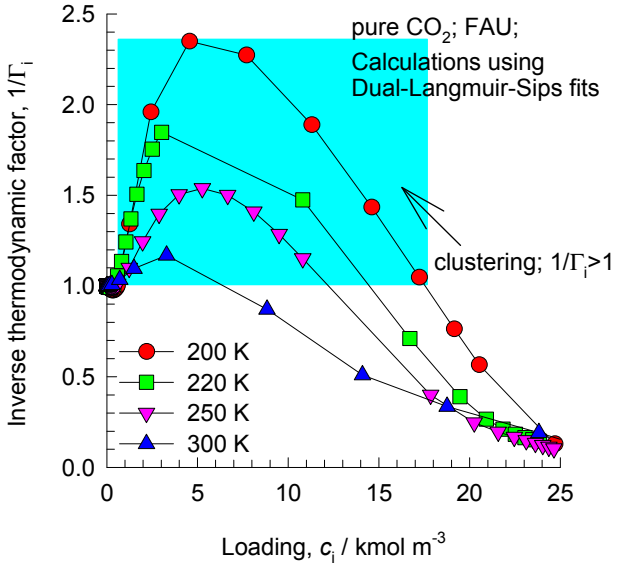

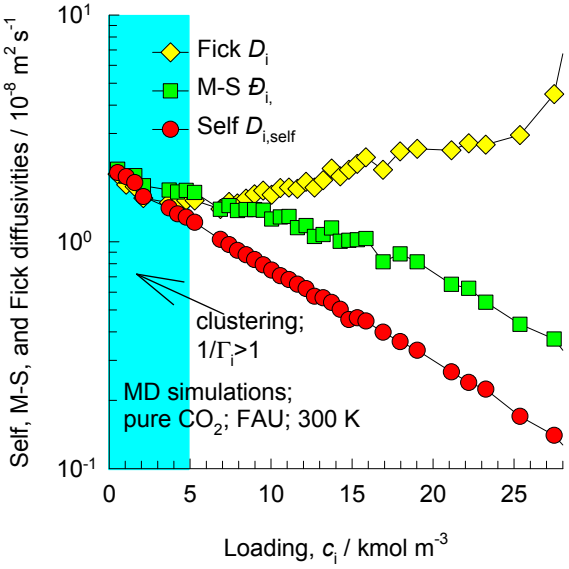

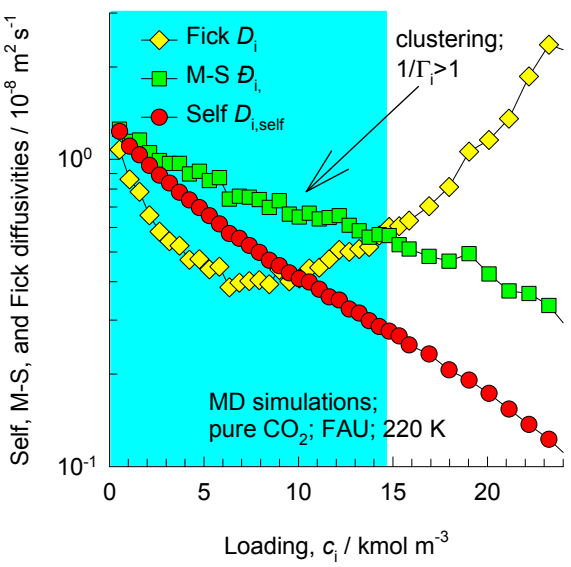

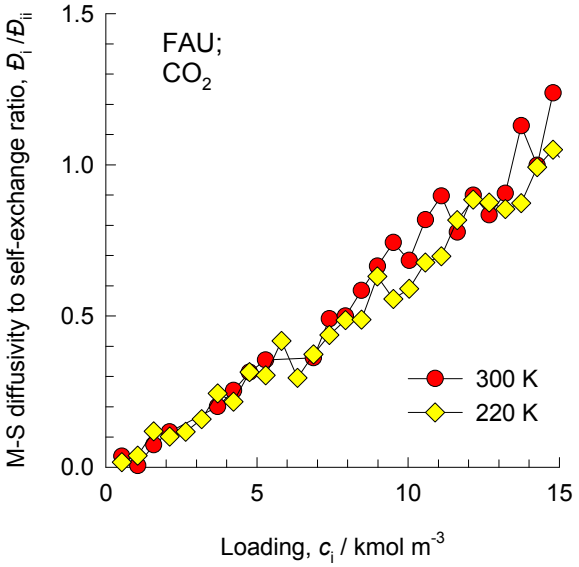

FAU-Si CH_4 adsorption and diffusion

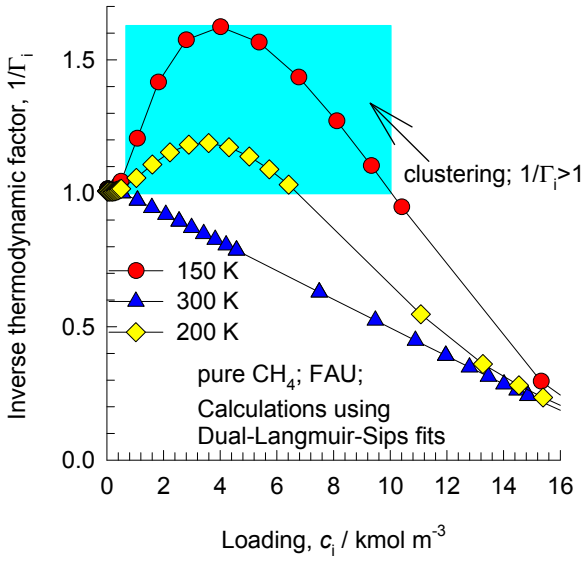

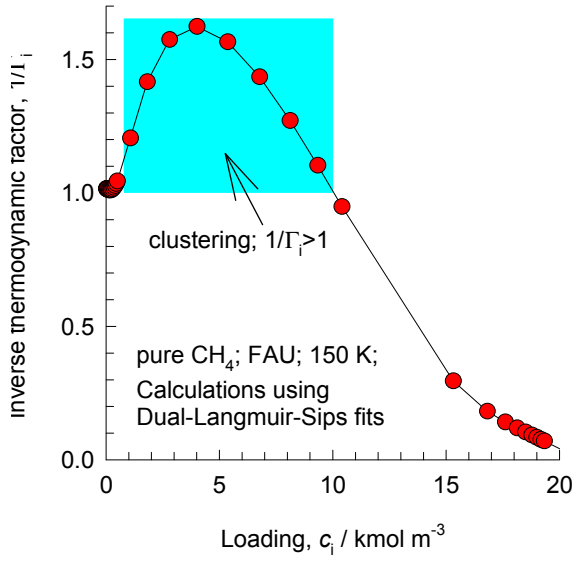

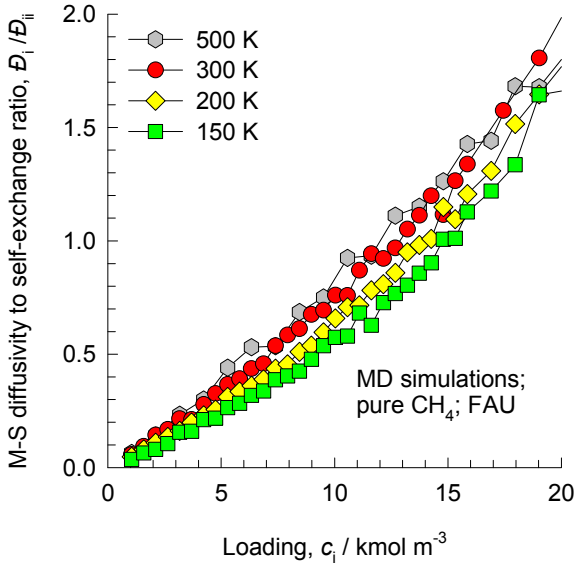

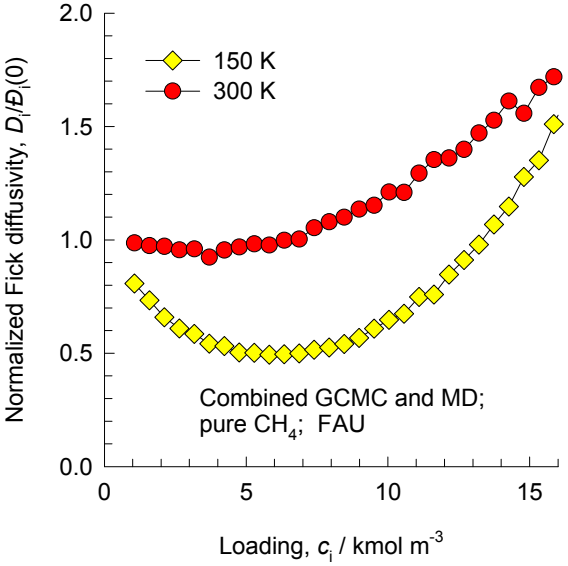

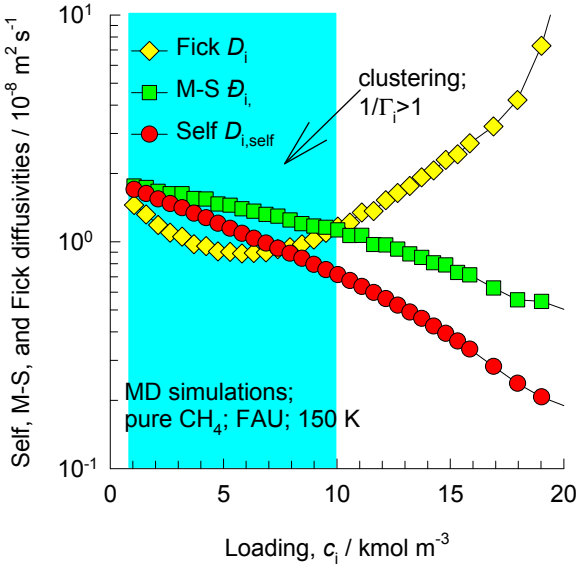

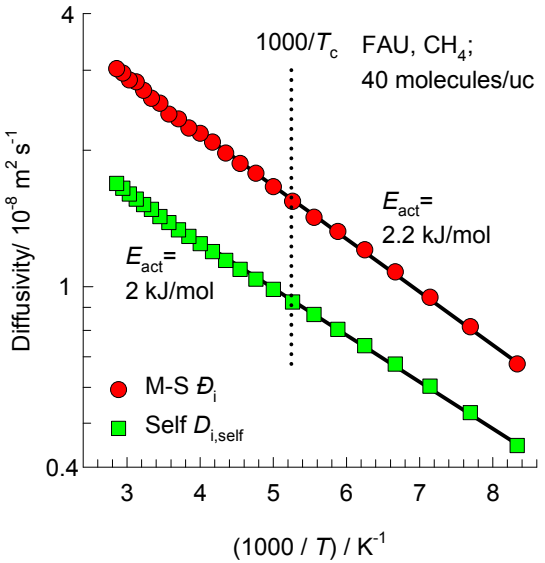

FAU-Si Ar adsorption and diffusion

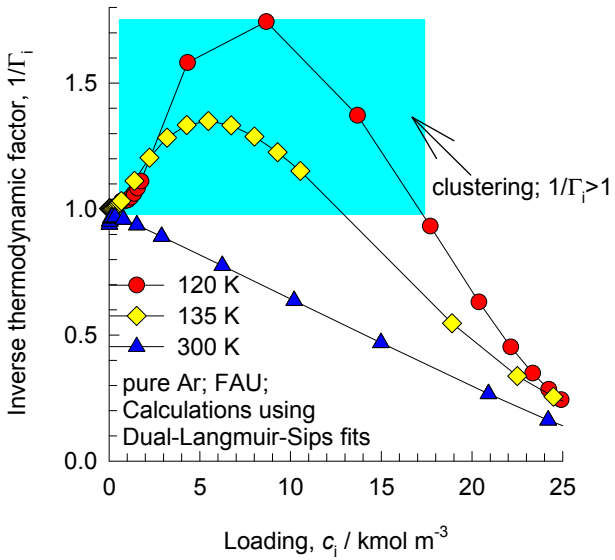

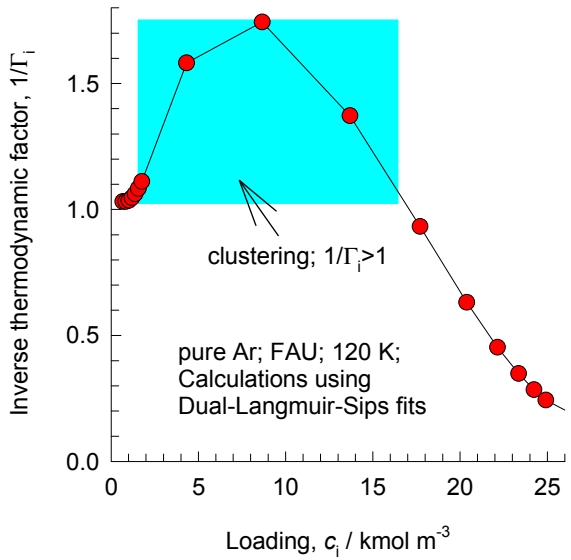

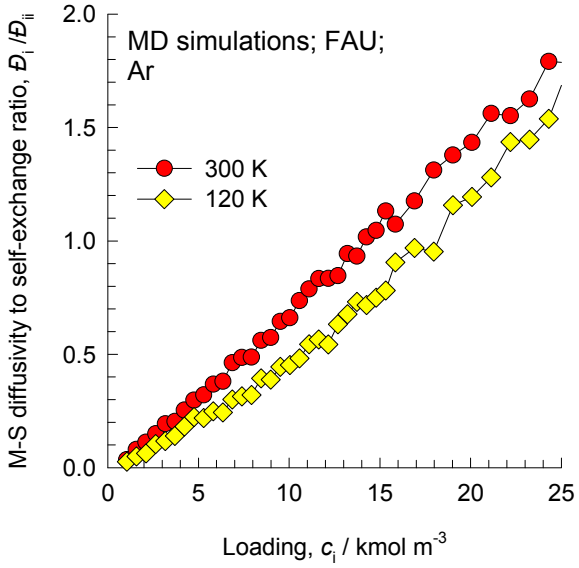

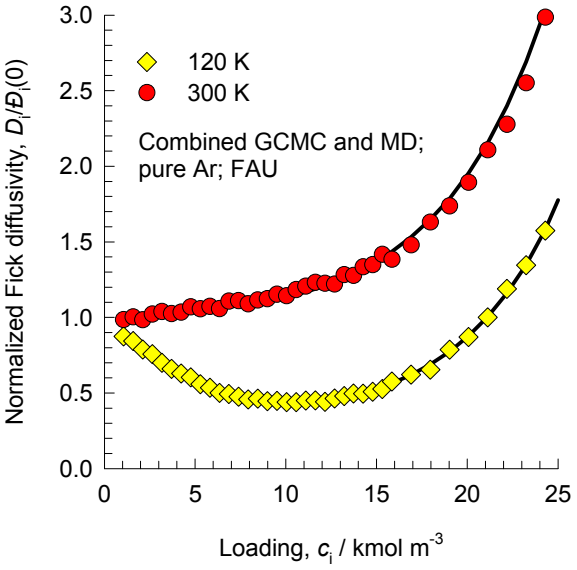

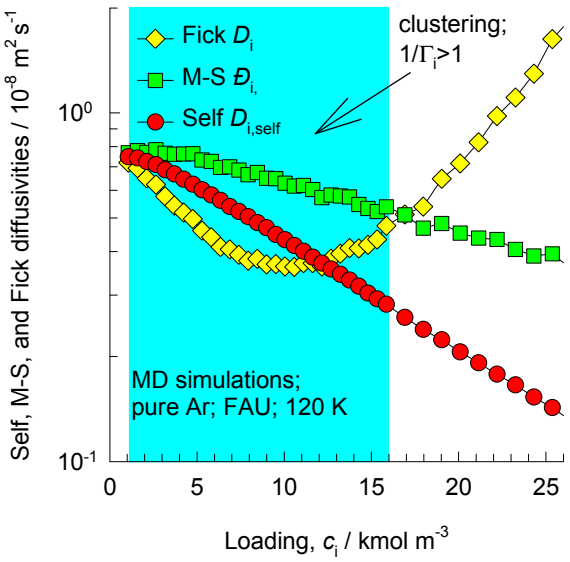

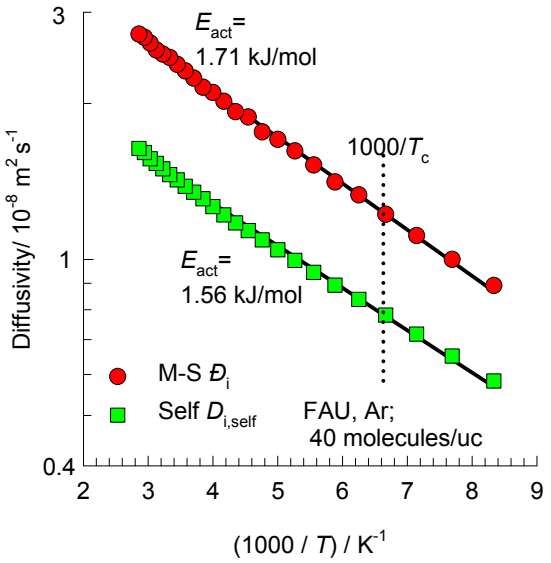

FAU-Si CBMC simulations of isotherms and thermodynamic factors for n-alkanes

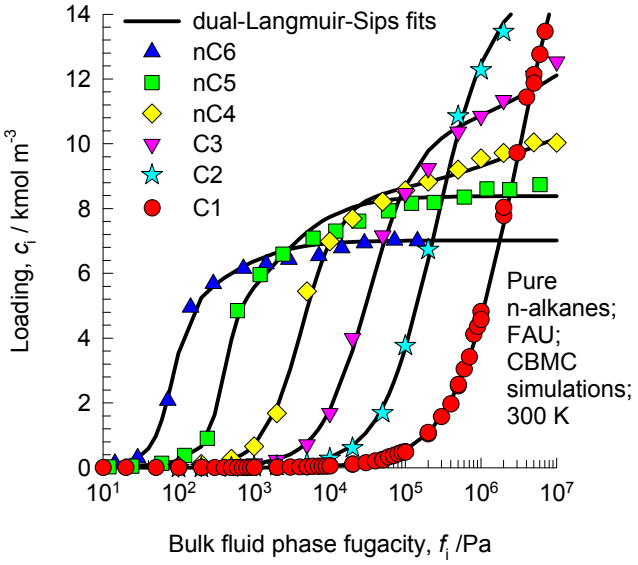

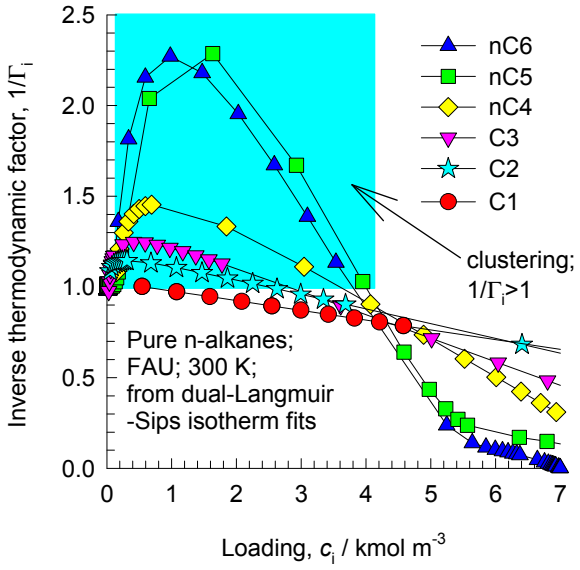

The degree of clustering increases with increasing chain length of n-alkanes.

Influence of Inverse Thermodynamic Factor on diffusivities

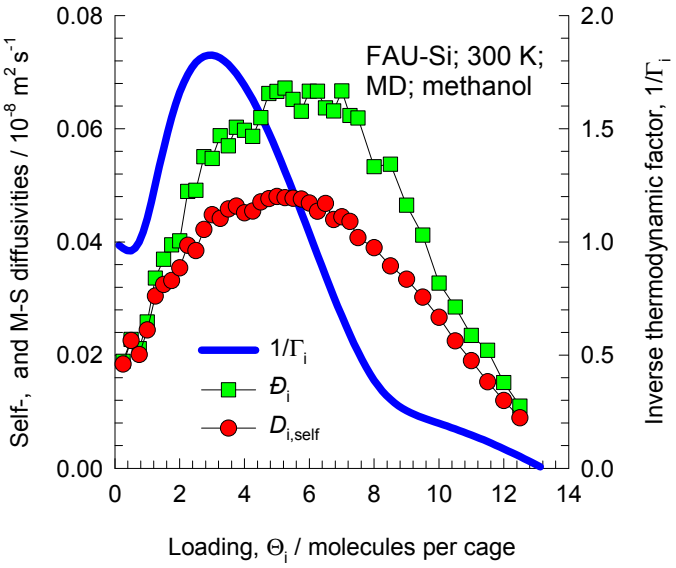

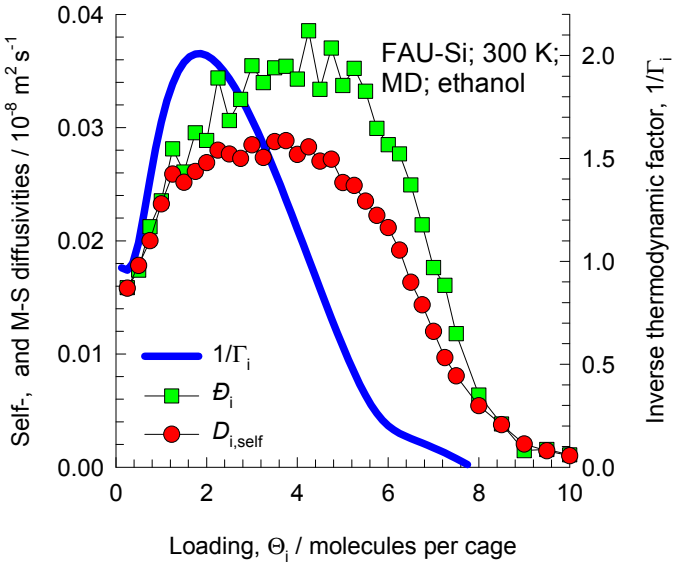

Electronic Supplementary Material (ESI) for Physical Chemistry Chemical Physics

NaY (138 Si, 54 Al, 54 Na+, Si/Al=2.55)

Blue spheres are cations

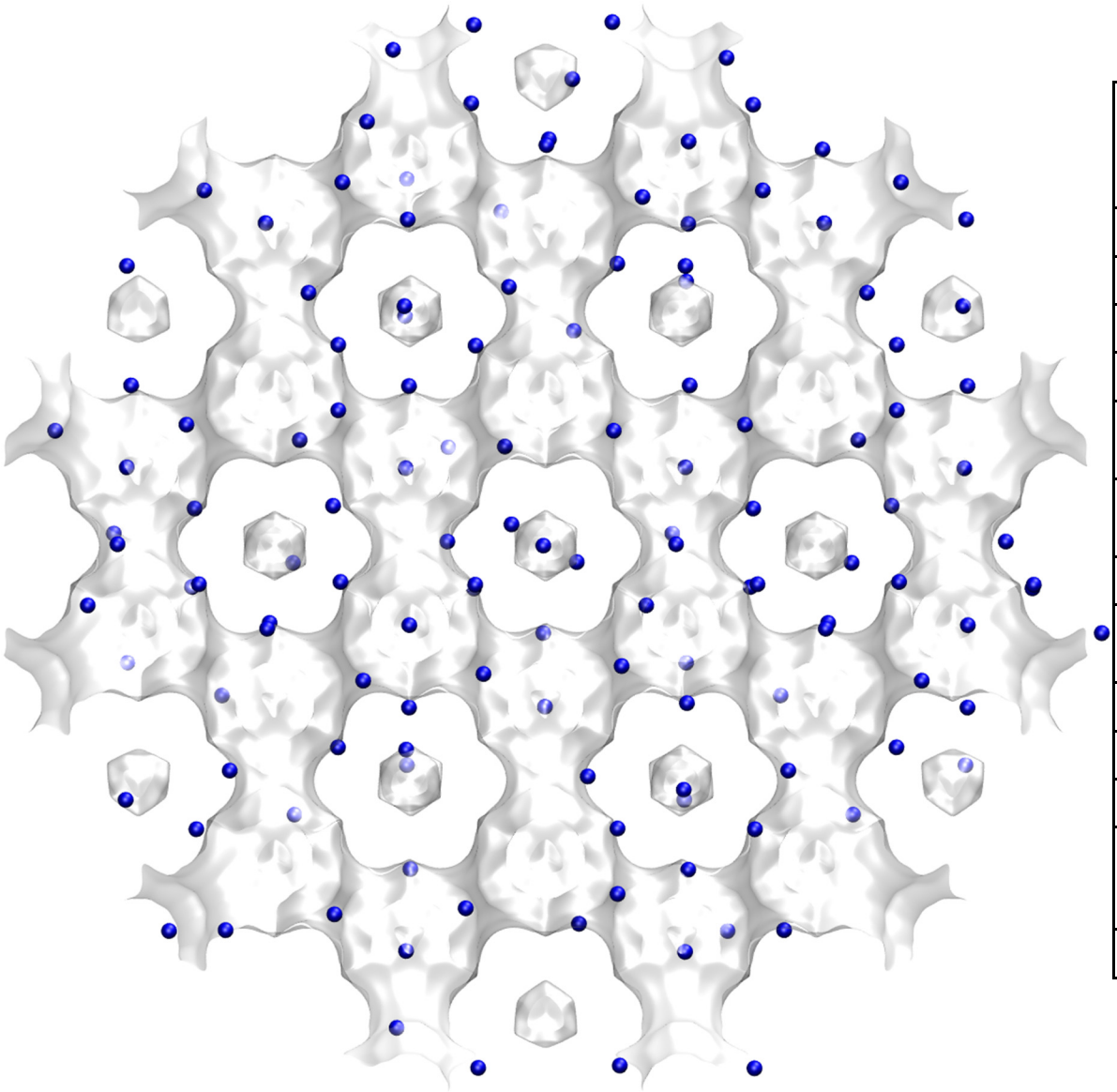

	FAU-54Al
a /Å	25.028
b /Å	25.028
c /Å	25.028
Cell volume / Å^3	15677.56
conversion factor for [molec/uc] to [mol per kg Framework]	0.0786
conversion factor for [molec/uc] to [kmol/m^3]	0.2596
ρ [kg/m3] (with cations)	1347.1
MW unit cell [g/mol(framework+cations)]	12718.08
ϕ, fractional pore volume	0.408
open space / Å^3/uc	6396.6
Pore volume / cm^3/g	0.303
Surface area /m^2/g	
DeLaunay diameter /Å	7.37

Influence of Inverse Thermodynamic Factor on diffusivities

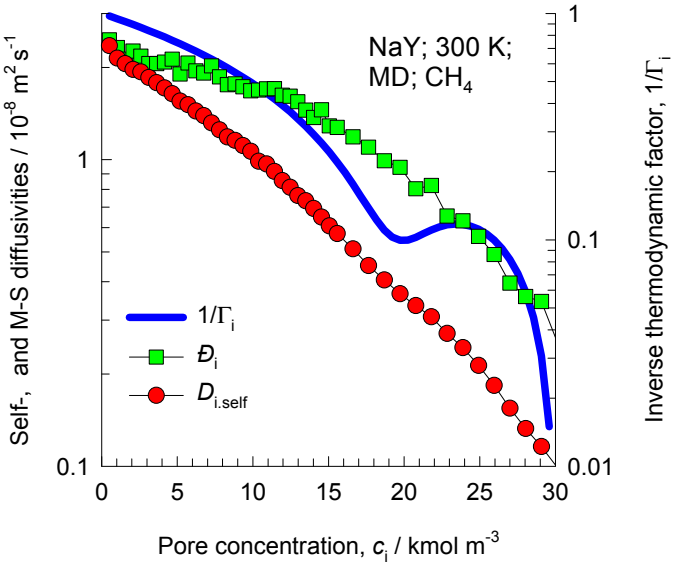

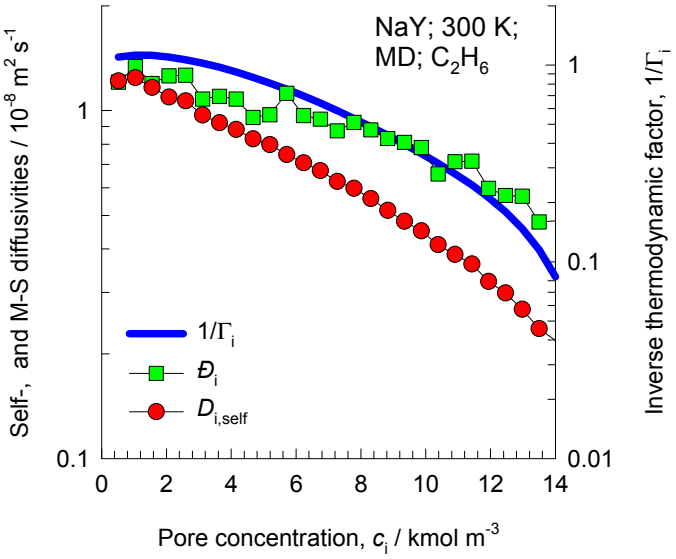

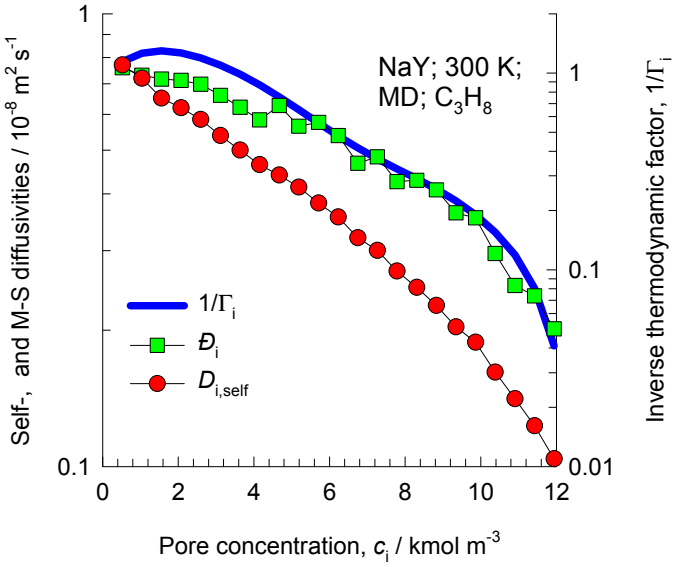

NaY CH_4 self-diffusivity at 200 K

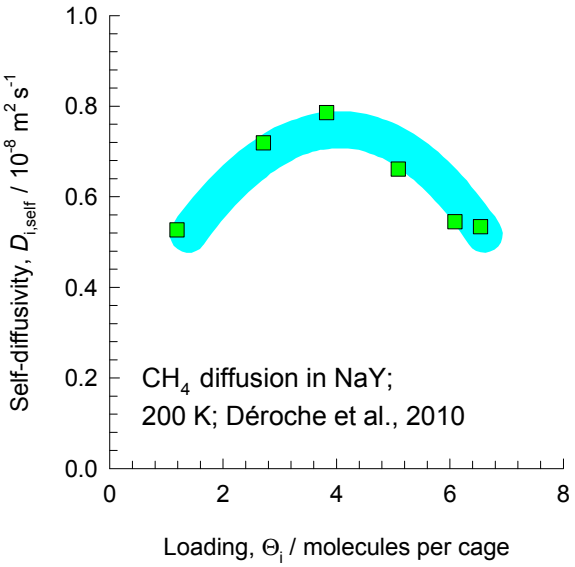

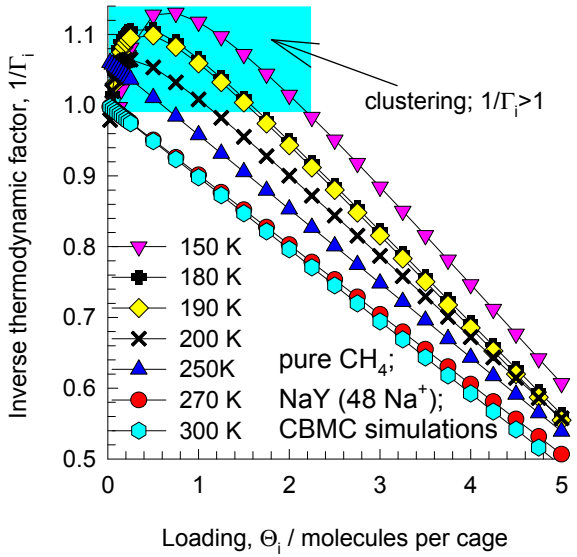

The QENS experimental data are re-plotted using the information in:
I. Déroche, G. Maurin, B.J. Borah, H. Jobic, S. Yashonath, Diffusion of pure CH4 and its binary mixture with CO2 in Faujasite NaY: A combination of neutron scattering experiments and Molecular Dynamics simulations, J. Phys. Chem. C 114 (2010) 5027-5034.

The CBMC simulations of the inverse thermodynamic factor are from our earlier works:
R. Krishna, J.M. van Baten, Investigating cluster formation in adsorption of CO2, CH4, and Ar in zeolites and metal organic frameworks at sub-critical temperatures, Langmuir 26 (2010) 3981-3992.
R. Krishna, J.M. van Baten, A rationalization of the Type IV loading dependence in the Kärger-Pfeifer classification of self-diffusivities, Microporous Mesoporous Mater. 142 (2011) 745-748.

Electronic Supplementary Material (ESI) for Physical Chemistry Chemical Physics

NaX (106 Si, 86 Al, 86 Na+, Si/Al=1.23)

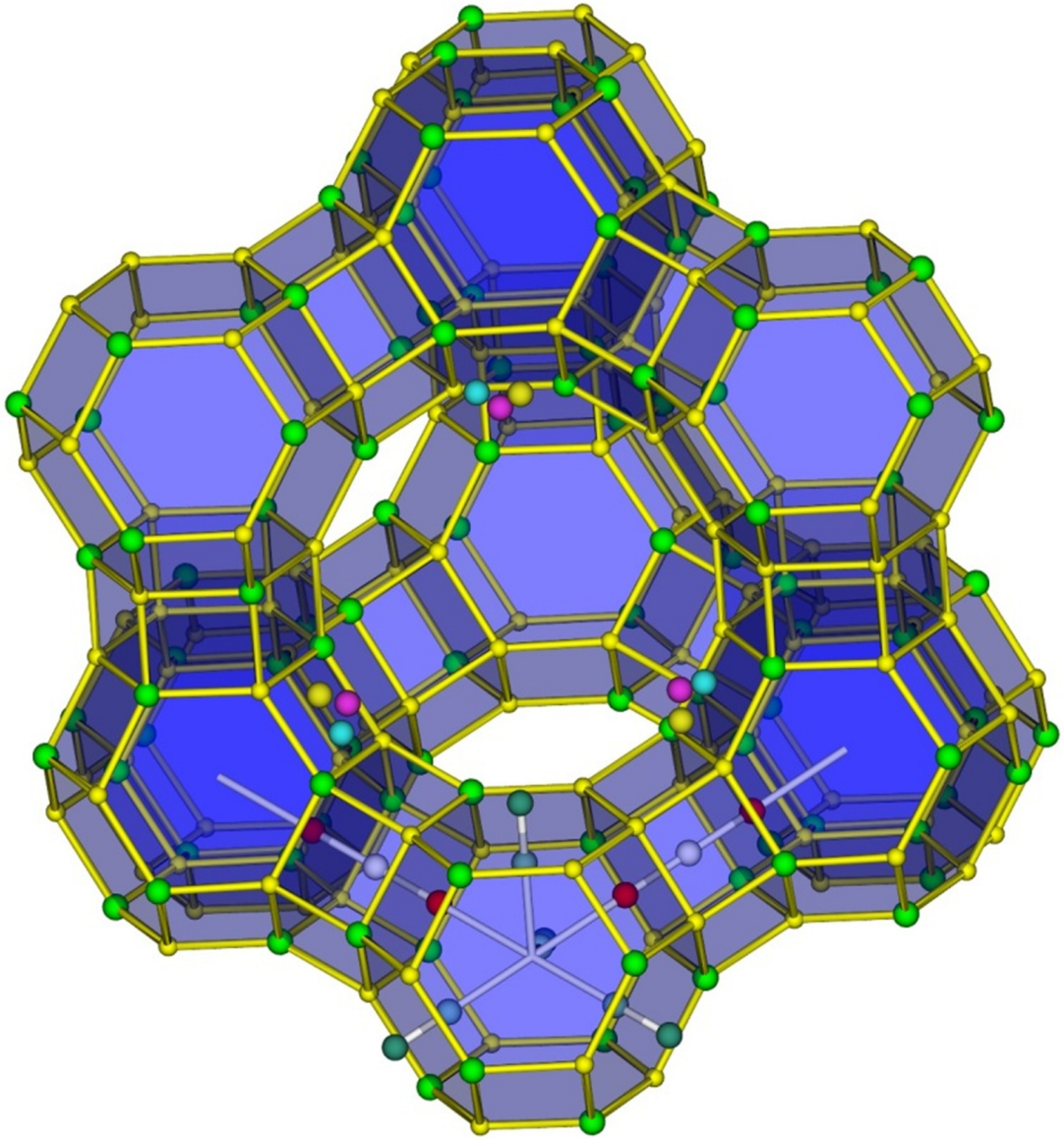

NaX (106 Si, 86 Al, 86 Na+, Si/Al=1.23)

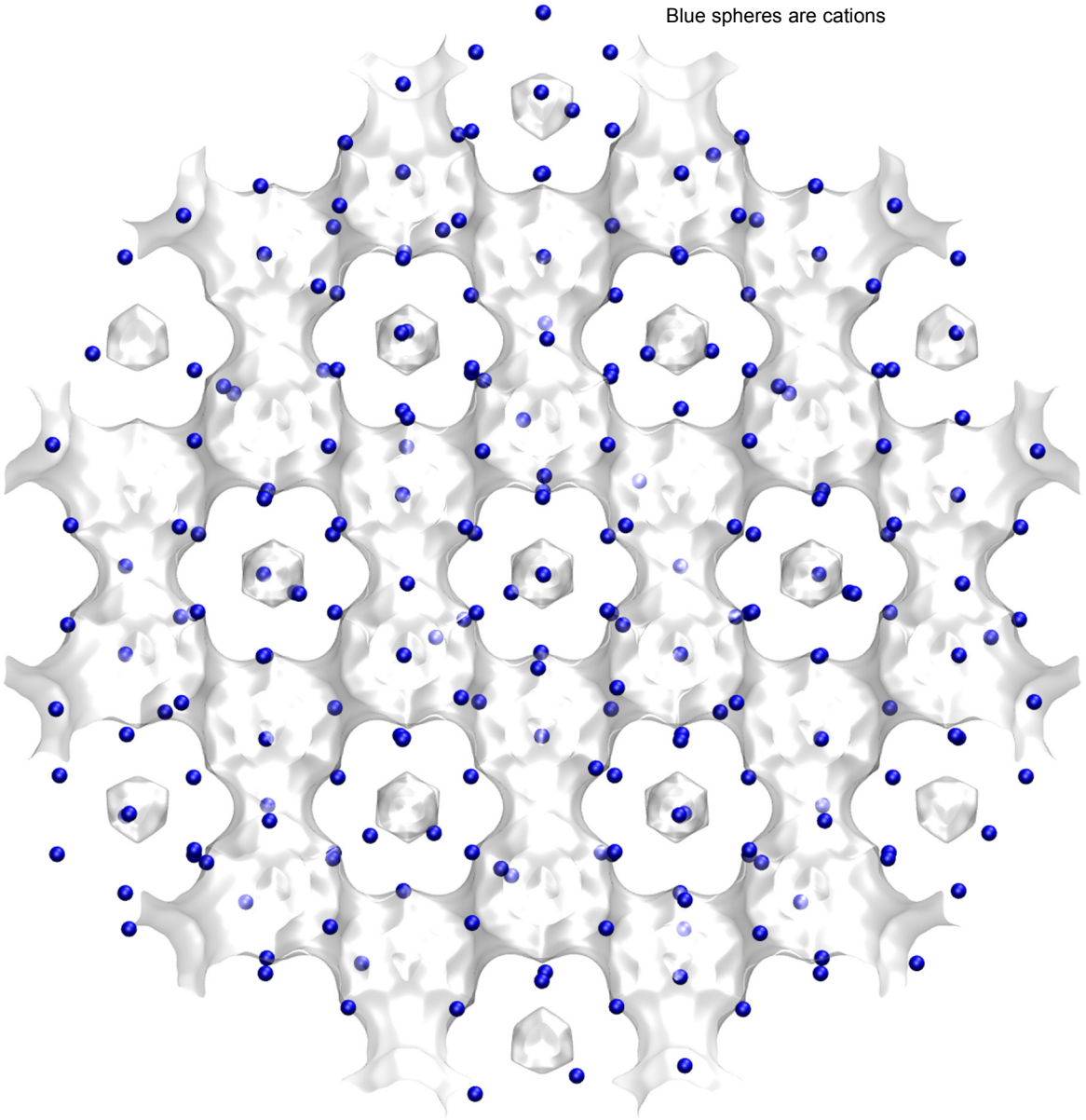

	FAU-86Al
a /Å	25.028
b /Å	25.028
c /Å	25.028
Cell volume / Å^3	15677.56
conversion factor for [molec/uc] to [mol per kg Framework]	0.0745
conversion factor for [molec/uc] to [kmol/m^3]	0.2658
ρ [kg/m3] (with cations)	1421.277
MW unit cell [g/mol(framework+cations)]	13418.42
ϕ, fractional pore volume	0.399
open space / Å^3/uc	6248.0
Pore volume / cm^3/g	0.280
Surface area /m^2/g	
DeLaunay diameter /Å	7.37

Influence of Inverse Thermodynamic Factor on diffusivities

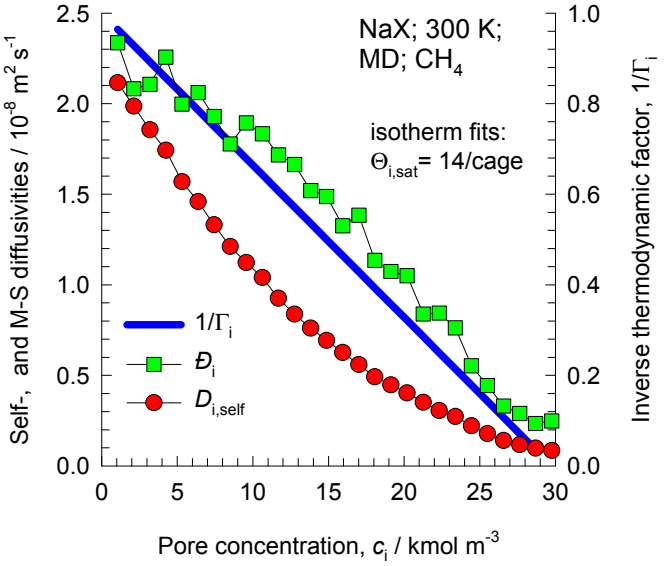

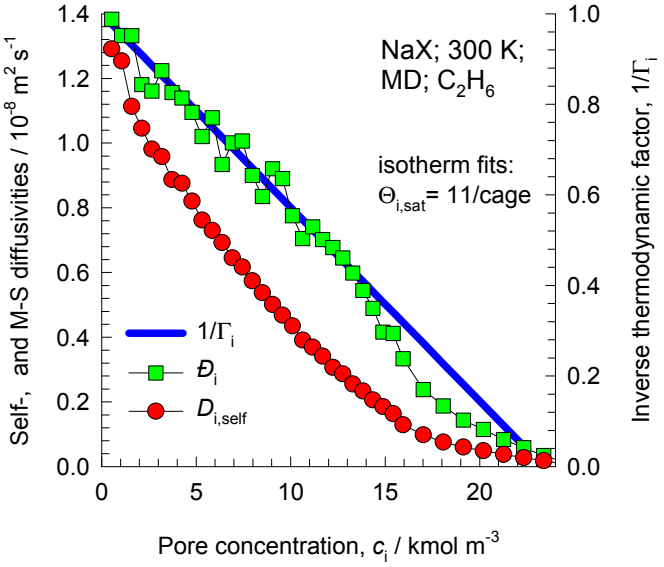

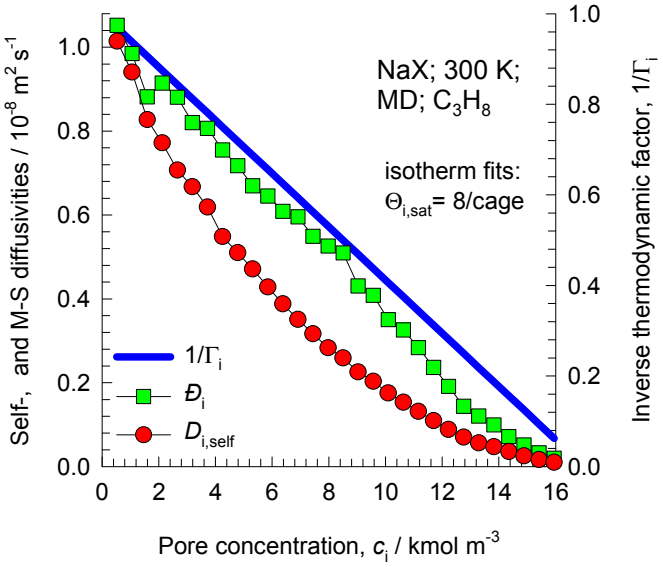

NaX NMR experiments of Caro

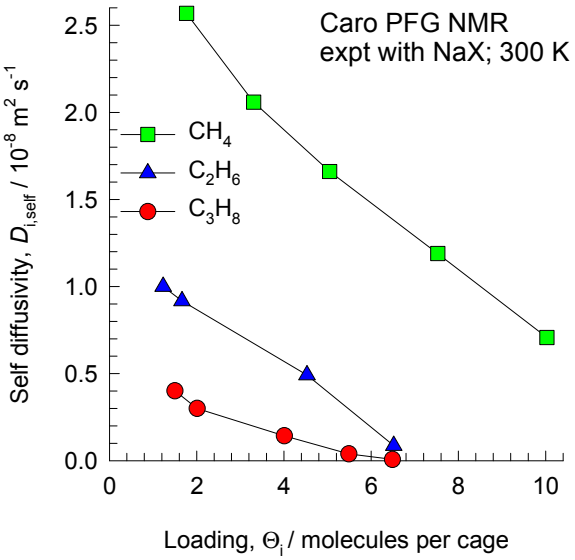

The experimental data are from
Caro, J.; Bülow, M.; Schirmer, W.; Kärger, J.; Heink, W.; Pfeifer, H. Microdynamics of methane, ethane and propane in ZSM-5 type zeolites. Journal of the Chemical Society, Faraday Transactions 1985, 81, 2541-2550.

NaX: Transient uptake of n-heptane and benzene

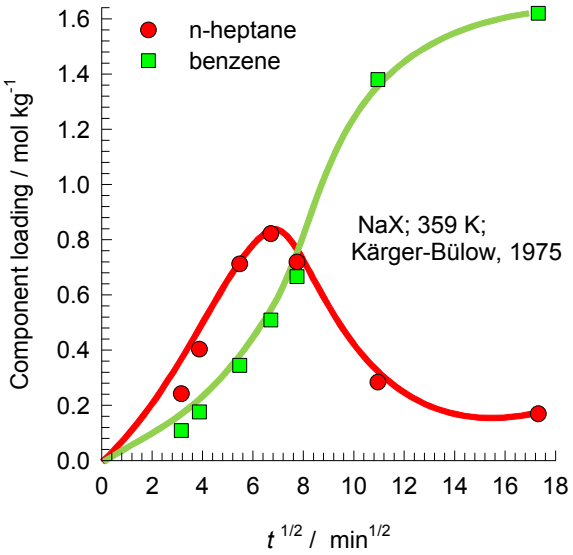

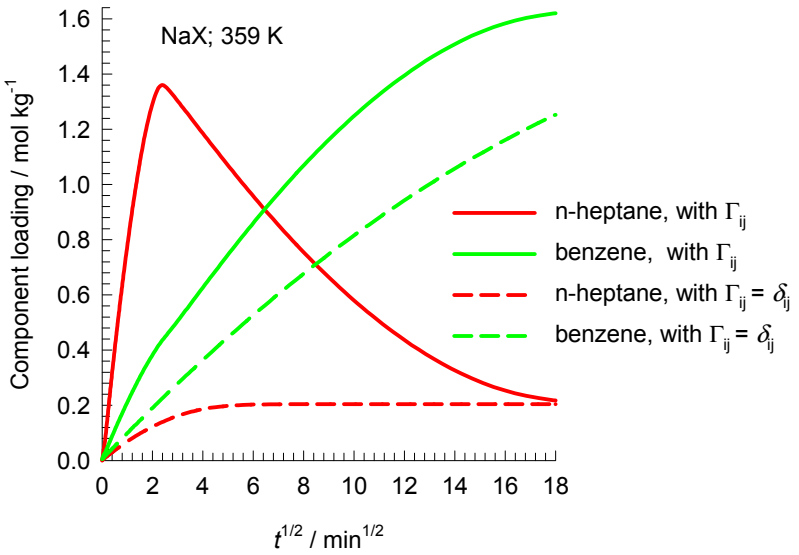

The data are re-plotted using the information contained in
Kärger, J.; Bülow, M. Theoretical prediction of uptake behaviour in adsorption kinetics of binary gas mixtures using irreversible thermodynamics, Chem. Eng. Sci. 1975, 30, 893-896.

The overshoot in the nC7 uptake is a direct consequence of thermodynamic coupling caused by the off-diagonal elements of $\begin{bmatrix} \Gamma_{11} & \Gamma_{12} \\ \Gamma_{21} & \Gamma_{21} \end{bmatrix}$ where $\Gamma_{ij} = \frac{q_i}{f_i}\frac{\partial f_i}{\partial q_j}$

This has been demonstrated by
Krishna, R. Multicomponent surface diffusion of adsorbed species - A description based on the generalized Maxwell-Stefan equations, Chem. Eng. Sci. 1990, 45, 1779-1791.

If the thermodynamic coupling is ignored, i.e. we assume $\begin{bmatrix} \Gamma_{11} & \Gamma_{12} \\ \Gamma_{21} & \Gamma_{21} \end{bmatrix} = \begin{bmatrix} 1 & 0 \\ 0 & 1 \end{bmatrix}$

the nC7 overshoot disappears.

CuBTC pore landscapes

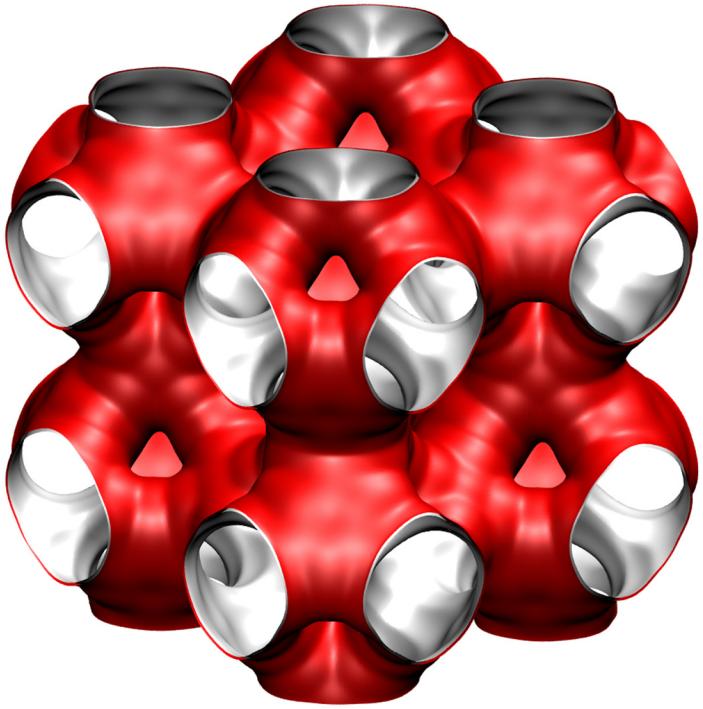

The structural information for CuBTC (= $Cu_3(BTC)_2$ with BTC = 1,3,5-benzenetricarboxylate) have been taken from

S.S.Y. Chui, S.M.F. Lo, J.P.H. Charmant, A.G. Orpen, I.D. Williams, A chemically functionalizable nanoporous material $[Cu_3(TMA)_2(H2O)_3]_n$, Science 283 (1999) 1148-1150.
The crystal structure of Chui et al. includes axial oxygen atoms weakly bonded to the Cu atoms, which correspond to water ligands. Our simulations have been performed on the dry CuBTC with these oxygen atoms removed.

Q. Yang, C. Zhong, Electrostatic-Field-Induced Enhancement of Gas Mixture Separation in Metal-Organic Frameworks: A Computational Study, ChemPhysChem 7 (2006) 1417-1421.

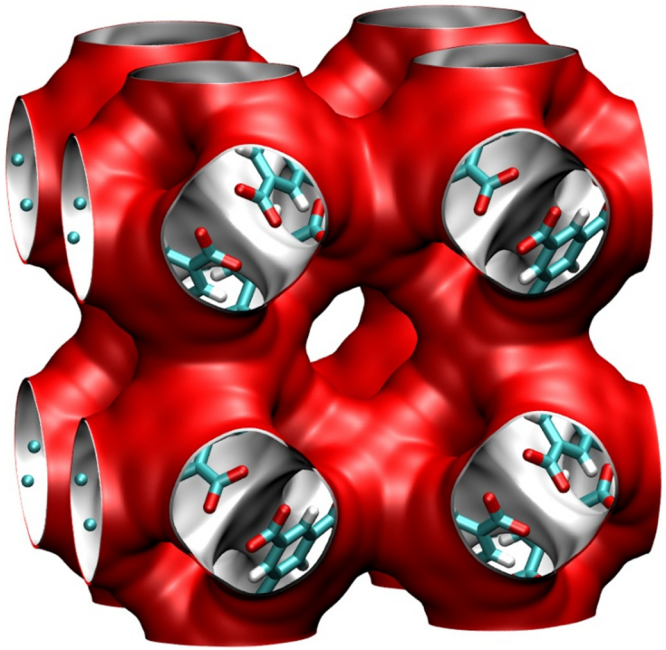

Snapshot of CO_2/CH_4 mixture

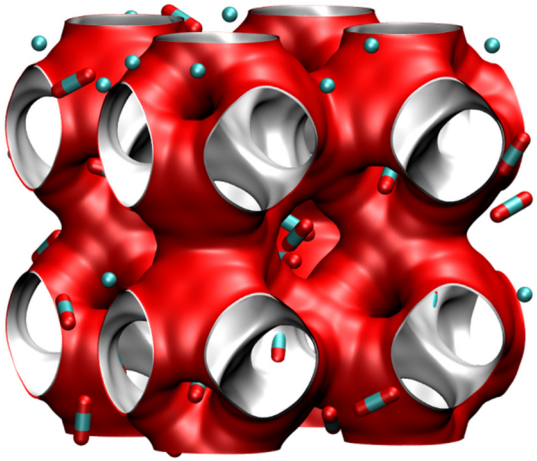

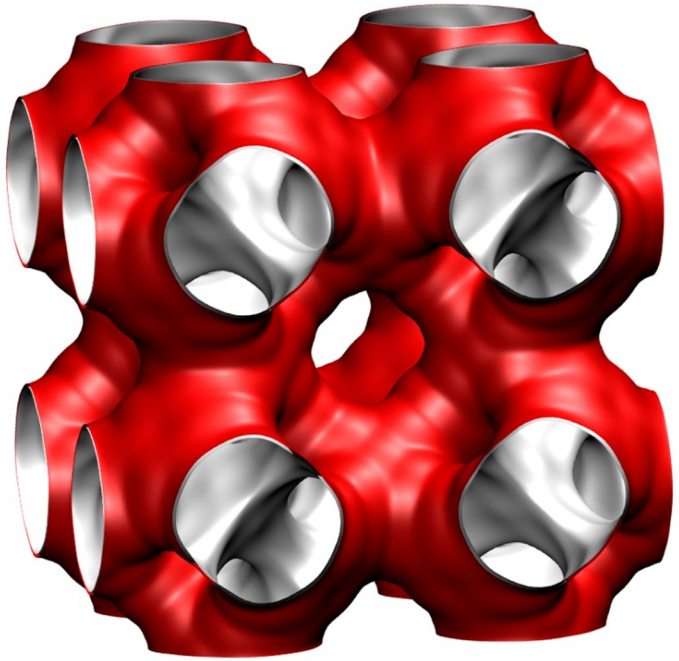

CuBTC pore dimensions

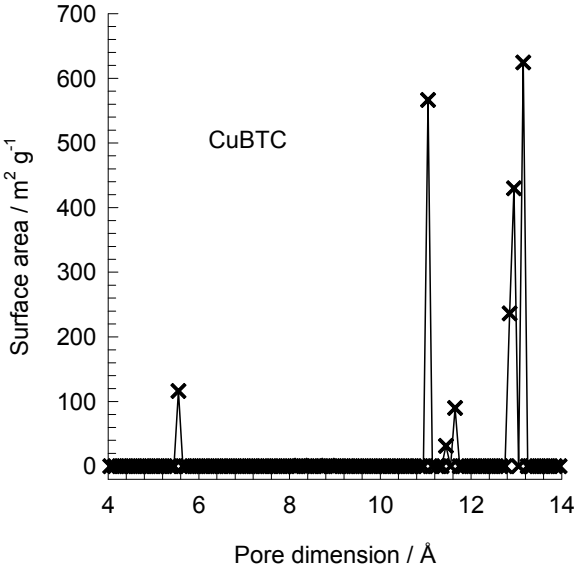

This plot of surface area versus pore dimension is determined using a combination of the DeLaunay triangulation method for pore dimension determination, and the procedure of Düren for determination of the surface area.

	CuBTC
a /Å	26.343
b /Å	26.343
c /Å	26.343
Cell volume / Å^3	18280.82
conversion factor for [molec/uc] to [mol per kg Framework]	0.1034
conversion factor for [molec/uc] to [kmol/m^3]	0.1218
ρ [kg/m3]	878.8298
MW unit cell [g/mol(framework)]	9674.855
ϕ, fractional pore volume	0.746
open space / Å^3/uc	13628.4
Pore volume / cm^3/g	0.848
Surface area /m^2/g	2097.0
DeLaunay diameter /Å	6.23

The CuBTC structure consists of two types of “cages” and two types of “windows” separating these cages. Large cages are inter-connected by 9 Å windows of square cross-section. The large cages are also connected to tetrahedral-shaped pockets of ca. 6 Å size through triangular-shaped windows of ca. 4.6 Å size

CuBTC CBMC simulations of isotherms, and isosteric heats of adsorption

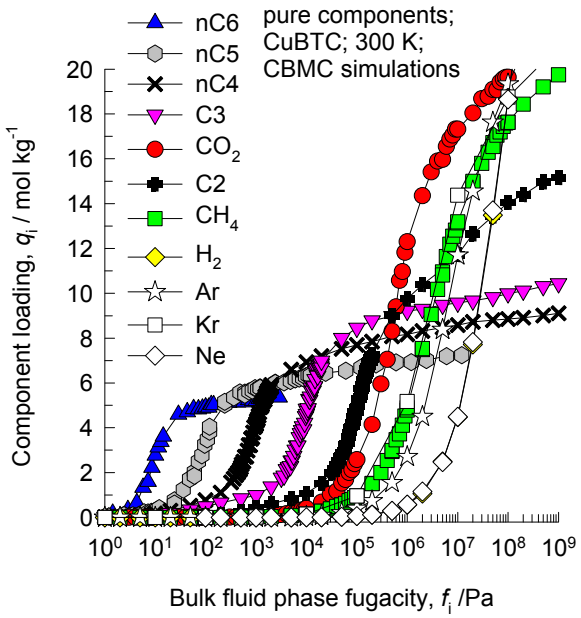

Note that C2 and C3 refer to saturated alkanes

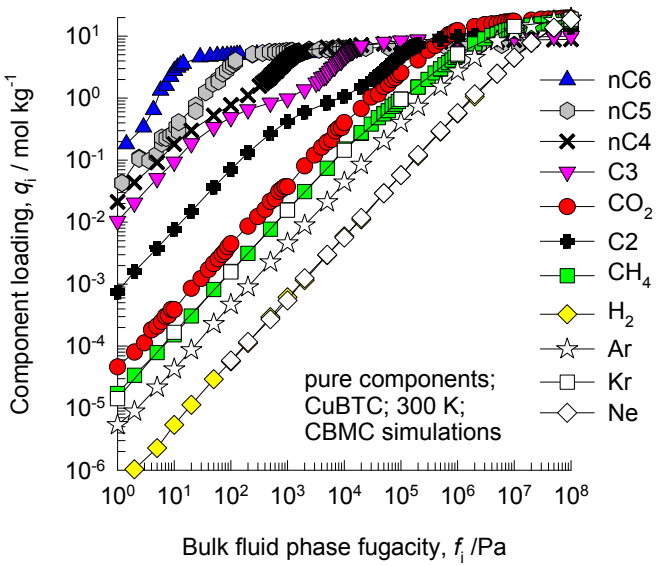

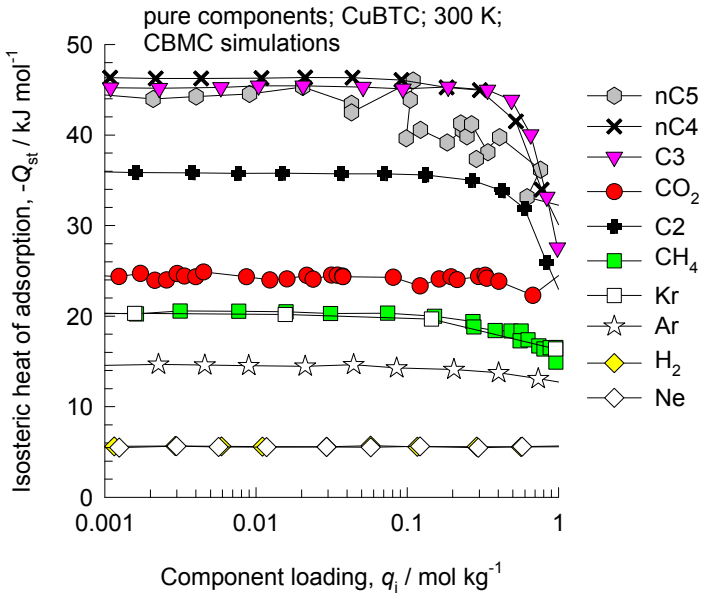

Influence of $-Q_{st}$ on diffusivities

Location of CH_4 inside the tetrahedral pockets

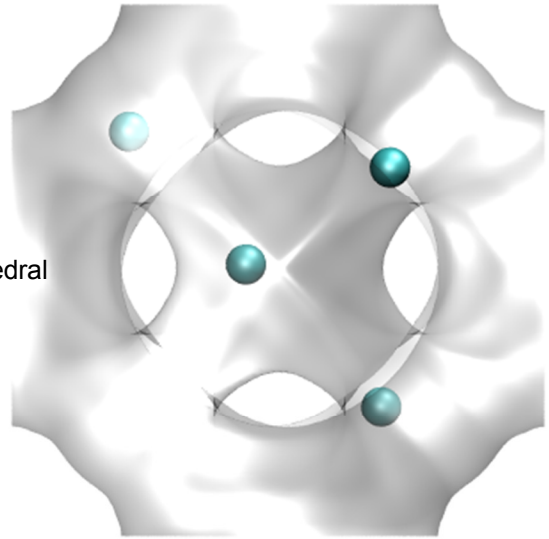

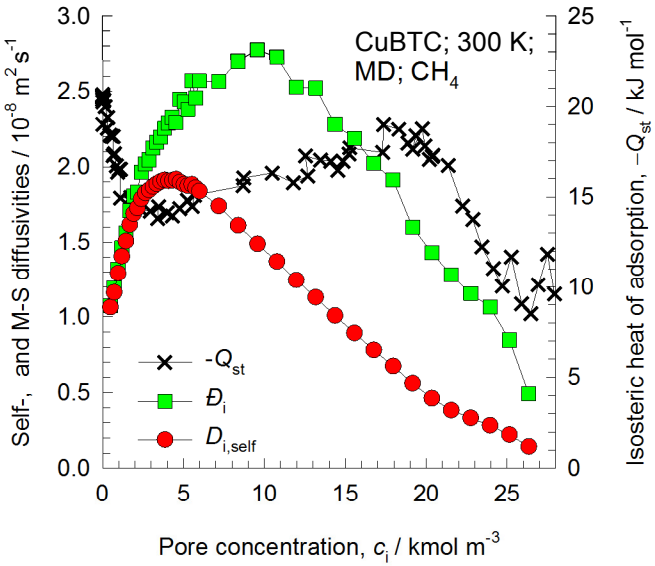

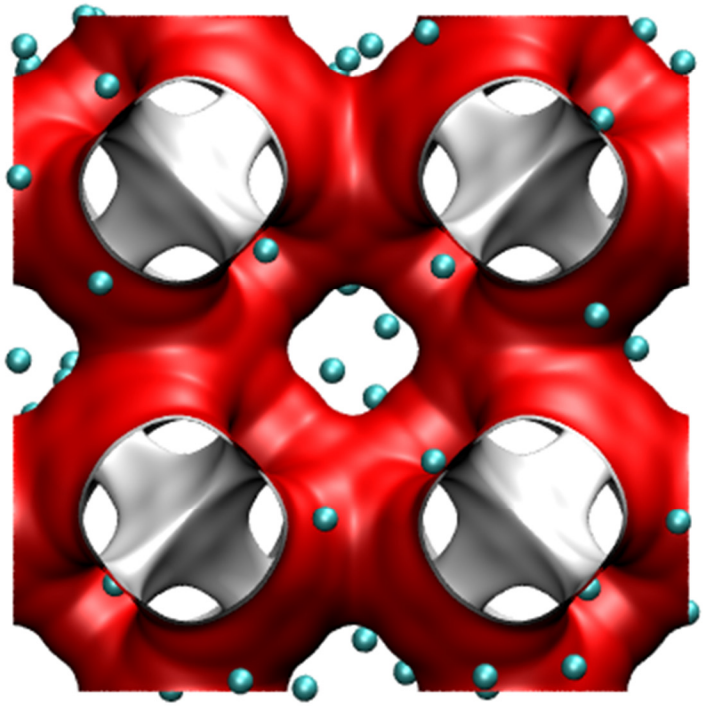

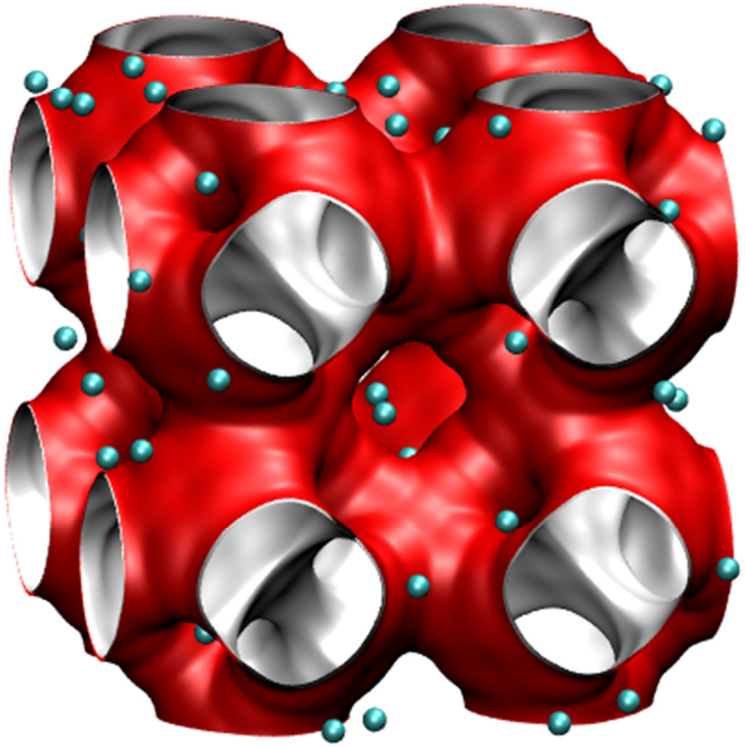

Influence of $-Q_{st}$ on diffusivities

Location of C_2H_6 inside the tetrahedral pockets

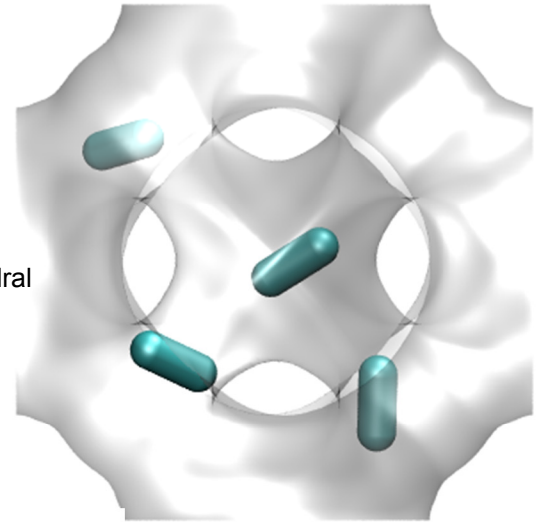

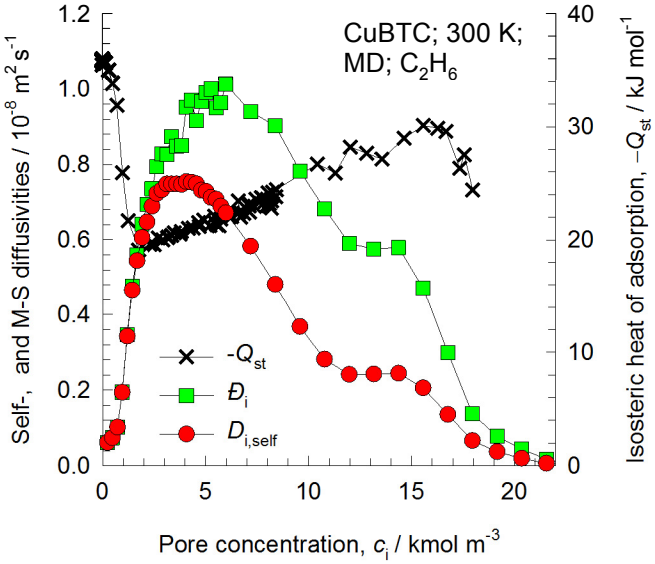

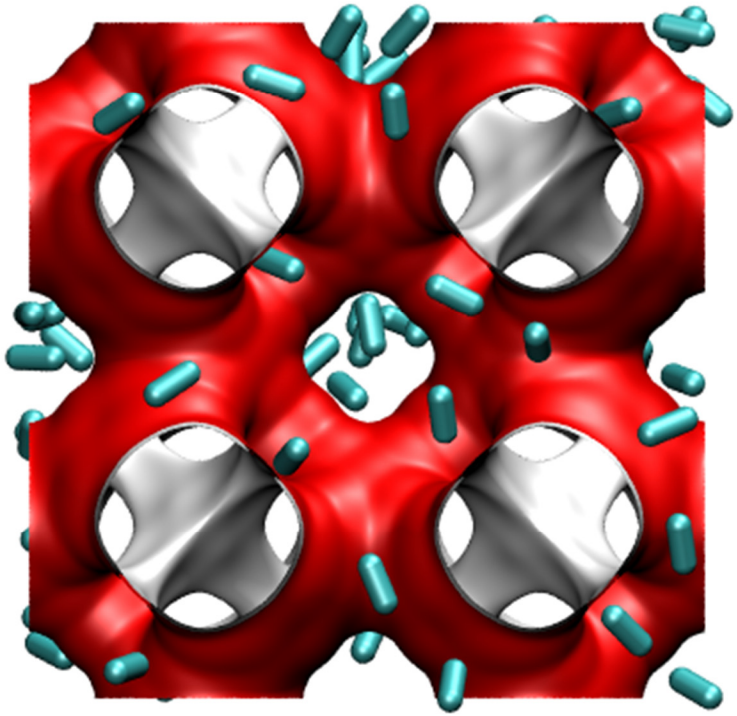

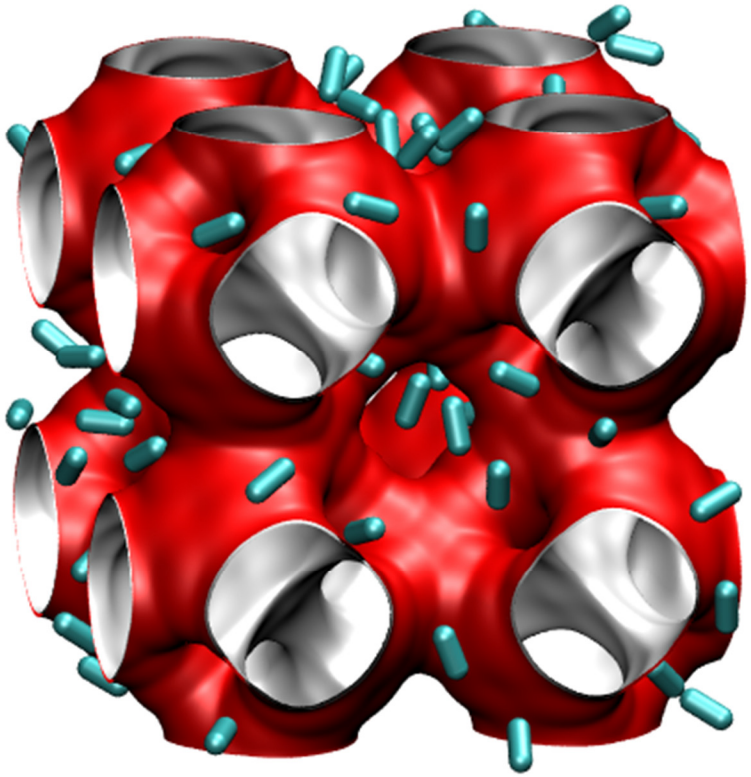

Influence of $-Q_{st}$ on diffusivities

Location of C_3H_8 inside the tetrahedral pockets

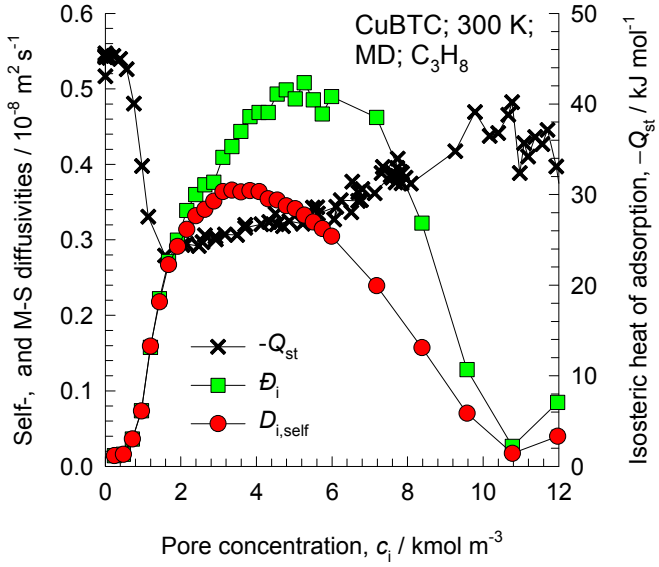

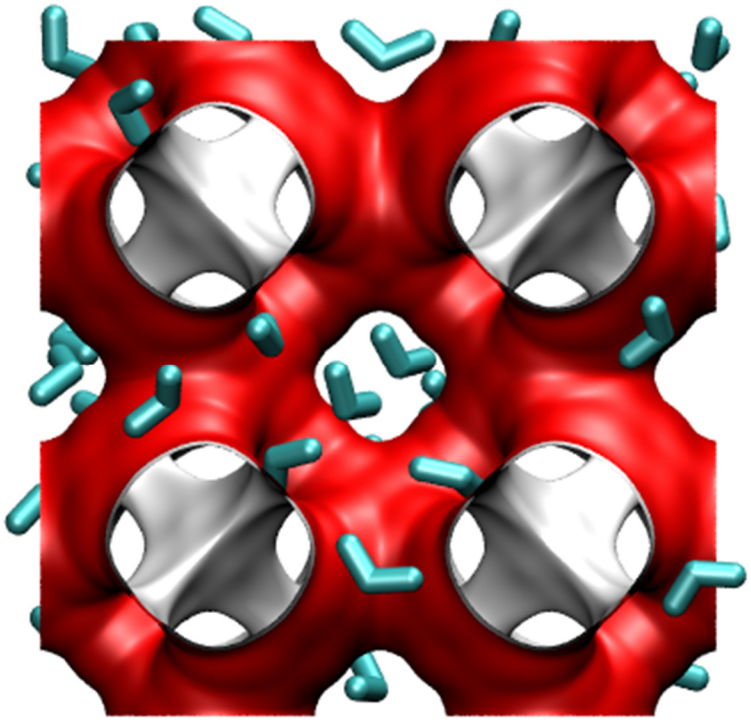

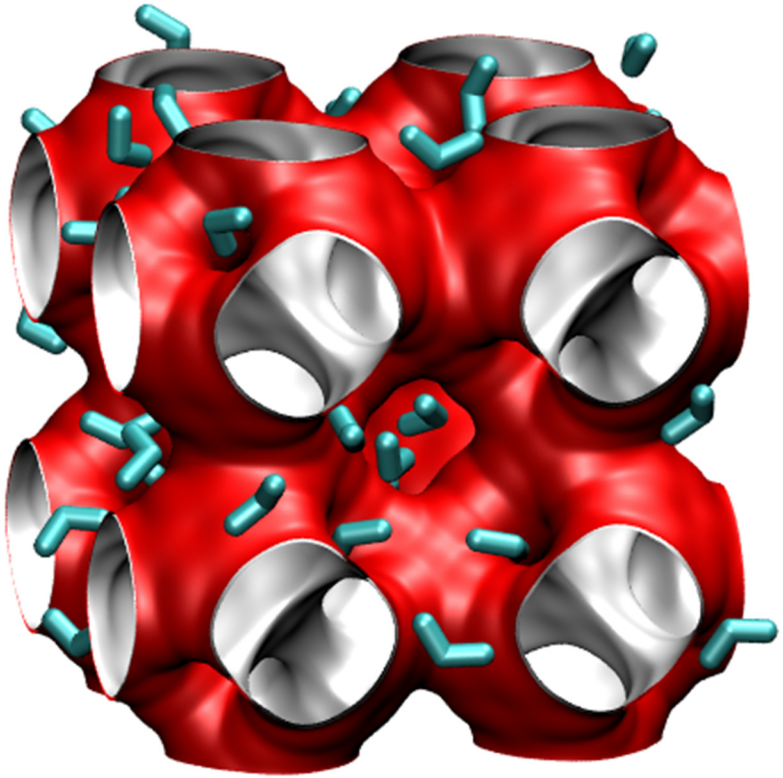

Influence of $-Q_{st}$ on diffusivities

Location of nC_4H_{10} inside the tetrahedral pockets

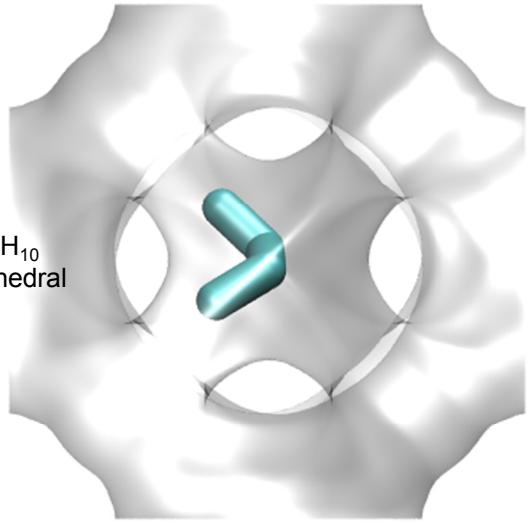

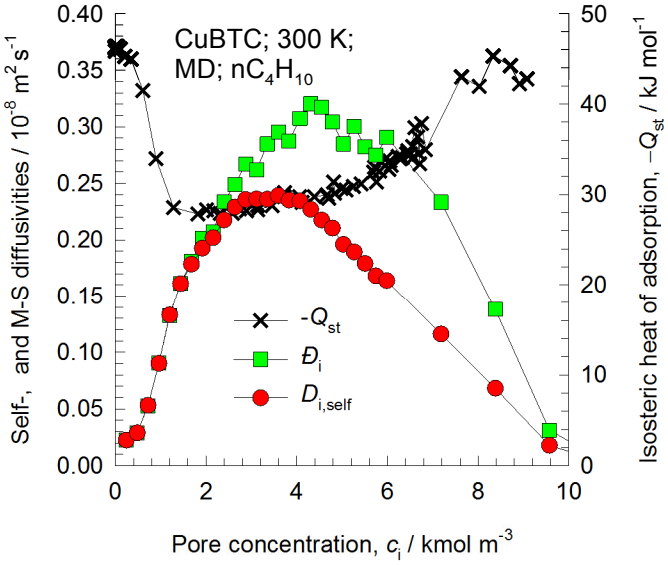

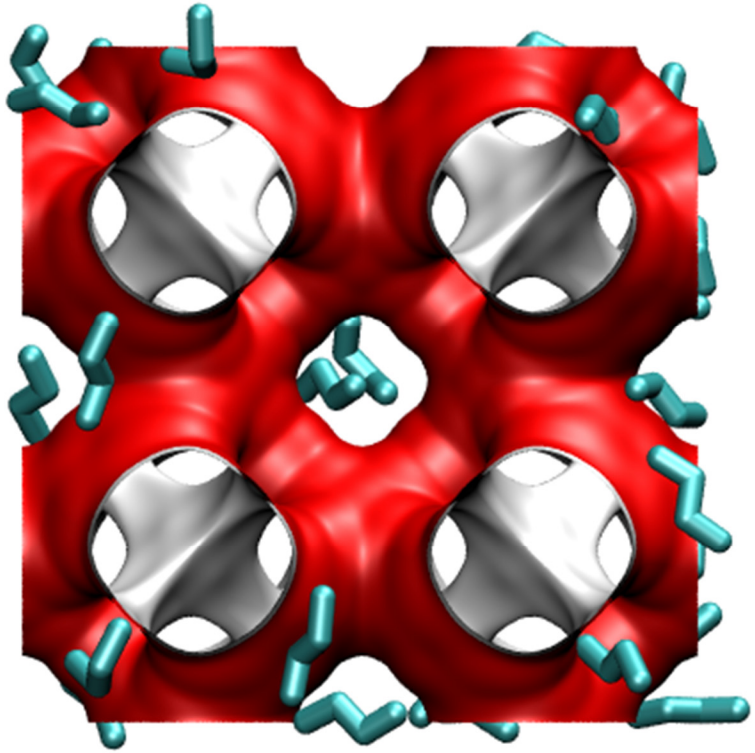

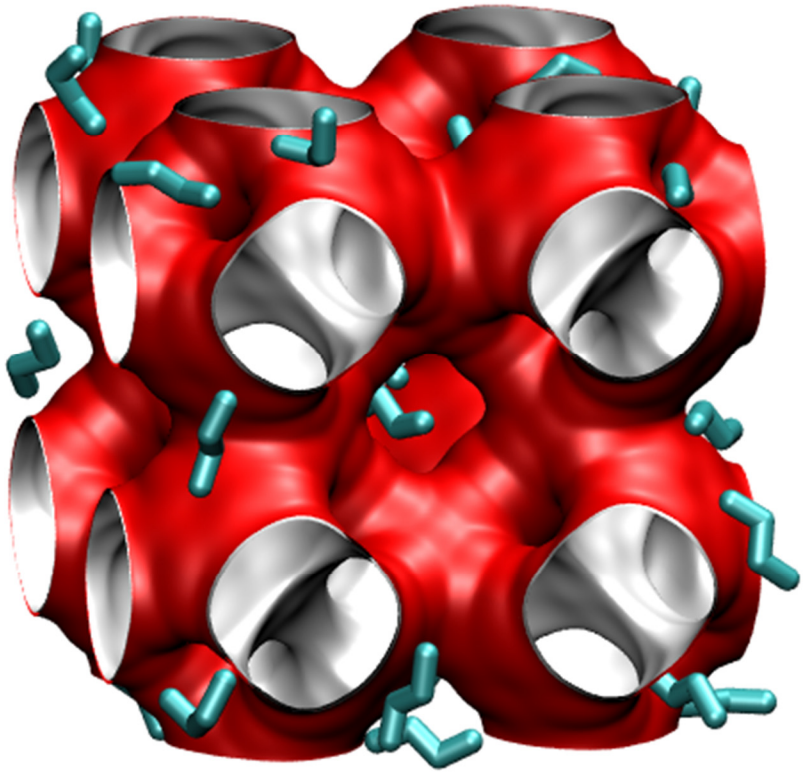

Influence of $-Q_{st}$ on diffusivities

Location of iC_4H_{10} inside the tetrahedral pockets

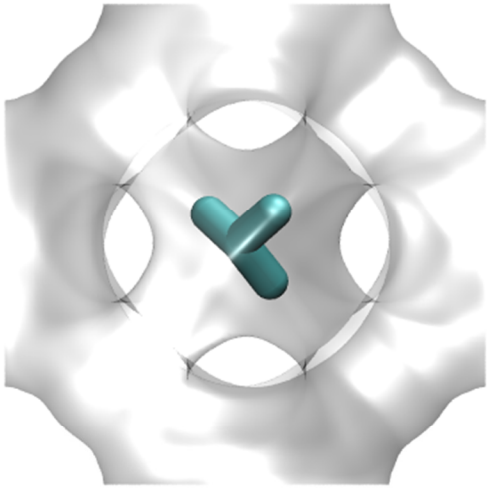

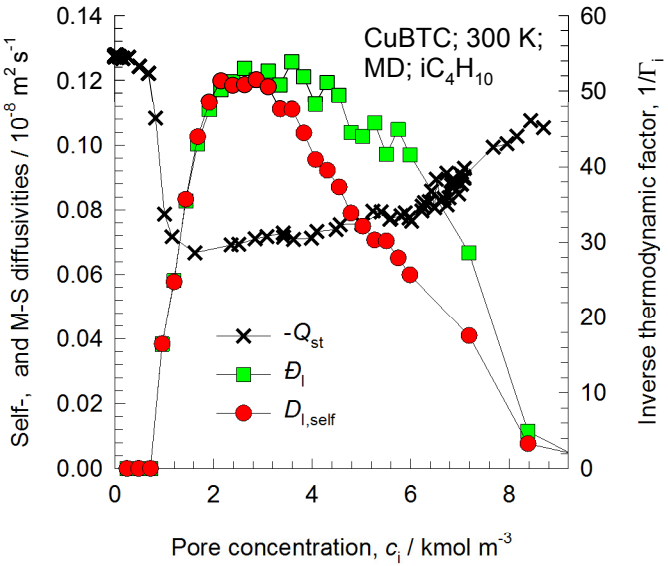

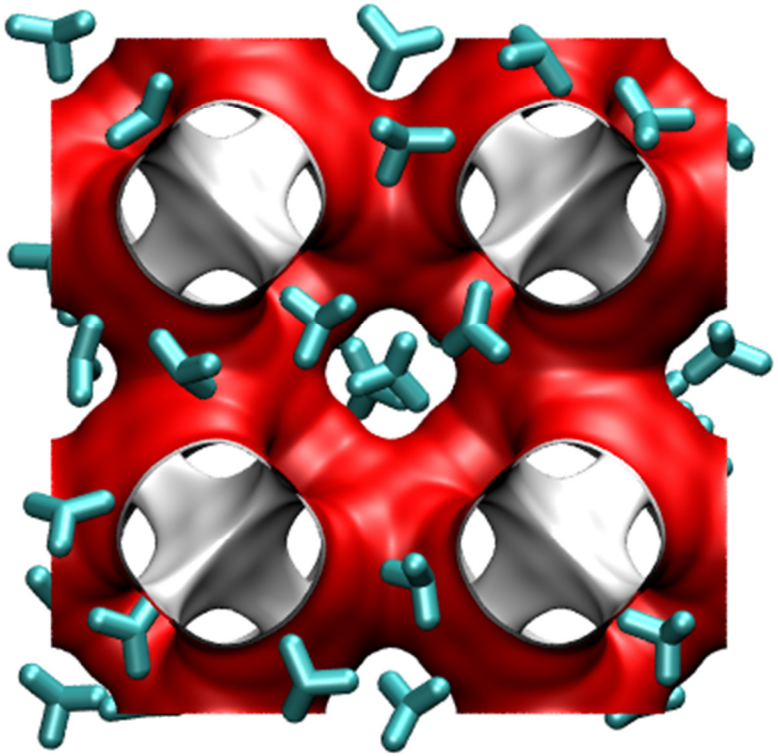

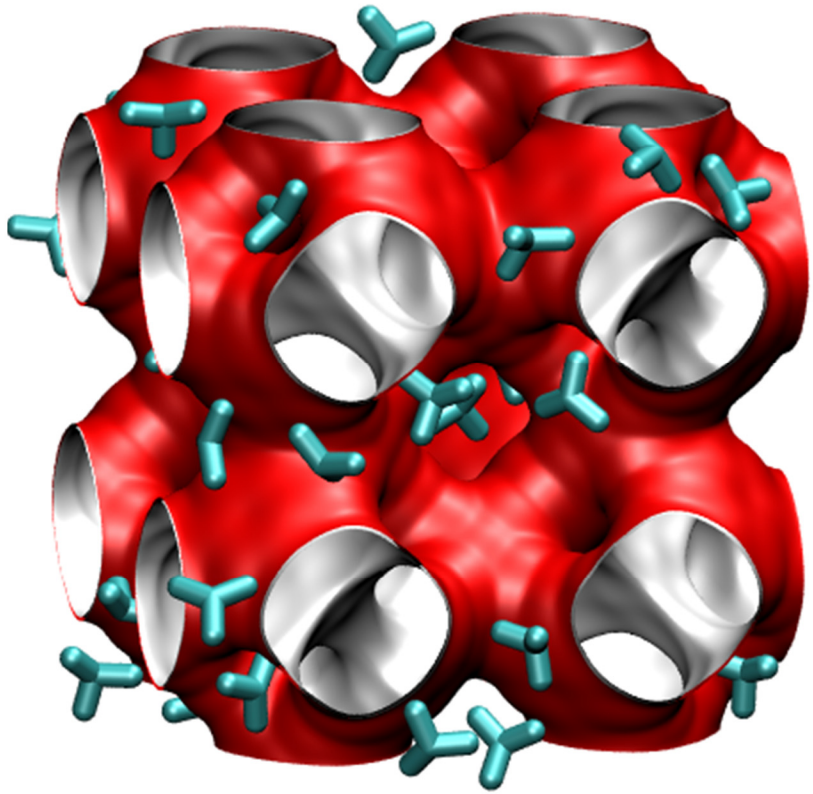

CuBTC MD simulations of unary self- , and M-S diffusivities

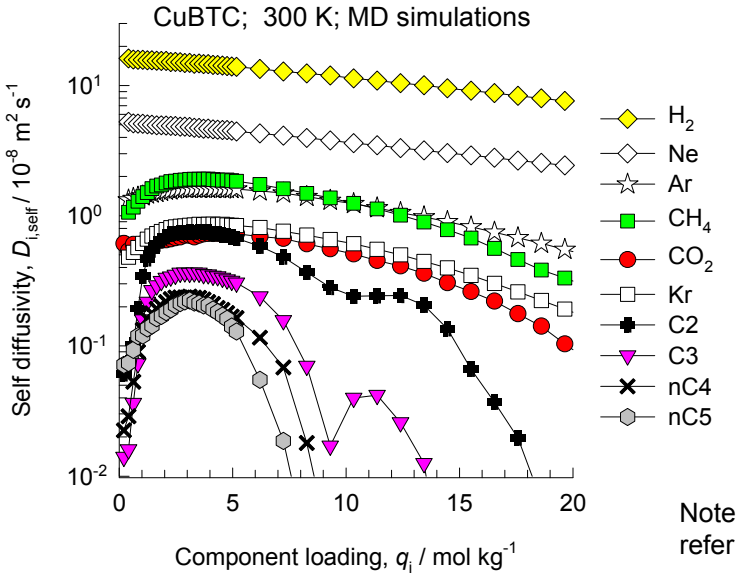

Note that C2 and C3 refer to saturated alkanes

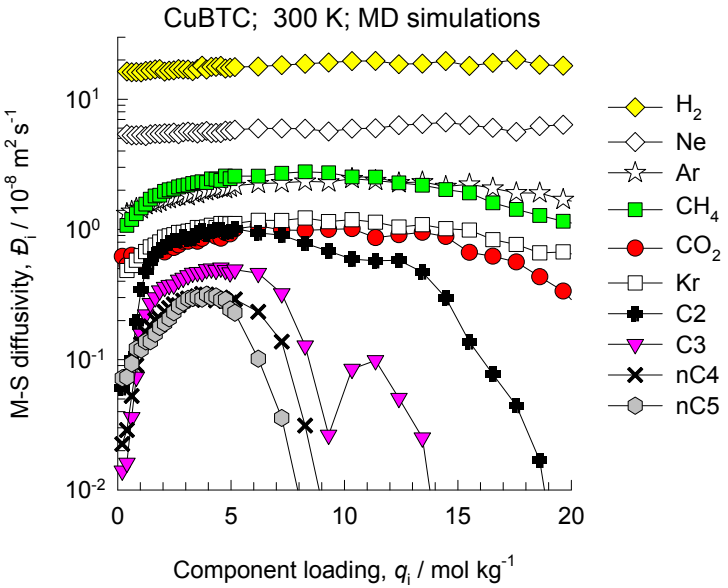

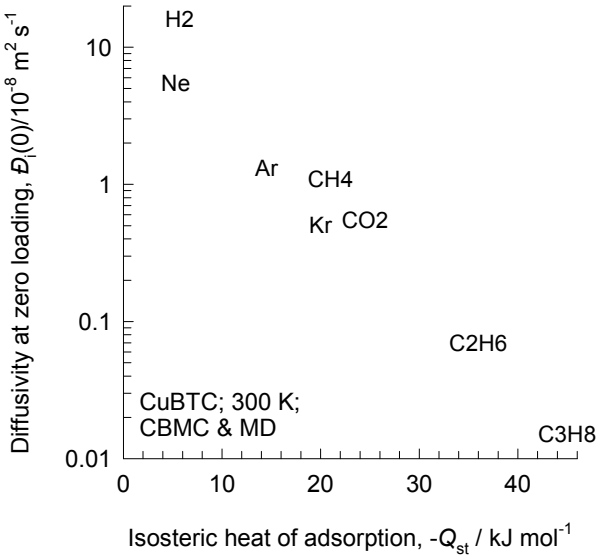

IRMOF-1 pore landscape

For IRMOF-1 (= MOF 5 = $Zn_4O(BDC)_3$ with BDC^{2-} = 1-4 benzenedicarboxylate) the structural information was obtained from

D. Dubbeldam, K.S. Walton, D.E. Ellis, R.Q. Snurr, Exceptional Negative Thermal Expansion in Isoreticular Metal–Organic Frameworks, Angew. Chem. Int. Ed. 46 (2007) 4496-4499.

D. Dubbeldam, H. Frost, K.S. Walton, R.Q. Snurr, Molecular simulation of adsorption sites of light gases in the metal-organic framework IRMOF-1, Fluid Phase Equilib. 261 (2007) 152-161.

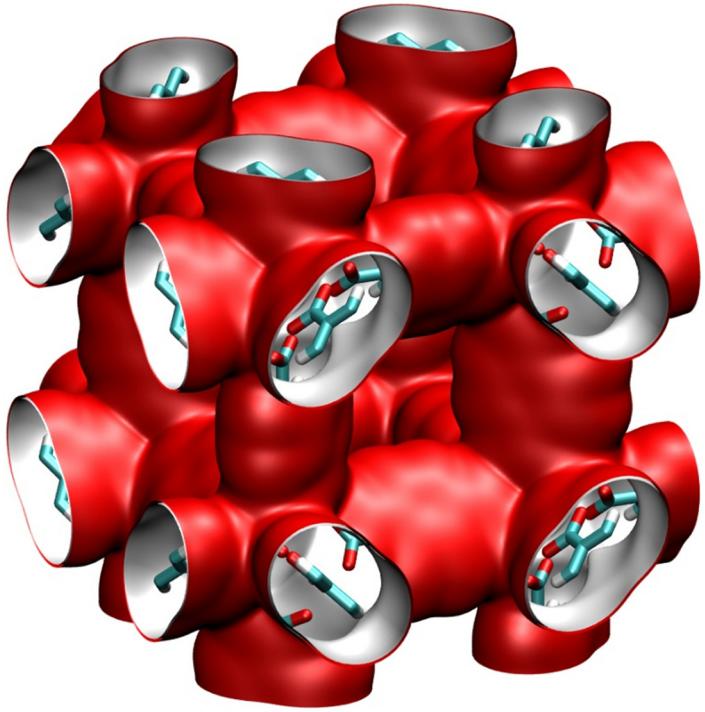

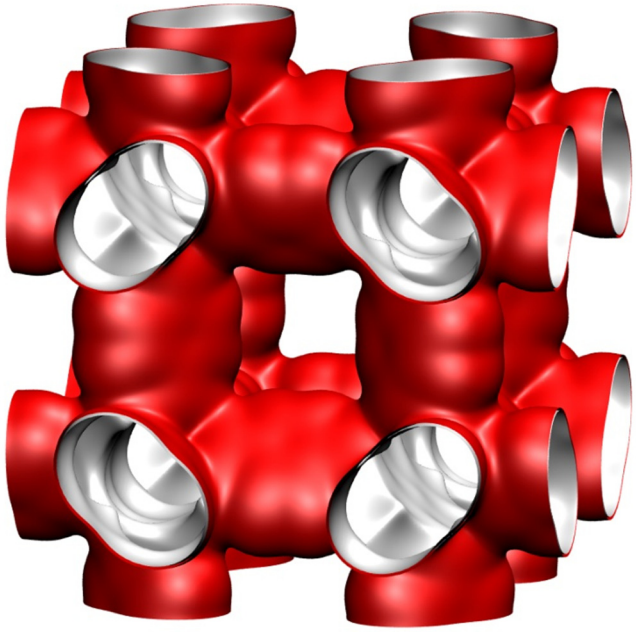

Snapshot of CO_2/CH_4 mixture

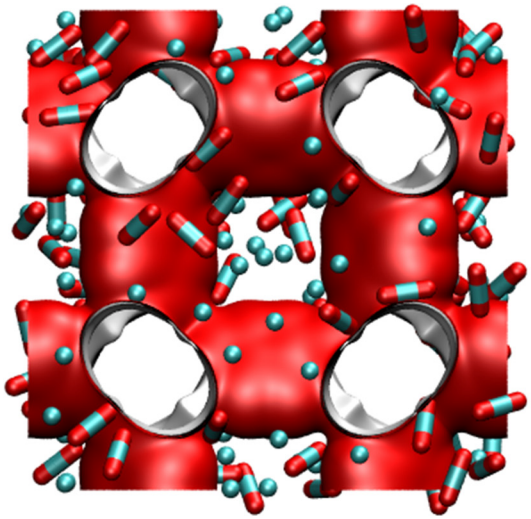

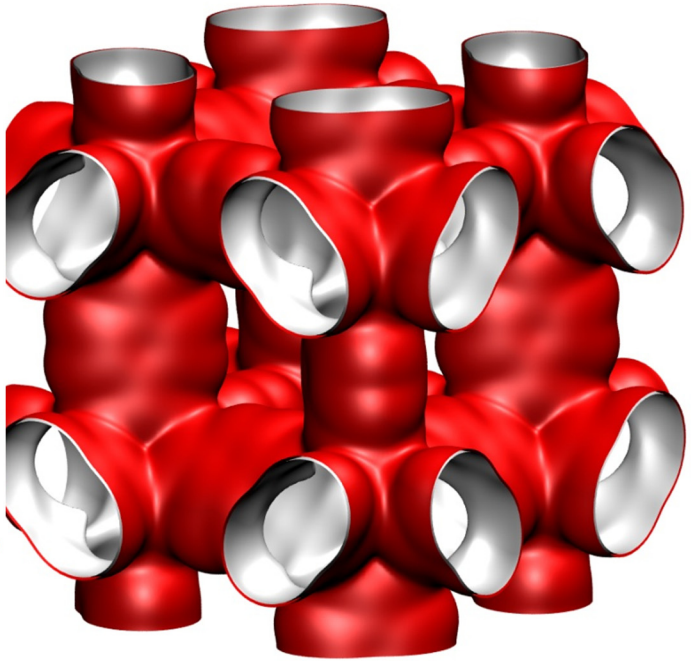

IRMOF-1 pore dimensions

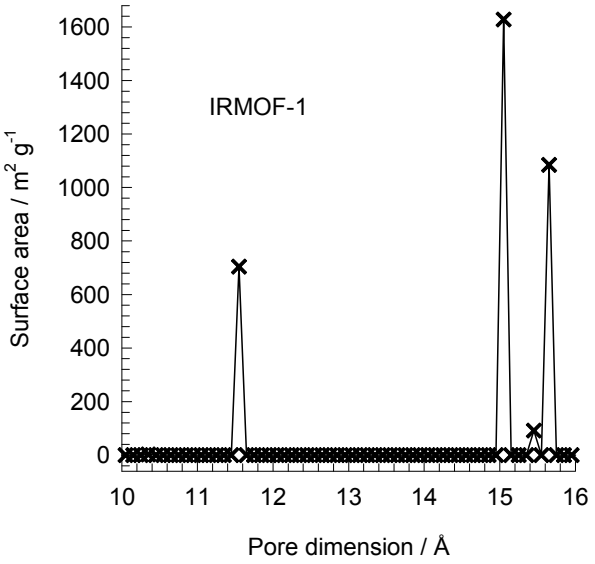

This plot of surface area versus pore dimension is determined using a combination of the DeLaunay triangulation method for pore dimension determination, and the procedure of Düren for determination of the surface area.

	IRMOF-1
a /Å	25.832
b /Å	25.832
c /Å	25.832
Cell volume / Å^3	17237.49
conversion factor for [molec/uc] to [mol per kg Framework]	0.1624
conversion factor for [molec/uc] to [kmol/m^3]	0.1186
ρ [kg/m3]	593.2075
MW unit cell [g/mol(framework)]	6157.788
ϕ, fractional pore volume	0.812
open space / Å^3/uc	13996.3
Pore volume / cm^3/g	1.369
Surface area /m^2/g	3522.2
DeLaunay diameter /Å	7.38

Two alternating, inter-connected, cavities of 11 Å and 15 Å with window size of 8 Å.

IRMOF-1 CBMC simulations of isotherms, and isosteric heats of adsorption

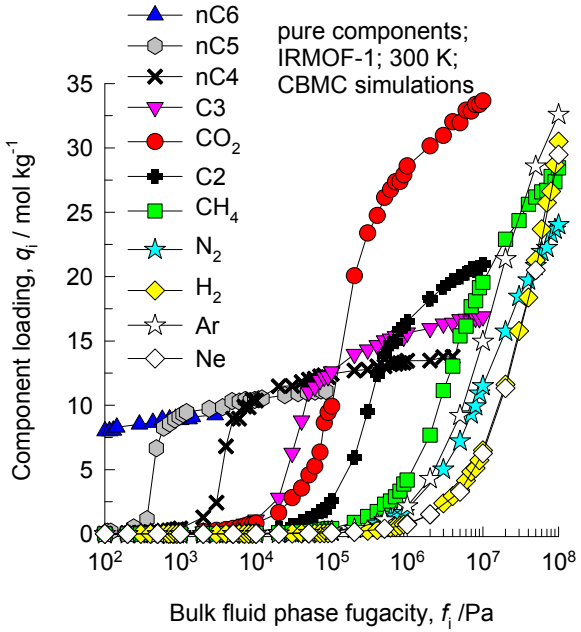

Note that C2 and C3 refer to saturated alkanes

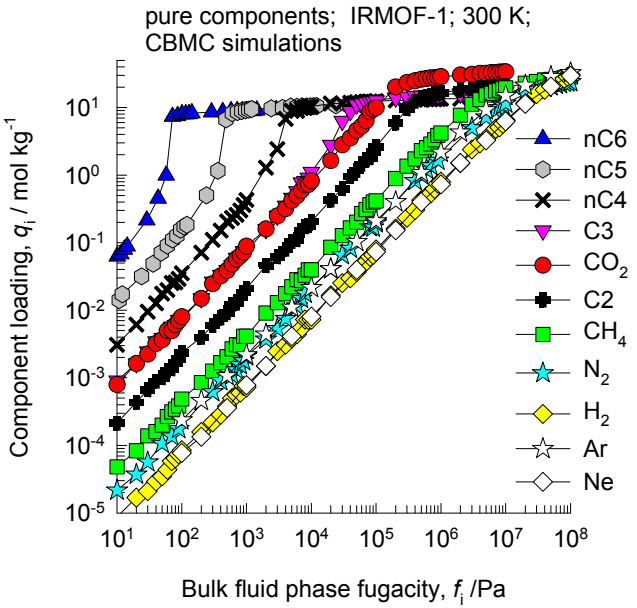

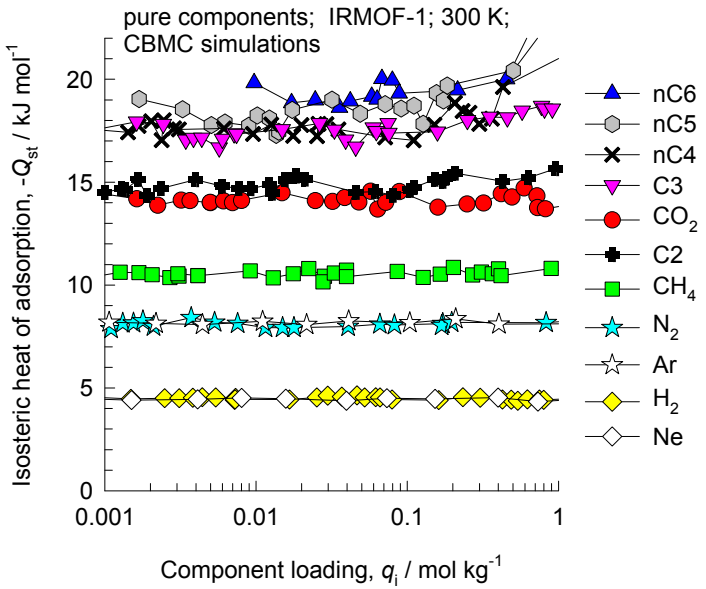

IRMOF-1 CO_2 adsorption and diffusion

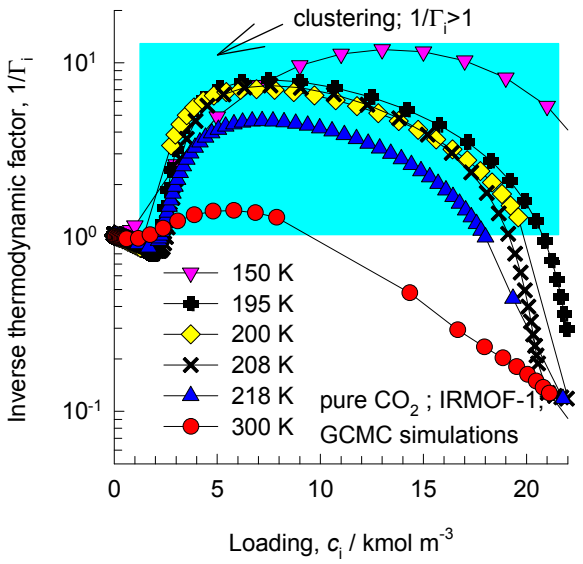

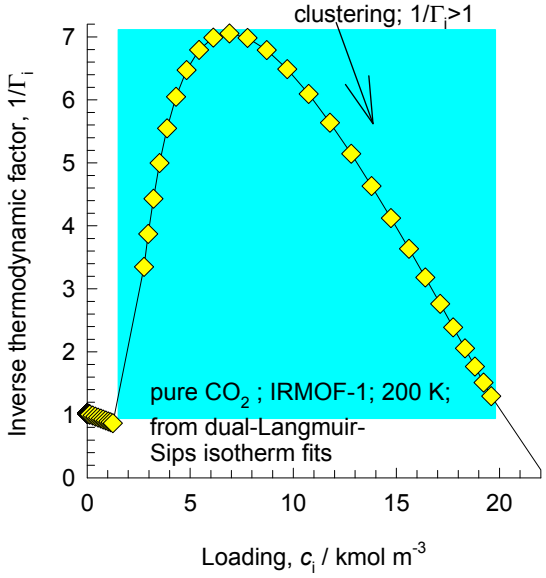

The RDFs show that the degree of clustering increases as the temperature is decreased.

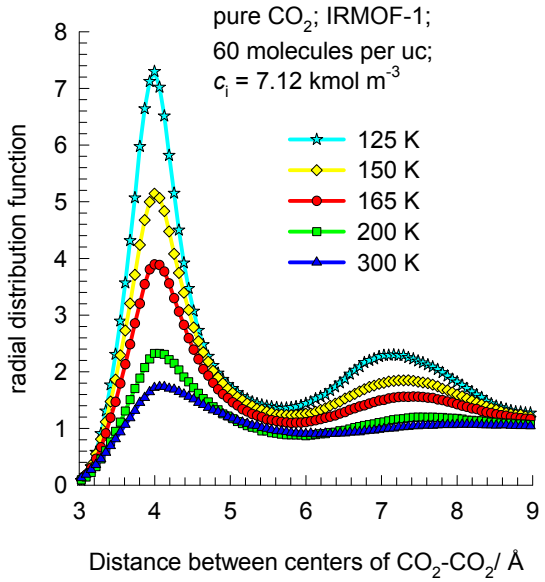

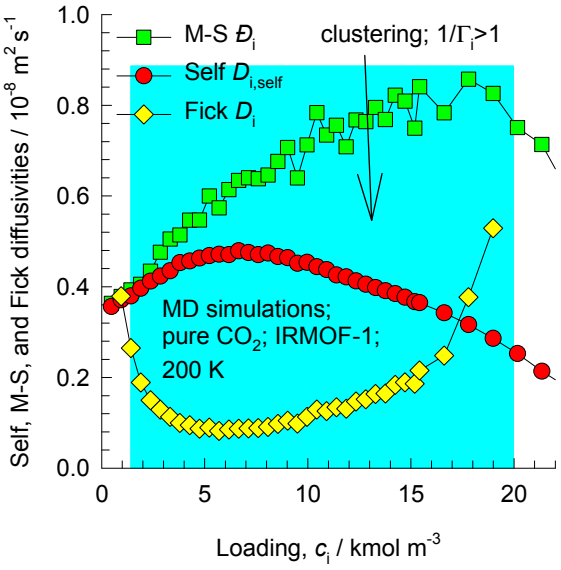

IRMOF-1 CH_4 adsorption and diffusion

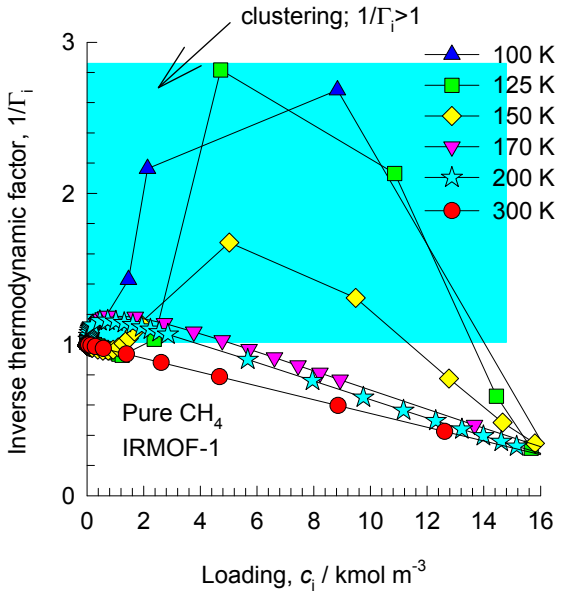

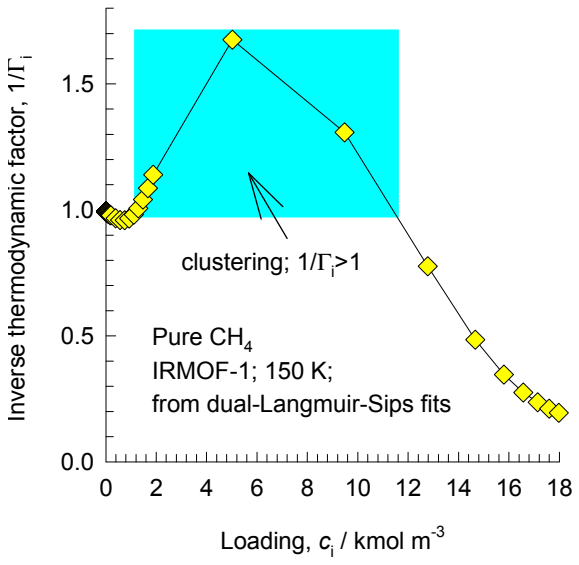

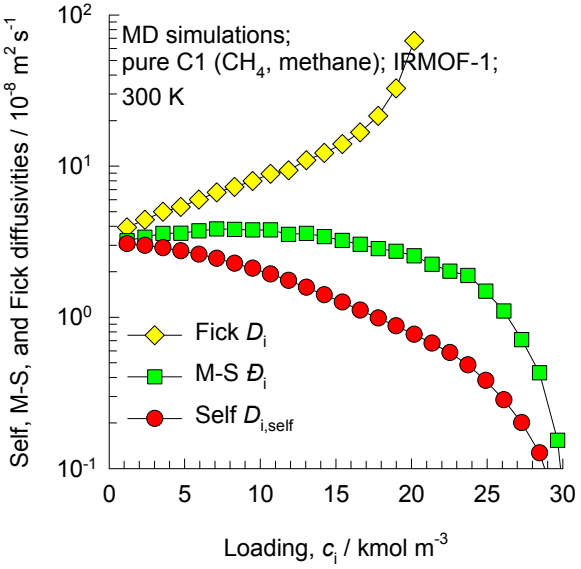

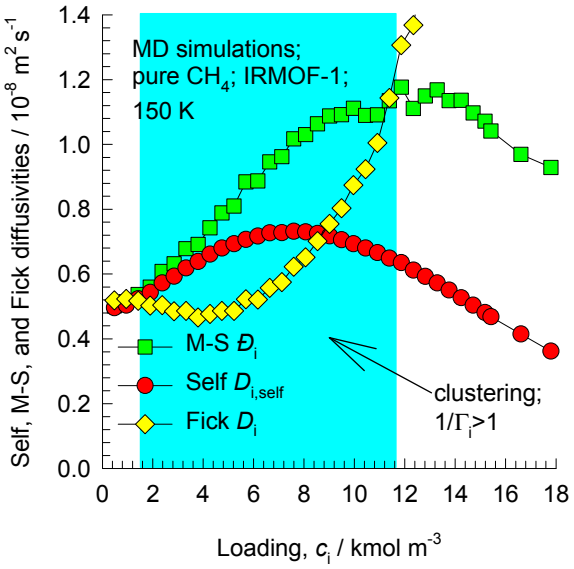

Electronic Supplementary Material (ESI) for Physical Chemistry Chemical Physics

IRMOF-1 Ar adsorption and diffusion

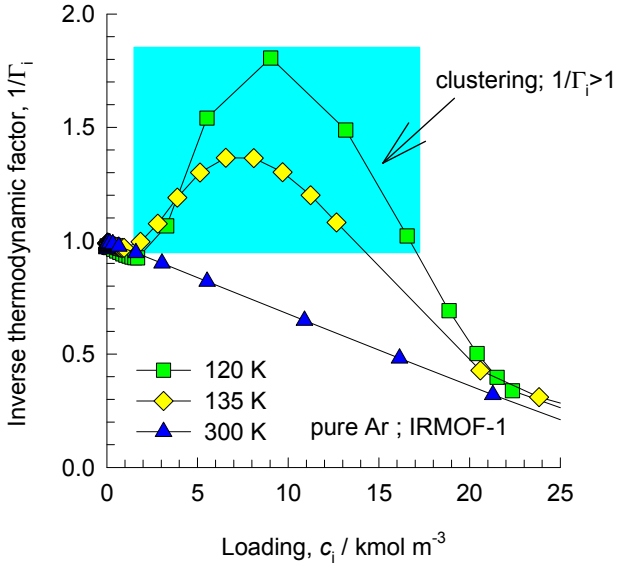

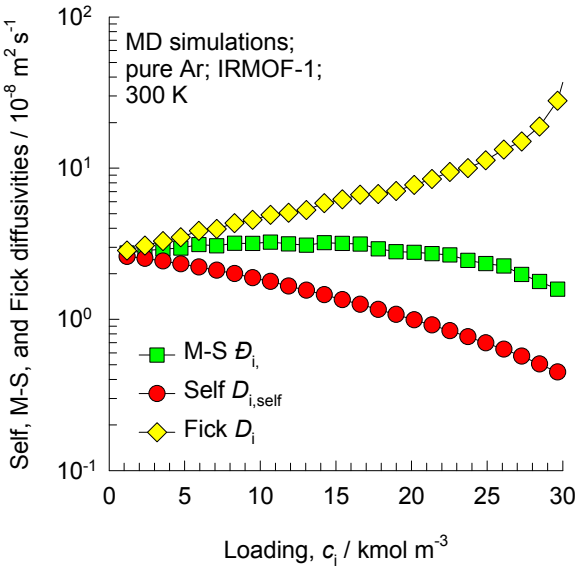

IRMOF-1 CBMC simulations for linear alkanes

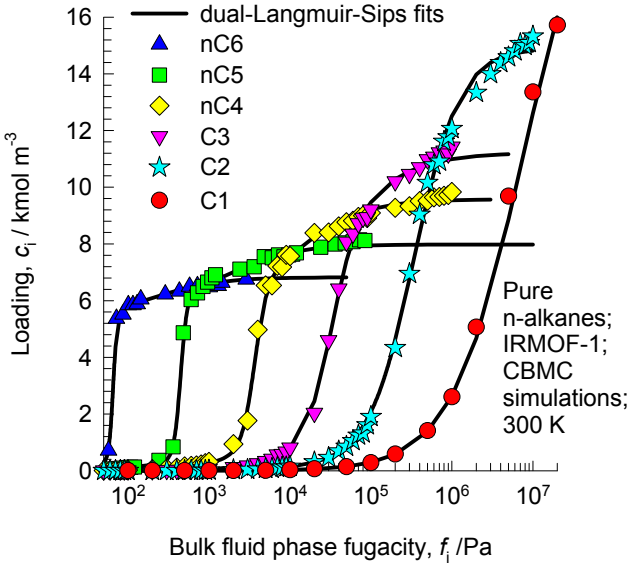

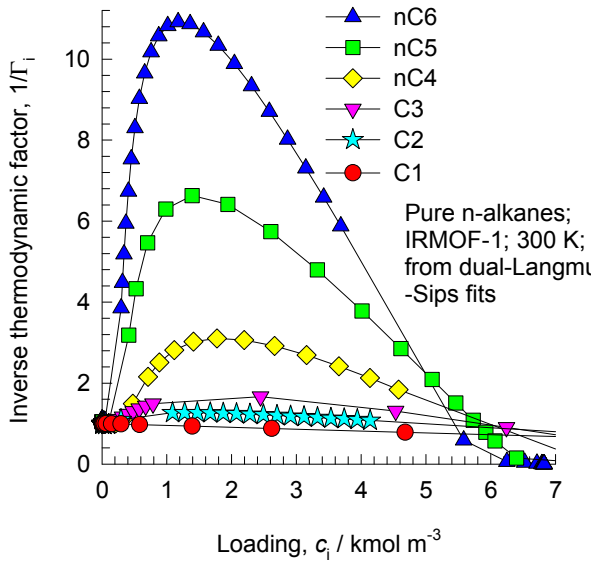

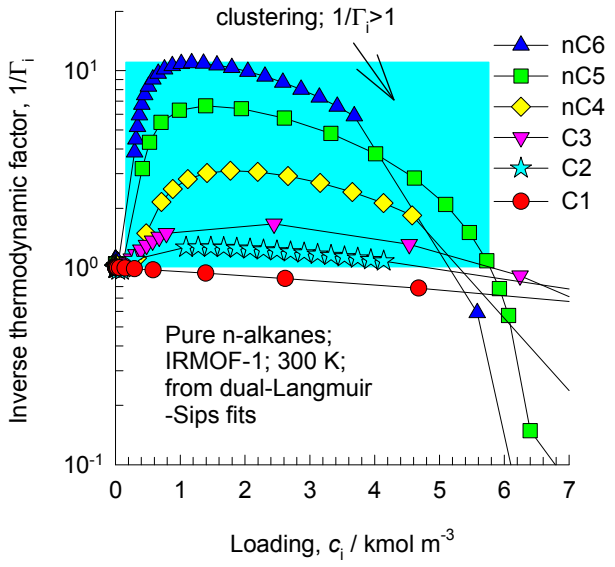

IRMOF-1 CBMC simulations for pure C4 and C5 isomers

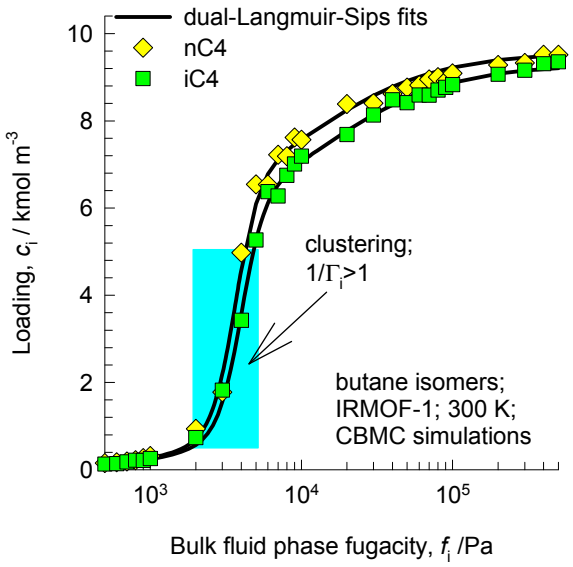

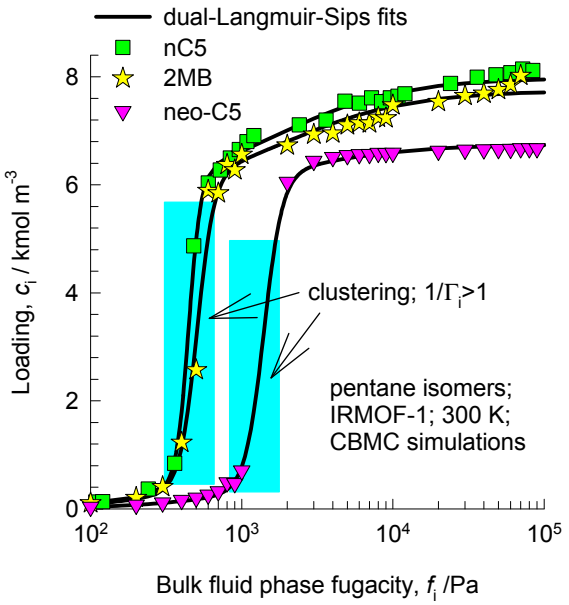

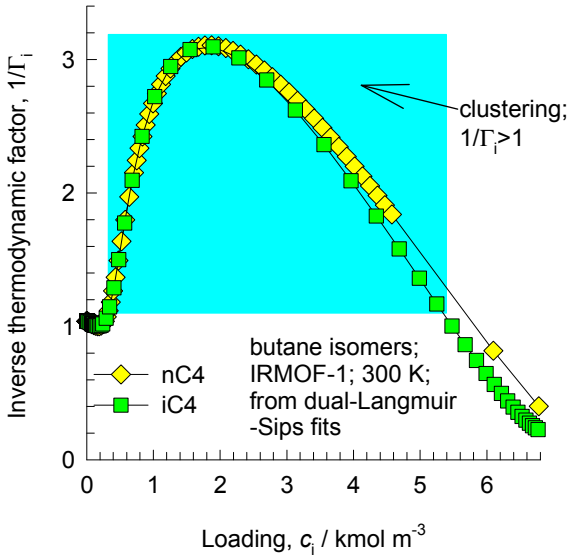

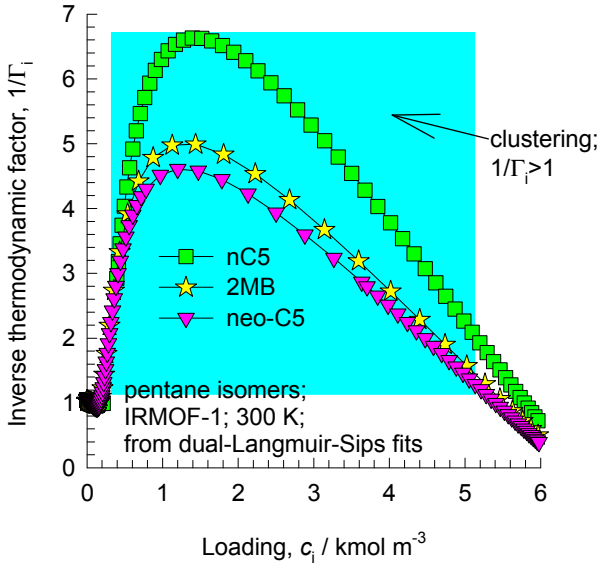

Electronic Supplementary Material (ESI) for Physical Chemistry Chemical Physics

IRMOF-1 RDFs for pure alkanes

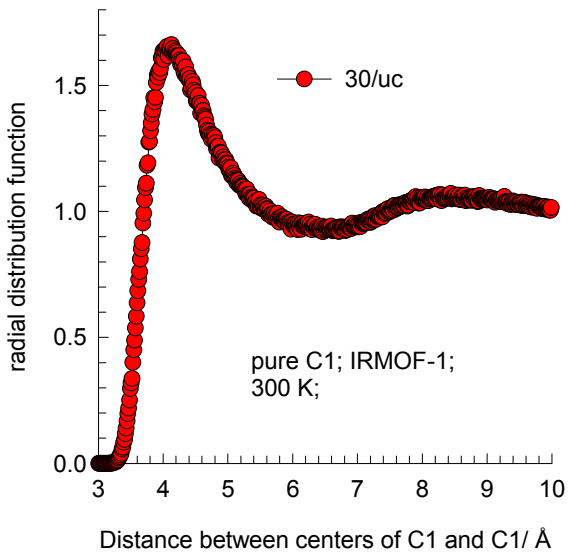

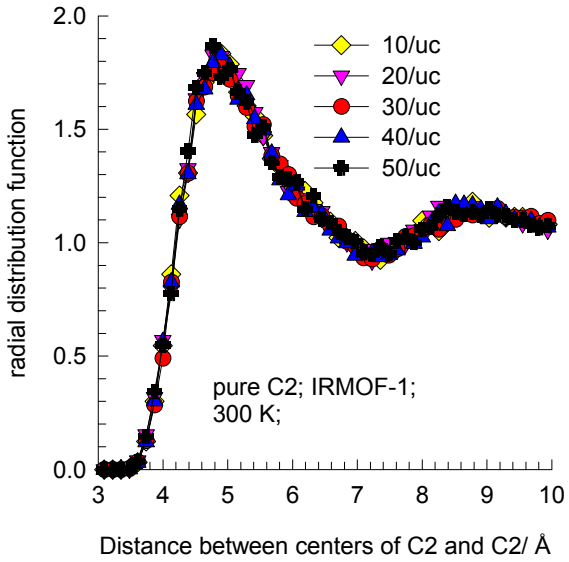

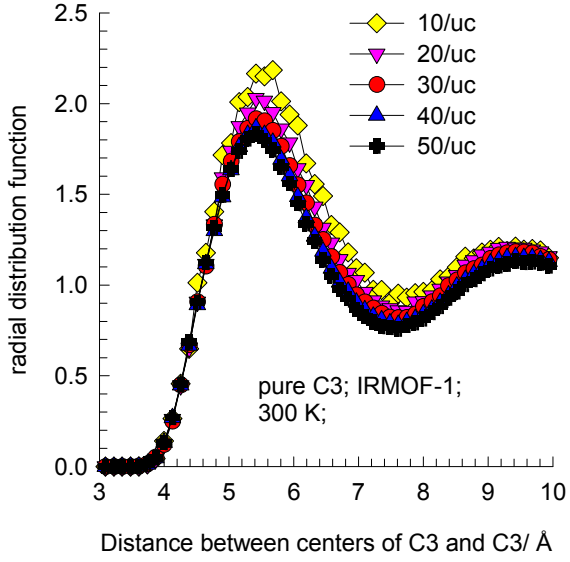

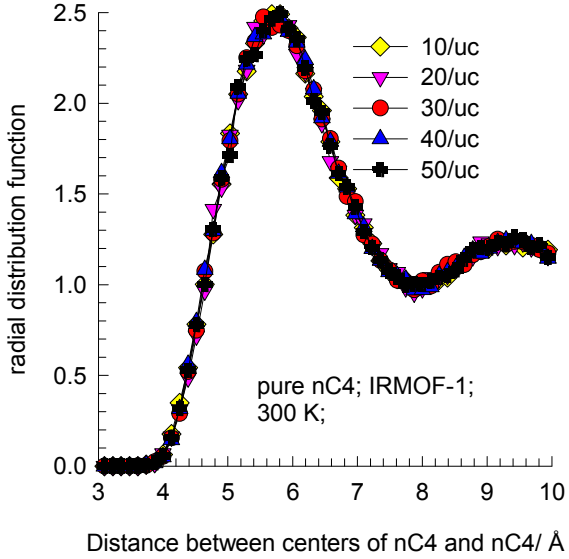

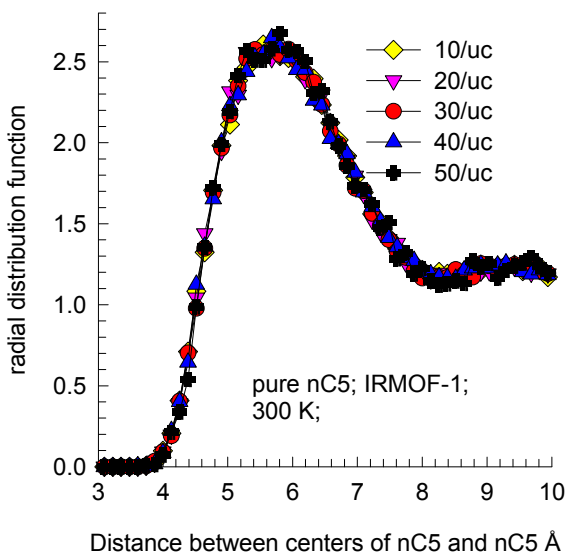

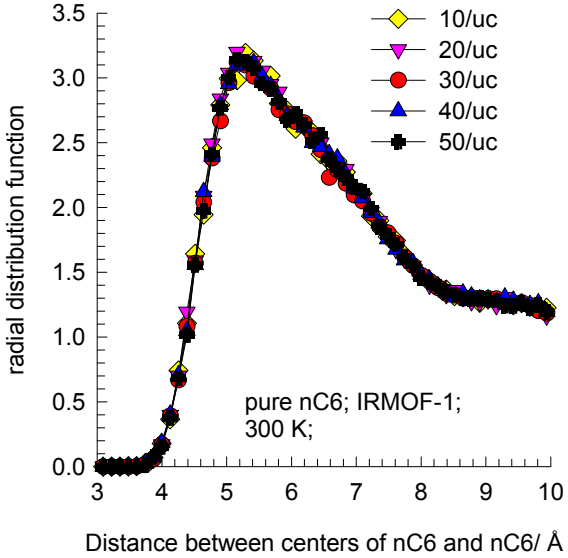

IRMOF-1 Comparison of RDFs of n-alkanes

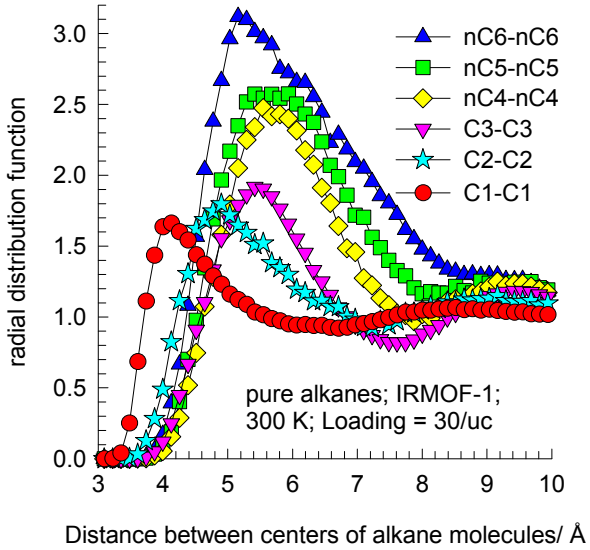

These RDFs are constructed on the basis of distances between centers of mass of n-alkane molecules

IRMOF-1 RDF comparison of linear and branched alkanes

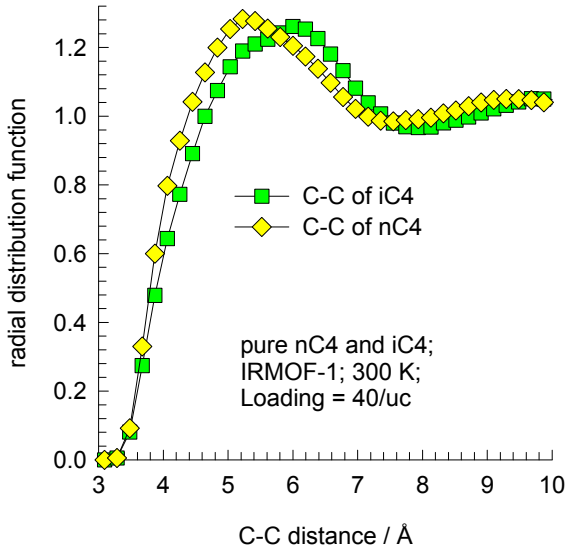

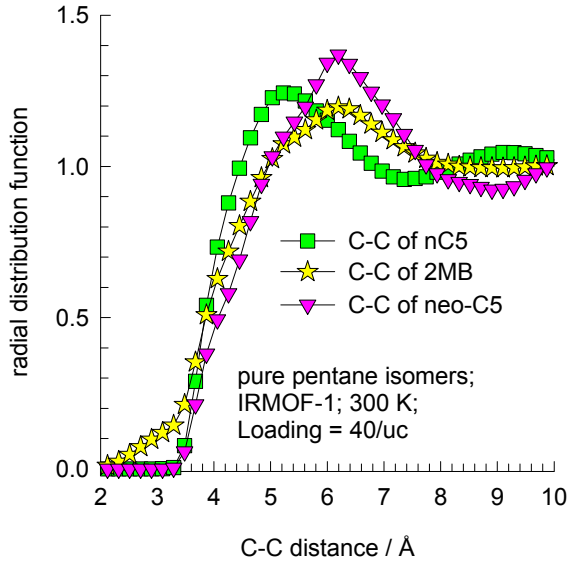

These RDFs are constructed on the basis of distances between every intermolecular C-C pairs

Electronic Supplementary Material (ESI) for Physical Chemistry Chemical Physics

MOF-177 pore landscape

The structural information for MOF-177 (= $Zn_4O(BTB)_2$ with (BTB^{3-} = 1,3,5-benzenetribenzoate)) is provided by

H.K. Chae, D.Y. Siberio-Pérez, J. Kim, Y.B. Go, M. Eddaoudi, A.J. Matzger, M. O'Keeffe, O.M. Yaghi, A route to high surface area, porosity and inclusion of large molecules in crystals, Nature 427 (2004) 523-527.

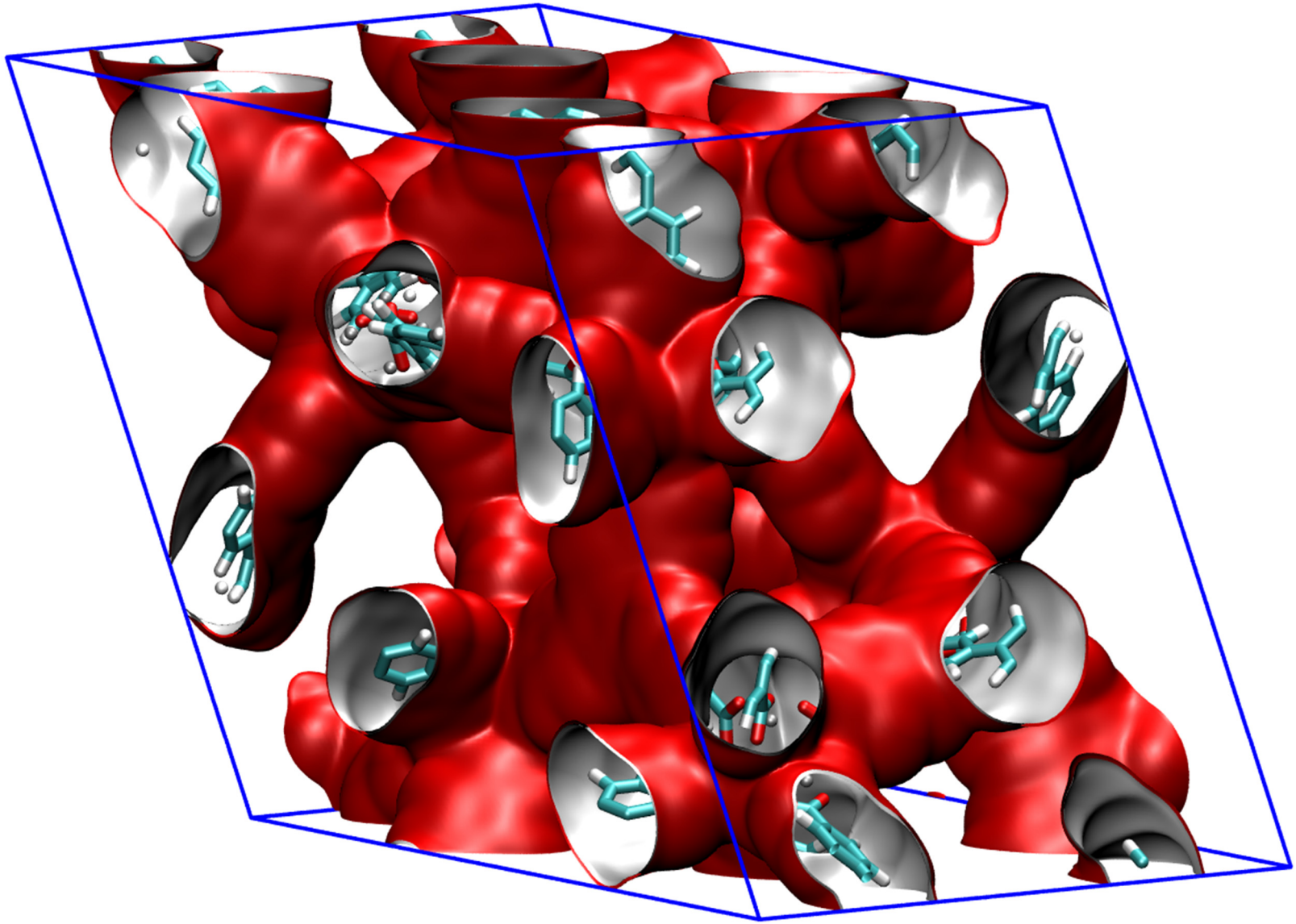

MOF-177 pore dimensions

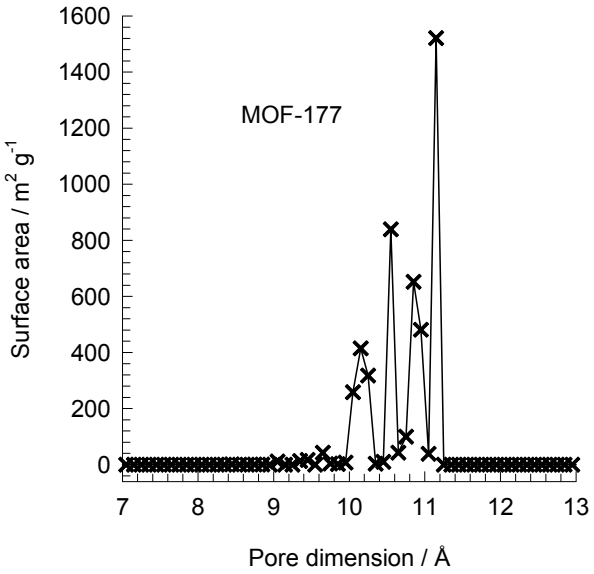

This plot of surface area versus pore dimension is determined using a combination of the DeLaunay triangulation method for pore dimension determination, and the procedure of Düren for determination of the surface area.

	MOF-177
a /Å	37.072
b /Å	37.072
c /Å	30.033
Cell volume / Å^3	35745.5
conversion factor for [molec/uc] to [mol per kg Framework]	0.1089
conversion factor for [molec/uc] to [kmol/m^3]	0.0553
ρ [kg/m3]	426.5952
MW unit cell [g/mol(framework)]	9182.931
ϕ, fractional pore volume	0.840
open space / Å^3/uc	30010.9
Pore volume / cm^3/g	1.968
Surface area /m^2/g	4781.0
DeLaunay diameter /Å	10.1

Tetrahedral $[Zn_4O]^{6+}$ units are linked by large, triangular tricarboxylate ligands. Six diamond-shaped channels (upper) with diameter of 10.8 Å surround a pore containing eclipsed BTB^{3-} moieties.

MOF-177 CBMC simulations of isotherms, and isosteric heats of adsorption

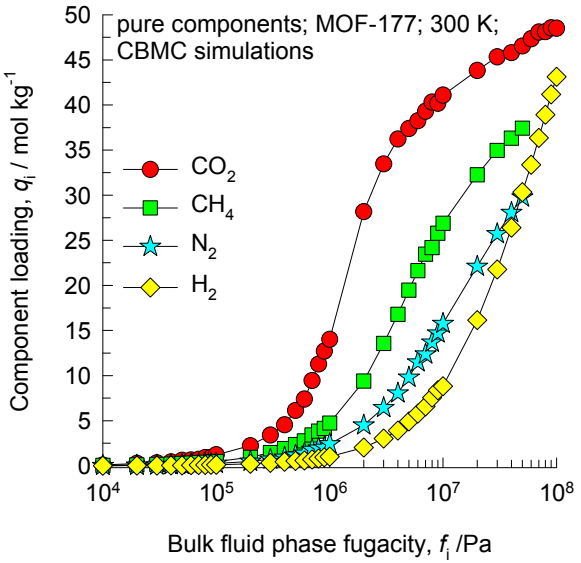

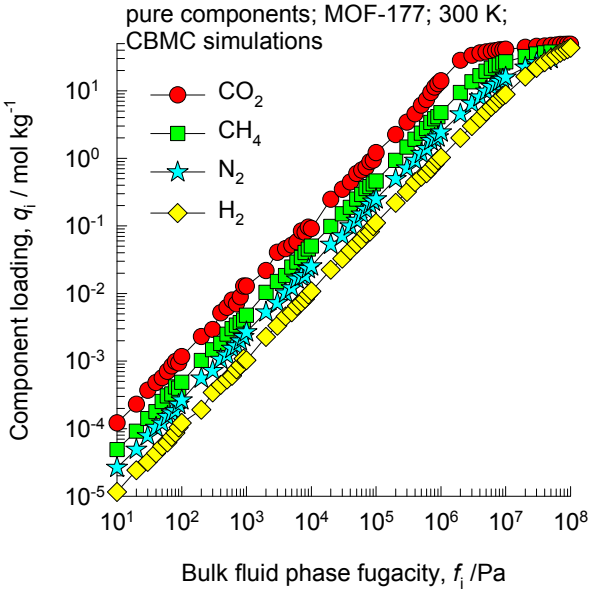

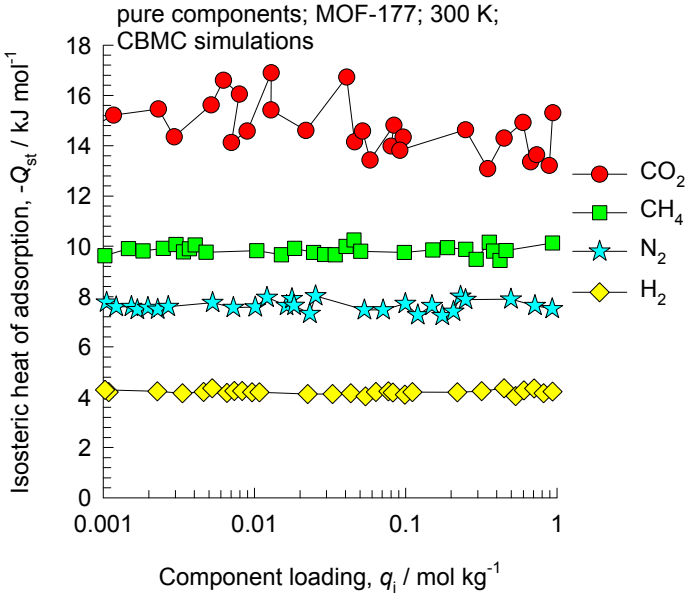

MOF-177 MD simulations of unary self- , and M-S diffusivities

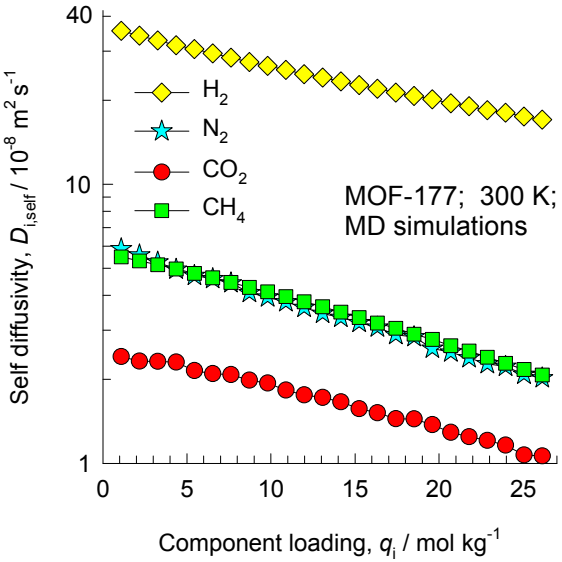

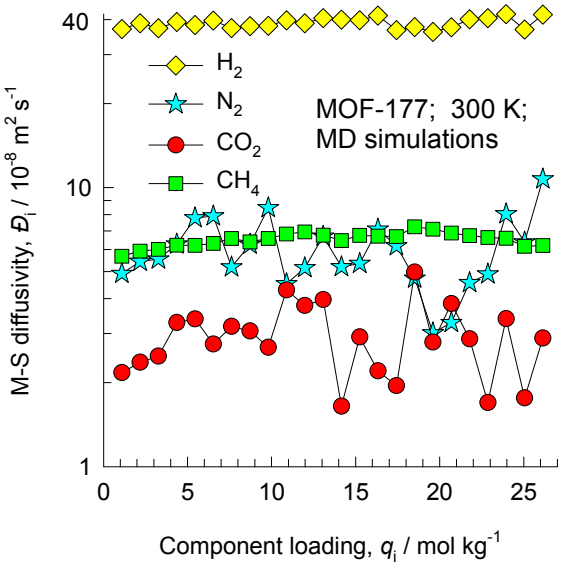

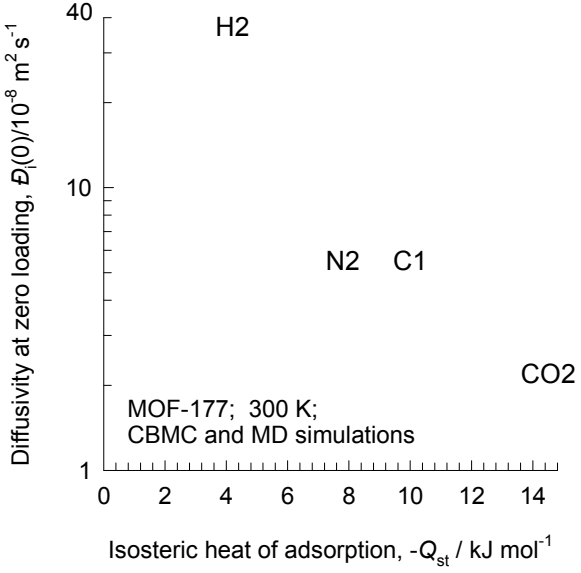

Electronic Supplementary Material (ESI) for Physical Chemistry Chemical Physics

Intersecting channels

BEA pore landscape

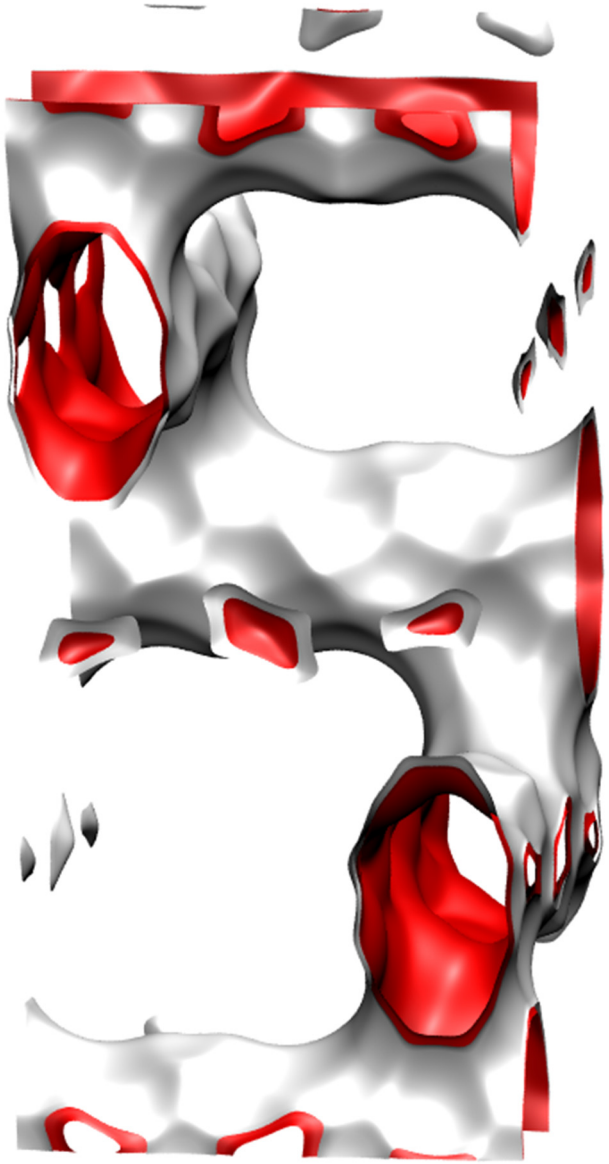

Intersecting channels of two sizes:
12-ring and 10-ring

	BEA
a /Å	12.661
b /Å	12.661
c /Å	26.406
Cell volume / Å^3	4232.906
conversion factor for [molec/uc] to [mol per kg Framework]	0.2600
conversion factor for [molec/uc] to [kmol/m^3]	0.9609
ρ [kg/m3]	1508.558
MW unit cell [g/mol(framework)]	3845.427
ϕ, fractional pore volume	0.408
open space / Å^3/uc	1728.1
Pore volume / cm^3/g	0.271
Surface area /m^2/g	923.0
DeLaunay diameter /Å	5.87

Structural information from: C. Baerlocher, L.B. McCusker, Database of Zeolite Structures, International Zeolite Association, http://www.iza-structure.org/databases/

Electronic Supplementary Material (ESI) for Physical Chemistry Chemical Physics

BEA pore dimensions

This plot of surface area versus pore dimension is determined using a combination of the DeLaunay triangulation method for pore dimension determination, and the procedure of Düren for determination of the surface area.

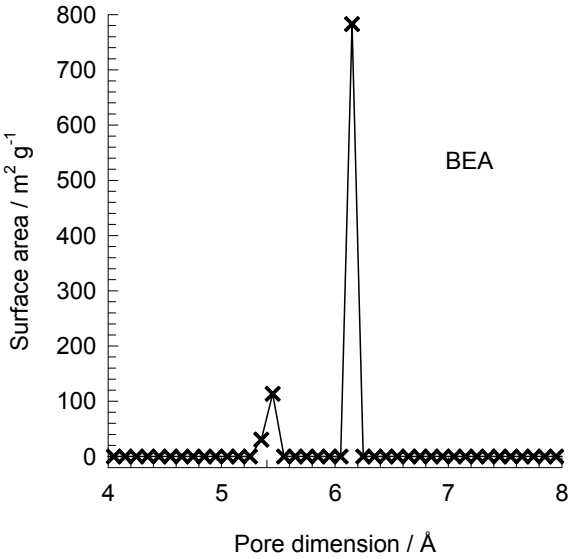

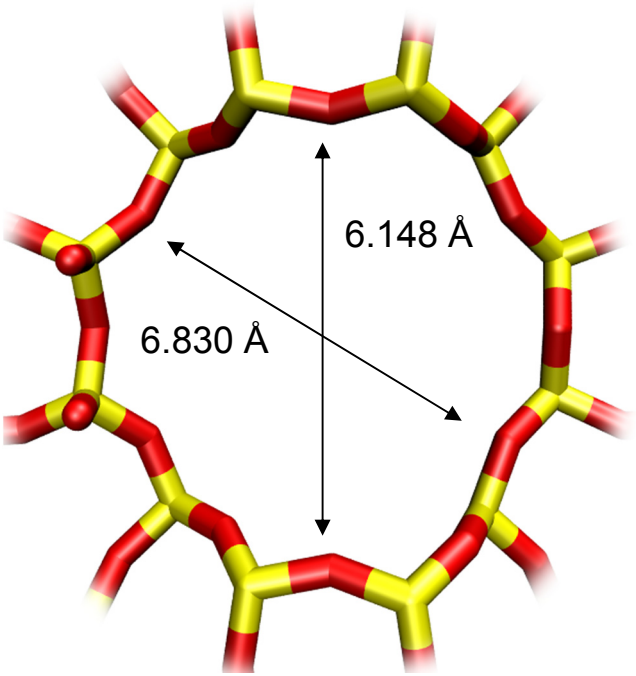

BEA [1 0 0]

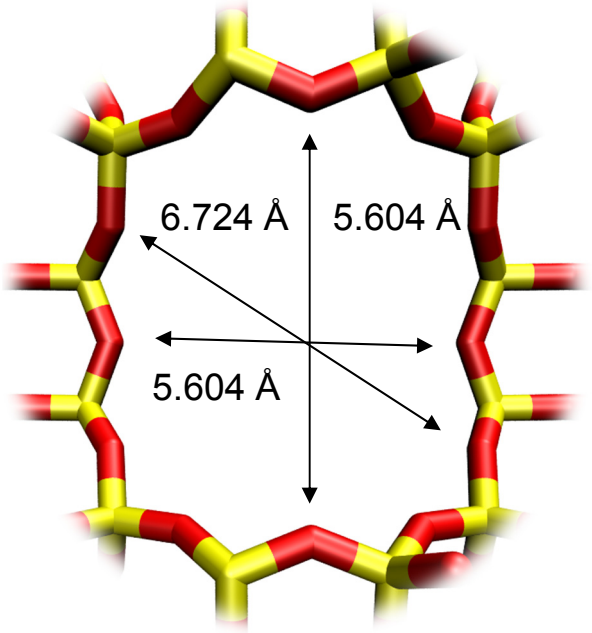

BEA [0 0 1]

Influence of Inverse Thermodynamic Factor on diffusivities

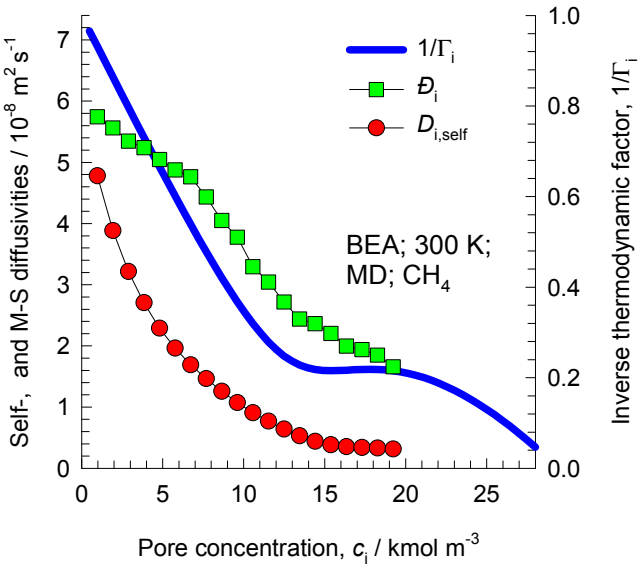

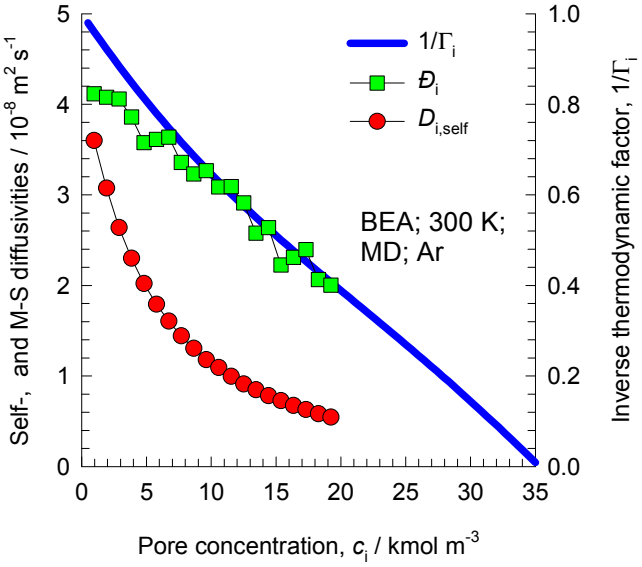

A detailed analysis of the loading dependence of CH_4 in BEA is contained in

E. Beerdsen, D. Dubbeldam and B. Smit, J Phys Chem B, 2006, 110, 22754-22772.

E. Beerdsen, D. Dubbeldam and B. Smit, Phys. Rev. Lett., 2006, 96, 044501.

BOG pore landscape

Intersecting channels:
12-ring and 10-ring

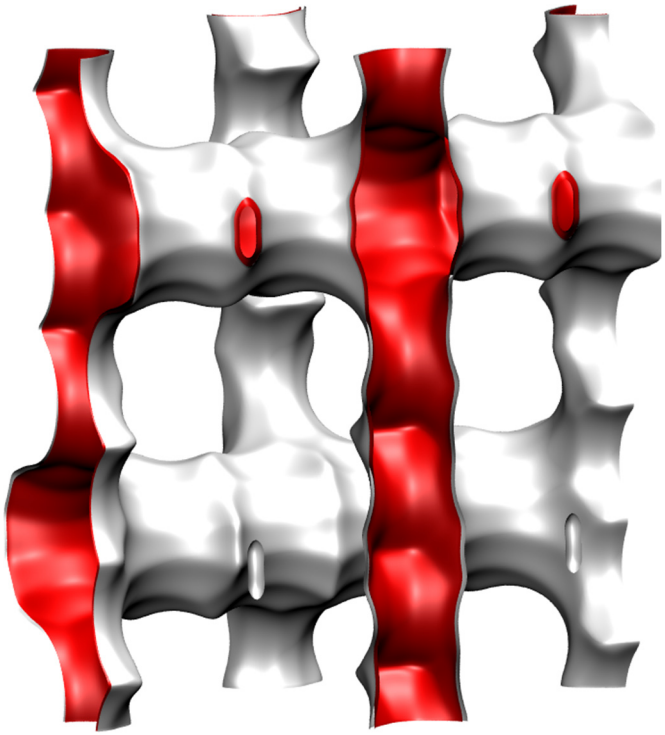

	BOG
a /Å	20.236
b /Å	23.798
c /Å	12.798
Cell volume / Å^3	6163.214
conversion factor for [molec/uc] to [mol per kg Framework]	0.1734
conversion factor for [molec/uc] to [kmol/m^3]	0.7203
ρ [kg/m3]	1995.523
MW unit cell [g/mol(framework)]	5768.141
ϕ, fractional pore volume	0.374
open space / Å^3/uc	2305.4
Pore volume / cm^3/g	0.241
Surface area /m^2/g	758.0
DeLaunay diameter /Å	5.02

Structural information from: C. Baerlocher, L.B. McCusker, Database of Zeolite Structures, International Zeolite Association, http://www.iza-structure.org/databases/

Electronic Supplementary Material (ESI) for Physical Chemistry Chemical Physics

BOG pore dimensions

This plot of surface area versus pore dimension is determined using a combination of the DeLaunay triangulation method for pore dimension determination, and the procedure of Düren for determination of the surface area.

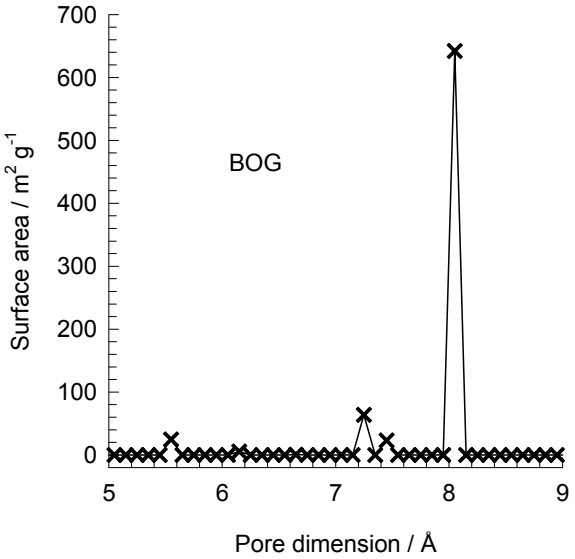

BOG has an intersecting channel system:
12-ring channels intersecting with 10-ring channels

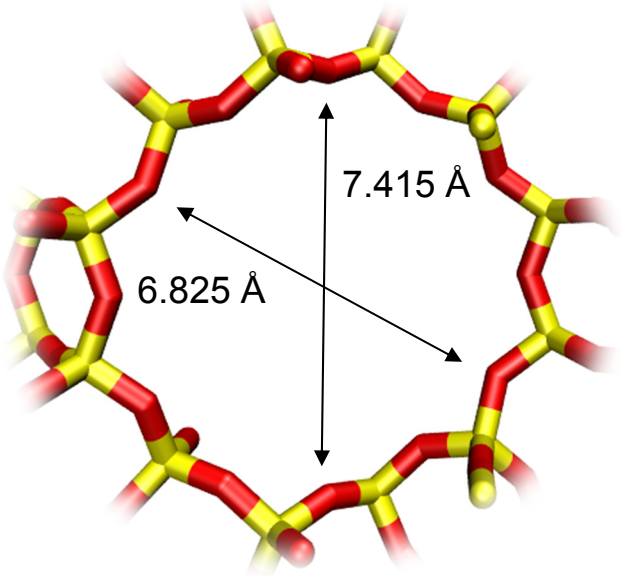

BOG [1 0 0]

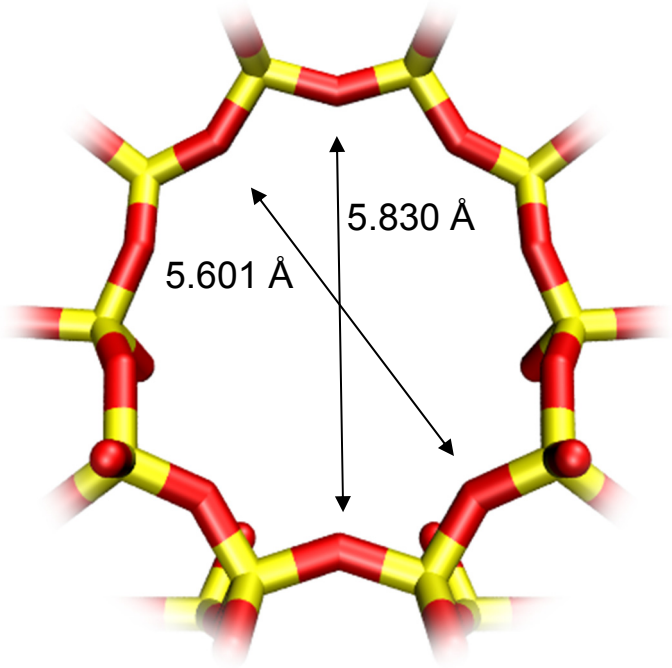

BOG [0 1 0]

Loading dependence of diffusivities

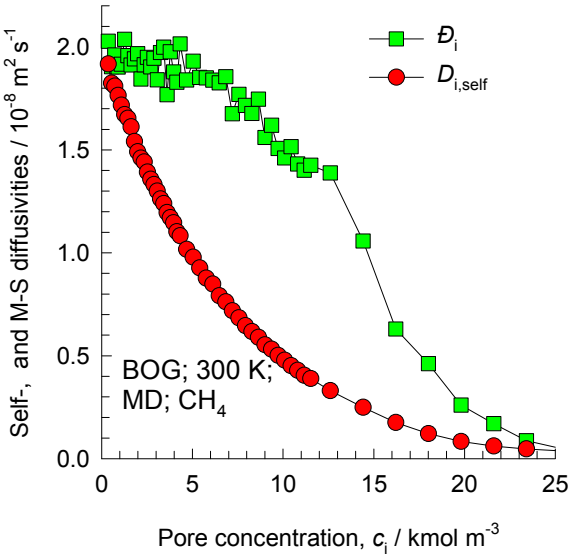

A detailed analysis of the loading dependence of CH_4 in BOG is contained in

E. Beerdsen, D. Dubbeldam and B. Smit, J Phys Chem B, 2006, 110, 22754-22772.

E. Beerdsen, D. Dubbeldam and B. Smit, Phys. Rev. Lett., 2006, 96, 044501.

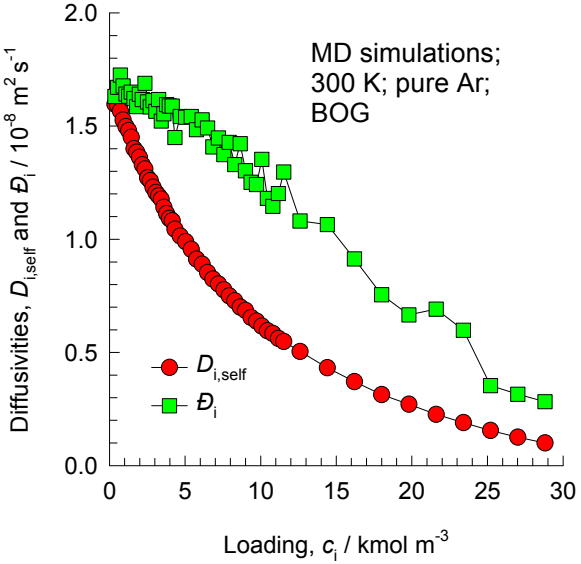

FER pore landscape

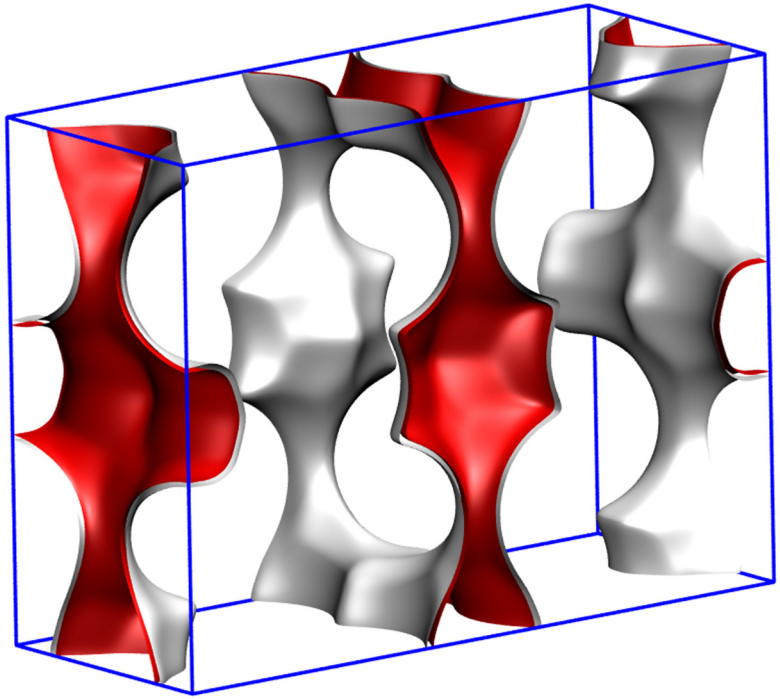

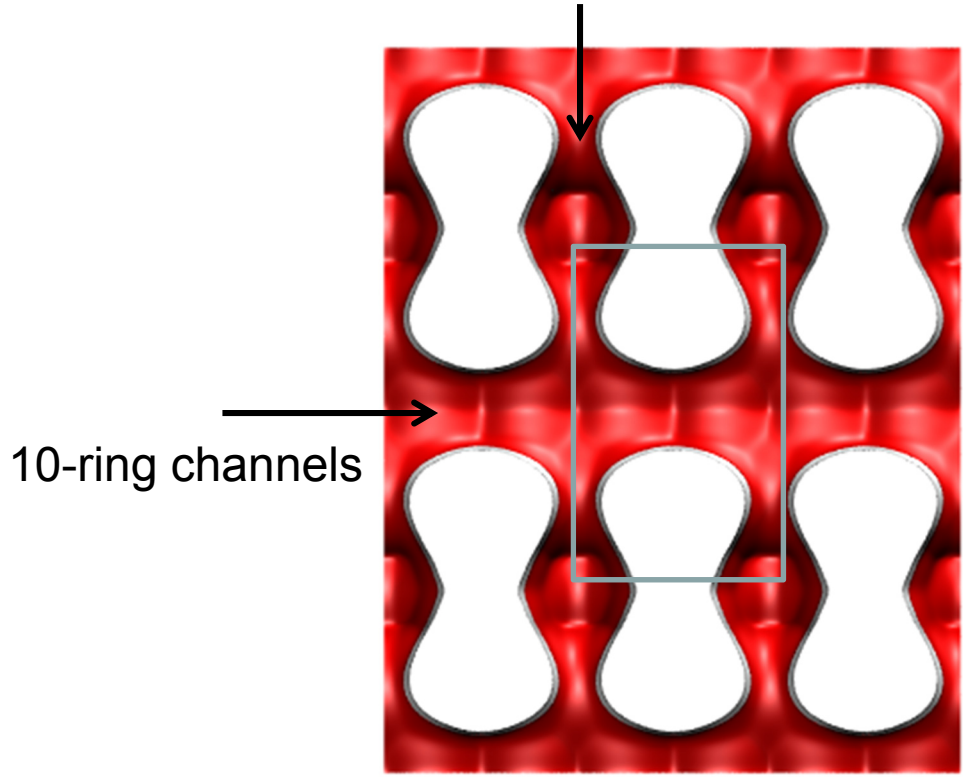

This is one unit cell

There are two 10-ring channels
There are two 8-ring channels

Structural information from: C. Baerlocher, L.B. McCusker, Database of Zeolite Structures, International Zeolite Association, http://www.iza-structure.org/databases/

Electronic Supplementary Material (ESI) for Physical Chemistry Chemical Physics

FER pore landscape

10-ring channels

8-ring channels

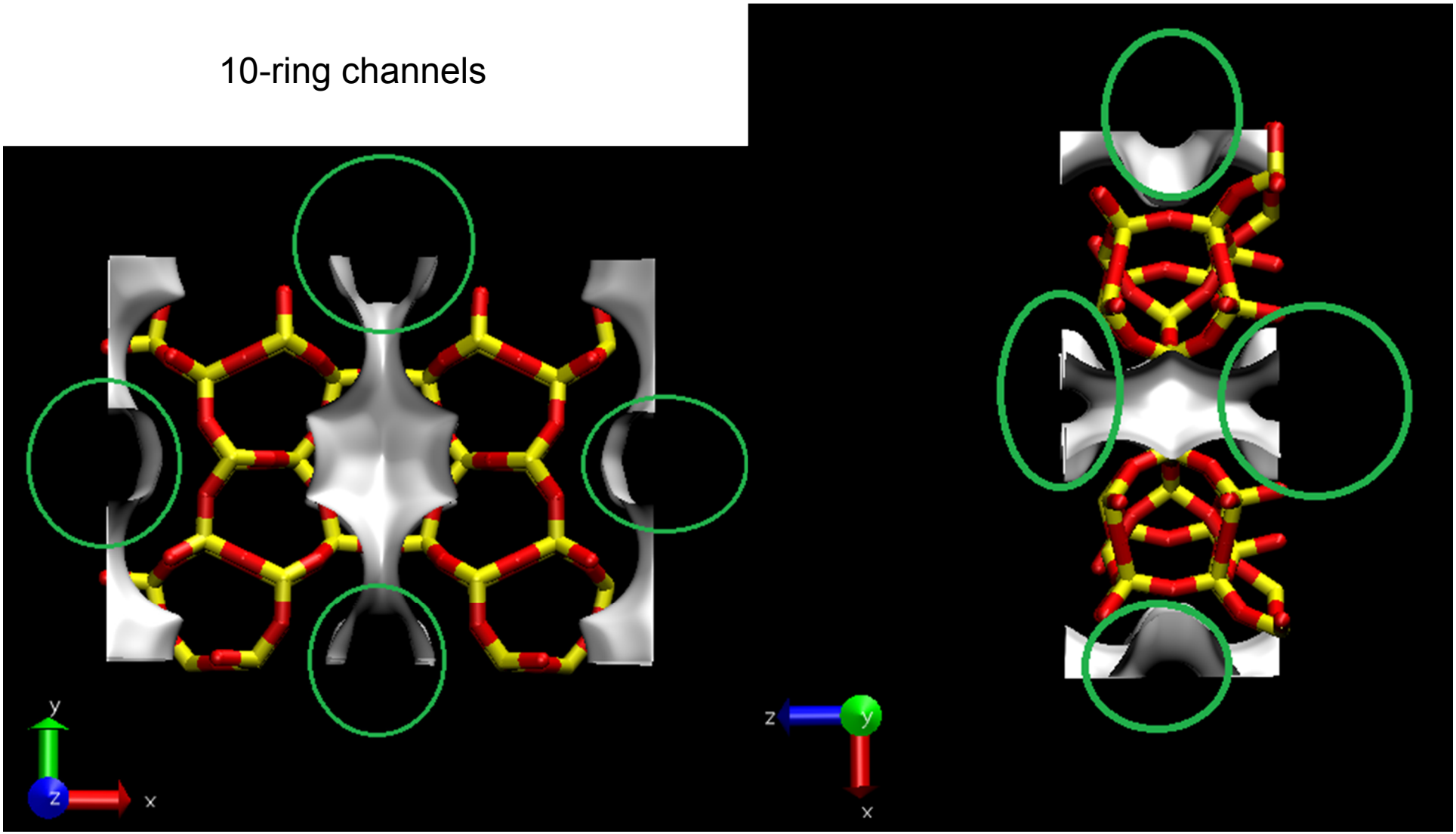

FER pore dimensions

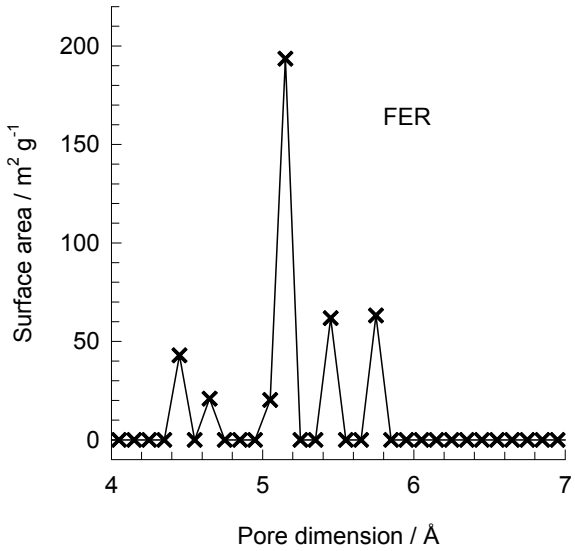

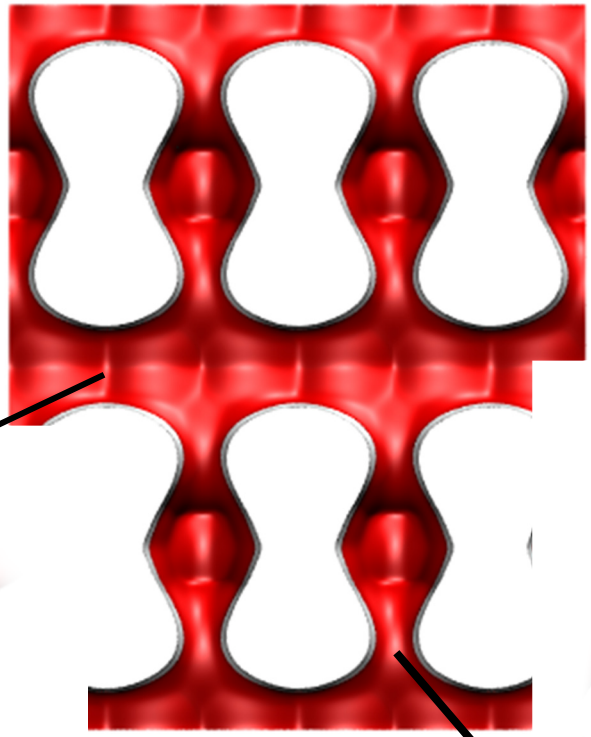

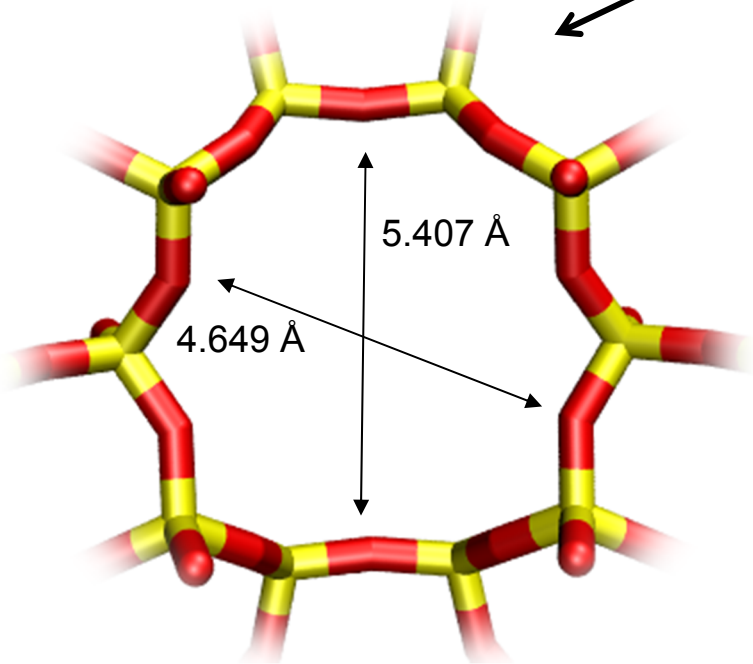

FER channel [0 0 1]

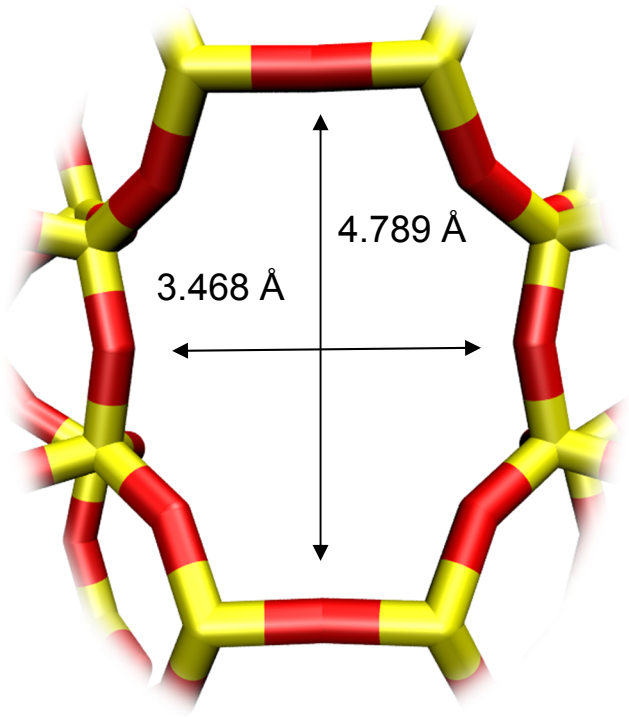

FER [0 1 0]

Electronic Supplementary Material (ESI) for Physical Chemistry Chemical Physics

FER pore landscape

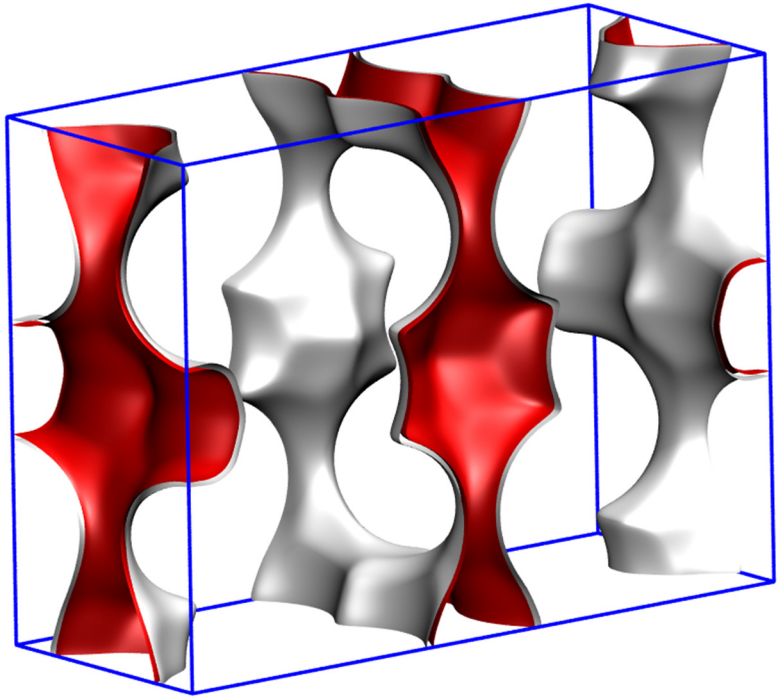

	FER
a /Å	19.156
b /Å	14.127
c /Å	7.489
Cell volume / Å^3	2026.649
conversion factor for [molec/uc] to [mol per kg Framework]	0.4623
conversion factor for [molec/uc] to [kmol/m^3]	2.8968
ρ [kg/m3]	1772.33
MW unit cell [g/mol (framework)]	2163.053
ϕ, fractional pore volume	0.283
open space / Å^3/uc	573.2
Pore volume / cm^3/g	0.160
Surface area /m^2/g	403.0
DeLaunay diameter /Å	4.65

FER CBMC simulations of isotherms, and -Q_{st}; MD simulations of diffusivities

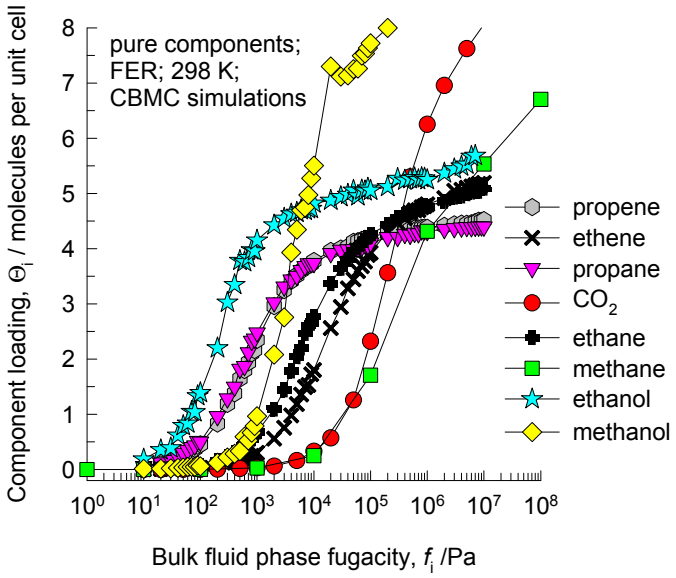

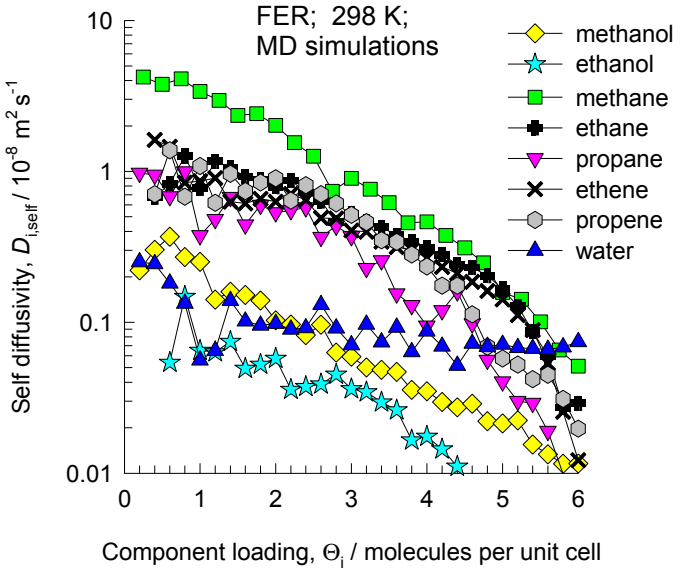

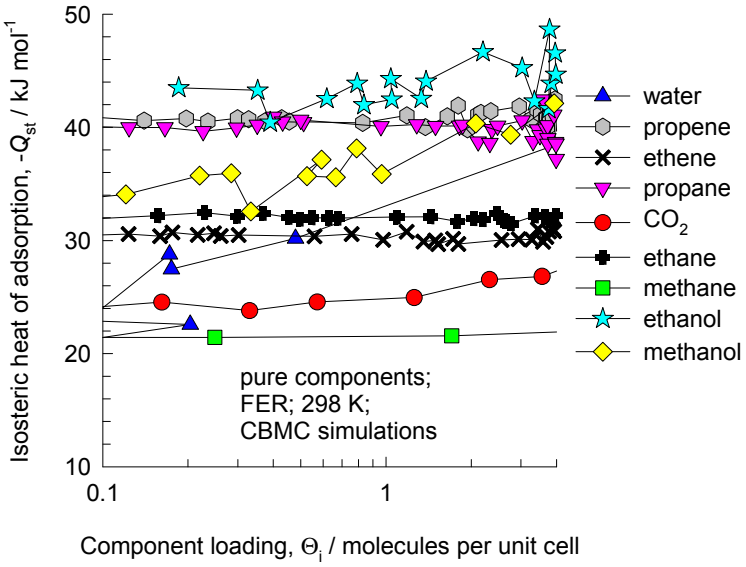

The diffusivities are along the 10-ring channels. The diffusivities in the other directions are too small to monitor accurately with MD.

ISV pore landscape

Intersecting 12-ring channels structure

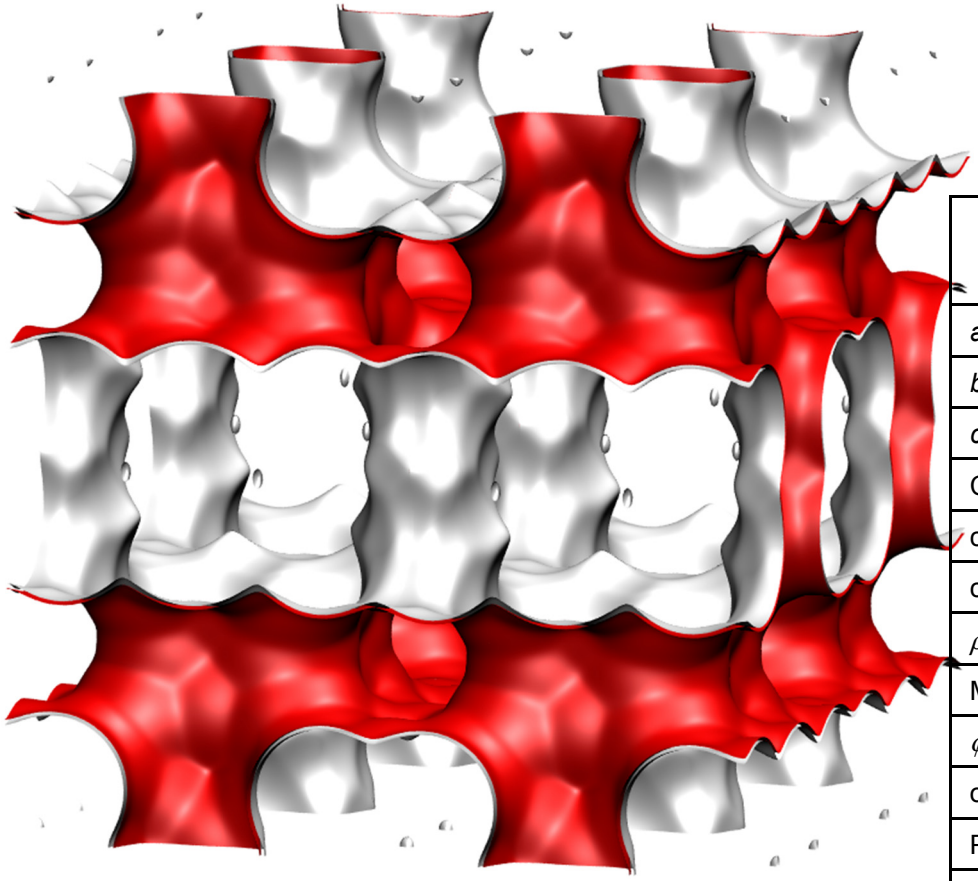

	ISV
a /Å	12.853
b /Å	12.853
c /Å	25.214
Cell volume / Å^3	4165.343
conversion factor for [molec/uc] to [mol per kg Framework]	0.2600
conversion factor for [molec/uc] to [kmol/m^3]	0.9361
ρ [kg/m3]	1533.027
MW unit cell [g/mol(framework)]	3845.427
ϕ, fractional pore volume	0.426
open space / Å^3/uc	1773.9
Pore volume / cm^3/g	0.278
Surface area /m^2/g	911.0
DeLaunay diameter /Å	5.96

Structural information from: C. Baerlocher, L.B. McCusker, Database of Zeolite Structures, International Zeolite Association, http://www.iza-structure.org/databases/

ISV pore dimensions

This plot of surface area versus pore dimension is determined using a combination of the DeLaunay triangulation method for pore dimension determination, and the procedure of Düren for determination of the surface area.

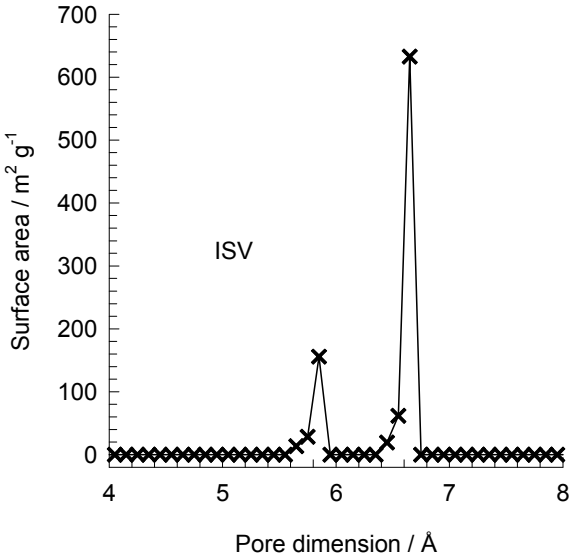

Intersecting 12-ring channels structure

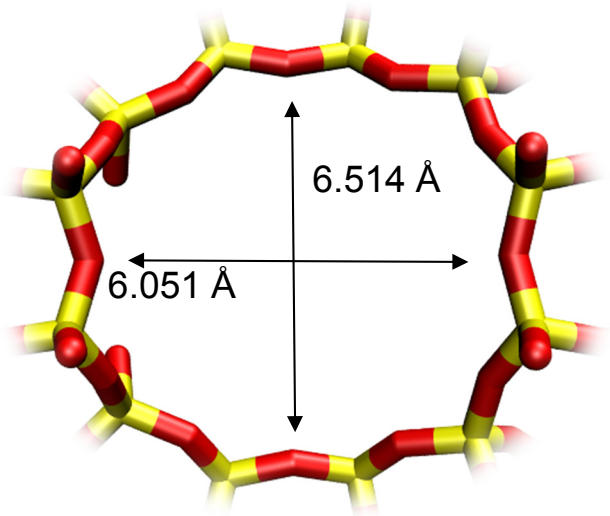

ISV [1 0 0]

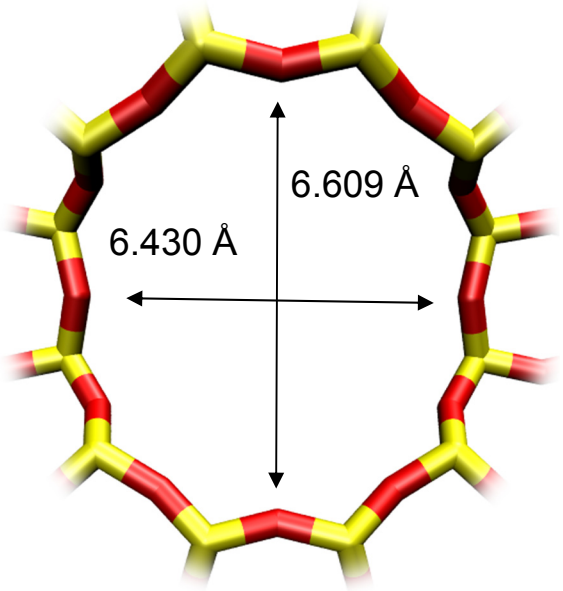

ISV [0 0 1]

Influence of Inverse Thermodynamic Factor on diffusivities

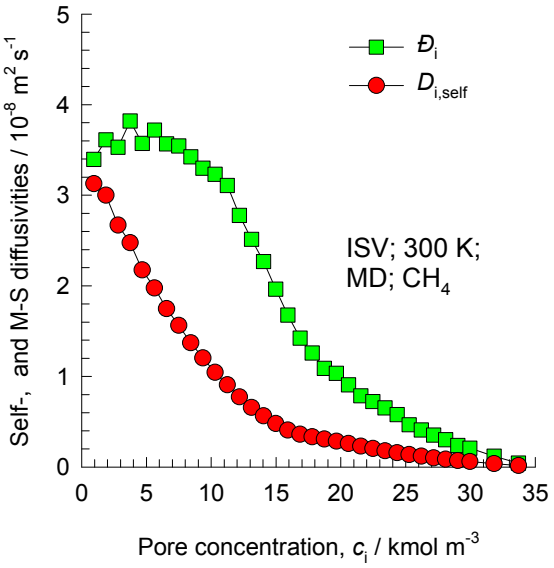

A detailed analysis of the loading dependence of CH_4 in ISV is contained in

E. Beerdsen, D. Dubbeldam and B. Smit, J Phys Chem B, 2006, 110, 22754-22772.

E. Beerdsen, D. Dubbeldam and B. Smit, Phys. Rev. Lett., 2006, 96, 044501.

MFI pore landscape

	MFI
a /Å	20.022
b /Å	19.899
c /Å	13.383
Cell volume / Å^3	5332.025
conversion factor for [molec/uc] to [mol per kg Framework]	0.1734
conversion factor for [molec/uc] to [kmol/m^3]	1.0477
ρ [kg/m3]	1796.386
MW unit cell [g/mol(framework)]	5768.141
ϕ, fractional pore volume	0.297
open space / Å^3/uc	1584.9
Pore volume / cm^3/g	0.165
Surface area /m^2/g	487.0
DeLaunay diameter /Å	5.16

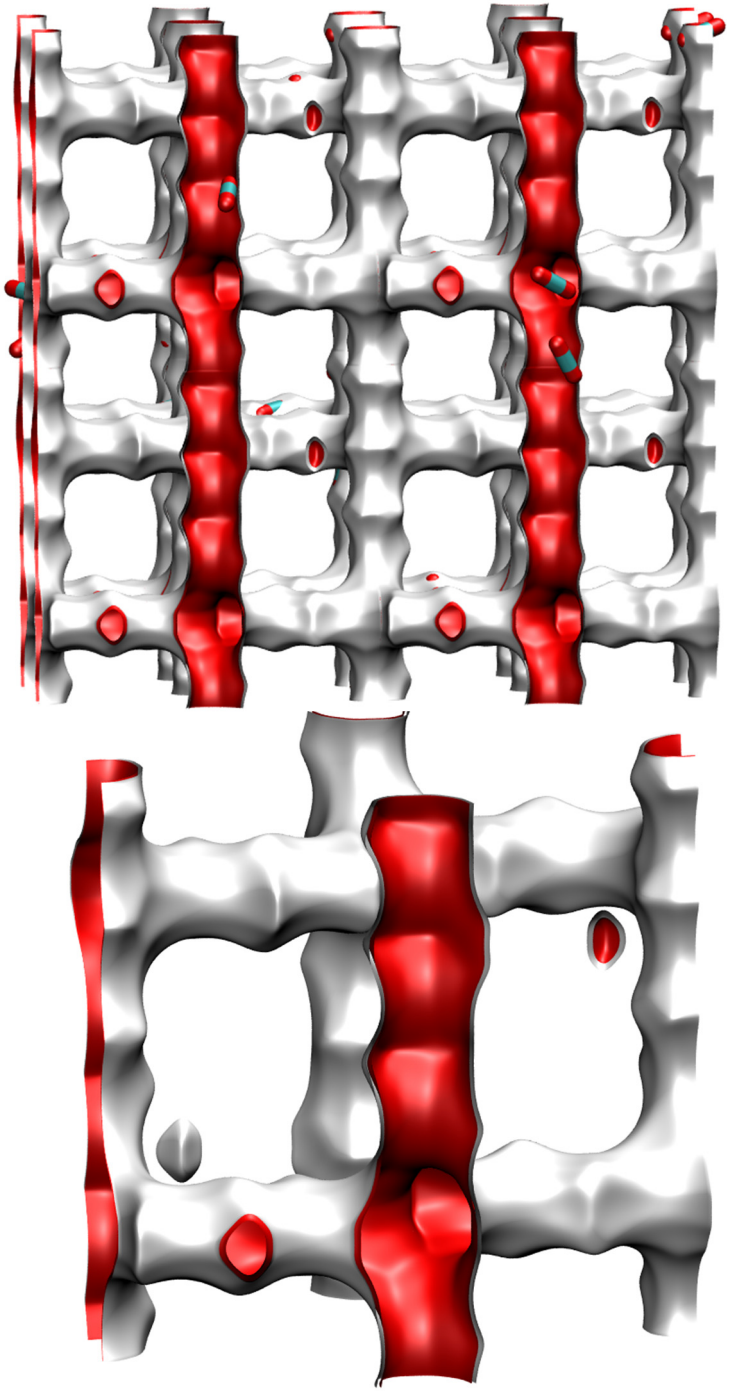

Structural information from: C. Baerlocher, L.B. McCusker, Database of Zeolite Structures, International Zeolite Association, http://www.iza-structure.org/databases/

MFI pore dimensions

10 ring channel of MFI viewed along [100]

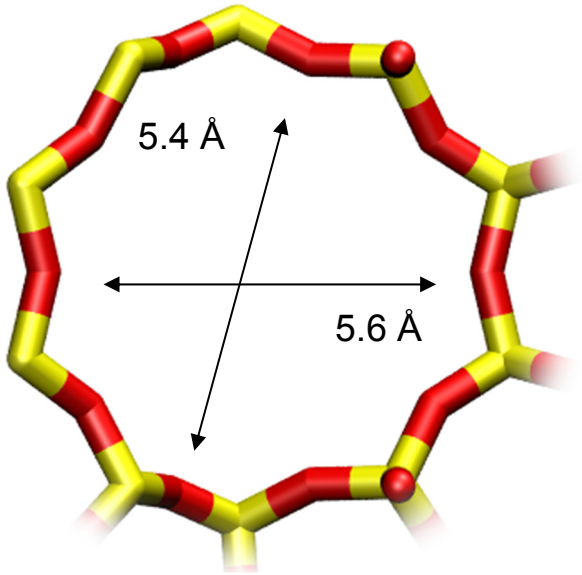

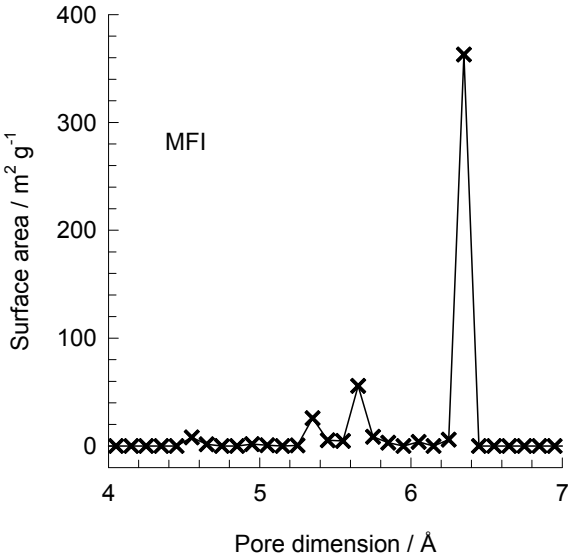

10 ring channel of MFI viewed along [010]

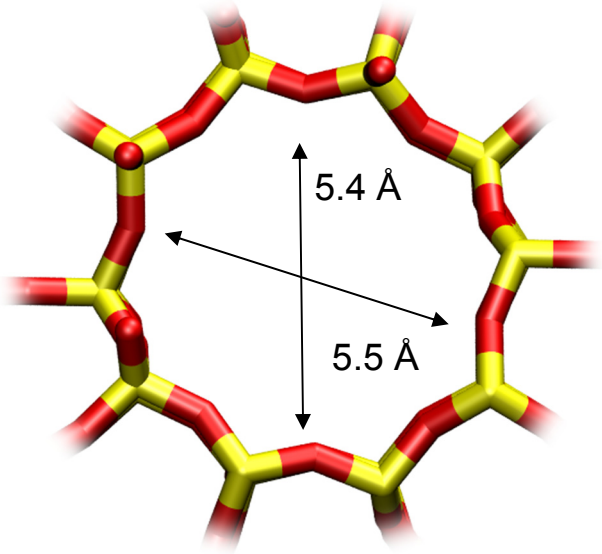

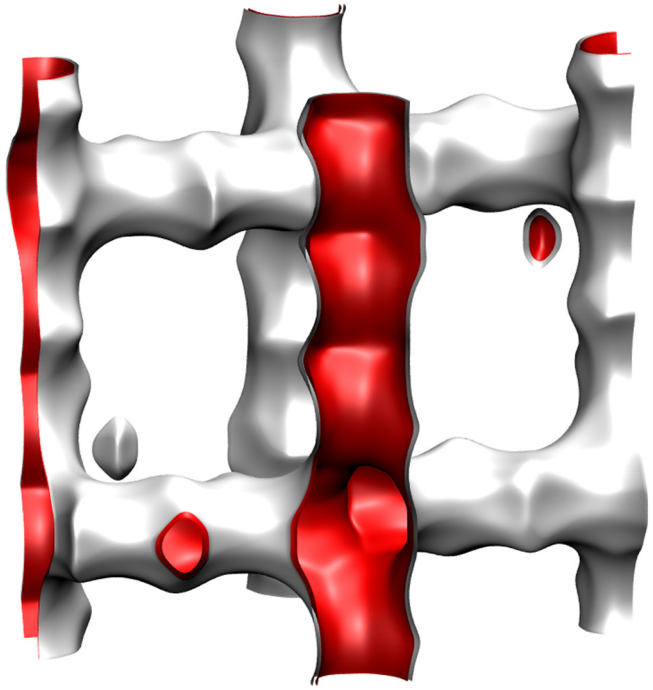

MFI CBMC simulations of isotherms, and isosteric heats of adsorption

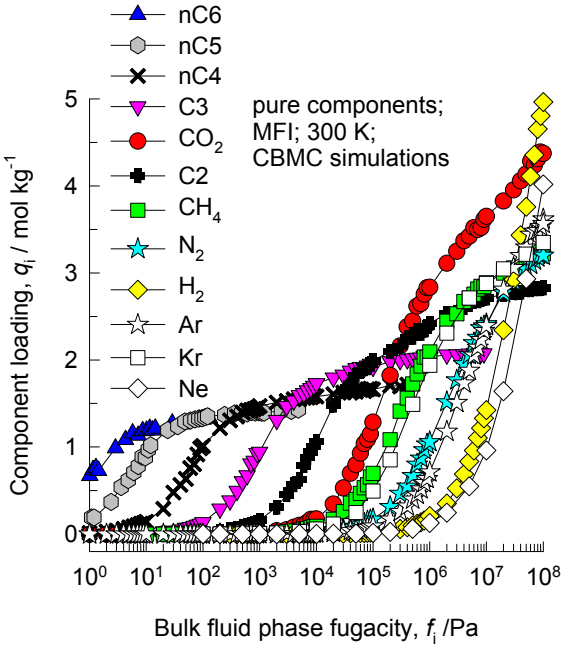

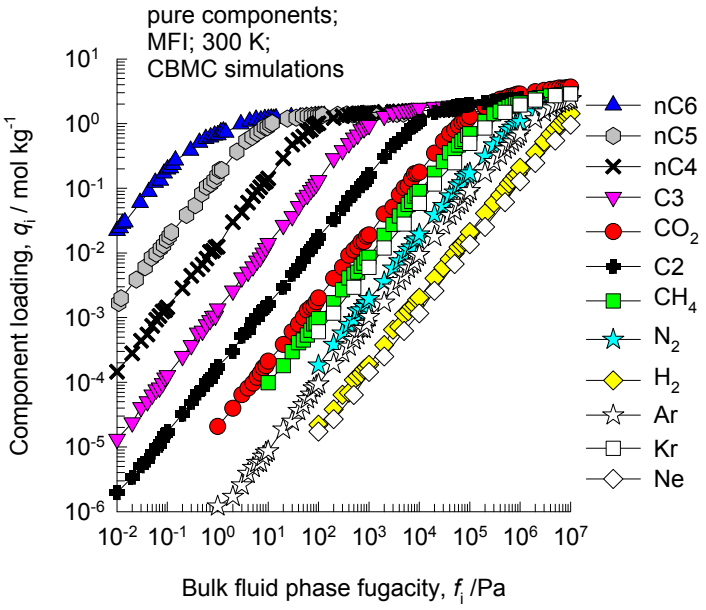

Note that C2 and C3 above refer to saturated alkanes

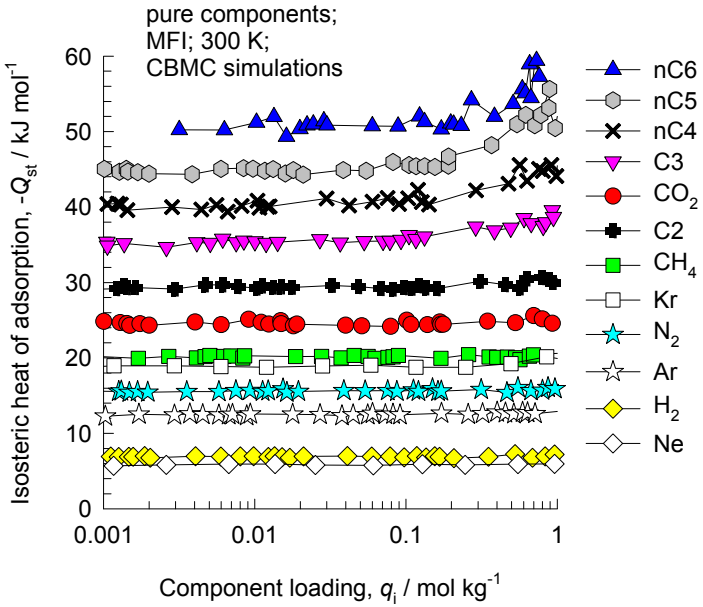

Influence of Inverse Thermodynamic Factor on diffusivities

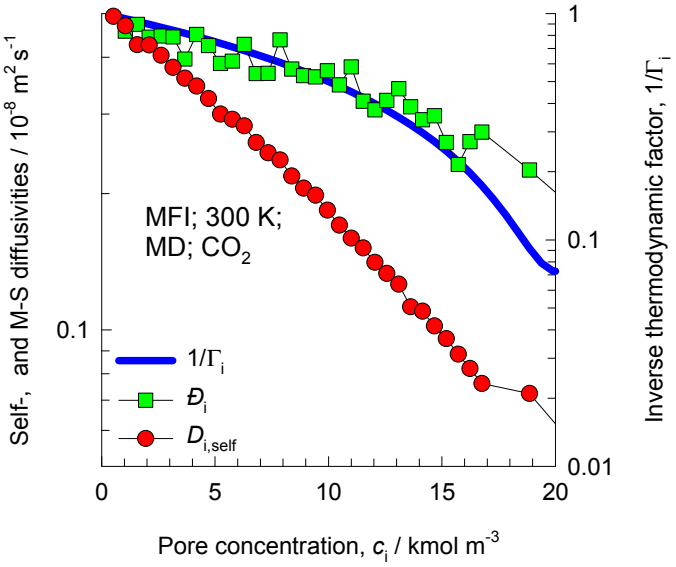

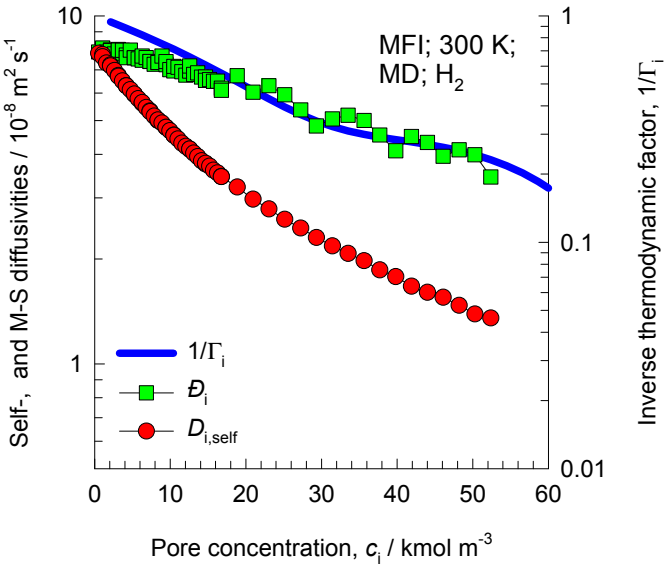

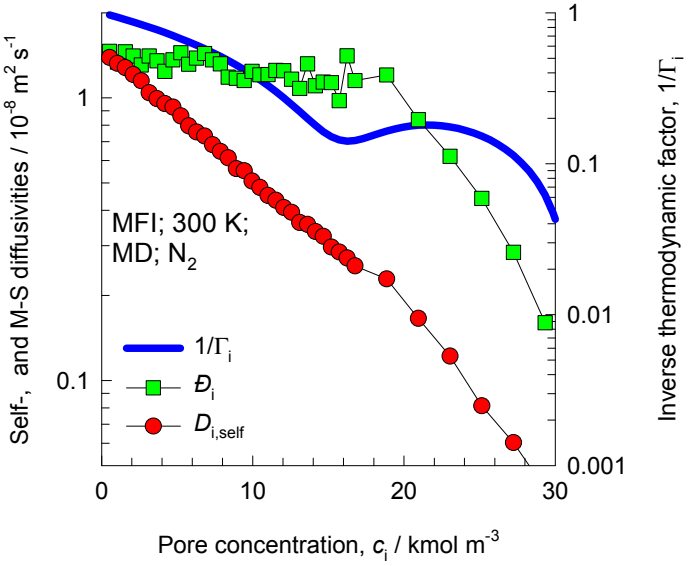

Influence of Inverse Thermodynamic Factor on diffusivities

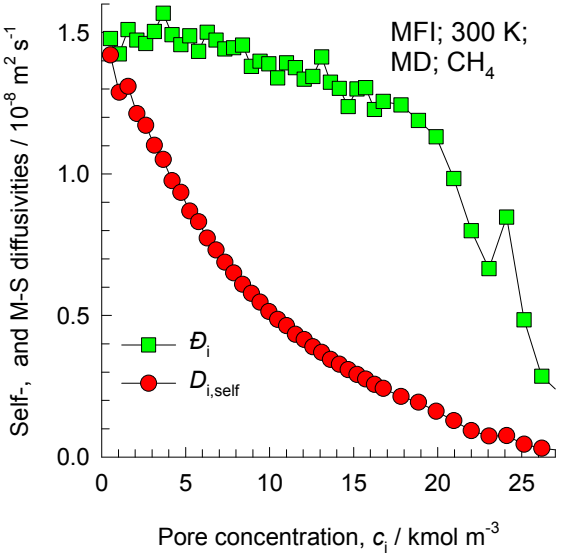

A detailed analysis of the loading dependence of CH_4 in MFI is contained in

E. Beerdsen, D. Dubbeldam and B. Smit, *Phys. Rev. Lett.*, 2005, **95**, 164505.

E. Beerdsen, D. Dubbeldam and B. Smit, J Phys Chem B, 2006, 110, 22754-22772.

E. Beerdsen, D. Dubbeldam and B. Smit, Phys. Rev. Lett., 2006, 96, 044501.

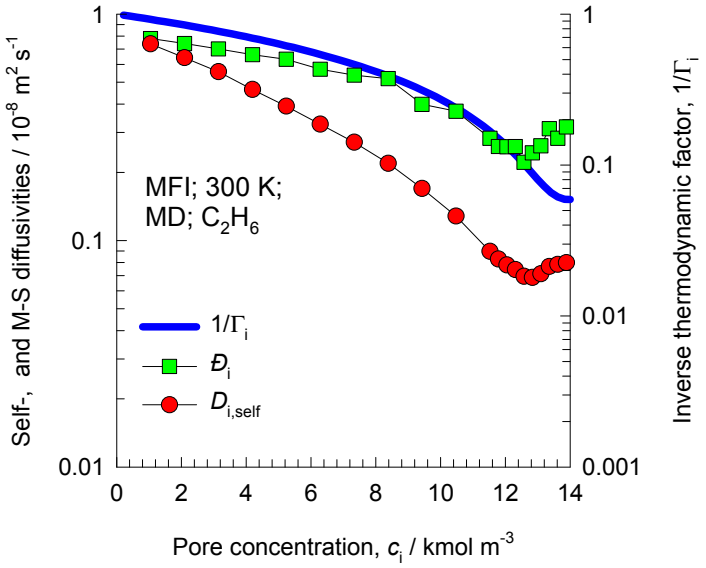

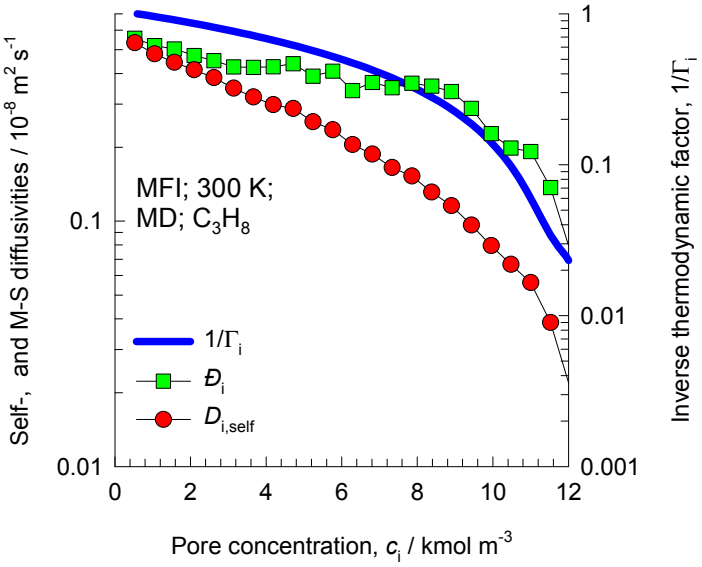

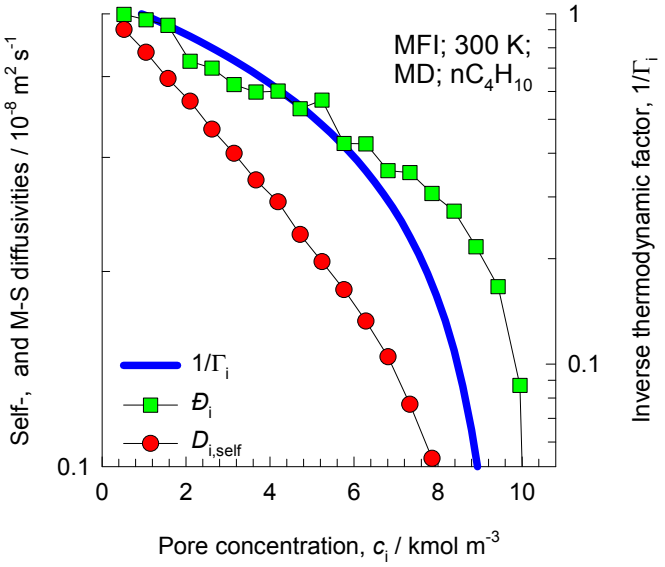

Influence of Inverse Thermodynamic Factor on diffusivities

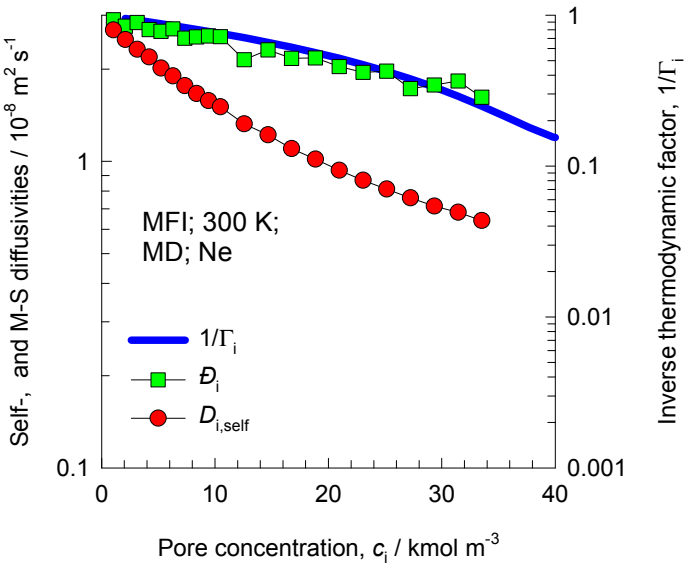

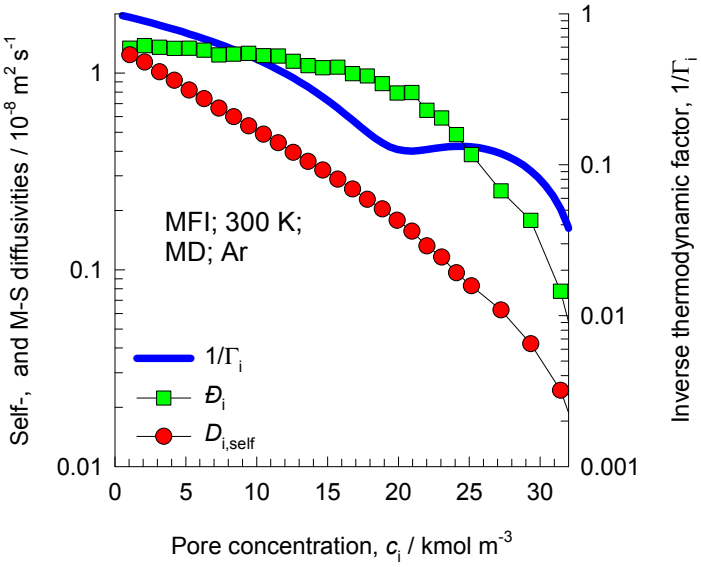

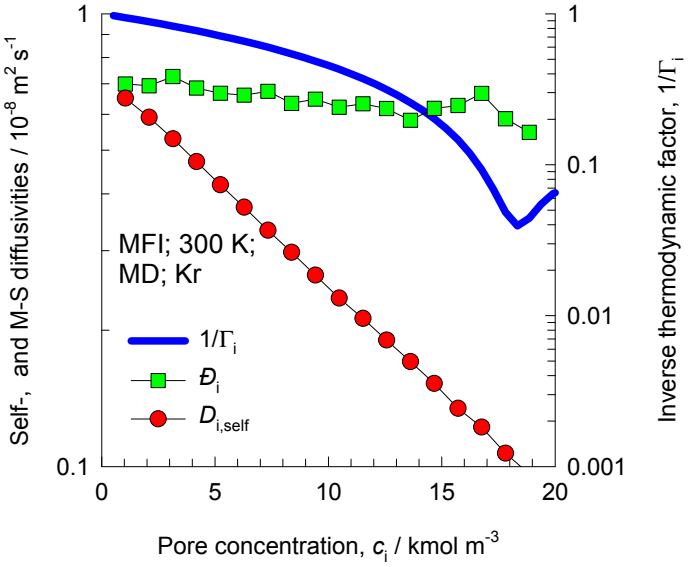

nC6 diffusivity in MFI zeolite

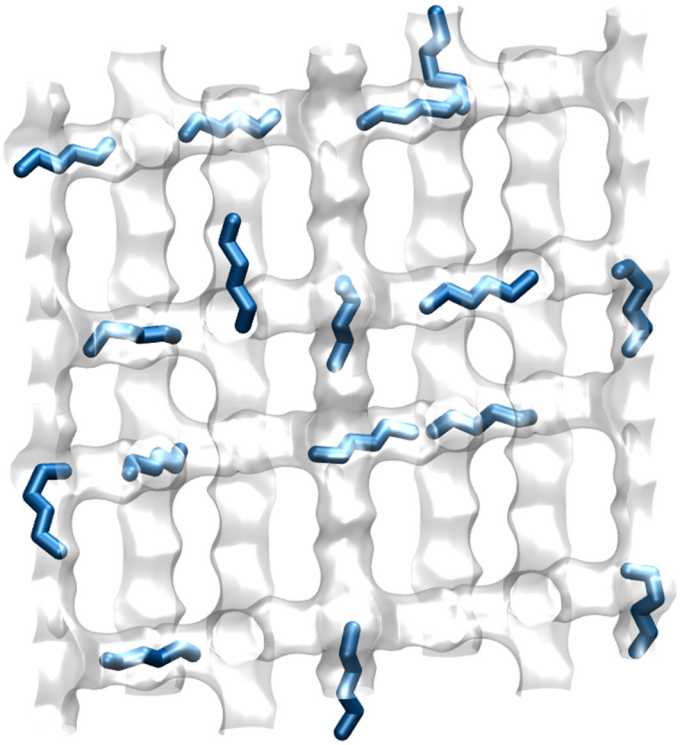

Linear, chain, alkanes can locate anywhere along the channels of MFI. The length of nC6 is commensurate with the distance between two intersections

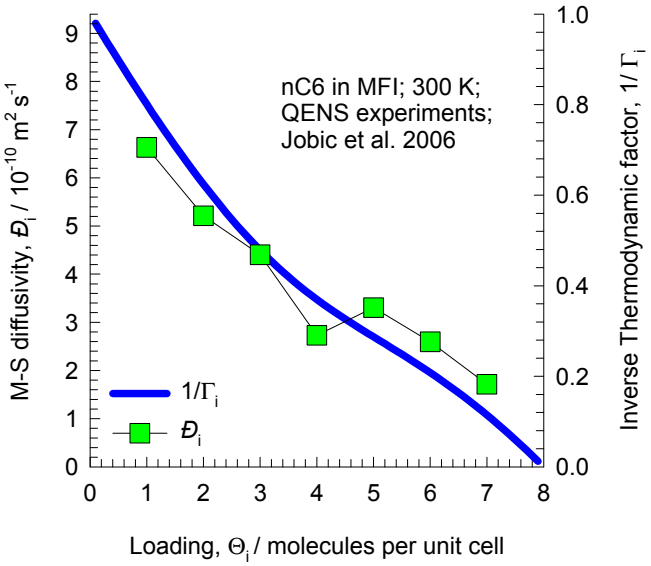

The QENS experimental data are re-plotted using the information in:

H. Jobic, C. Laloué, C. Laroche, J.M. van Baten, R. Krishna, Influence of isotherm inflection on the loading dependence of the diffusivities of n-hexane and n-heptane in MFI zeolite. Quasi-Elastic Neutron Scattering experiments supplemented by molecular simulations, J. Phys. Chem. B 110 (2006) 2195-2201.

nC7 diffusivity in MFI zeolite

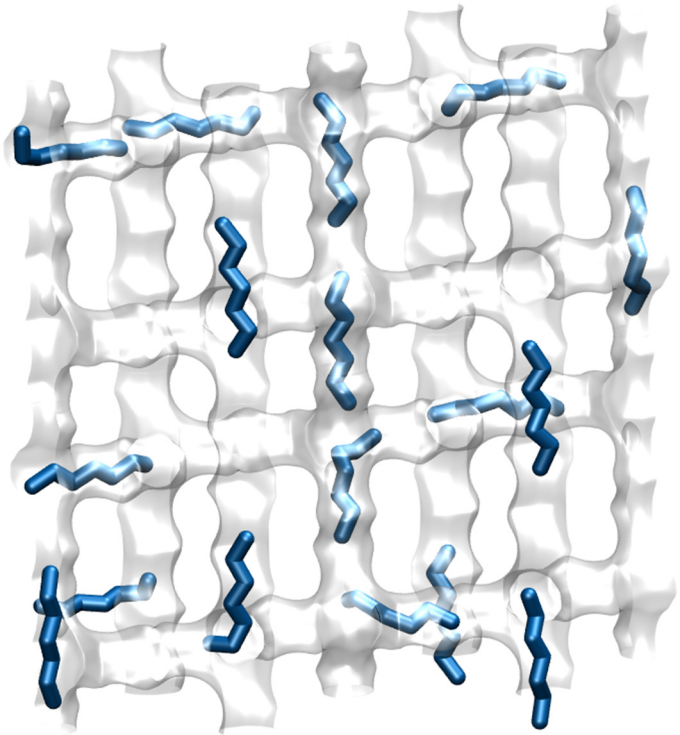

The length of nC7 is not commensurate with the distance between two intersections

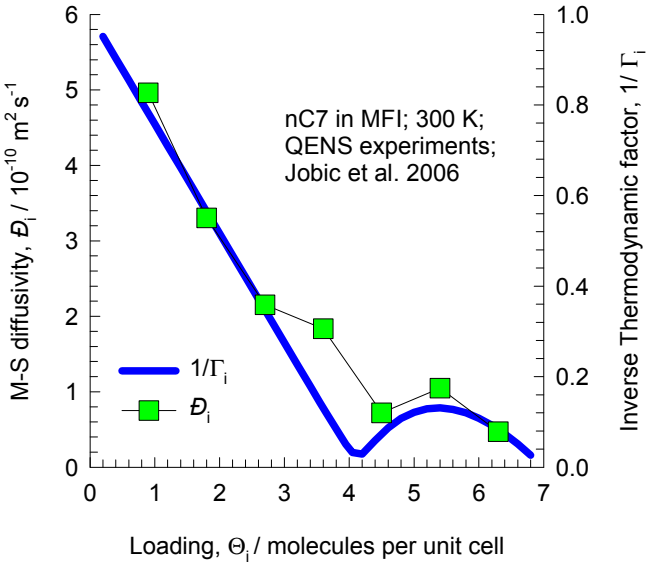

The QENS experimental data are re-plotted using the information in:

H. Jobic, C. Laloué, C. Laroche, J.M. van Baten, R. Krishna, Influence of isotherm inflection on the loading dependence of the diffusivities of n-hexane and n-heptane in MFI zeolite. Quasi-Elastic Neutron Scattering experiments supplemented by molecular simulations, J. Phys. Chem. B 110 (2006) 2195-2201.

Benzene diffusivity in MFI zeolite

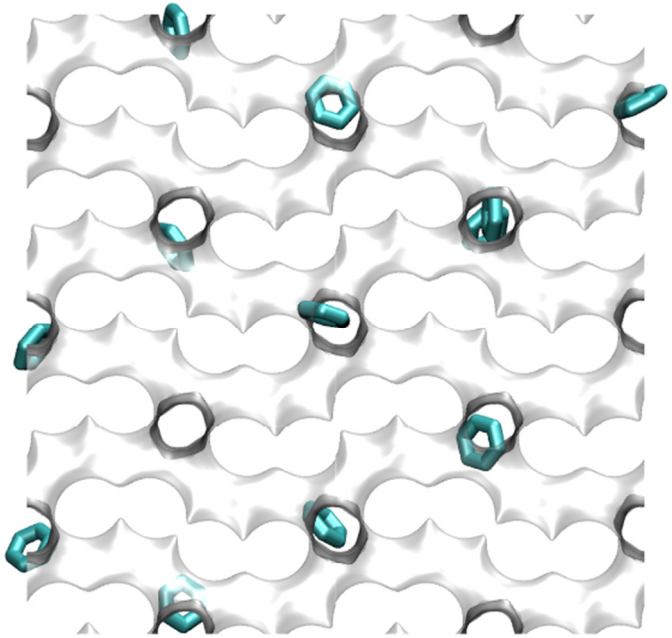

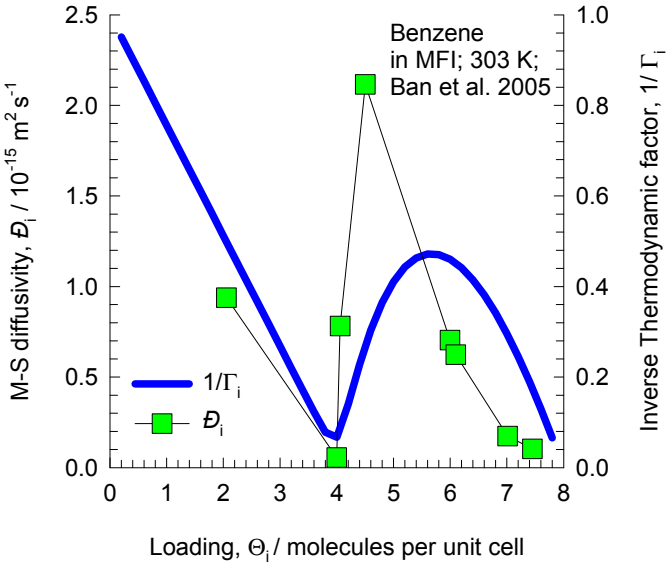

The experimental data are re-plotted after converting Fick diffusivities to Maxwell-Stefan diffusivities using:

Ban, H.; Gui, J.; Duan, L.; Zhang, X.; Song, L.; Sun, Z. Sorption of hydrocarbons in silicalite-1 studied by intelligent gravimetry. Fluid Phase Equilib. 2005, 232, 149-158.

MFI: Traffic junction effects for nC4/iC4 mixture diffusion

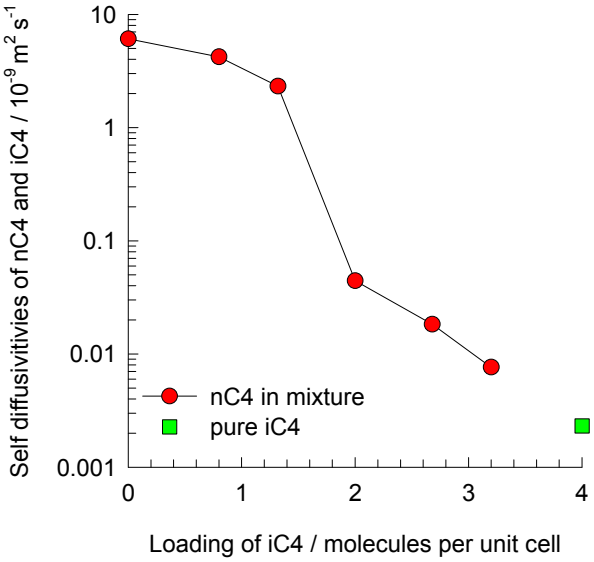

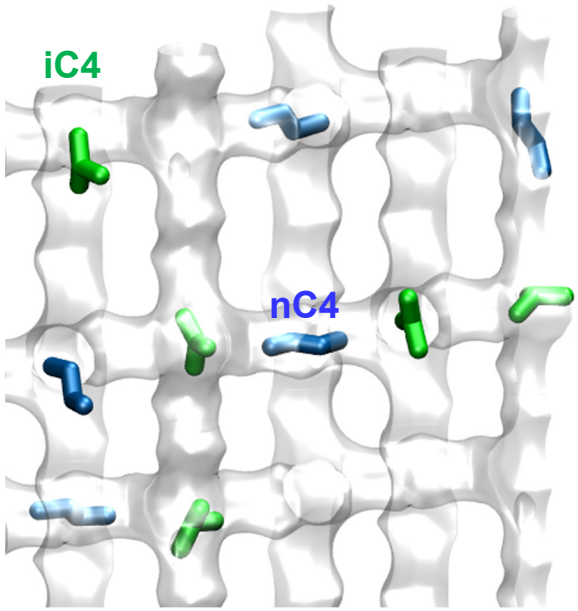

The experimental data are re-plotted using the data of:

Fernandez, M.; Kärger, J.; Freude, D.; Pampel, A.; van Baten, J. M.; Krishna, R. Mixture diffusion in zeolites studied by MAS PFG NMR and molecular simulation, Microporous Mesoporous Mater. 2007, 105, 124-131.

MFI: Traffic junction effects for CH4/Benzene mixture diffusion

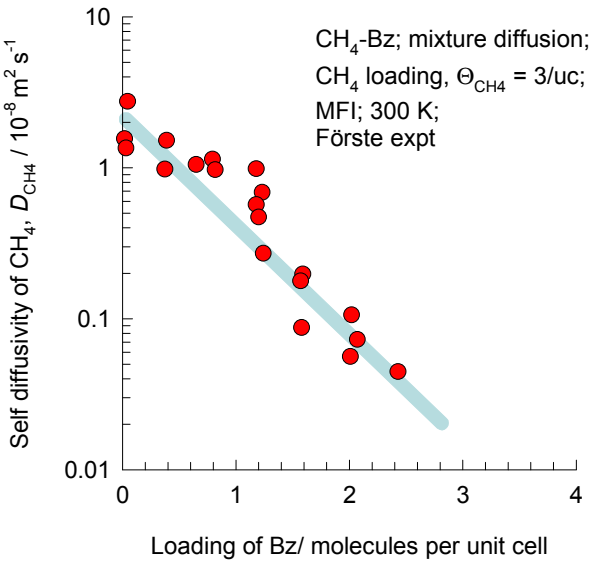

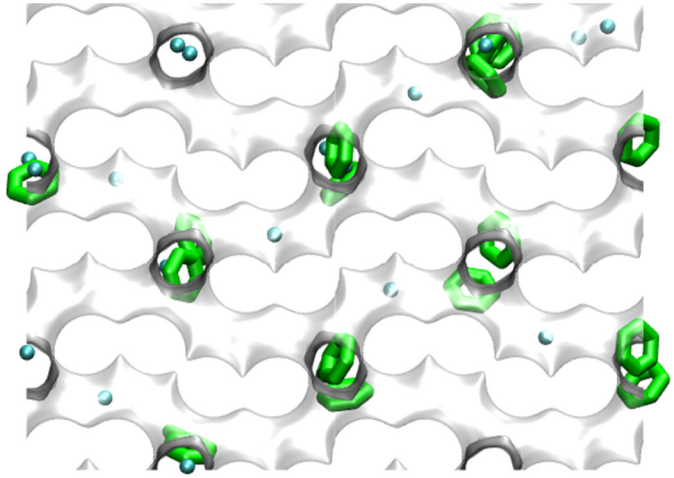

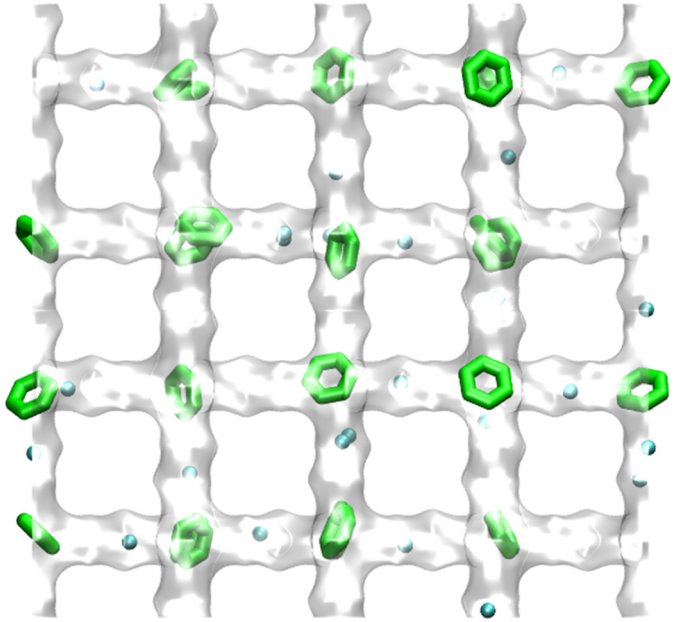

The experimental data are re-plotted using the data of:

Förste, C.; Germanus, A.; Kärger, J.; Pfeifer, H.; Caro, J.; Pilz, W.; Zikánóvá, A. Molecular mobility of methane adsorbed in ZSM-5 containing co-adsorbed benzene, and the location of benzene molecules, J. Chem. Soc., Faraday Trans. 1. 1987, 83, 2301-2309.

MFI: Traffic junction effects for nC6/2MP mixture diffusion

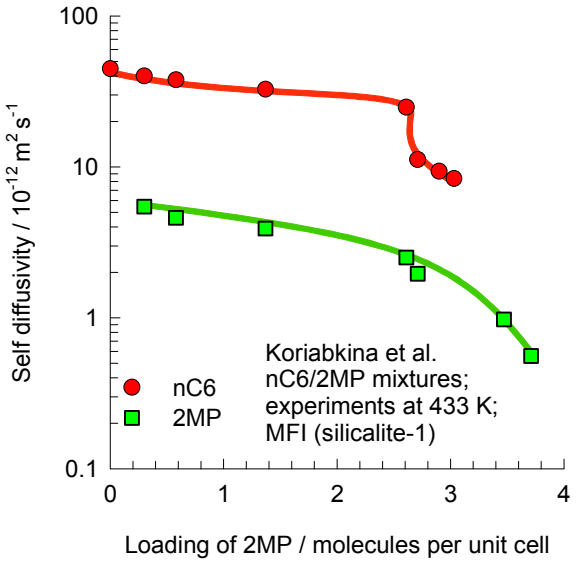

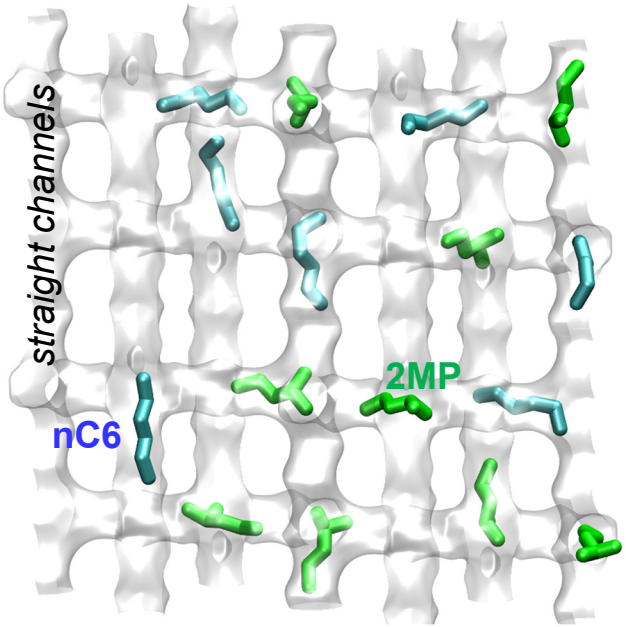

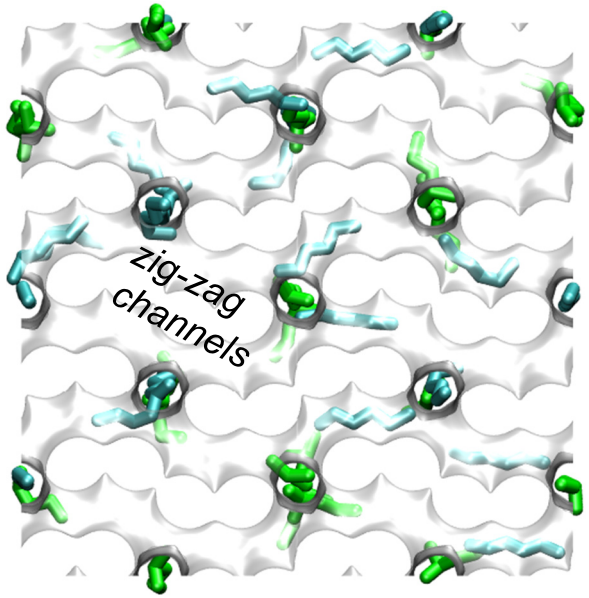

The experimental data are re-plotted using the data of:

Koriabkina, A. O.; de Jong, A. M.; Schuring, D.; van Grondelle, J.; van Santen, R. A. Influence of the acid sites on the intracrystalline diffusion of hexanes and their mixtures within MFI-zeolites, J. Phys. Chem. B 2002, 106, 9559-9566.

Zn(bdc)dabco landscapes

The structural information for $Zn(bdc)(dabco)_{0.5}$, commonly simply referred to as Zn(bdc)dabco, is from

P.S. Bárcia, F. Zapata, J.A.C. Silva, A.E. Rodrigues, B. Chen, Kinetic Separation of Hexane Isomers by Fixed-Bed Adsorption with a Microporous Metal-Organic Framework, J. Phys. Chem. B 111 (2008) 6101-6103.

J.Y. Lee, D.H. Olson, L. Pan, T.J. Emge, J. Li, Microporous Metal–Organic Frameworks with High Gas Sorption and Separation Capacity, Adv. Funct. Mater. 17 (2007) 1255-1262.

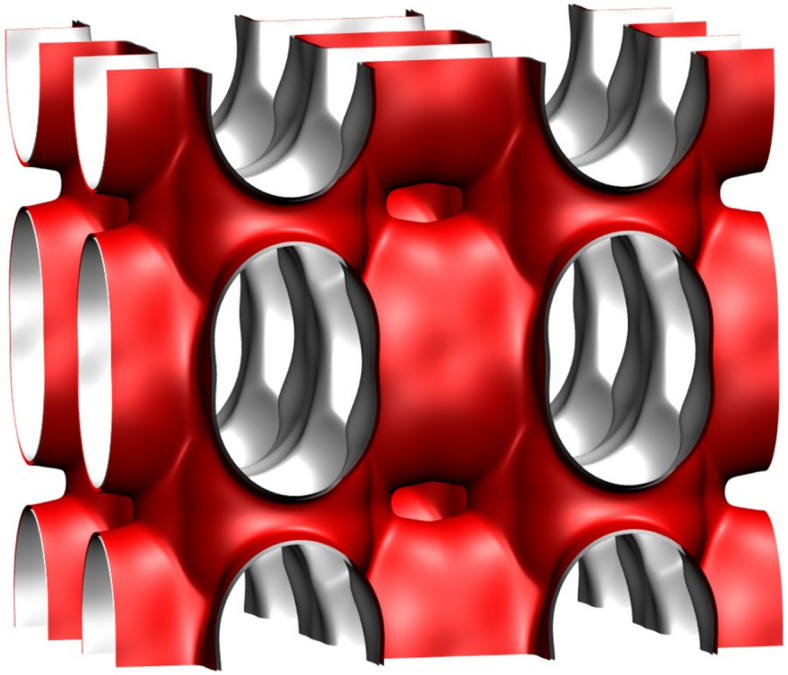

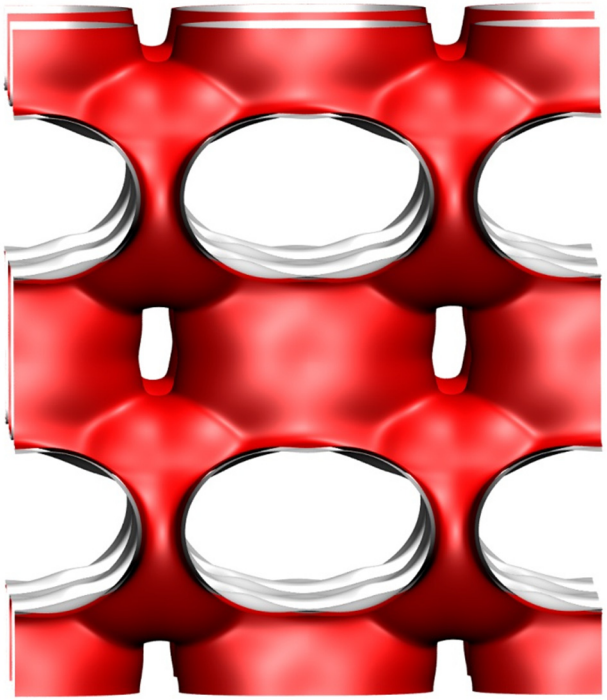

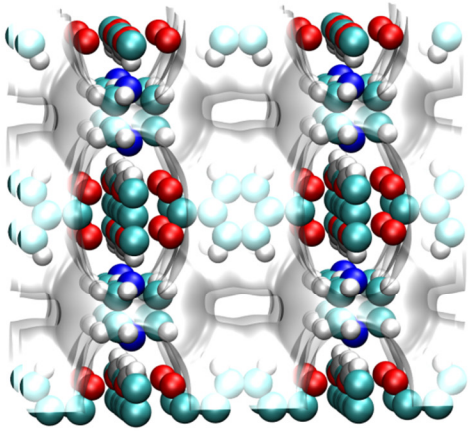

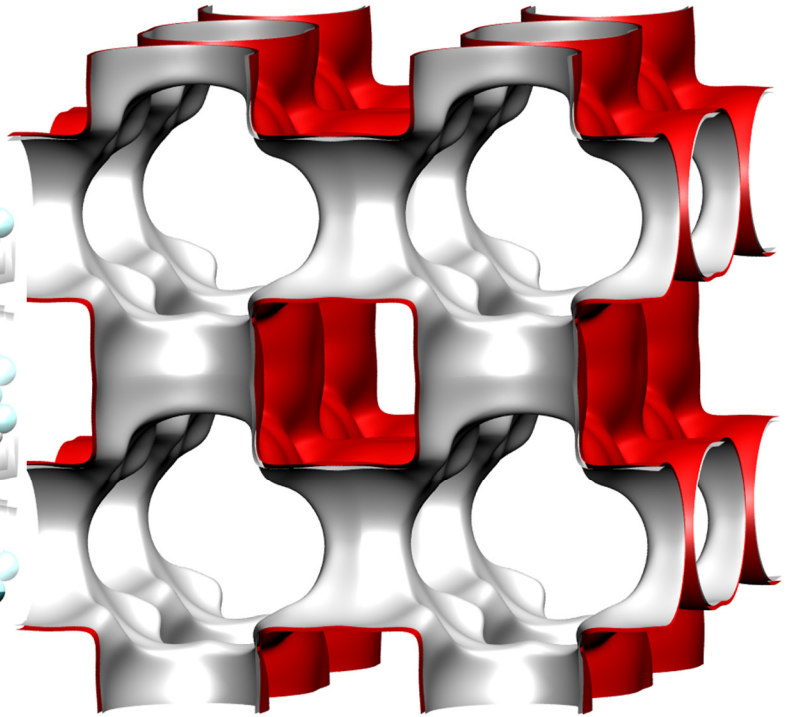

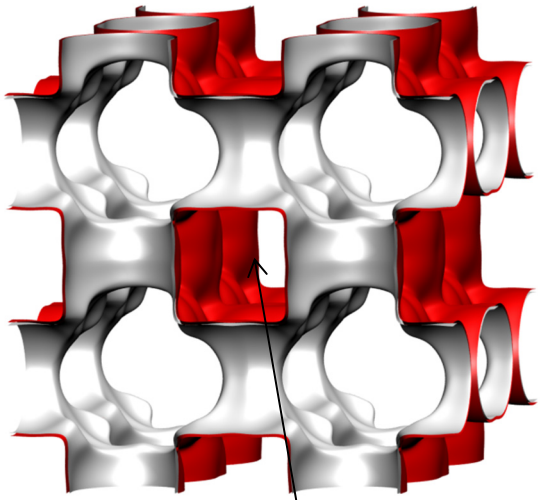

Zn(bdc)dabco
landscapes

3D intersecting channels

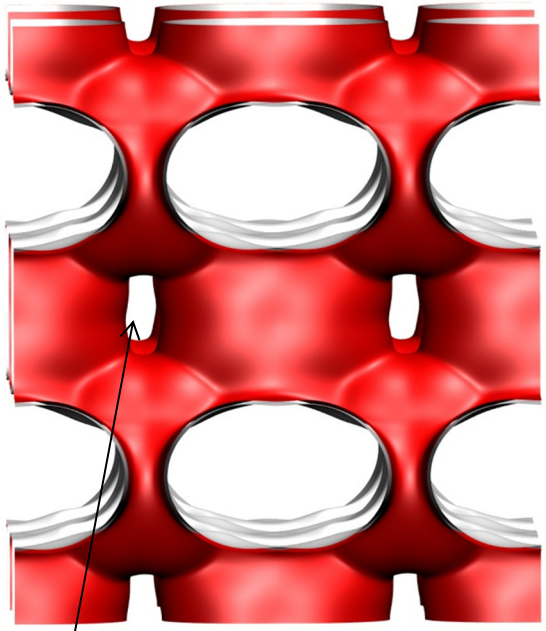

There exist two types of intersecting channels of about 7.5 Å × 7.5 Å along the *x*-axis and channels of 3.8 Å × 4.7 Å along *y* and *z* axes.

Wide channels

7.5 Å x 7.5 Å

Narrow channels

4.7 Å x 3.8 Å

Zn(bdc)dabco pore dimensions

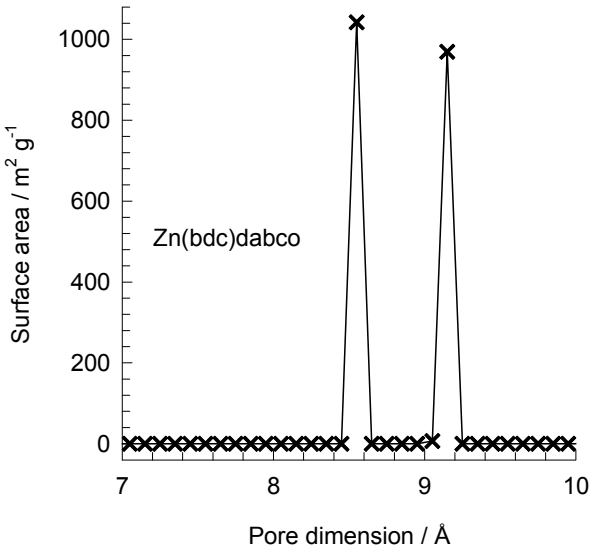

This plot of surface area versus pore dimension is determined using a combination of the DeLaunay triangulation method for pore dimension determination, and the procedure of Düren for determination of the surface area.

	Zn(bdc)dabco
a /Å	10.9288
b /Å	10.9288
c /Å	9.6084
Cell volume / Å^3	1147.615
conversion factor for [molec/uc] to [mol per kg Framework]	1.7514
conversion factor for [molec/uc] to [kmol/m^3]	2.1867
ρ [kg/m3]	826.1996
MW unit cell [g/mol(framework)]	570.9854
ϕ, fractional pore volume	0.662
open space / Å^3/uc	759.4
Pore volume / cm^3/g	0.801
Surface area /m^2/g	2022.5
DeLaunay diameter /Å	8.32

Electronic Supplementary Material (ESI) for Physical Chemistry Chemical Physics

Influence of Inverse Thermodynamic Factor on diffusivities